

**Development of
Chemical-hydraulic
Models for the Prediction
of Long-term Sealing
Capacity of Concrete-
based Sealing Materials
in Rock Salt**

Development of Chemical-hydraulic Models for the Prediction of Long-term Sealing Capacity of Concrete- based Sealing Materials in Rock Salt

Kyra Jantschik
Oliver Czaikowski
Uwe Hertes
Thorsten Meyer
Helge C. Moog
Bernd Zehle

Mai 2018

Remark:

This report was prepared under funding reference no. 02 E 11324 of the German Federal Ministry for Economic Affairs and Energy (BMWi).

The work was conducted by the Gesellschaft für Anlagen- und Reaktorsicherheit (GRS) gGmbH.

The authors are responsible for the content of this report.

Key Words:

Advection, Corrosion, Diffusion, Geochemical Modelling, Laboratory Tests, Permeability, Salt Concrete, Sorel Concrete

Table of contents

1	Introduction.....	1
1.1	Background	1
1.2	Long-term chemical stability of cement based sealing materials	2
1.3	Aim and approach.....	4
2	Analytical methods.....	7
3	Description of available concrete based sealing materials	9
3.1	Sorel concrete	9
3.1.1	Chemical and hydraulic properties	9
3.1.2	Temperature dependent hardening of sorel concrete.....	11
3.1.3	Production of sorel concrete samples in laboratory	13
3.2	Salt concrete.....	14
3.2.1	Chemical and hydraulic properties	15
3.2.2	Derivation of available salt concrete.....	19
3.3	Fabrication of saline solutions for experiments	20
3.4	Analysation of materials.....	21
3.4.1	Analysis of used concrete	21
3.4.2	Analysis of saline solutions	25
4	Laboratory investigations	27
4.1	Batch experiments	27
4.1.1	Setup of batch experiments	27
4.1.2	Laboratory results of batch experiments	29
4.1.2.1	System sorel concrete – old / NaCl solution.....	29

Tables of contents

4.1.2.2	System sorel concrete – old / MgCl ₂ solution	34
4.1.2.3	System salt concrete / NaCl solution.....	38
4.1.2.4	System salt concrete / MgCl ₂ solution.....	42
4.1.2.5	Results of tracer tests	46
4.1.3	Interpretation and discussion	48
4.1.3.1	Thermodynamic stability in the system sorel concrete – old / NaCl solution	49
4.1.3.2	Thermodynamic stability in the system sorel concrete – old / MgCl ₂ solution	51
4.1.3.3	Thermodynamic stability in the system salt concrete / NaCl solution.....	52
4.1.3.4	Thermodynamic stability in the system salt concrete / MgCl ₂ solution.....	53
4.1.3.5	Applicability of tracers caesium and lithium in the various systems with sorel and salt concrete	55
4.2	Cascade experiments	55
4.2.1	Setup of cascade experiments.....	55
4.2.2	Laboratory results of cascade experiments.....	58
4.2.2.1	System sorel concrete – A1 / NaCl solution	58
4.2.2.2	System salt concrete / MgCl ₂ solution.....	62
4.2.3	Interpretation and discussion	67
4.2.3.1	Dissolution-precipitation processes in the system sorel concrete – A1 / NaCl solution	67
4.2.3.2	Dissolution-precipitation processes in the system salt concrete / MgCl ₂ solution.....	70
4.3	Through-diffusion experiments.....	71
4.3.1	Setup of through-diffusion experiments.....	71
4.3.2	Results of through-diffusion experiments	74
4.3.3	Interpretation and discussion	83
4.4	Advection experiments.....	88
4.4.1	Setup of advections experiments	88
4.4.2	Laboratory results of advection experiments.....	93
4.4.2.1	Advection experiments with sorel concrete – A1	93

Tables of contents

4.4.2.2	Advection experiments with combined samples of rock salt and salt concrete.....	107
4.4.3	Interpretation and discussion	116
4.4.3.1	Development of the permeability of sorel concrete during percolation with saline solutions and its influence to the sealing capacity	116
4.4.3.2	Development of the contact seam between sealing element and host rock during percolation with saline solutions and its influence to the sealing capacity	122
4.5	PET-measurements on salt concrete – halite contact zone.....	125
4.5.1	Set up of PET-measurements.....	125
4.5.2	Results of PET-measurements	127
4.5.3	Interpretation and discussion	130
5	Model investigations	137
5.1	Model methods	137
5.2	Database	137
5.3	Calculation and adjustments.....	138
5.3.1	Calculation of saturation indices from the composition of experimental solutions	138
5.3.2	Calculations and adjustments in the system sorel concrete / NaCl solution	139
5.3.4	Calculations and adjustments in the system salt concrete / MgCl ₂ solution	144
5.4	Modelling results.....	151
5.4.1	Calculation of saturation indices from experimental solutions in batch experiments	152
5.4.2	Calculation of saturation indices from experimental solutions in cascade experiments.....	159
5.4.3	Calculation of saturation indices from experimental solutions in advection experiments with sorel concrete.....	162

Tables of contents

5.4.4	Modelling of the reaction of sorel concrete with NaCl solution.....	165
5.4.5	Modelling of the reaction of salt concrete with MgCl ₂ solution	170
5.5	Interpretation and discussion	184
5.5.1	Comparison between modelling and experimental results in the system sorel concrete – A1 / NaCl solution.....	184
5.5.2	Comparison between modelling and experimental results in the system salt concrete / MgCl ₂ solution.....	186
6	Evaluation of cement based sealing materials	193
6.1	Evaluation of sorel concrete with respect to its geo-chemical material behaviour and its sealing capacity	193
6.2	Evaluation of salt concrete with respect to its geo-chemical material behaviour and its sealing capacity	195
7	Conclusions	199
8	Summary and outlook	201
9	Zusammenfassung und Ausblick	205
	References	211
	Glossary, Symbols and Abbreviations.....	221
	List of tables	229
	List of figures.....	233
	Appendix	245
A 1	Experimental data.....	245
A 1.1	Detection limits of ICP-OES and ICP-MS.....	245
A 1.2	Solution analysis batch experiments	246
A 1.3	Solution analysis cascade experiments	250

Tables of contents

A 1.4	Tracer concentrations through-diffusion experiments.....	252
A 1.5	Solution analysis advection experiments – soresl concrete – A1	256
A 1.6	Solution analysis and permeability measurements advection experiments – combined samples.....	260
A 1.7	Tracer test	263
A 1.8	X-ray analysis	264
A 1.9	Permeability measurements to gas – soresl concrete – A1.....	267
A 1.10	Permeability measurements to gas – combined samples.....	268
A 2	Modelling data	269
A 2.1	Calculated saturation indices from batch experiments	269
A 2.2	Calculated saturation indices from cascade experiments.....	276
A 2.3	Calculated saturation indices from advection experiments.....	279
A 2.4	Potential equilibrium phases in modelling with PHREEQC.....	286
A 2.5	Translation of logK from cemdata07.dat to THEREDA.....	288
A 2.6	Modelled concentrations cascade experiment – soresl concrete – A1 / NaCl solution	290
A 2.7	Modelled concentrations cascade experiment – salt concrete / MgCl ₂ solution	291
A 3	Calculation of pc_H	292

1 Introduction

1.1 Background

For the safe disposal of radioactive waste in Germany the emplacement of nuclear waste in deep geological formations is foreseen. Several safety principles are involved in the German safety requirements for a repository of heat-generating nuclear waste /BMU 2010/. The most significant ones are:

- Radionuclides and other contaminants have to be concentrated in the containment-providing rock zone and must be isolated from the biosphere as long as possible.
- The risks from natural radiation exposure should be enhanced only insignificantly by the release of radionuclides from waste disposal.

A multiple barrier system shall ensure the safe enclosure of radioactive waste. The system consists of the geological barrier (host rock), the geotechnical barriers (backfill and sealing elements) and the technical barriers (canisters and over packs) /BRA 2008/.

Three options of host rock are investigated in Europe: Rock salt, clay stone and crystalline rock. This thesis deals with the salt option. Rock salt is characterized by a natural porosity about 0.2 %, in which the pores are not connected continuous. The undisturbed rock salt is tight against fluids and gases. Voids in the host rock are able to be closed by time under compressive stress because of the viscoplastic material behaviour of rock salt. This circumstance is used for backfilling mine openings with crushed salt. Pores and pathways are able to be closed over the time if the crushed salt is compacted as results of the convergence from the host rock. Until the backfill satisfy its sealing capacity shafts and drifts of the disposal system could be closed with cement based plugs and seals. The integrity of the geological barrier and the stabilization of the disturbed rock zone at the contour shall be preserved by the sealing elements. In addition the inflow of solution and the release of radionuclides shall be decelerated.

The sealing capacity of sealing elements depends on the structurally engineered properties of the materials itself and on the long-term interaction between the sealing material and the host rock. A sealing element may be regarded to consist of three compartments: the excavation damaged zone (EDZ), the sealing element itself and the contact seam between sealing element and EDZ /RÜB 2014/. Additionally, the geomechanics consider the undisturbed and impermeable rock salt as fourth compartment. It aimed at considering the interaction between host rock and sealing element related to the safety case. Especially, the contact seam between sealing element and EDZ presents a preferred pathway for saline solutions, brines and gases, which may generate if water enters in rock salt repositories. But also the sealing element itself and the EDZ presents possible pathways for saline solutions. The presence of saline solution to cement based sealing materials can result in corrosion processes which influence the sealing capacity of plugs and seals. Hence, the chemical-hydraulic material behaviour of cement based sealing materials has to be well known to ensure the safe enclosure of radioactive waste in the host rock.

The research projects "LAVA" and "LAVA-2", conducted at the Gesellschaft für Anlagen- und Reaktorsicherheit (GRS gGmbH) were cofunded by the BMWi under contract no. 02E11122 and 02E11324. LAVA was additionally cofunded by the European Union's European Atomic Energy Community's (Euratom) Seventh Framework Programme FP7/2007-2013 under Grant Agreement no. 323273, the DOPAS Project /JAN 2016a/. Within these projects the cement based sealing materials salt and sored concrete were investigated in presence of saturated NaCl and MgCl₂ solution. The development of phase composition while corrosion process as well as the impact on corrosion of advective and diffusive transport were investigated.

1.2 Long-term chemical stability of cement based sealing materials

The longevity of a sealing element depends significantly of the chemical stability of the cement based sealing materials. The porosity and subsequently the mechanical stability of a cement based sealing element might be affected by dissolution and precipitation processes when a saline solution enters to a repository. In general, two scenarios are conceivable /MEY 2003a/: first, porosity decreases caused by an increase of solid phase volume. This would result in a decrease of permeability. Secondly, mechanical stability decreases because porosity and consequently the permeability increase.

The ambient host rock formation has a significant impact on the composition of the saline solution. Most important minerals in rock salt are Halite (NaCl), Anhydrite (CaSO_4), Gypsum ($\text{CaSO}_4 \cdot 2\text{H}_2\text{O}$), Sylvite (KCl), Kieserite ($\text{MgSO}_4 \cdot \text{H}_2\text{O}$), Polyhalite ($\text{K}_2\text{Ca}_2\text{Mg}[\text{SO}_4] \cdot 2\text{H}_2\text{O}$), Carnallite ($\text{KMgCl}_3 \cdot 6\text{H}_2\text{O}$) and Kainite ($\text{K}_4\text{Mg}_4[\text{Cl}_4\text{SO}_4]_4 \cdot 11\text{H}_2\text{O}$) /HER 2000/. Solutions in rock salt always equilibrate with respect to Halite. Dependent to the other mineral phases the solution had equilibrated with, quinary solutions (without calcium) or hexary solutions (with calcium) are formed. Equilibration with potash salts results in brines which are dominated by magnesium and chloride.

The corrosion processes of sealing elements depend significantly on the composition of the saline solutions and the used construction material /KRA 2008/. Salt concrete is stable in solutions saturated with respect to Halite or to Halite and calcium-sulphate containing phases. Salt concrete corrodes in solutions with high magnesium-chloride concentrations. Sorel concrete behaves oppositely and corrodes in solutions which are saturated with respect to Halite only and is stable in solution with high magnesium-chloride content.

In general, two scenarios are conceivable which result in a fail of the sealing function of a cement based sealing element resulting from intrusion of saline solution to the repository: Firstly, a solution enters a repository, encounters a sealing element and the sealing element may saturate with the solution. In this case, it is possible that radionuclides from the repository can be released by diffusive transport through the saturated sealing element. Secondly, the present solution corrodes the sealing element and generates a flow path. In that case, solution can penetrate to the repository by advection or contaminated solutions can leave the containment-providing rock zone (CRZ). Furthermore, the contact seam between the sealing element and the EDZ seems to be the primary pathway for solution as long as permeability of the contact seam is high.

Hence, for a better understanding of the interaction between corrosion processes, dependent to the composition of sealing material and saline solution and its impact on the sealing capacity, through-diffusion and advection experiments were performed.

Process of diffusion may be relevant to sealing elements when a saline solution entered to a repository and saturated a sealing element without generating pathways for advective flow. Saturation of a sealing element may affect in release of

radionuclides from the repository by diffusive transport, if containers and over packs which represent the technical barrier, were also damaged. The setup of through-diffusion experiments offers the possibility to determine diffusion coefficients to saturated concrete cores within relative small periods of time. In through-diffusion experiments the diffusion coefficient is calculated from the cumulated mass of tracer, which passed the sample. In contrast, in in-diffusion experiments the diffusion coefficient is calculated from the deep of intrusion of tracer in relation to its concentration in the sample and the time of diffusion. The setup of through-diffusion experiments was more practicable in case of the available concretes.

In advection experiments the impact of saline solutions to the permeability of cement based sealing materials was investigated. It should be estimated if the equilibration with various saline solution results in improve or fail of the sealing function of the sealing material itself as well as of the contact seam and EDZ. Partly, advection experiments were performed as “stop-and-flow” experiments in which the solution was enclosed in the samples for a while. Development of permeability and solution composition dependent to the time of enclosure was investigated to determine kinetic effects during the equilibration.

1.3 Aim and approach

Aim of the projects LAVA and LAVA-2 was the investigation of the chemical-hydraulic behaviour of salt and sored concrete in contact with saturated NaCl and MgCl₂ solution and its impact on the sealing capacity. The presence of saline solutions at a cement based sealing element may result in the dissolution and formation of solid phases. The phase composition can influence the material properties significantly, for example stability under load or hydraulic permeability, thus affecting the integral sealing capacity. Consequently, it is necessary to get a better understanding of the corrosion processes of salt and sored concrete in contact with high saline solutions and its impact on the sealing function.

In the beginning, a literature research about the sealing material properties of salt and sored concrete and its material behaviour was conducted. The results were summarized in chapters 3.1 (sored concrete) and 3.2 (salt concrete).

In the next step, a comprehensive laboratory program was carried out. It started with batch experiments (chapters 4.1.1 and 4.1.2). Aim of batch experiments was to define the reaction time between powdered concrete and saline solution until the equilibrium was achieved approximately. Batch experiments were performed in the systems sorel concrete / NaCl solution, sorel concrete / MgCl₂ solution, salt concrete / NaCl solution and salt concrete / MgCl₂ solution.

In cascade experiment powdered concrete was reacted with saline solution for a defined reaction time (chapters 4.1.2 and 4.2.2). The time allowed for equilibration was determined in batch experiments. The reacted solution was separated from concrete in the end of each cascade and was reacted with unreacted concrete again. Based on cascade experiments the reaction path between concrete and saline solution can be described within very short periods of time resulting from the large specific surface area of the powdered concrete.

Furthermore, advective and diffusive transport experiments were performed. Diffusion experiments aimed at determining diffusion coefficients for the concrete. The diffusion coefficient is relevant to the release of radionuclides from the disposal to the biosphere after a sealing element was saturated by saline solution as result of brine intrusion to the disposal. Therefore through-diffusion experiments were performed. A pilot test of through-diffusion experiments was performed in the beginning. The pilot test aimed at testing and improving the proceeding of through-diffusion experiments. Additionally, should be tested, which length of samples are workable for laboratory tests within a realistic time period. Based on experience of the pilot test a further through-diffusion experiment was performed. Results of both experiments were shown in chapters 4.2.2 and 4.3.2.

Advective transport process was investigated in comprehensive laboratory program of advection experiments (chapters 4.3.2 and 4.4.2). This process describes the intrusion of solution to a disposal. Advection experiments have to be divided in experiments with sorel concrete, by that the pure sorel concrete samples were percolated with saline solution and in advection experiments with salt concrete, which were performed to combined samples of a hollow rock salt cylinder in which a salt concrete core was inserted. Experimental set up of combined samples allows investigations to the development of a sealing element at laboratory scale under influence of saline

solutions and comprehensive load. The most relevant parameter of advection experiments was the development of permeability.

In a further procedure the geochemical cascade experiments were modelled using the program code PHREEQC and the THEREDA database release 6.0. This approach aimed at verifying and improving the understanding of geochemical processes, which occur while sored and salt concrete, respectively were corroded by high saline solutions. The various steps of calculation and their results, also in comparison to laboratory results, were shown in chapters 4.4.2 and 5.4.

Methods and results of laboratory testing program and of modelling were interpreted and discussed in chapter 5.5. Therefore, results from various laboratory tests were related among each other and compared with data from literature as available. Additionally, the information value of modelling results was evaluated. Finally, the suitability of salt and sored concrete based on results before was summarized and discussed.

2 Analytical methods

Determination of aluminium, calcium, magnesium, potassium, silicon, sodium and sulfur was conducted with ICP-OES (Type: iCAP 7400 ICP-OES Duo, Thermo Fisher Scientific). Chloride was determined by using titration. Caesium and lithium were analysed by ICP-MS (Type: X Series II ICP-MS System, Thermo Scientific). Limits of detection are given in appendix A 1.1 (Tab. A.1.1 and Tab. A.1.2) The pH was measured using Orion pH Elektrode ROSS™ in combination with pH meter Metrohm 826 pH lab. Because of the high ionic activity in high saline solution measured pH was converted in p_{cH} according to /HAG 2014/ (appendix A 3). Density was measured with Dichteschwinger DMA 5000M (Anton Paar GmbH). X-ray diffraction was conducted by means of a X-ray diffraction camera X'Pert Pro MPD of PANalytical. Software X'Pert Highscore Version 3.0 was used for analysis of X-ray diffractograms using ICSD database 2009 – 2 (Type-no. PW3213/92), release version 1.5 from 1st December 2009.

3 Description of available concrete based sealing materials

3.1 Sorel concrete

Experiences with sorel concrete for the construction of sealing elements in rock salt exist for more than 100 years. Sealing elements of sorel concrete are foreseen in drift sections, where the intrusion of $MgSO_4$ and $MgCl_2$ solutions is expected, for example in Carnallite (40-60 % Carnallite ($KMgCl_3 \cdot 6H_2O$), 30 – 40 % Halite ($NaCl$) and up to 20 % Kieserite ($MgSO_4 \cdot H_2O$) /PRI 2006/). There exist various recipes and procedures for the production of sorel concrete. Sorel concrete composition A1 was used for laboratory experiments described in this thesis. It consists of crushed salt, magnesium oxide (MgO) and $MgCl_2$ solution. The composition is defined in Tab. 3.1.

Tab. 3.1 Composition of sorel concrete A1 according to /FRE 2015a/ and /TEI 2009/

Component	Composition [kg/m ³]	Composition [mass-%]
Magnesium oxide (Reactivity 200-250 s)	218	11.3
Crushed salt	1237	63.7
$MgCl_2$ solution (4-5 molal)	485	25
Sum	1940	100

The so called 318-phase ($3Mg(OH)_2 \cdot MgCl_2 \cdot 8H_2O$) is formed during the hardening process of sorel concrete A1 /FRE 2007/. For formation of 318-phase it is necessary to consider the reactivity of magnesium oxide and molality of $MgCl_2$ solution as described in Tab. 3.1 /FRE 2015a/. Additionally, it seems to be necessary for phase formation that sorel concrete A1 hardens in a defined temperature regime as described in chapter 3.1.2.

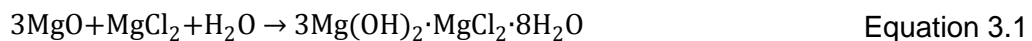
3.1.1 Chemical and hydraulic properties

Chemical and hydraulic properties of sorel concrete depend on each other. Hence, both properties are considered together within this chapter.

The porosity of sorel concrete was determined for compacted and non-compacted sorel concrete samples by DBE-Tec (Deutsche Gesellschaft zum Bau und Betrieb von Endlagern – Technology GmbH). Porosity of compacted samples were determined to 17.9 V %, for non-compacted sorel concrete samples to 19.9 V % /TEI 2009/.

Permeability to gas was measured at 22 samples. Average gas permeability was determined to $2.24 \cdot 10^{-18} \text{ m}^2$. The confining pressure was 1 MPa and the gas injection pressure 0.6 MPa /TEI 2009/. Results conform to in situ gas permeability of $4.5 \cdot 10^{-18} \text{ m}^2$.

Stoichiometric ratios of magnesium oxide, MgCl_2 solution and water have to be considered for formation of 318-phase in the A1-formulation of sorel concrete. Correct molar ratios are given in Equation 3.1.



The corrosion behaviour of sorel concrete was investigated in MgCl_2 , MgSO_4^{2-} und MgCl_2 -NaCl systems by /FRE 2015/ and is summarized below:

In presence of MgCl_2 solution (System $\text{Mg}(\text{OH})_2$ - MgCl_2 - H_2O) no corrosion processes were detectable. Brucite ($\text{Mg}(\text{OH})_2$) and the 318-phase are thermodynamically stable in this milieu. Brucite forms at low concentrations of MgCl_2 . It can also be formed in higher MgCl_2 concentrations at higher temperatures. 318-phase becomes stable at increasing MgCl_2 concentrations. Brucite and 318-phase are stable simultaneously at MgCl_2 concentrations between 1.5 and 2.0 $\text{MgCl}_2/\text{kg H}_2\text{O}$ ("Two-salt-point"). The concentration of the two-salt-point depends on the temperature. The so called high-temperature phases are formed at temperature above 80°C . The high-temperature phases are not considered below, because following investigations corresponds to hardened sorel concrete. Temperatures above 80°C are not expected in rock salt repositories after the hardening process /MÜL 2012/. When the saturation of MgCl_2 is attained the formation of Bischofite ($\text{MgCl}_2 \cdot 6\text{H}_2\text{O}$) was observed /PAN 2017/.

An influence of sulphate concentrations in saline solutions on the stability of sorel concrete was not detectable in investigations up to now. Solubility of various phases in the system $\text{Mg}(\text{OH})_2\text{-MgSO}_4\text{-H}_2\text{O}$ was investigated by the TU Bergakademie Freiberg. Results show, that magnesium-hydroxide-sulphate hydrates ($x \text{Mg}(\text{OH})_2 \cdot y \text{MgSO}_4 \cdot z \text{H}_2\text{O}$) are formed in this system /DIN 2013/. The thermodynamically stable phase of the system $\text{Mg}(\text{OH})_2\text{-MgSO}_4\text{-H}_2\text{O}$ up to 120 °C is the 512-phase. With increasing MgSO_4 concentration, Epsomite ($\text{MgSO}_4 \cdot 7\text{H}_2\text{O}$), Hexahydrate ($\text{MgSO}_4 \cdot 6\text{H}_2\text{O}$) or Kieserite are formed dependent on the temperature. Epsomite forms up to 50 °C, Hexahydrate at circa 60°C and Kieserite at temperatures above 70 °C. Results from investigations of the system $\text{Mg}(\text{OH})_2\text{-MgCl}_2\text{-MgSO}_4\text{-H}_2\text{O}$, which are in agreement with the intrusion of magnesium-sulphate-containing solution to sorel concrete are not available at present.

Further investigations were performed in the system $\text{Mg}(\text{OH})_2\text{-MgCl}_2\text{-NaCl-H}_2\text{O}$ with MgCl_2 solution saturated with respect to NaCl. Stable phases are Brucite and the 318-phase in agreement with the system without NaCl. NaCl decreases the solubility of the 318-phase and consequently the two-salt-point switch to MgCl_2 concentrations of circa 0.5 mol $\text{MgCl}_2/\text{kg H}_2\text{O}$. When saturation of MgCl_2 is attained Bischofite is additionally formed as stable phase. Corrosion of sorel concrete occurs only until the concentration of Mg^{2+} in the NaCl solutions is at least 0.5 mol $\text{Mg}^{2+}/\text{kg H}_2\text{O}$ /FRE 2015/, /KRA 2008/.

Investigations of a system with pure saturated NaCl solution are not available yet.

3.1.2 Temperature dependent hardening of sorel concrete

The heat of reaction, induced from the binder, can generate high temperatures during the hardening process of sorel concrete. Maximal temperatures up to 110 °C can be formed during hardening process /KUD 2009/. Measurements in an in-situ sealing element yielded temperatures of some 80 °C /HEY 2015/.

The development of mineral phases in sorel concrete is clearly influenced by the hardening temperature. The hardening process and the influence of temperature to the formation of phases were investigated at TU Bergakademie Freiberg. The hardening behaviour and phase formation were analysed in the context of various Temperature Time Frames (TTF). The laboratory program and results are described in detail in

/FRE 2015/. The continuous hardening regime of 90°C TTF is mostly representative for the hardening process of sorel concrete in rock salt repositories. The hardening process should involve 200 days at least /FRE 2015a/. Hence, the phase formation in agreement with this TTF is described below.

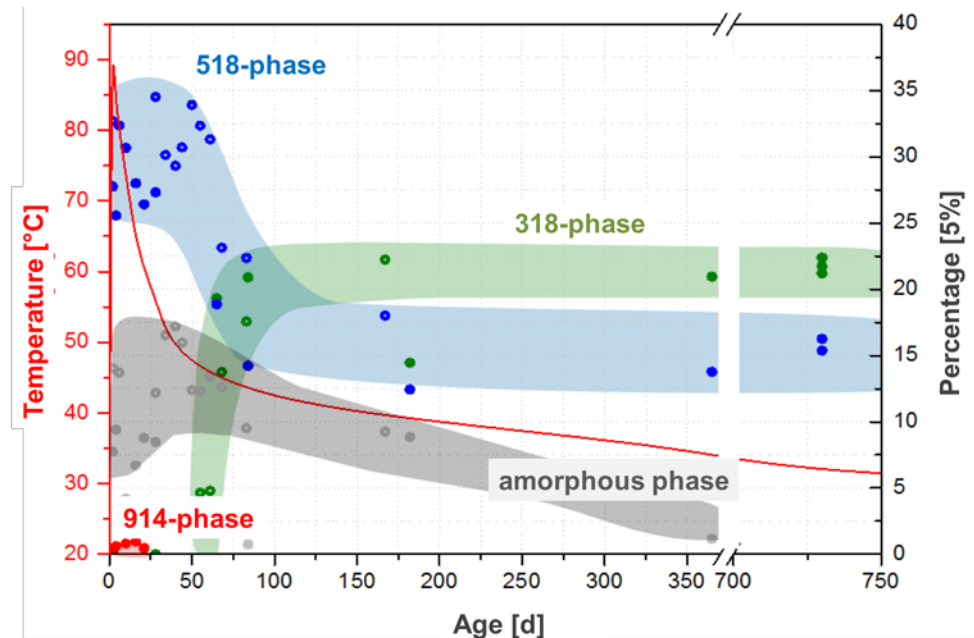


Fig. 3.1 Continuous temperature time frame (TTF) of 90 °C for sorel concrete A1 /PAS 2015/

The highest temperatures are expected in the initial phase of the hardening process. First the metastable 518- and 914-phases are formed. Furthermore, amorphous phases are formed. The 914-phase is stable at temperatures > 80°C. If the temperature decreases the high-temperature 914-phase dissolves. The rate of the 518-phase also decreases from 35 % to 17 %. Formation of 318-phase occurs simultaneously at a temperature < 50 °C and reaches a maximum content of 25 % during the experimental time. The 318-phase is stable in temperature ranges between 25°C and 80 °C /PAN 2015/. The 518-phase can exist between 25 °C and 60 °C as metastable phase. The 318-phase is always formed from the 518-phase, partly from the 914-phase and amorphous phases in sorel concrete composition A1. The point of time, at which secondary crystallization begins, depends on the temperature profile and the reactivity of MgO. In general: at high reactivity the hardening temperature is low and the 518-phase exists for longer times. The hardening process is completed when

the amorphous phase is completely transformed. This process needs a duration of months up to years /PAN 2015/.

3.1.3 Production of sorel concrete samples in laboratory

The development of sorel phases depends on the composition of the sorel concrete, on the temperature profile during the hardening process and on the reactivity of magnesium oxide as shown in chapter 3.1.2. The knowledge of these boundary conditions during production of sorel concrete is needed for reproducible and reliable experimental results. Hence, sorel concrete was produced in laboratory with consideration of required conditions:

- Composition and requirements on components must conform to Tab. 3.1.
- Sorel concrete is mixed in a compulsory mixer. Entry of air shall be minimized by slow mix.
- Concrete hardens in air tight vessels to avoid evaporation of pore solution. The pore solution is required for the formation of 318-phase /FRE 2015/.
- Concrete samples harden over 200 days at a continuous TTF of 90 °C as described in chapter 3.1.2: Hardening process starts at temperature of 90 °C and the temperature decreases continuously within the time period of hardening process.



Fig. 3.2 Production of sorel concrete A1 in laboratory: Mixing of sorel concrete in compulsory mixer (left) and hardening of samples in air tide vessels in climate cabinet (right)

Sorel concrete, produced in consideration of conditions described above, was not available at the beginning of the research project. Consequently, preliminary experiments had to be executed with the sorel concrete, which was produced under unknown conditions and hardening regime before. In general, these experiments were used as pre-experiments for testing experimental set ups and estimation of equilibration times. Experiments, executed with these undefined sorel concrete are identified by “sorel concrete – old” in this thesis. Significant experiments were repeated with the new sorel concrete, produced as described above. This concrete is called “sorel concrete - A1”. The significance of experimental results using sorel concrete - old can be estimated by comparison of this results with the new experiments, in which sorel concrete - A1 was used.

3.2 Salt concrete

The salt concrete available for laboratory experiments below consists of saturated NaCl solution, crushed salt and blast furnace cement (Tab. 3.2). Consequently, salt concrete is stable in saturated NaCl solutions /SCH 2009/. Hence, the installation of sealing element of salt concrete is foreseen in halite horizons. The set concrete consists of a cement matrix with inclusions of crushed salt. The grain size of the used crushed salt is 16.00 mm in maximum /MÜL 2010/. Salt concrete is characterized by the typical

calcium-silicate-hydrates (CSH), which are formed during the hardening process /LEA 1998/.

Tab. 3.2 Composition of salt concrete /MÜL 2010/

Component	Composition [kg/m ³]	Composition [mass-%]
Blast furnace cement (HOZ 25 HS/NW)*	380	18.3
Crushed salt	1496	72.1
NaCl solution (saturated)	198	9.5
Sum	2074	100 (99.9)

* corresponds to cement CEM III/B according to DIN 1164 [Hewlett, 1998]; the sum of mass-% is given to 100 % in [Müller-Hoeppel, 2010], calculated the sum is only 99.9 %.

A significant impact on the material properties of salt concrete is not expected. Crushed salt consists of Halite and Anhydrite /ENG 2008/.

3.2.1 Chemical and hydraulic properties

Chemical and hydraulic properties of concrete are interdependent thus both properties are described together within this chapter. The used salt concrete was produced of blast furnace cement, which presents a special variation of Portland cement /HEW 1998/. Because there are no applicable studies of the corrosion behaviour of blast furnace cement the following descriptions refer to the investigation of corrosion behaviour of Portland cement.

The velocity of the corrosion process depends significantly of the pore structure. If the pores are well connected the corrosion will influence the whole sealing element more quickly. The degree of cross-linking depends on the water cement ratio (w/c-value) of the concrete. It describes the ratio between water and cement, which influence the velocity of cement hardening process. If the w/c-value is < 0.45 the concrete is hardening in a few days. The hardening process needs a couple of weeks if the w/c-value is > 0.45 and a complete hardening of the concrete is probably never reached for values > 0.7. The faster the hardening process is completed the smaller is the degree of cross-linking. In addition the w/c-value influences the porosity. If the w/c-value is > 0.5 the porosity increases significantly (Powers 1958/59, cited in /HAG 2009/).

The w/c-value of the used salt concrete is 0.38. That means, according to /ENG 2008/, that there is still unreacted cement in the concrete matrix, because in proportion there is more cement included in the concrete than can react with the available water. Based on the information of /HAG 2009/ the salt concrete must be a fast hardening type with a small degree of cross-linked pores. Furthermore, /ENG 2008/ describes a crystallisation of salts from the pore solution during the hardening process. Hence, there is Halite with inclusions of liquids in the cement-gel-matrix. The air void volume is estimated to 1.5 V-%. Air voids are primarily in the cement-gel-matrix /MÜL 2010/.

In consideration of the chemical cement corrosion /BIC 1968/ distinguishes three types of corrosion. The denotation of following corrosion processes refers to the definition of corrosion processes in civil engineering. Relevant chemical processes are described in section below:

- Leaching corrosion
- Corrosion resulting from exchange reactions
- Corrosion resulting from swelling reactions

Normally these corrosion processes proceed simultaneously and influence each other. The most relevant concrete damaging ions are Mg^{2+} , NH_4^+ , H^+ , SO_4^{2-} , Cl^- , HCO_3^- und OH^+ /BIC 1968/.

Leaching corrosion

The leaching corrosion describes processes which result in the dissolution from the cement-matrix without formation of new phases. This process is relevant for porous cements, which repeatedly are in contact with solutions, which are not in equilibrium with the cement.

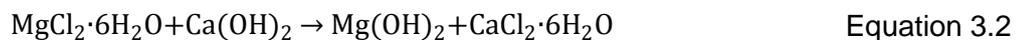
Aqueous solutions in equilibrium with cement exhibit a pH of 12 – 13. The alkaline properties of the cement are mostly caused by the presence of Portlandite ($Ca(OH)_2$) /BIC 1968/. The cement is thermodynamically not stable anymore in neutral or acid solutions. The acid reacts with Portlandite whereby water soluble salts are formed. These salts can be leached from the cement matrix. Eventually, the cement loses its

alkaline buffering and pH decreases as result of the complete dissolution of Portlandite. Subsequently, characteristic and stabilizing CSH-phases are dissolved. Finally, the concrete completely loses its stability. The final product from acid attack is silica-gel (SiO₂-gel) /HAG 2009/.

Corrosion resulting from exchange reactions

Corrosion resulting from exchange reactions describes the exchange of ions between cement and solution, which results in formation of new phases. These phases remain in the concrete matrix or are flushed out by percolation of solution if phases are not in a stable compound with the concrete matrix.

The presence of magnesium chloride (MgCl₂) induces magnesia corrosion in cement. Brucite and calcium chloride (CaCl₂) are formed. The simplified reaction describes Equation 3.2:



Brucite can generate a film at the surface and can delay further corrosion of the cement. However, /BIC 1968/ suggests, that the Brucite-film is stable in stagnant waters only because it will be leached quickly by advective flow. When the Brucite is leached the corrosion retarding effect is lost.

Brucite and Gypsum (CaSO₄·2H₂O) are formed by the attack of magnesium sulphate (MgSO₄) according to Equation 3.3:



Consequences of the formation of Gypsum will be described in section “corrosion resulting from swelling reactions”.

Corrosion caused by exchange reactions results also in dissolution of Portlandite and the decrease of pH. Consequently, CSH-phases are dissolved and SiO₂-gel is formed just as during corrosion by acids. Brucite precipitates and forms a deposit at the surface of SiO₂-gel. In contrast to CSH-phases, magnesium-silicate-hydrate-phases

(MSH) do not exert a stabilizing effect on the cement matrix, resulting in a lower mechanical stability. Moreover, MSH-phases do not form a stable compound with the cement matrix and are therefore to a much higher extent subject to leaching by ingressing solution.

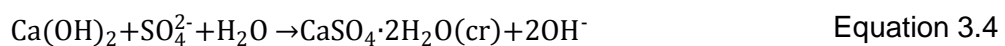
Corrosion resulting from swelling reactions

Reactions with salt result especially in swelling reactions. Crystallisation of salts results primary in hardening of concrete caused by the clogging of pores resulting from the higher specific volume of salt crystals. Clogging of the pore volume can result in strains, which damage the concrete.

The swelling reaction in the cement, which is relevant to the following laboratory tests, is primarily induced by the sulphate ion. W.W. Kind (cited in /BIC 1968/) divides three types of sulphate attack: sulphate corrosion, Ettringite corrosion and magnesium-Gypsum corrosion.

a. Sulphate corrosion

Sulphate corrosion is characterised by the reaction of sulphate ions with the Portlandite of the cement:



Due to the higher specific volume of Gypsum the reaction results in an increase of volume of circa 17.7 % (R.H. Bogue, cited in /BIC 1968/). The volume extension causes strain in the cement matrix, which can result in a failure of the cement. However, a failure of the cement is only expected, if its stability is already diminished by chemical attacks to Portlandite and CSH-phases /HAG 2009/.

b. Ettringite corrosion

At high pH-values, Ettringite ($3\text{CaO} \cdot \text{Al}_2\text{O}_3 \cdot 3\text{CaSO}_4 \cdot 31\text{H}_2\text{O}$) is thermodynamically more stable in comparison to Gypsum. Hence, Ettringite corrosion is expected at $\text{pH} > 11.6$ if adequate masses of aluminium or iron are available. Sulphate, calcium hydroxide and

tricalcium aluminate (C_3A) reacts to Ettringite. Formation of Ettringite induces a volume expansion of 227 %. This is 2.3 times higher than the initial volume of sulphate and tricalcium aluminate according to calculations of R.H. Bogue, W. Lerch and W.C.Taylor (cited in /BIC 1968/). Consequently, this volume extension can result in a failure of the cement. The Portlandite content is minimized by the formation of Ettringite, which causes a decrease of pH. If the pH becomes too low, Ettringite is not stable anymore and Gypsum is formed.

c. Magnesium-Gypsum corrosion

The magnesium-Gypsum corrosion induces formation of Gypsum and attack by magnesium ion at once. Corrosions processes occur simultaneously. Hence, the combined corrosion process is very harmful to the cement /BIC 1968/.

The type of corrosion depends on following factors after /BIC 1968/ and /HAG 2009/:

- pH: if $pH < 10.6$ to 11.6 Ettringite transforms to Gypsum.
- $MgSO_4$ concentration: for concentrations between 1000 mg/l and 4000 mg/l Gypsum corrosion is expected, at concentrations between 4000 mg/l and 7500 mg/l Ettringite corrosion is preferred and concentrations over 7500 mg/l results in magnesium-Gypsum corrosion. The limits cannot be exactly determined and depend on the composition of the cement.
- C_3A content: At high C_3A contents the Ettringite corrosion is preferred. In addition certain rates of Al^{3+}/Ca^{3+} need to be met (Jones, 1938, 1945, J.D. Ans and H. Eick (1945) cited in /BIC 1968/).
- Chloride and carbonate concentrations: chloride and carbonate can delay the Ettringite corrosion. Very high chloride or carbonate concentrations can avoid Ettringite corrosion.

3.2.2 Derivation of available salt concrete

The salt concrete used in laboratory experiments derives from an in situ sealing element of a former German salt mine. The sealing element was constructed in

1991/1992 /STO 1994/. The samples were drilled in 2002. Hence, the concrete was exposed to ambient conditions of the host rock for about ten years. After drilling concrete cores were stored in core boxes by BfS / Asse GmbH until 2012 and afterwards by GRS in laboratory until laboratory experiments were started. Salt concrete samples were exposed to ambient conditions of particular storage within this period of time.

3.3 Fabrication of saline solutions for experiments

Saturated NaCl solution and MgCl₂ solution were used in experiments with salt and sored concrete for investigation of the corrosion behaviour. The saturated NaCl solution is called NaCl solution below. The MgCl₂ solution composition is very similar to IP21 solution. IP21 solution is formed by entry of water in potash levels and is saturated with Carnallite, Sylvite (KCl), Kainite (K₄Mg₄[Cl₄SO₄]₄·11H₂O), Halite and Polyhalite (K₂Ca₂Mg[SO₄]₂·2H₂O).

NaCl and MgCl₂ solution were fabricated by the mixture of H₂O with various evaporate minerals. Components need to be added to solution in the order as given in Tab. 3.3.

Tab. 3.3 Evaporite minerals of NaCl and MgCl₂ solution fabricated in laboratory

Component	NaCl solution [mass-%]	MgCl ₂ solution mass-%]
H ₂ O	73.53	40.10
CaCl ₂	-	0.01
Na ₂ SO ₄	-	0.01
KCl	-	3.26
NaCl	26.47	1.85
MgSO ₄	-	2.32
MgCl ₂ ·6H ₂ O	-	52.41

3.4 Analysation of materials

3.4.1 Analysis of used concrete

Three concrete types were used in the following experiments: salt concrete, sorel concrete – old and the new fabricated sorel concrete - A1 (chapter 3.1). Within this chapter phase composition of all concretes based on X-ray-diffraction analysis and elemental composition is shown.

The sorel concrete for following investigations was produced in GRS laboratory. Sorel and salt concrete samples are shown in Fig. 3.4.

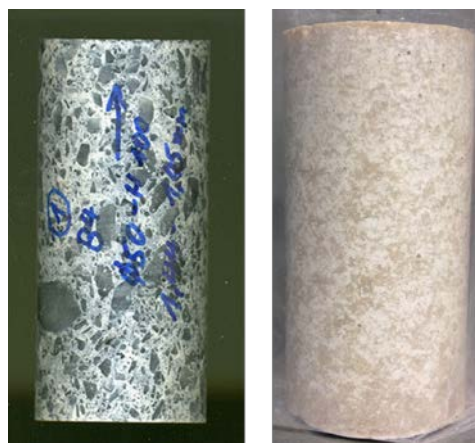


Fig. 3.3 Left: sample of salt concrete - dark-grey areas present the crushed salt inclusions, light-grey areas the cement-gel-matrix; Right: sample of sorel

Description of available concrete based sealing materials

concrete: dark areas describe inclusions of crushed salt, light areas the MgO-matrix

Tab. 3.4 shows the elemental and Tab. 3.5 the phase composition of all concretes.

Tab. 3.4 Composition of concretes according to decomposition

Element	Sorel concrete – old [mol/kg]	Sorel concrete A1 [mol/kg]	Salt concrete [mol/kg]
Al	0.000	0.000	0.369
Ca	0.120	0.165	1.814
Cl	11.958	11.716	13.693
K	n.m.	0.007	0.042
Mg	0.945	2.250	0.368
Na	11.127	11.574	13.693
Si	0.000	0.000	0.660
SO ₄	0.133	0.094	0.376

Tab. 3.5 Mineral phase composition of concretes based on X-ray diffraction

Mineral phase	Sorel concrete – old	Sorel concrete A1	Salt concrete
Anhydrite	X	X	X
Brucite		X	
Chlorartinite	X		
Friedels'salt			X
Halite	X	X	X
Portlandite			X
318-phase	X	X	

The unreacted sorel concrete – old consists of the characteristic 318-phase of Anhydrite and Halite (Fig. 3.4). In addition Chlorartinite ($Mg_2[ClOHCO_3] \cdot 3H_2O$) was detectable. Chlorartinite results from the carbonation of sorel concrete, because this sorel concrete did not harden with exclusion of carbon dioxide. The content of Anhydrite and Halite derives from the crushed salt, which was used for production of sorel concrete. The formation of 318-phase is induced by reaction of magnesium oxide and $MgCl_2$ solution during the hardening process.

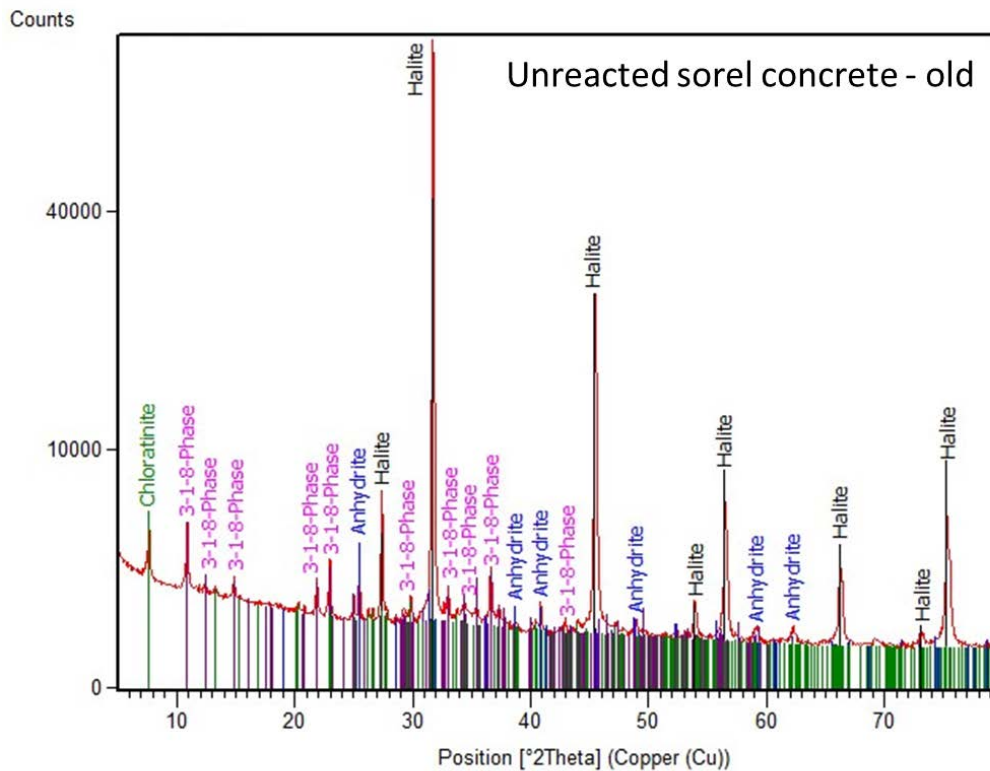


Fig. 3.4 Initial phase composition of unreacted sorel concrete – old

The new fabricated sorel concrete - A1 consists of the characteristic 318-phase, Anhydrite, Brucite and Halite (Fig. 3.5). Compared to the sorel concrete – old no Chloratinitite was formed caused by the exclusion of carbon dioxide during hardening process. The crushed salt, used for production of sorel concrete – A1, was investigated by X-ray-diffraction. It consists essentially of Halite and Anhydrite (CaSO_4).

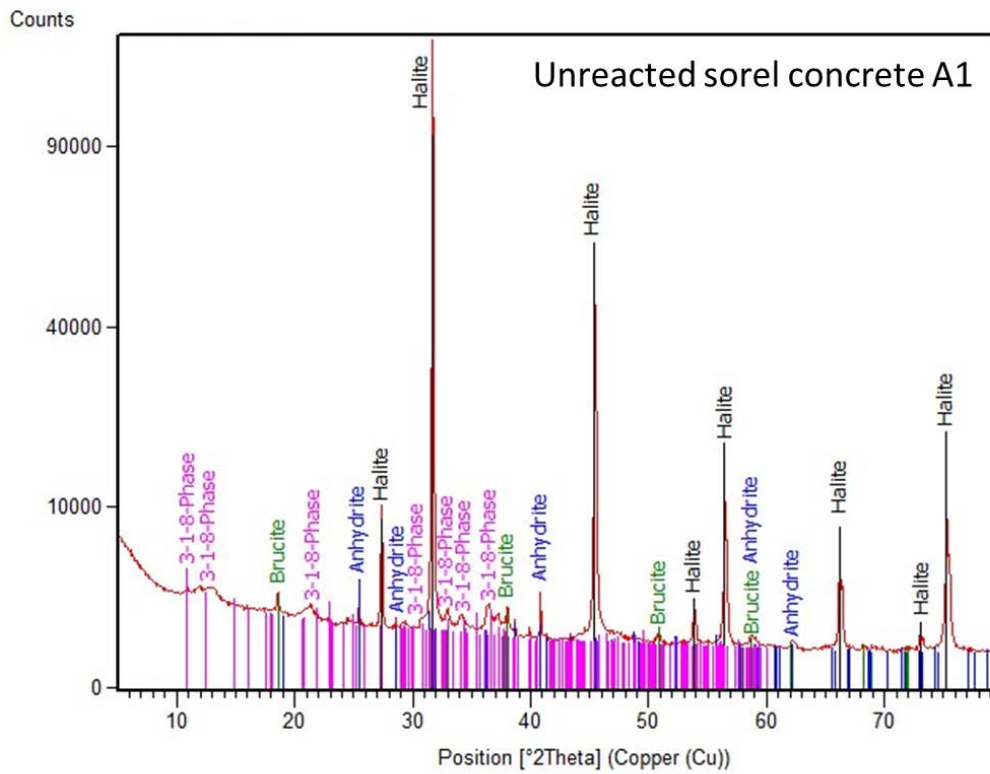


Fig. 3.5 Initial phase composition of unreacted sorel concrete – A1

X-ray-diffraction of unreacted salt concrete is shown in Fig. 3.6. It consists of Halite, Anhydrite, Portlandite and Friedels' salt ($3\text{CaO}\cdot\text{Al}_2\text{O}_3\cdot\text{CaCl}_2\cdot 10\text{H}_2\text{O}$).

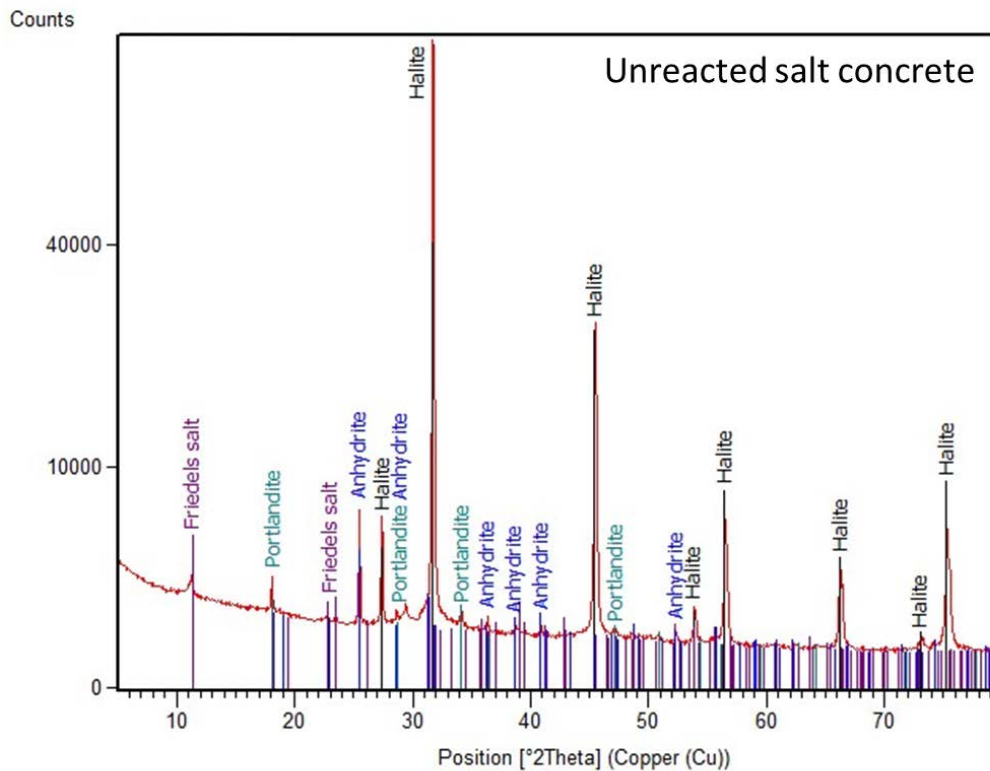


Fig. 3.6 Initial phase composition of unreacted salt concrete

3.4.2 Analysis of saline solutions

The production of a solution which is exactly in agreement with IP21 solution was not possible in the laboratory. The IP21 solution is very sensitive for temperature changes, which could not be excluded in laboratory. Furthermore, phase precipitation depends on very complex boundary conditions, which are not completely known. Hence, a “MgCl₂ solution” was used, which is very similar to the composition of IP21-solution. Compositions of the solutions are given in Tab. 3.4

Tab. 3.6 Composition of saturated NaCl solution, IP21-solution /MEY 2003a/ and MgCl₂ solution

	NaCl solution [mol/kg H ₂ O]	IP21-solution [mol/kg H ₂ O]	MgCl ₂ solution* [mol/kg H ₂ O]
Density [kg/m ³]	1200	1292	1290
p _{cH} [-]	6.75	-	7.15
Viscosity [Ns/m ²]	2.04·10 ⁻³	1.16·10 ⁻³	-
Temperature [°C]	25	25	25
Na ⁺	6.100	0.463	0.486
K ⁺	-	0.556	0.569
Mg ²⁺	-	4.250	4.362
Ca ²⁺	-	0.001	0.001
Cl ⁻	6.100	8.892	9.013
SO ₄ ²⁻	-	0.314	0.294
Saturated of	NaCl	Halite, Sylvite, Carnallite, Kainite, Polyhalite	

* Average values of produced MgCl₂ solutions in GRS laboratory

4 Laboratory investigations

4.1 Batch experiments

4.1.1 Setup of batch experiments

Batch experiments are very simple experiments for investigating the equilibration between solids and solutions. Solids and solutions are mixed in a defined ratio for reaction. The equilibration is monitored by the development of solid phase assemblage and solution composition. Aim of the batch experiments is to determine the duration necessary for an approximate equilibrium to be attained.

For reaction of salt concrete and sorel concrete with saline solution the ratio between solid and solution was chosen to be 1:3.

Additionally, it was checked, if tracers of caesium and lithium are sorbed on the solid material. Therefore, saline solutions were spiked with tracers and analysed with regard to its tracer concentration before the batch experiments. Batch experiments were performed with tracer spiked solution and analysed with regard to its tracer concentration in the seven samplings in addition to residual element analysis. Blind samples were analysed simultaneously.

Batch experiments were executed for four systems:

- Sorel concrete / NaCl solution
- Sorel concrete / MgCl₂ solution
- Salt concrete / NaCl solution
- Salt concrete / MgCl₂ solution

Concrete and saline solution were filled in PE-bottles at the beginning of experiments after PE-bottles were flushed with argon to prohibit carbonation of concrete. Afterwards, bottles were shaken by hand until concrete and solution were mixed. All PE-bottles were kept in an exsiccator, which was flushed with argon, to ascertain exclusion of CO₂. The PE-bottles were shaken by hand once a day.



Fig. 4.1 Preparation of batch experiments in PE-bottles (left) and storage of PE-vessels in exsiccator (right)

Solid and solutions samples were taken after 2, 4, 7, 9, 11 and 18 days during the mean experiment. Further samples were taken after 46, 158 and 552 days (systems with NaCl solution) respectively after 88, 200 and 510 days (systems with MgCl₂ solution). Sampling was executed in the glovebox for CO₂ elimination. Solid and solution were filled in a test tube and centrifuged for separation of solid and solution. Afterwards, solution was extracted by pipette and was analysed by ICP-OES, ICP-MS and titration. Additionally, ensity and pH was measured. The measured pH (= pH_{mes}) was converted into pc_H (negative decade logarithm of hydrogen ion concentration) because of the high ionic activity of high saline solutions.

$$pc_H = pH_{mes} - \Delta pH \quad \text{Equation 4.1}$$

ΔpH is calculated as function of concentration in saline solutions by density of solution and element concentrations of calcium, chloride, magnesium, potassium, sodium and sulphate based on /HAG 2014/. Background to this method is defined in appendix A 3 .

The solid samples were dried in vacuum in an exsiccator with silica gel. Solid phase composition was analysed by X-ray diffraction.

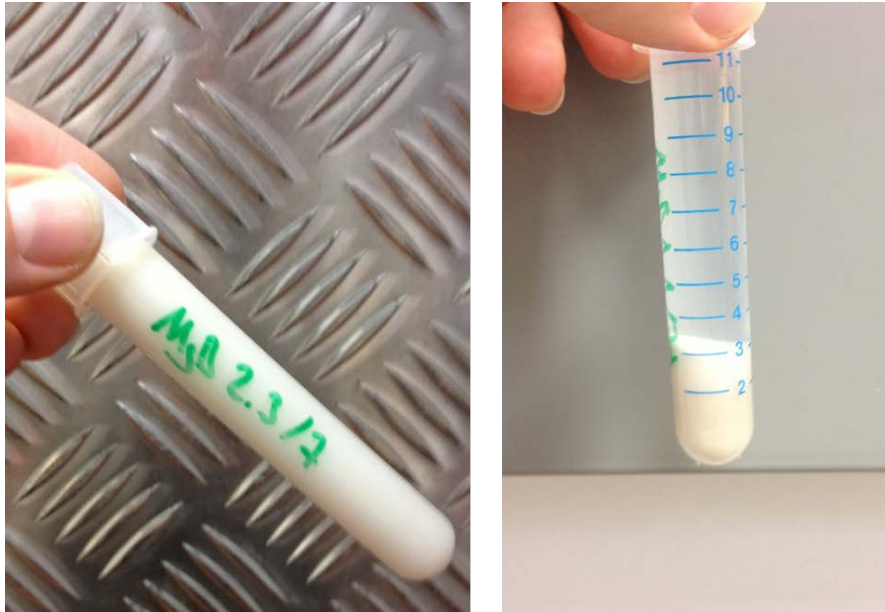


Fig. 4.2 Test tube with mixture of saline solution and concrete after sample drawing and before centrifugation (left) and sample after centrifugation with explicit separation of concrete and solution (right)

4.1.2 Laboratory results of batch experiments

Batch experiments aimed at determining the significant equilibration time between concrete and saline solution for following cascade experiments. In systems with sored concrete they were performed using the sored concrete – old. Results are shown below. Subsequent sections describe the change of solution and mineral phase composition in each system.

4.1.2.1 System sored concrete – old / NaCl solution

The typical 318-phases of sored concrete are not stable in contact with NaCl solution. The dissolution of 318-phase and Anhydrite could be detected by X-ray-diffraction of the reacted sored concrete – old. Both phases were completely dissolved after eleven days of reaction. Merely Halite was detectable by X-ray-diffraction anymore (Fig. 4.3). There were some reflection patterns in the reacted concrete whose positions were very similar to the position of 318-phase. But analysis using the Highscore software showed no agreement with 318-phase reference pattern. Probably, these visible reflexes result from less crystalline phases.

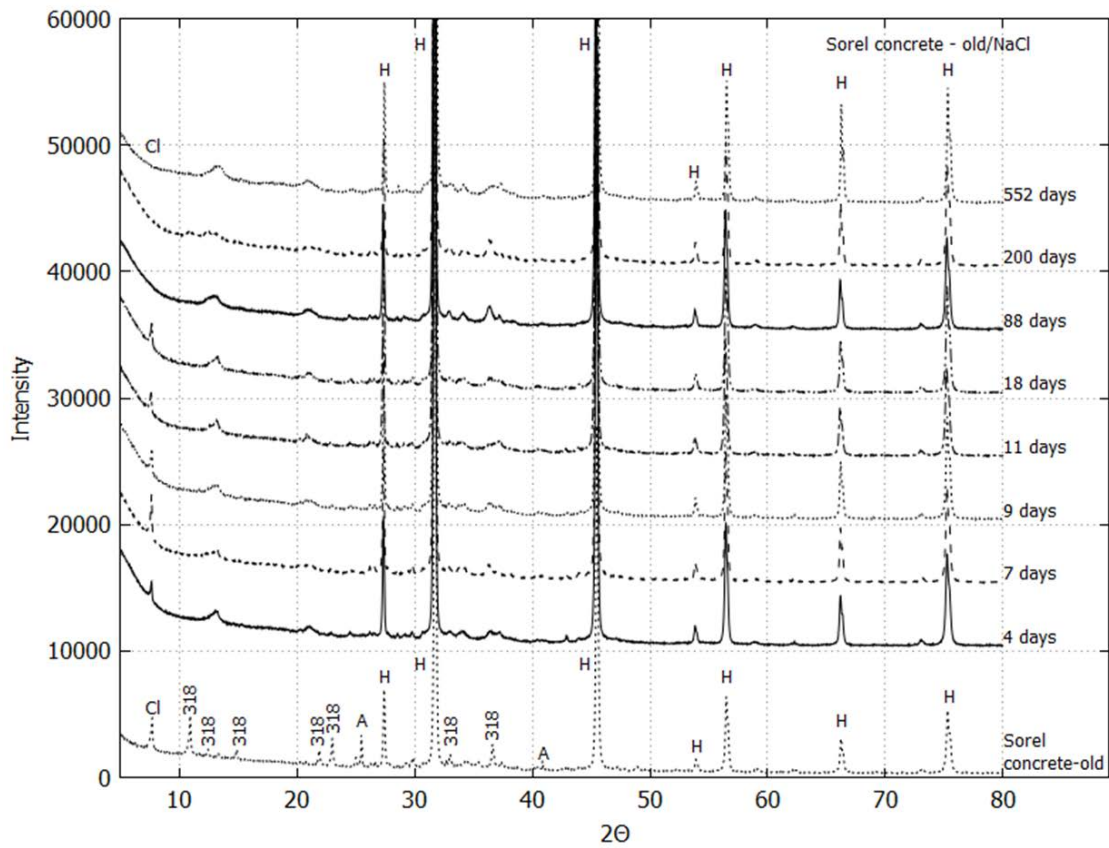


Fig. 4.3 X-ray-diffraction of sorel concrete – old after reaction with NaCl solution; A – Anhydrite, Cl – Chlorartinite, H – Halite, 318 – 318-phase

The sodium and chloride concentrations of initial NaCl solution were about 6.13 - 6.45 mol/kg H₂O. In batch experiments concentrations of sodium and chloride increased to 6.84 – 7.52 mol/kg H₂O within the first reaction period of two days (Fig. 4.4). This value was nearly constant up to 18 days, merely in one batch sodium and chloride concentrations had decreased to 5.92 – 6.00 mol/kg H₂O at this point of time. With ongoing equilibration time concentrations decreased in all batches down to values of about 4.79 – 5.44 mol/kg H₂O.

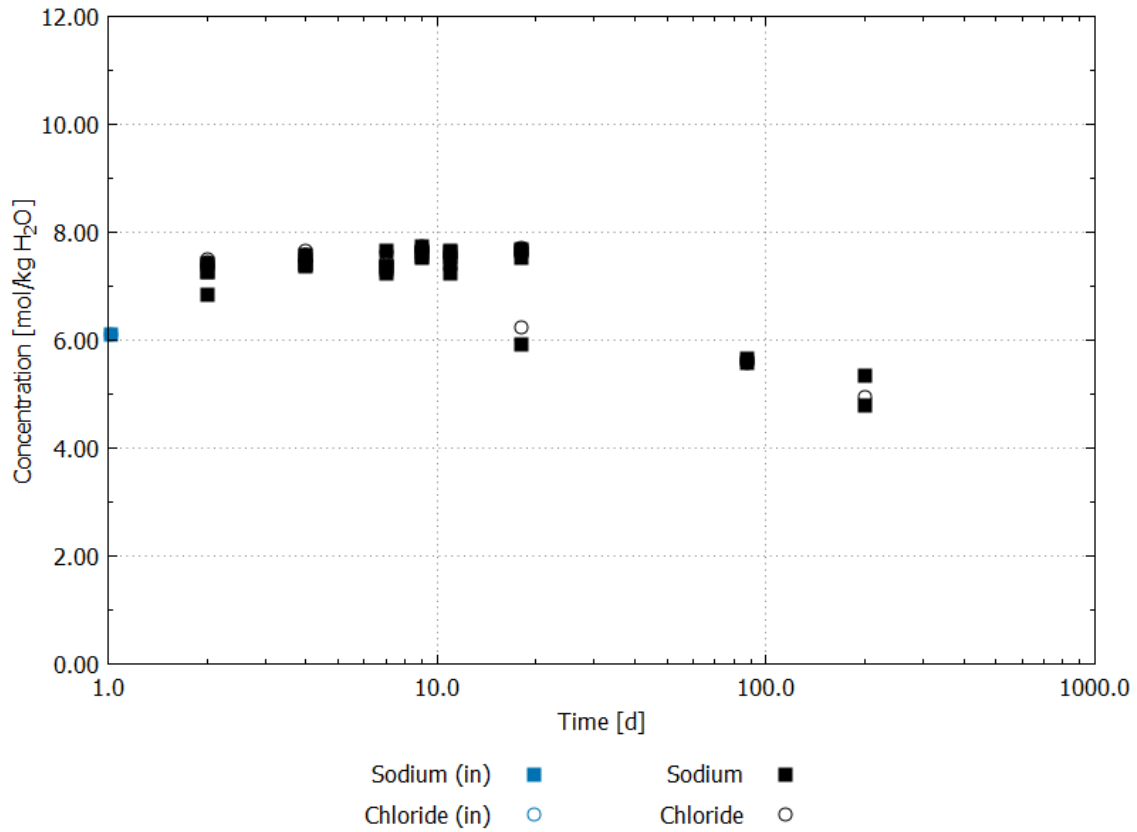


Fig. 4.4 Batch experiments in the system sorel concrete – old / NaCl solution: Development of chloride and sodium concentrations. Blue data points describe solution composition of initial NaCl solution

Concentrations of calcium increased not significantly within the first reaction period to 0.001 mol/kg H₂O, concentrations of potassium to 0.003 mol/kg H₂O (Fig. 4.5). Ongoing changes of calcium and potassium concentrations were not detected.

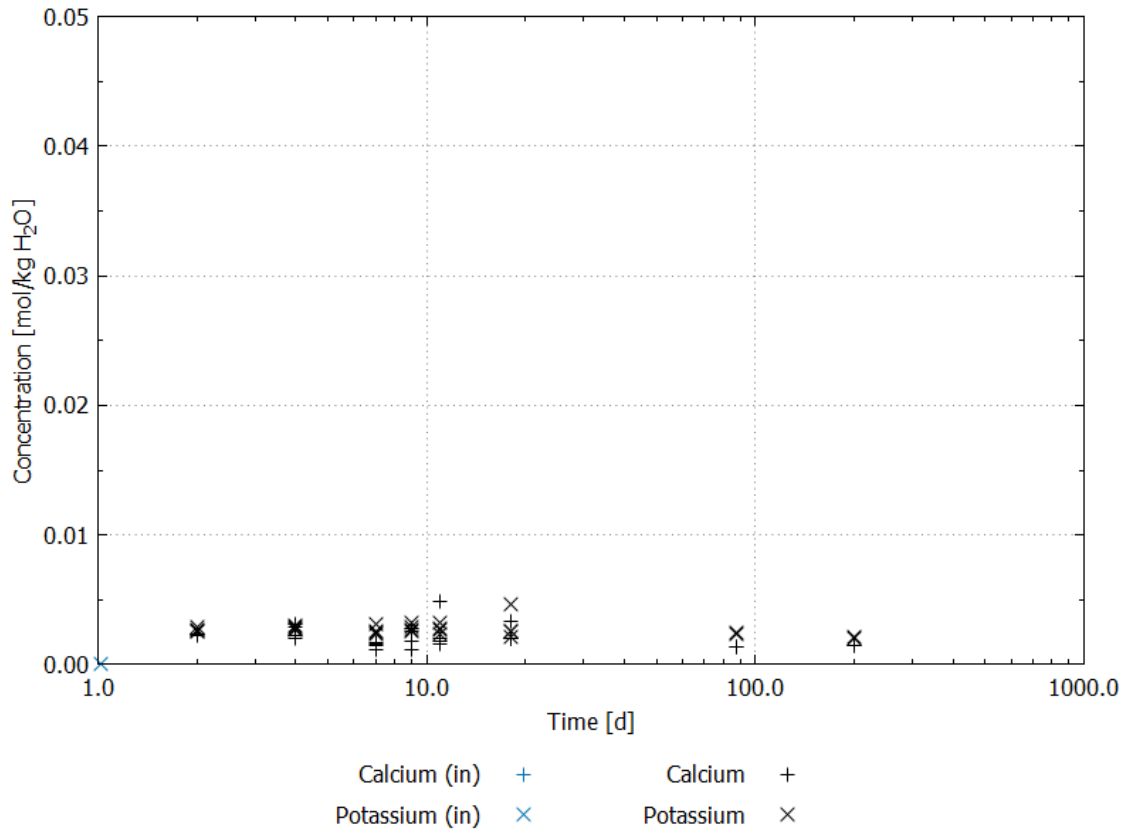


Fig. 4.5 Batch experiments in the system sorel concrete – old / NaCl solution: Development of calcium and potassium concentrations in the solution. Blue data points describe solution composition of initial NaCl solution

Magnesium concentrations increased to 0.12 mol/kg H₂O and sulphate concentrations to 0.07 – 0.09 mol/kg H₂O within a time period of 18 days (Fig. 4.6). The high deviation in concentration between singuer batches is noticeable, especially of magnesium. Magnesium and sulphate concentrations decreased further after 18 days. Sulphate concentrations were 0.03 – 0.06 mol/kg H₂O, magnesium concentrations 0.10 – 0.11 mol/kg H₂O at the end of batch experiment.

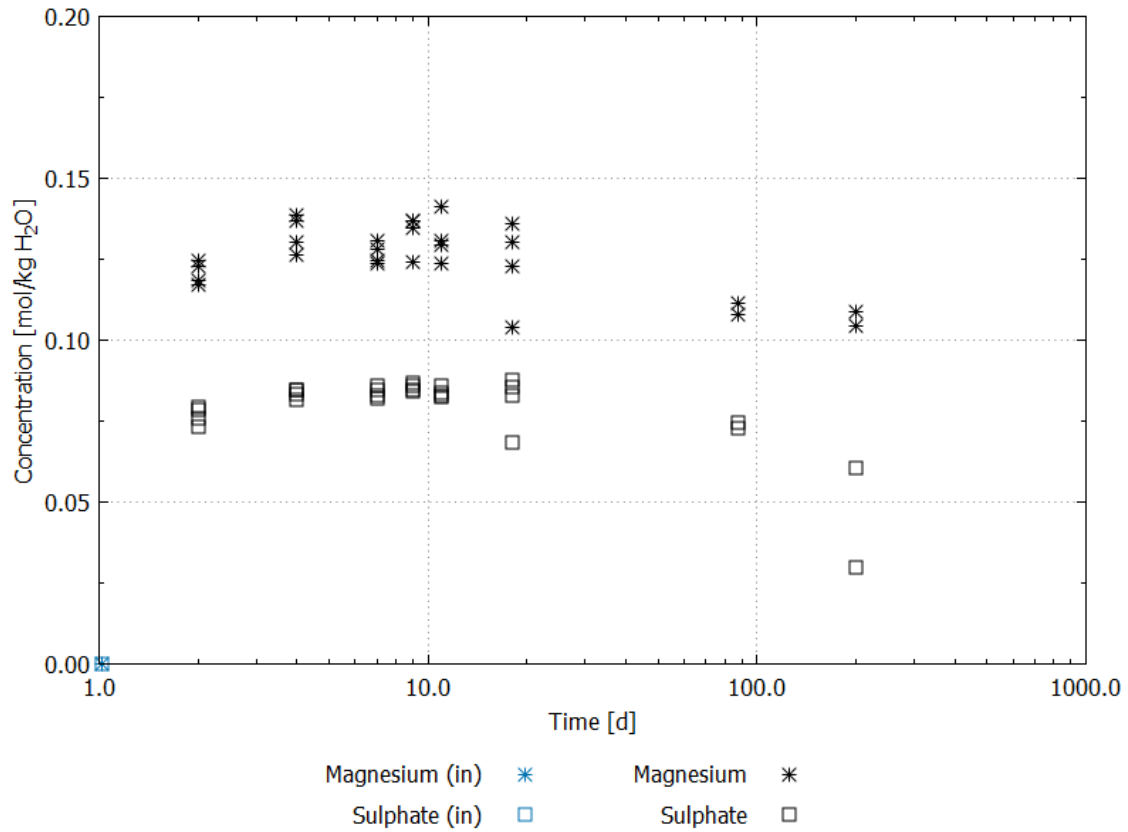


Fig. 4.6 Batch experiments in the system sorel concrete – old / NaCl solution: Development of magnesium and sulphate concentrations in the solution. Blue data points describe solution composition of initial NaCl solution

The p_{cH} increased in batch experiments from 6.75 in the initial solution to 10.03 - 10.18. Significant changes could not be detected with ongoing reaction time. Density changed not significantly in comparison with initial NaCl solution. It was 1.20 - 1.21 g/cm³ during total experimental time.

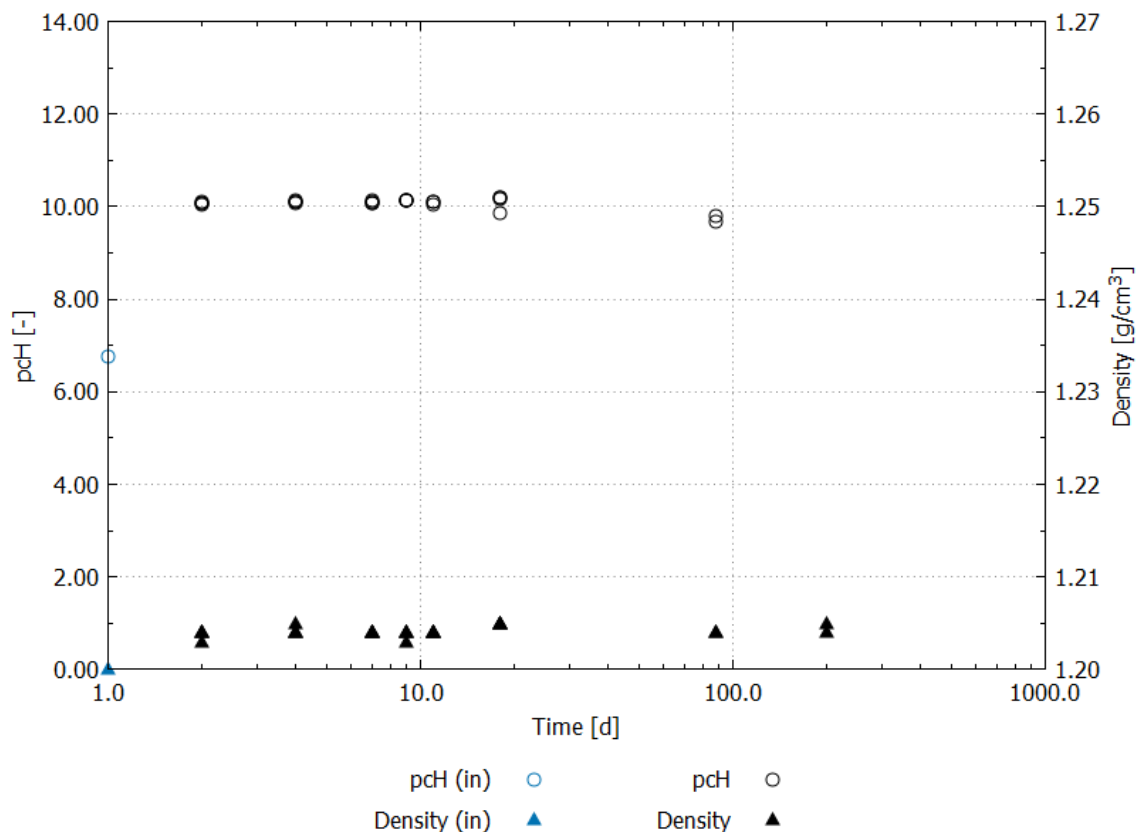


Fig. 4.7 Development of pc_H and density in the system sorel concrete – old / NaCl solution. Blue data points describe pc_H and density of initial NaCl solution

4.1.2.2 System sorel concrete – old / $MgCl_2$ solution

Analysis of powdered concrete showed that the characteristic and stabilizing 318-phase of the unreacted sorel concrete - old (Fig. 3.4) was stable in presence of $MgCl_2$ solution (Fig. 4.8). Halite and Anhydrite were also stable. The formation of Carnallite could be identified after two days of reaction. After four days Bischofite was also formed. Significant changes of phase composition based on X-ray-diffraction analysis were not detected in the further course of batch experiments.

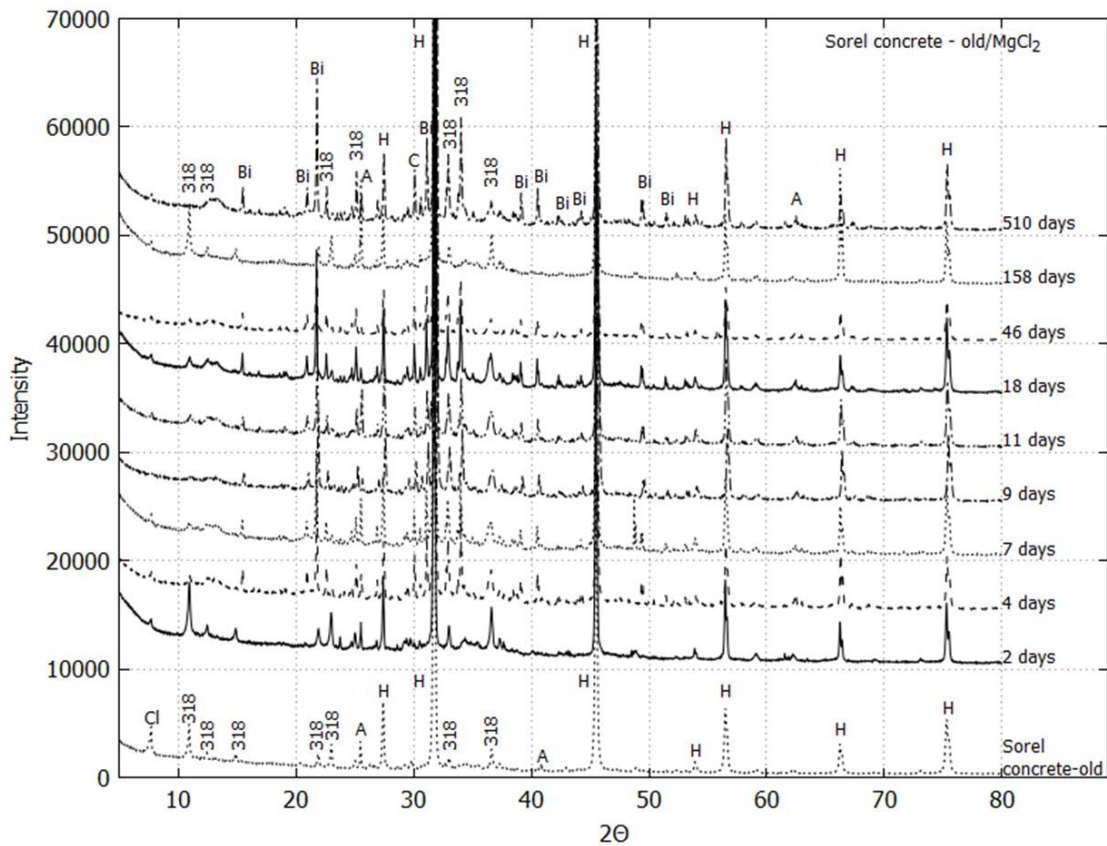


Fig. 4.8 X-ray-diffraction of sorel concrete – old after reaction with MgCl₂ solution; A – Anhydrite, Bi – Bischofite, C- Carnallite, Cl – Chlorartinite, H – Halite, 318 – 318-phase

Compared to the initial composition of the MgCl₂ solution (Tab. 3.6) an increase of chloride from 9.01 mol/kg H₂O to 11.02 – 11.16 mol/kg H₂O and of magnesium from 4.36 mol/kg H₂O to 5.31 – 5.36 mol/kg H₂O could be detected (Fig. 4.9). The concentrations did not change significantly within 18 days. Afterwards, both concentrations decreased to values near to initial concentrations.

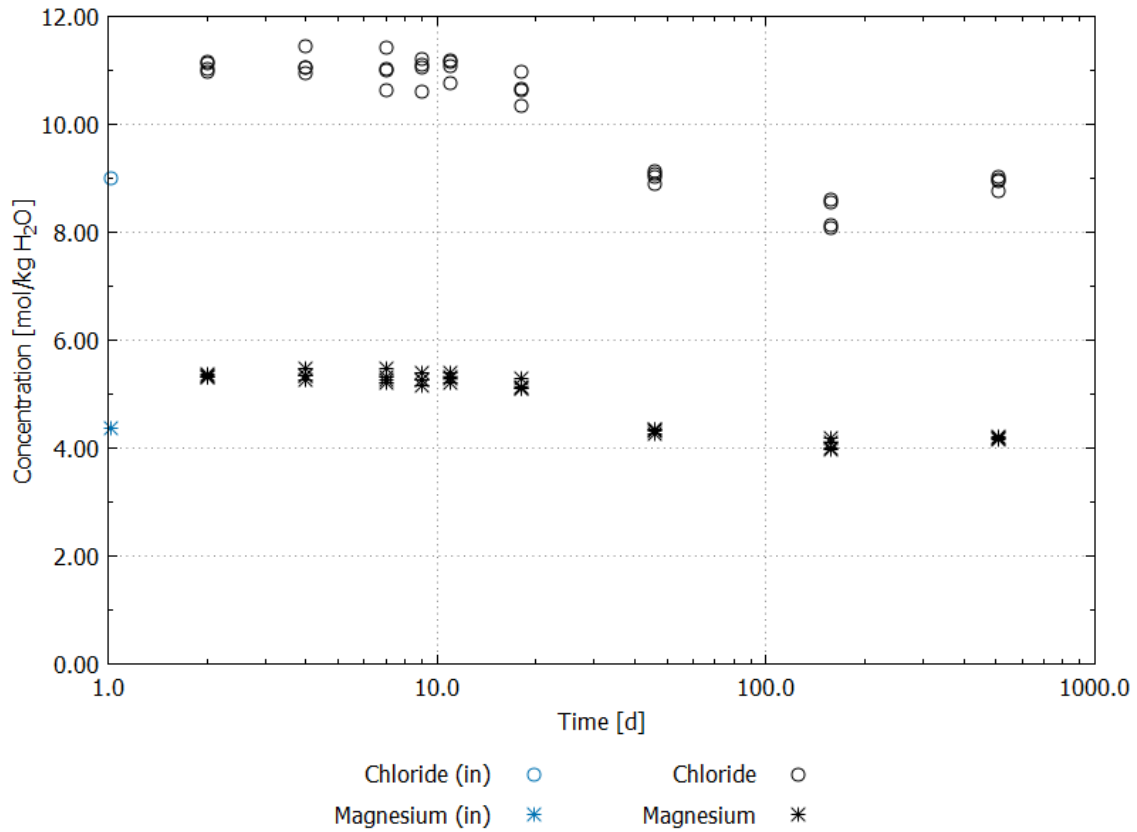


Fig. 4.9 Batch experiments in the system soresl concrete – old / MgCl₂ solution: Development of chloride and magnesium concentrations. Blue data points describe solution composition of initial MgCl₂ solution

Concentrations of sodium, calcium, potassium and sulphate showed no significant changes compared to the initial solution during the whole reaction time. But all these concentrations varied during the whole experiment without a clear trend. Sodium concentration of one batch deviated significantly from sodium concentrations of residual batches.

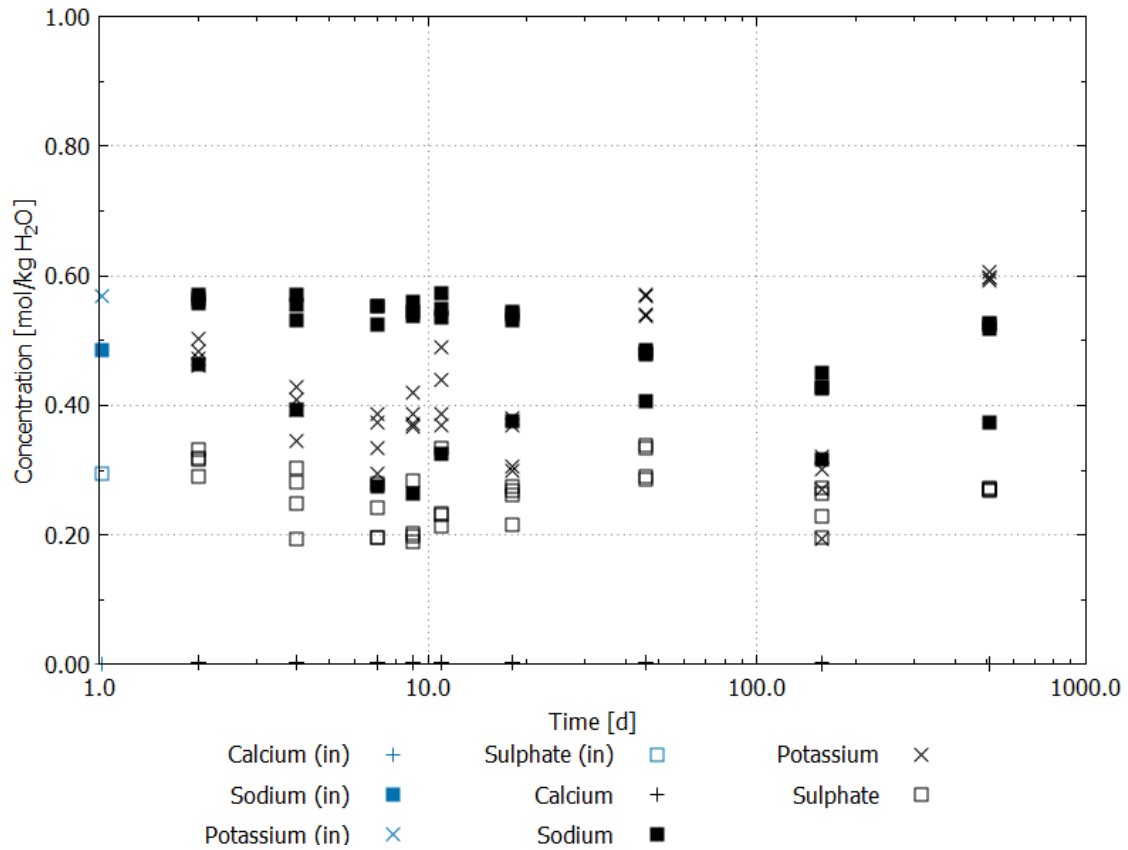


Fig. 4.10 Batch experiments in the system soresl concrete – old / MgCl₂ solution: Development of calcium, potassium, sodium and sulphate concentrations in the solution (below). Blue data points describe solution composition of initial MgCl₂ solution

The p_{cH} increased in comparison with the initial concentration from 6.75 to circa 9.56 – 9.58 in the beginning of experiments. During the ongoing reaction p_{cH} decreased to circa 8.90 – 8.93. The density showed no significant change in comparison to the initial solution. Density is about 1.29 g/cm³, but showed some scattering between the measurements (Fig. 4.11).

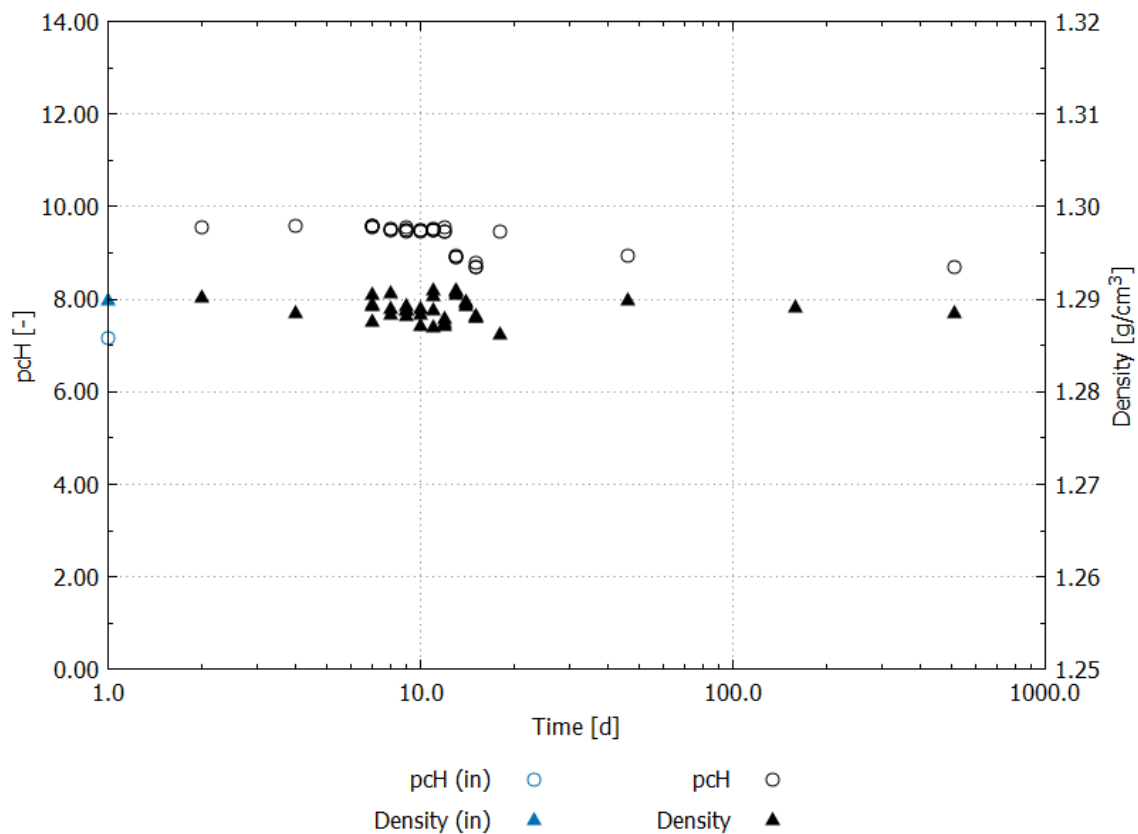


Fig. 4.11 Development of pc_H and density in the system sorel concrete – old / $MgCl_2$ solution. Blue data points describe pc_H and density of initial $MgCl_2$ solution

4.1.2.3 System salt concrete / NaCl solution

X-ray diffraction of the salt concrete showed that Anhydrite, Friedels' salt, Halite were still detectable after reaction in all samples. Portlandite was only detectable in single samples (Fig. 4.12).

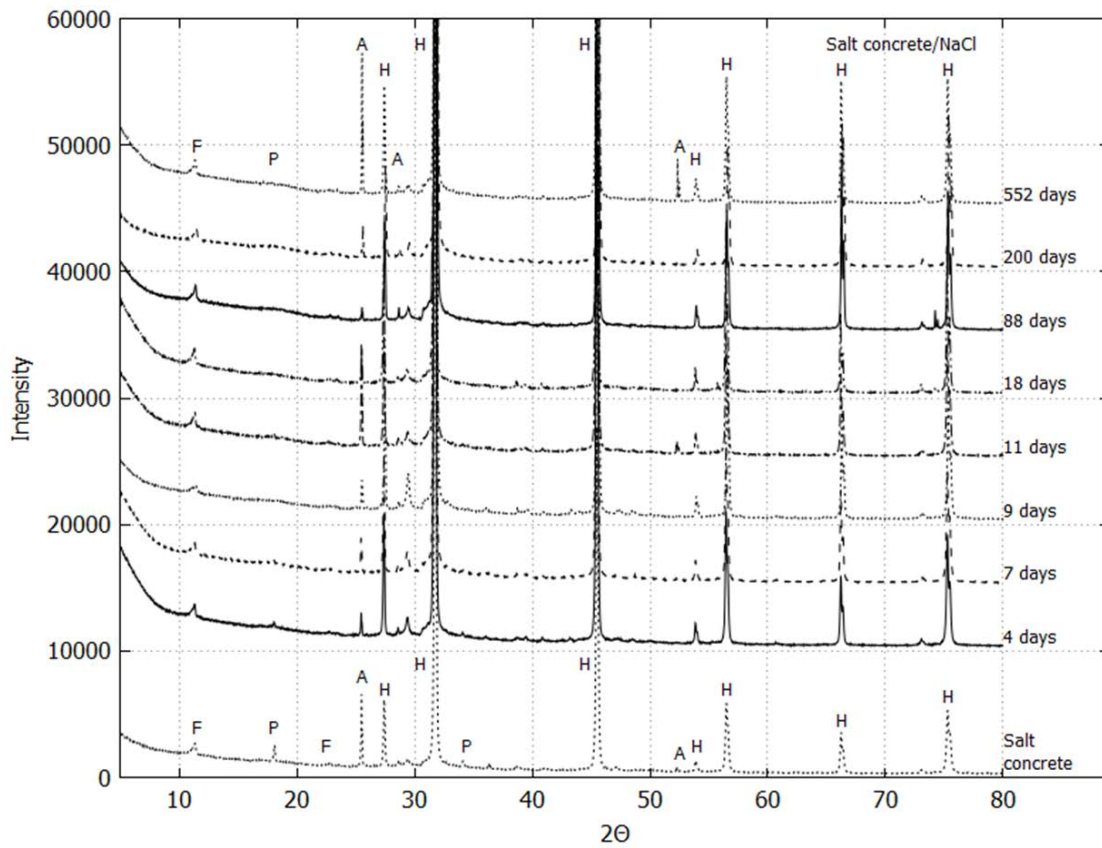


Fig. 4.12 X-ray-diffraction of salt concrete after reaction with NaCl solution; A – Anhydrite, F- Friedel's salt, H – Halite, P - Portlandite

Concentrations of sodium and chloride increased in comparison with the initial NaCl solution from 6.10 mol/kg H₂O to values between 6.84 mol/kg H₂O and 7.70 mol/kg H₂O. Especially, during measurements between seven to 18 days concentrations varied significantly between various approaches. After 18 days both concentrations decreased significantly. At 200 days concentrations were 4.79 mol/kg H₂O to 5.44 mol/kg H₂O, which was less than the initial concentration in NaCl solution.

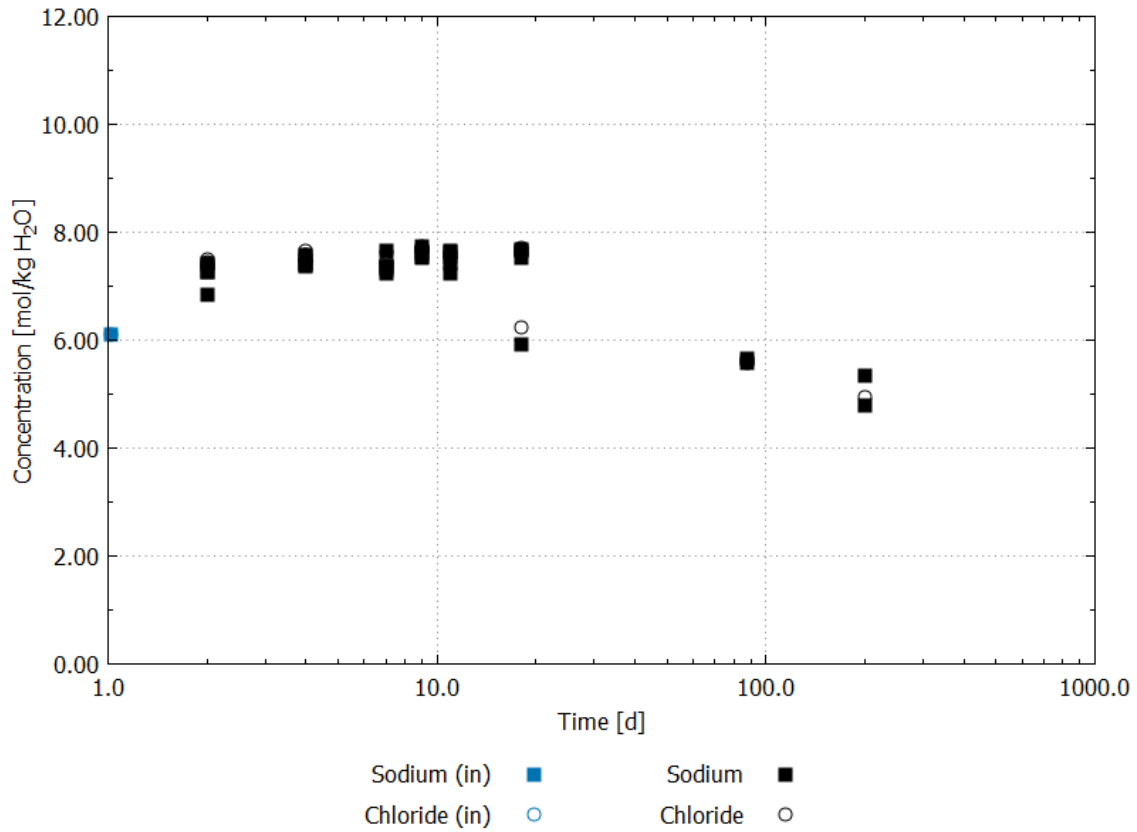


Fig. 4.13 Batch experiments in the system salt concrete / NaCl solution: Development of chloride and sodium concentrations. Blue data points describe solution composition of initial NaCl solution

Concentrations of calcium, potassium and sulphate increased in comparison to the initial solution. But all concentrations were very low (< 0.08 mol/kg H₂O) and showed no significant trend (Fig. 4.14). Concentration of magnesium was below detection limit during the whole experiment.

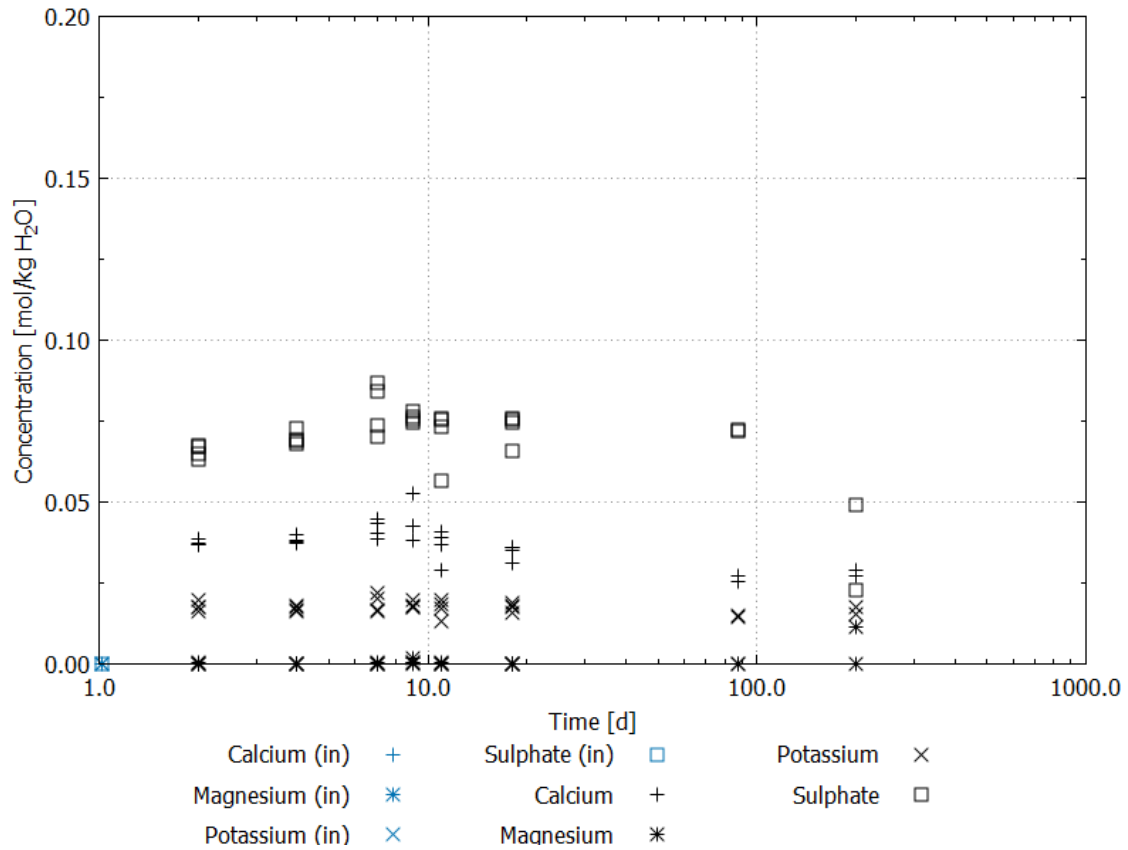


Fig. 4.14 Batch experiments in the system salt concrete / NaCl solution: Development of calcium, magnesium, potassium and sulphate concentrations. Blue data points describe solution composition of initial NaCl solution

Aluminium and silicon concentrations were also analysed. Concentration of aluminium was 0.000 – 0.001 mol/kg H₂O and concentrations of silicon 0.001 – 0.006 mol/kg H₂O. Concentrations of both elements decreased with ongoing reaction time below the limit of quantification.

The p_{cH} increased in experiments in comparison with initial solution from 6.75 to circa 13.04 – 13.44. The p_{cH} changed not significantly in time period of batch experiments. The density changed not significantly in comparison with the initial NaCl solution. It was about 1.21 g/cm³ during total reaction time.

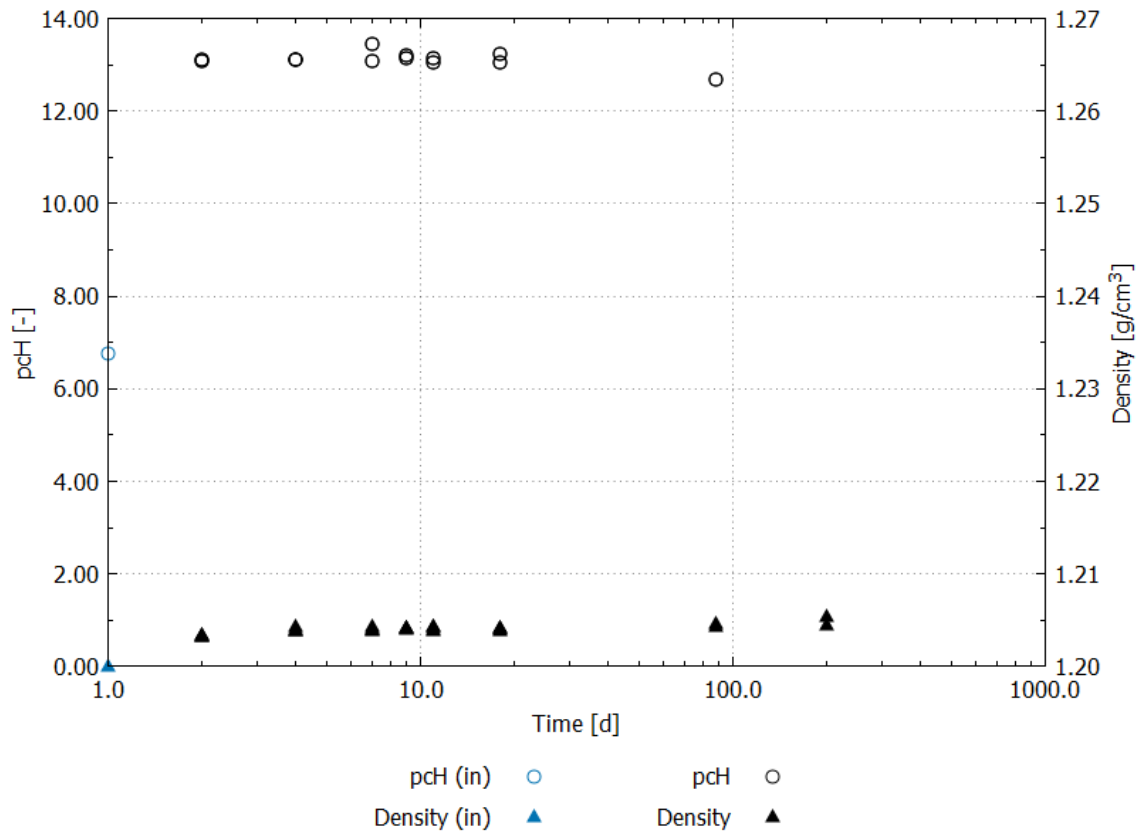


Fig. 4.15 Development of pH and density in the system salt concrete / NaCl solution. Blue data points describe pH and density of initial NaCl solution

4.1.2.4 System salt concrete / MgCl₂ solution

Batch experiments in the system salt concrete / MgCl₂ solution showed that this system is thermodynamically instable. Portlandite and Friedel's salt dissolved in presence of MgCl₂ solution. Bischofite and Carnallite were formed after 11 days of reaction (Fig. 4.16). Formation of Gypsum could be detected by X-ray diffraction after 18 days of reaction. Further significant changes in its phase composition could not be identified during the following reaction time up to 510 days.

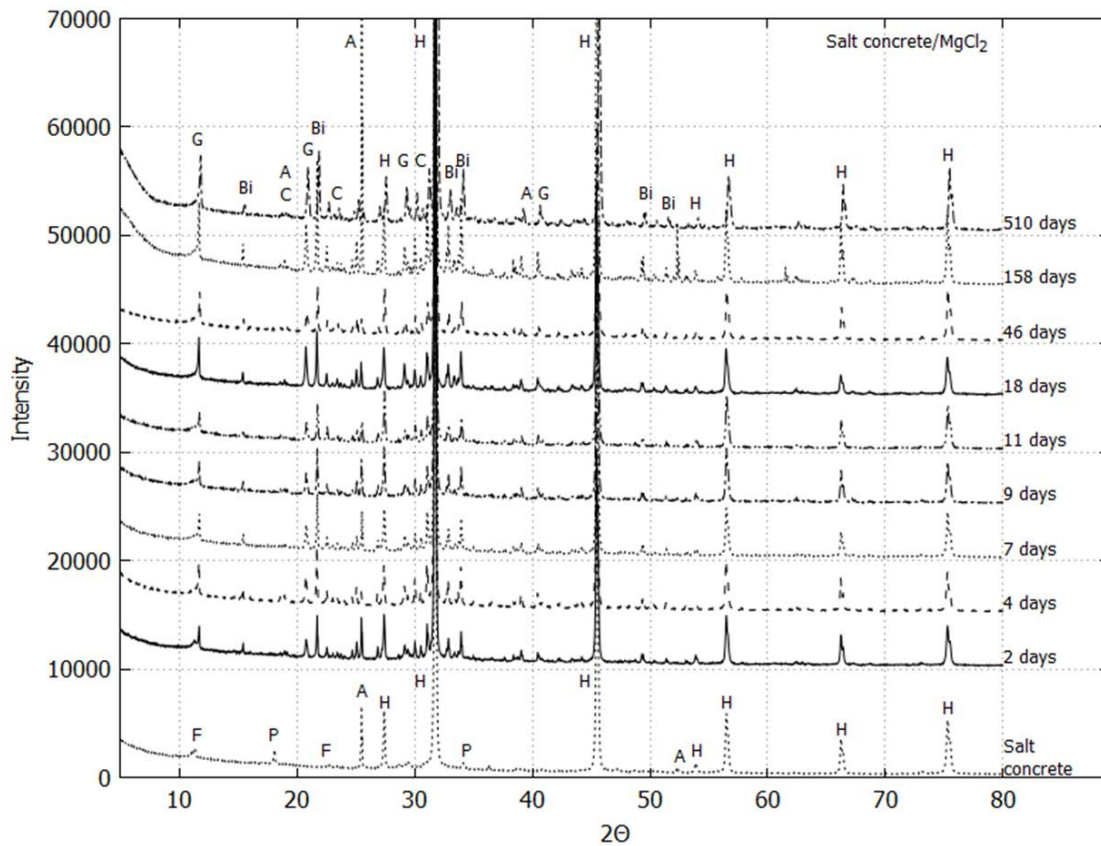


Fig. 4.16 X-ray diffraction of salt concrete after reaction with $MgCl_2$ solution; A – Anhydrite, Bi – Bischofite, C – Carnallite, F– Friedels’ salt, G – Gypsum, H – Halite, P – Portlandite.

Note: Diffraction pattern of Gypsum around $11.0 2\theta$ is displaced about $0.3 2\theta$ to higher angles in comparison with Friedels’ salt

Both magnesium and chloride concentrations increased in batch experiments (Fig. 4.17). Chloride concentrations increased from 6.13 - 6.45 mol/kg H_2O to 10.80 - 11.25 mol/kg H_2O within four days. Concentrations decreased to 8.24 - 9.20 mol/kg H_2O after 18 days of equilibration. Magnesium concentration increased from 4.36 mol/kg H_2O to values between 4.87 - 5.10 mol/kg H_2O within four days and decreased again after seven days of equilibration. Concentration decreased to values < 4.0 mol/kg H_2O . After 46 days concentration was nearly constant in following measurements. Sodium concentration showed no significant changes in comparison to initial concentration. Its concentration was 0.40 - 0.67 mol/kg H_2O .

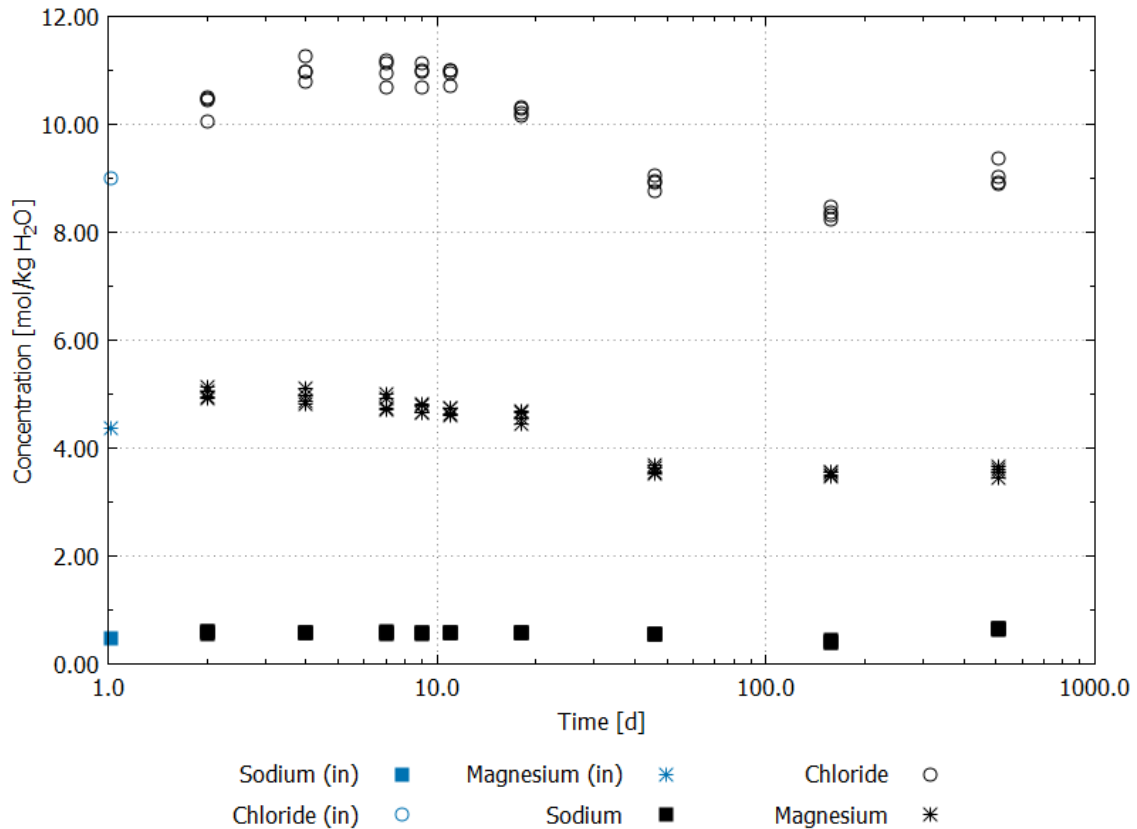


Fig. 4.17 Batch experiments in the system salt concrete / $MgCl_2$ solution: Development of chloride, sodium and magnesium concentrations. Blue data points describe solution composition of initial NaCl solution

Concentrations of potassium decreased within two days, but concentrations deviate from 0.39 - 0.54 mol/kg H_2O between the batches at this point of time (Fig. 4.18). In following analysis concentrations deviated less and decreased in comparison to the initial $MgCl_2$ solution. Concentrations was 0.37 - 0.39 mol/kg H_2O . After 18 days of equilibration potassium concentrations increased again but changed significantly from 0.56 mol/kg H_2O at 46 days and 510 days to 0.17 - 0.21 mol/kg H_2O at 158 days. Sulphate concentrations decreased from 0.29 mol/kg H_2O in initial solution to 0.024 - 0.03 mol/kg H_2O after seven days of reaction. There were no significant changes in further process. Calcium concentration increased from 0.001 mol/kg H_2O in initial solution to 0.33 - 0.35 mol/kg H_2O after 18 days. Concentrations were 0.27 - 0.33 mol/kg H_2O in the following equilibration time.

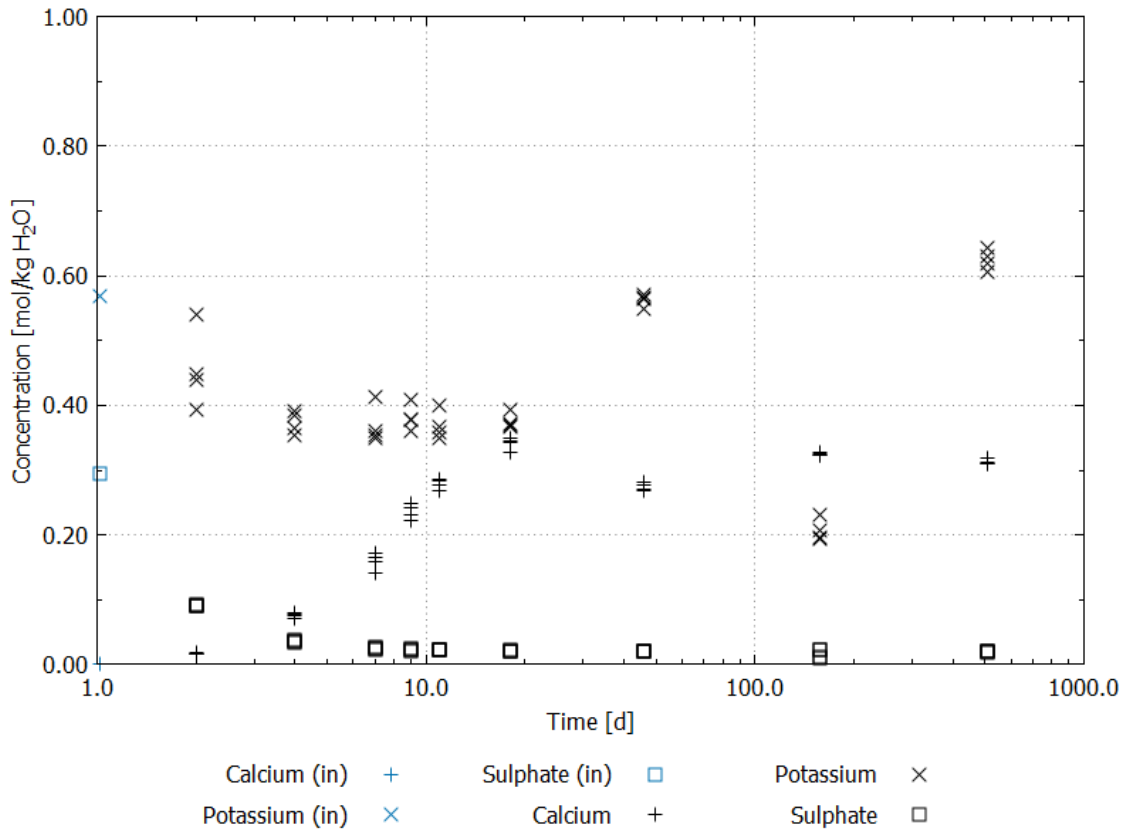


Fig. 4.18 Batch experiments in the system salt concrete / $MgCl_2$ solution: Development calcium, potassium and sulphate concentrations in the solution. Blue data points describe solution composition of initial NaCl solution

Aluminium and silicon concentrations were analysed too. But concentrations were below the detection limit.

The p_{cH} increased during batch experiment from 7.15 in the initial solution to circa 9.62 – 9.75 in first step of reaction. With ongoing reaction time p_{cH} decreased again to 7.90 - 8.00. Density decreased from 1.29 g/cm^3 in the initial solution to approximately 1.27 g/cm^3 . The spread of density is higher between seven days and 18 days of reaction in comparison to remaining measurements.

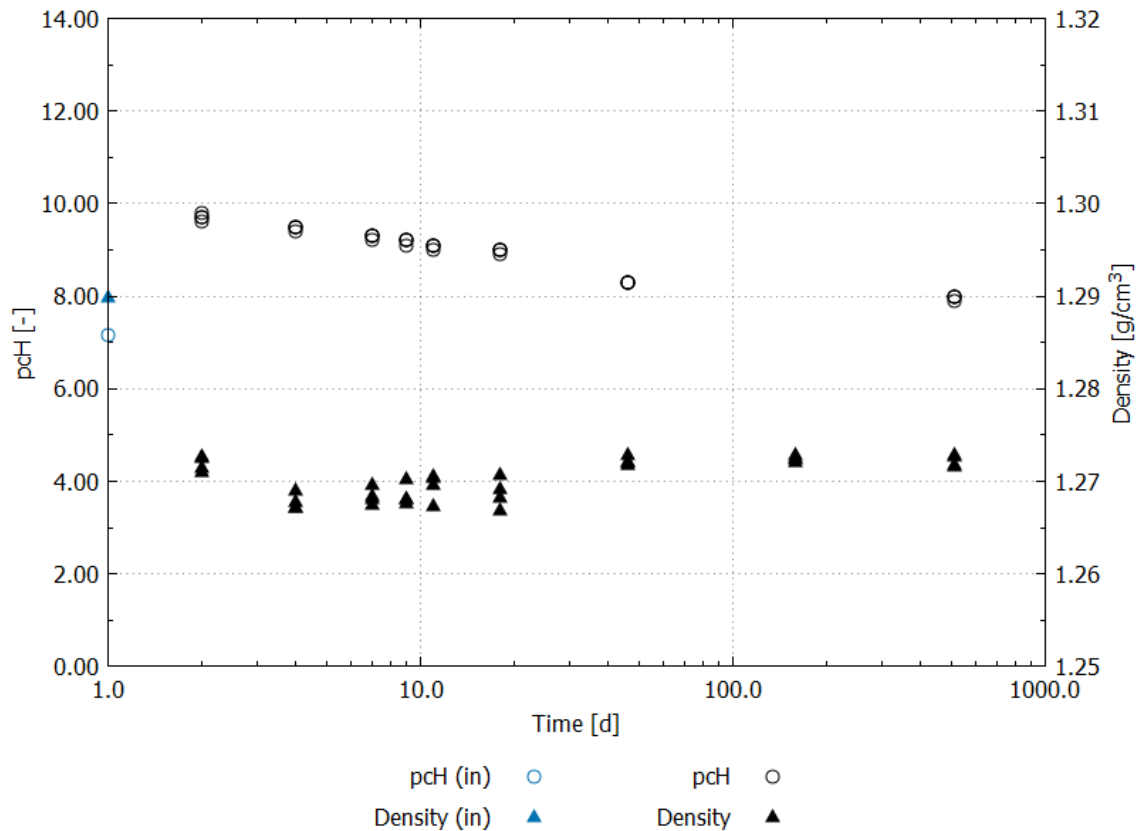


Fig. 4.19 Development of pc_H and density in the system salt concrete / $MgCl_2$ solution. Blue data points describe pc_H and density of initial $MgCl_2$ solution

4.1.2.5 Results of tracer tests

Both caesium and lithium concentrations were constant during whole reaction time in the blind sample of NaCl solution (Fig. 4.20). (Caesium concentrations in blind sample were equal to concentrations in NaCl solution with salt concrete; Hence, data points of blind sample are overlaid by salt concrete sample.) Lithium concentrations in NaCl solution, which were exposed to salt concrete, was a bit lower than in the blind sample (lithium concentration of salt concrete samples is overlaid by lithium concentration of the sored concrete sample at 88 days), but showed no significant decrease of concentration during reaction time. Caesium concentrations in NaCl solution with salt concrete decreased a little within reaction period. Concentration of caesium and lithium in NaCl solution with sored concrete changed not significantly with time.

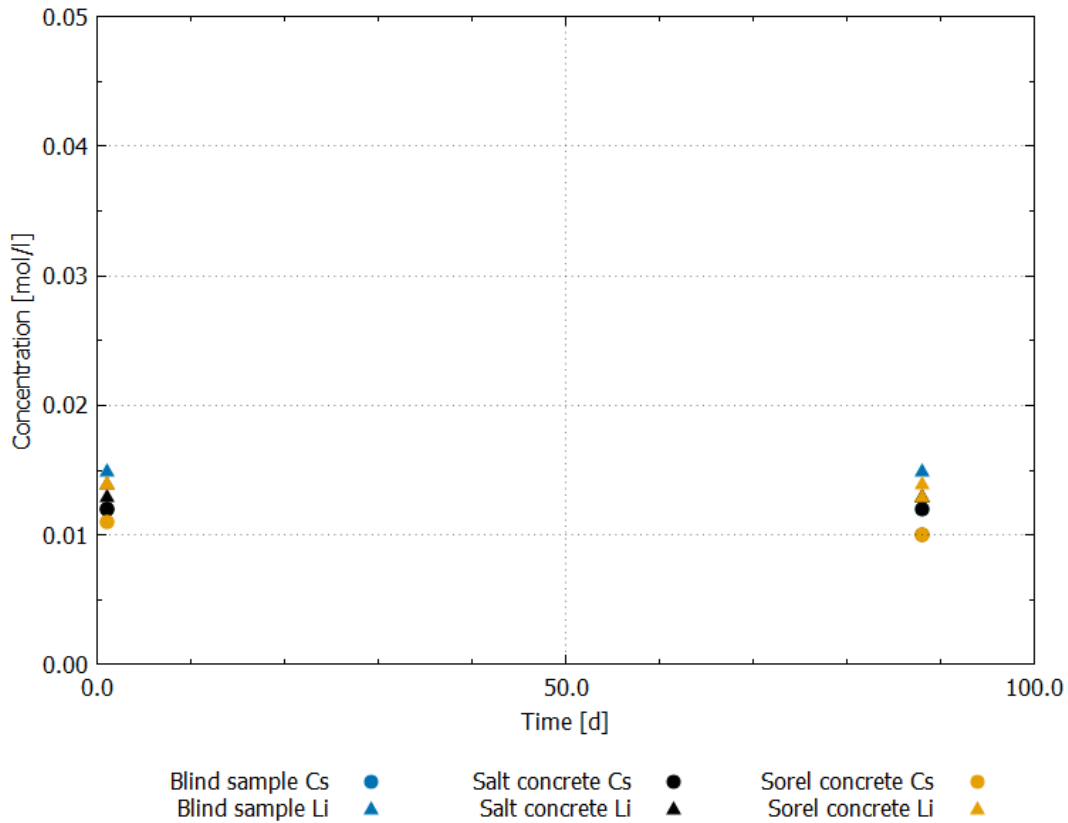


Fig. 4.20 Results of tracer test in NaCl solution. Blind sample of caesium is equal to caesium concentration in salt concrete samples in the beginning and end of tracer test

Caesium and lithium concentrations in the blind sample of $MgCl_2$ solution were constant with time (Lithium concentration of blind sample is overlaid by caesium concentration of $MgCl_2$ solution with salt concrete). Caesium concentrations changed not significantly during the tracer test in both solutions. (Caesium concentration in $MgCl_2$ solution with salt concrete and sorel concrete were identically, hence, data points are overlaid in Fig. 4.20.) Lithium concentrations finally decreased in both systems: in $MgCl_2$ solution with salt concrete concentration decreased about nearly 50 %, with sorel concrete about 25 %.

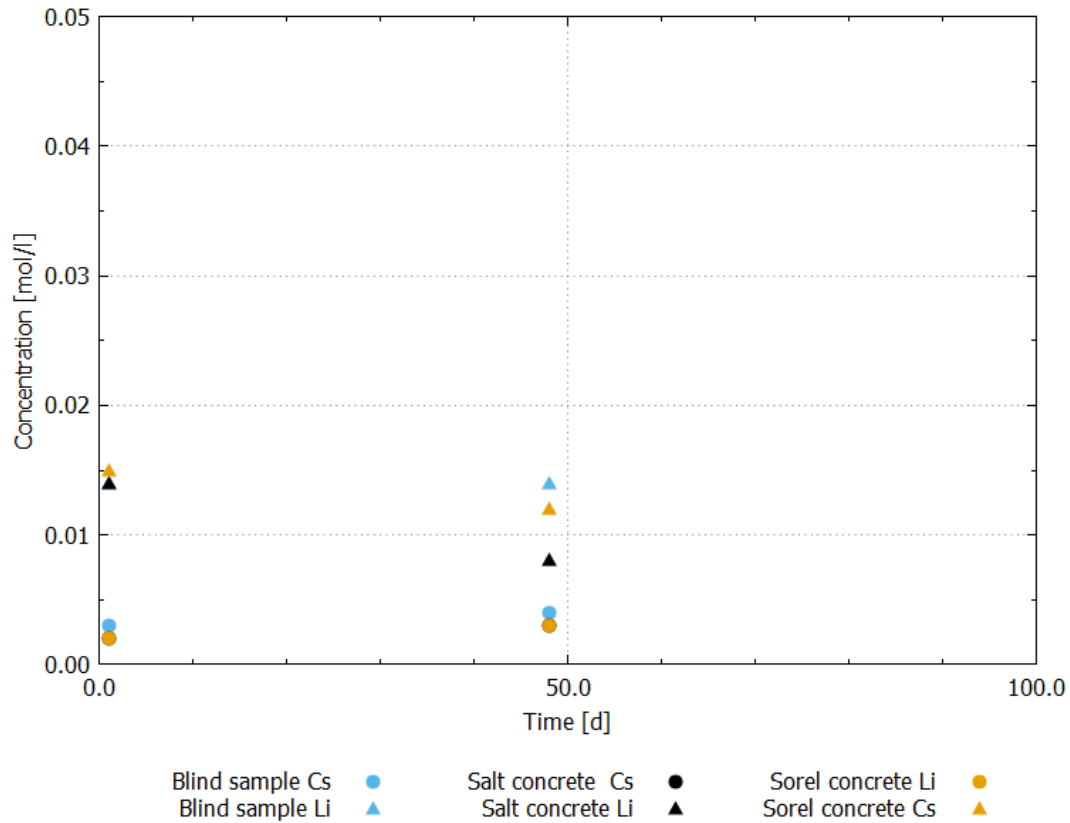


Fig. 4.21 Results of tracer test in $MgCl_2$ solution. Blind sample of lithium is equal to lithium concentration in $NaCl$ solution with salt concrete sample in the beginning of tracer test. Additionally, lithium concentrations of $NaCl$ solution with salt and sorel concrete are identically

4.1.3 Interpretation and discussion

The execution of batch experiments aimed primarily at determining the equilibration times in the various systems for following cascade experiments. In earlier cascade experiments prior to this work, equilibration time was uniformly set to four days. Following, the reasonable assumption that for the overwhelming majority of dissolution- and precipitation reactions in rock salt, sorel concrete and salt concrete instantaneous equilibrium cannot be expected, the execution of pilot tests seemed mandatory, and should remain so in the future.

4.1.3.1 Thermodynamic stability in the system sorel concrete – old / NaCl solution

Based on experiences of /FRE 2015/ and /KRA 2008/ corrosion of sorel concrete by dissolution of the 318-phases in contact with NaCl solution was expected because the concentration of Mg^{2+} in solution was ≤ 0.5 mol/kg H_2O . X-ray diffraction showed that 318-phase and Anhydrite were dissolved within two days in batch experiments. But comparison of diffraction pattern showed additionally that phase composition changed within eleven days. However, most diffraction pattern could not be identified (Fig. 4.3). Probably, phases were formed with small degree of crystallisation or the percentage of total solid phases was too less for explicit determination by X-ray diffraction. After eleven days there were no significant changes in the diffraction pattern anymore.

Composition of solution changed most significantly within the first two days of reaction and showed an increase of calcium, chloride, magnesium, potassium, sodium and sulphate in the solution (Fig. 4.4 to Fig. 4.6). Increase of magnesium and sulphate was most significant. Increase of magnesium content can be attributed to dissolution of 318-phase, which is further supported by X-ray diffraction. Calcium and sulphate increase may be induced by the dissolution of Anhydrite, the increase of potassium by dissolution of Polyhalite. Polyhalite can be present in small amounts in the rock salt, which was used for the production of sorel concrete - old /GIE 1994/. But due to the proportion of 1:1 of calcium and sulphate in Anhydrite, an equal amount of concentrations would be expected. Although, Polyhalite contains calcium and sulphate in proportion 1:2 the dissolution of Portlandite cannot explain the higher sulphate content in the solution: the proportion of potassium to calcium in Polyhalite is 1:1. Experimental results showed that the increase of potassium is very low. Hence, the increase of calcium is very low too. Accordingly, increase of sulphate should be two times higher than of calcium and potassium. However, in experiments sulphate concentrations were by a factor 80 higher than calcium. Therefore the deviation of calcium and sulphate concentrations cannot be explained by the dissolution of Polyhalite. Another explanation for the deviation between calcium and sulphate concentrations is the simultaneous formation of other calcium containing phases, which are currently unknown. However, solution composition kept changing up to the end of batch experiments. Thus, even if according to XRD the phase assemblage remains constant, precipitation and dissolution processes continue to proceed.

Saturation indices in the reacted solution from batch experiments were calculated using PHREEQC (Fig. 5.1). Calculation of SI confirmed that solution was undersaturated with respect to 318-phase, confirming its assumed dissolution. Dissolution of Anhydrite is not reflected in the calculation, as solution was supersaturated with respect to Anhydrite for the first 18 days and became undersaturated only afterwards. Hence, dissolution of Anhydrite in experiments should be expected only after 18 days. It is conceivable, that Anhydrite lost its high crystalline structure in the beginning of batch experiment and could not be identified in X-ray-diffraction anymore although Anhydrite was still present in solid composition.

On the other hand, with regard to the concurrent increase of calcium and sulphate concentration, results can be explained with a partial dissolution of anhydrite.

Calculated saturation of the reacted solution showed also supersaturation with respect to Dansite. Verification of this phase in the solid composition was negative, which can be explained with retarded precipitation. Against the formation of Dansite argues the high sulphate content, because solution analysis of batch experiments showed higher increase of sulphate concentration than of calcium. By formation of Dansite more sulphate than calcium would be consumed. The thermodynamic stability of Halite was confirmed by the supersaturation of the reacted solution.

The simultaneous decrease of all SI after 18 days is affected by the significant decrease of the sulphate concentration in the reacted solution after 200 days (Fig. 4.6 and Fig. 5.1). An explicit reason for the decrease of sulphate concentration in comparison to solution compositions before could not be detected. Certainly, these samples had to be stored for a couple of weeks before analysis. Probably, analysis of these samples represents not the composition of the solution by sampling. For this reason the development of solution composition and SI seems to be not representative at experimental times of 200 days.

Dissolution of solid phases of sored concrete was confirmed by the increase of density after two days of reaction (Fig. 4.7). Also p_{cH} increased within two days, which can be associated with changes in solution composition. But p_{cH} did not change significantly in further reaction time. Consequently, it can be assumed that most significant processes occurred in the beginning of batch experiments although solution composition changed

up to end of batch experiments or a phase was formed in the beginning which buffered the p_{C_H} .

Finally, the equilibration time per cascade was set to eleven days based on changes in the solid phase. Much longer equilibration times had not been practicable and most significant corrosion processes seemed to be completed in the beginning of batch experiments.

4.1.3.2 Thermodynamic stability in the system sorel concrete – old / MgCl_2 solution

/FRE 2015/ and /KRA 2008/ specify that the stabilising 318-phases of sorel concrete are thermodynamically stable if concentration of Mg^{2+} in solution is ≥ 0.5 mol/kg H_2O . The Mg^{2+} content is 4.36 mol/kg H_2O in the used MgCl_2 solution. Hence, a corrosion of sorel concrete was not expected.

The results of X-ray diffraction showed that the initial phase composition of Anhydrite, Brucite, Halite and 318-phase was stable in contact with MgCl_2 solution (Fig. 4.8). In addition, the formation of Bischofite and Carnallite was detected. In investigations of /FRE 2015/ the formation of Bischofite was also observed when MgCl_2 solution was saturated with respect to NaCl. Based on the solution composition of Tab. 3.6 saturation with NaCl of the used MgCl_2 solution is expected.

Development of solution composition showed no significant trend and confirmed results from X-ray-diffraction (Fig. 4.9 and Fig. 4.10). Hence, significant corrosion of sorel concrete induced by MgCl_2 solution is not expected.

Consideration of calculated SI of the reacted solution from experiments confirmed that Anhydrite, Halite and the 318-phase were supersaturated and consequently thermodynamically stable in the system sorel concrete – old / MgCl_2 solution (Fig. 5.2). Saturation with respect to Halite also confirmed that formation of Bischofite could be expected according to /FRE 2015/. Calculated SI showed additionally that Bischofite and Carnallite were supersaturated and may precipitate consequently. Hence, formation of both phases is consistent with respect to solution composition. Additionally, brucite, Kainite, Kieserite, Loewite ($\text{Na}_{12}\text{Mg}_7(\text{SO}_4)_{13} \cdot 15\text{H}_2\text{O}$), Polyhalite and Sylvite were supersaturated during the complete batch experiment. The phases

Bloedite ($\text{Na}_2\text{Mg}(\text{SO}_4)_2 \cdot 4\text{H}_2\text{O}$), Epsomite, Gypsum, Hexahydrate, Sylvite, and Glauberite were temporarily saturated. But detection of these phases in solid phase by X-ray-diffraction was not possible. Probably, diffraction pattern of those phases were overlaid with other phases or the structure of those phases was not sufficient crystalline for detection using X-ray-diffraction.

Most significant was the increase of p_{cH} in the solution at the beginning of experiment (Fig. 4.11). Probably, this increase was induced by the reaction of unreacted magnesium oxide from the sorel concrete with MgCl_2 solution.

Based on these results, the system sorel concrete / MgCl_2 solution was not further investigated in geochemical experiments because of the thermodynamic stability of this system. However, further investigations were performed with regard to the advective and diffusive transport in sorel concrete.

4.1.3.3 Thermodynamic stability in the system salt concrete / NaCl solution

The available salt concrete for laboratory experiments was produced with saturated NaCl solution (chapter 3.2). Based on this fact it was assumed that salt concrete will be thermodynamically stable in saturated NaCl solutions. The X-ray diffraction analysis of reacted salt concrete of batch experiments confirmed this assumption because within the time period of up to 550 days no changes in solid phase composition could be detected (Fig. 4.12). Anhydrite, Friedels' salt and Halite were stable during the complete experimental time. Portlandite was only detectable in some of the solid samples without consistent pattern. Probably, the content of Portlandite was too low to be detectable by X-ray diffraction.

In solution a small increase of calcium, potassium and sulphate concentrations was measured and simultaneously a small increase of the density (Fig. 4.13 and Fig. 4.14). This indicated the partial dissolution of mineral phases from the powdered salt concrete, which also results in an increase of density. But the concentrations of the elements were less and showed no further increase in solution. Because the mineral phase composition of salt concrete remained unchanged within the experimental time, it is concluded that significant corrosion did not occur. This hypothesis is supported by /KRA 2008/, who described salt concrete as stable for corrosion in NaCl solutions.

Calculated SI of the reacted solution confirmed that Anhydrite and Halite were thermodynamically stable in this system (Fig. 5.3). In addition Gypsum, Glauberite and Pentasalt ($K_2Ca_5(SO_4)_6 \cdot H_2O$) were supersaturated in the reacted solution up to eleven days. But formation of those phases was not detected in the solid phase composition of batch experiments. This can again be attributed to minor masses of new phases formed, which were not detectable by X-ray-diffraction. Friedels' salt and Portlandite were not supersaturated, as well as the CSH phases, which should be included in salt concrete. Undersaturation of Portlandite confirmed results of X-ray diffraction because Portlandite was only detectable in a part of the samples without regularity as mentioned in the beginning of this chapter. SI of Friedels' salt and CSH phases were not able to be calculated, because both include aluminium and silicon, respectively and those elements were below the quantification limit in experiments.

The assumed dissolution of Portlandite is consistent with increase of the p_{cH} in the saline solution from 6.75 to circa 13.0, which may be induced by the increase of Portlandite content in the NaCl solution (Fig. 4.15). Portlandite is primarily responsible for the high pH of concretes, which is typically between 12.0 and 13.0 /BIC 1968/. The calculated p_{cH} of 13.0 corresponds to measured pH of circa 11.8 in the analysed solution.

Based on results of solid and solution analysis, the system salt concrete / NaCl solution was not further investigated in geochemical experiments because both composition of solid phases and solution showed no significant changes in experimental time.

4.1.3.4 Thermodynamic stability in the system salt concrete / $MgCl_2$ solution

From further investigations of /MEY 2003a/ is known, that salt concrete corrodes in presence of $MgCl_2$ solution. Batch experiments in this work verify these investigations, but aimed at considering the equilibration time. Hence, development of mineral phase and solution composition was analysed for longer time periods. Results confirmed that equilibration time of 2.5 to 4 days, assumed before in /MEY 2003a/, was not sufficient. Dissolution of Friedels' salt and Portlandite was indeed detectable within two days, but formation of new phases, such as Bischofite, Carnallite and Gypsum needed time periods up to 18 days until they was detectable by X-ray-diffraction (Fig. 4.16). Probably, phases formed earlier in experiments but the degree of crystallization was to low for detection with X-ray-diffraction in the beginning. Formation of further phases

could not be detected within the next 550 days. But based on the increase of reflex intensity of present phases it may be concluded that the degree of crystallization increased with reaction time.

Also the development of solution composition confirmed that equilibration time is longer than assumed in earlier investigations (Fig. 4.17 and Fig. 4.18). Based on the low pH of circa 5.0 of the initial MgCl_2 solution, firstly Portlandite and afterwards CSH-phases dissolved because these phases are thermodynamically unstable in neutral and acidic milieus (chapter 3.2.1). Consequently, calcium concentration increased. It can be assumed that Brucite formed simultaneously which explains the increase of pH to 7.0 in the beginning of batch experiments. Based on the small decrease of magnesium concentrations, neo-formation of Brucite is assumed to be low. Part of dissolved calcium reacted with sulphate of the initial solution to form Gypsum and potassium was consumed by the formation of Carnallite.

Calculation of SI from the reacted solution confirmed the stability of Anhydrite and Halite (Fig. 5.4). It also shows that the solution was supersaturated with respect to Bischofite, Carnallite and Gypsum. Hence, formation of these phases is thermodynamically possible, but may be retarded due to reaction kinetics. Portlandite was not supersaturated. Consequently, dissolution of Portlandite is thermodynamically possible. Furthermore, supersaturation with respect to Brucite, Pentasalt, Polyhalite and 318-phase was calculated. Kainite, Kieserite and Sylvite were temporarily supersaturated. But in X-ray diffraction only Anhydrite, Bischofite, Carnallite, Friedels' salt, Gypsum, Halite and Portlandite were detectable. Hence, it is hypothesized that accessory phases, which were supersaturated, were formed, but degree of crystallization was not sufficient for detection by X-ray diffraction. SI of Friedels' salt was not able to calculate, because it contains aluminium and aluminium was below the quantification limit in experiments.

The development of density and p_{cH} also confirmed longer equilibration times (Fig. 4.19). Constant density was measured after 46 days and p_{cH} decreased even up to 510 days. The continuous decrease of p_{cH} from 10 to 8 indicated a progressive process of equilibration. But equilibration times of more than 15 days could not be realized in this work. In consideration of solid and solution analysis it may be assumed, that the most relevant precipitation- and dissolution processes are finished within this term. Based on calculated SI of the reacted solution it was assumed that Gypsum was

also formed within this time period and an equilibration time of 15 days would be sufficient for an investigation of the reaction path.

4.1.3.5 Applicability of tracers caesium and lithium in the various systems with sores and salt concrete

Tracer test showed that caesium and lithium were not sorbed in systems with NaCl solution. In systems with MgCl₂ solution caesium was not sorbed too but lithium was sorbed significantly. Hence, the through-diffusion experiments with NaCl solution spiked with caesium and lithium and MgCl₂ spiked with caesium should be conducted without difficulties. In through-diffusion experiments with MgCl₂ and lithium it seemed to be useful that lithium and concrete will be in equilibrium before: when the maximum mass of lithium is sorbed by the concrete continuing lithium from the tracer spiked solution will diffuse through the concrete without. Based on this knowledge both the tracer spiked solution at the bottom and the non-spiked solution at the top of the diffusion cell were circulated until a break-through of tracers was measured. After break-through of tracer a stationary flux of tracers was expected and the cumulated mass of tracer could be calculated from tracer concentrations in the various samples (4.2.2).

4.2 Cascade experiments

4.2.1 Setup of cascade experiments

The cascade experiment is a succession of batch experiments. Cascade experiments aim at the investigation of the chemical reaction path between solid and solution. The principle of cascade experiments is shown in Fig. 4.22.

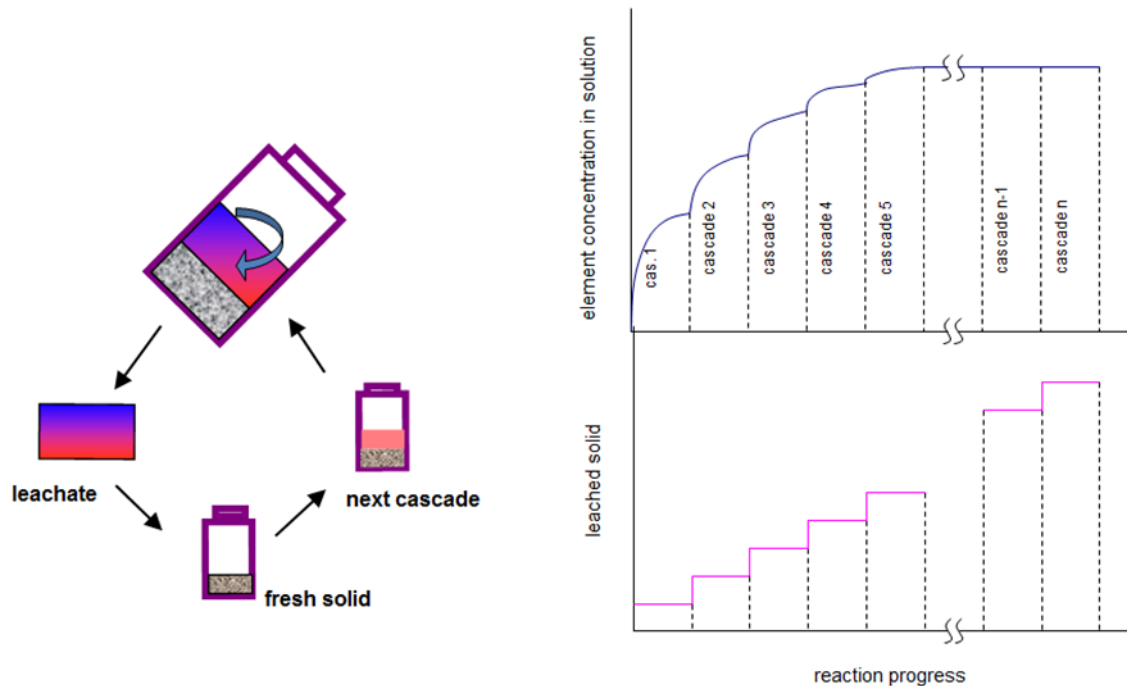


Fig. 4.22 Test procedure of the cascade experiment /HER 1996/

Defined masses of powdered concrete and saline solution were mixed in a pressure vessel in ratio 1:3. Afterwards, concrete and solution were shaken in an over-head shaker during the whole reaction time. The reaction time per cascade was based on results of batch experiments. Saline solution and concrete were separated in the end of each cascade by pressure filtration. New powdered concrete was exposed to the reacted solution in the defined ratio of 1:3. This procedure was repeated until no supernatant solution was left. In this way, the mass of concrete accumulates with that the saline solution has equilibrated. This results in an increase of solid solution ratio (SSR). Concrete and solutions samples were taken in the end of each cascade.

Cascade experiments are designed to characterize the maximum possible impact an aqueous solution might have on the evolution of mineral phase composition in the solid upon contact with aqueous solution in a minimum equilibration time. Thus, in comparison to the chemical reactivity of solid samples with aqueous solutions, this type of experiment tends to exaggerate the chemical turn-over. Hence, the real reactivity of solids can be expected to be much smaller due to the smaller active surface in contact with solution /JAN 2011/.

Laboratory investigations

Cascade experiments were only performed in the thermodynamically instable systems sored concrete / NaCl solution and salt concrete / MgCl_2 solution based on results of batch experiments.

Generally, the following boundary conditions have to be considered in cascade experiments:

- Grain size of concrete
- Composition of solution
- Ratio between solid and solution per cascade: 1:3
- Temperature: $25\text{ °C} \pm 1\text{ °C}$
- Revolutions per minute: 8

Cores of salt and sored concrete were first broken by a jaw breaker and afterwards ground by a ball mill (3 big and 2 small balls, period of mall: 30 minutes with 240 rotations per minute, interval: 5 minutes, counter-rotating). Sample preparation at identical conditions aims at receiving reproducible particle size distribution among all experiments.



Fig. 4.23 Execution of cascade experiment in laboratory: pressure vessels in overhead shaker (left) and separation of reacted solution from concrete at the end of cascade (right)

Finally, the phase composition of concrete was analysed by X-ray-diffraction and solutions were analysed with regard to its composition of calcium, chloride, magnesium, potassium, sodium, and sulphate (salt and sored concrete) so as aluminium and silicon (salt concrete), density and pH. The pH (= pH_{mes}) was converted into pC_H analogue to batch experiments (appendix A 3).

4.2.2 Laboratory results of cascade experiments

4.2.2.1 System sored concrete – A1 / NaCl solution

Cascade experiment in the system sored concrete – A1 / NaCl solution was performed in three batches simultaneously. The equilibration time per cascade was fixed to eleven days based on batch experiments. Experiment was performed using the new produced sored concrete – A1. Tab. 4.1 presents the exact equilibration times per cascade and temperature during the experiment.

Tab. 4.1 Reaction time per cascade and temperature during cascade experiments in the system sored concrete – A1 / NaCl solution

Cascade	Reaction time	Temperature
	[days] Vessel 1, 2 + 3	[°C] Vessel 1, 2 + 3
1	12	24.6
2	11	25.4
3	11	25.3
4	13	25.1
5	17	24.4
6	13	24.3
7	12	24.4

Results from X-ray-diffraction analysis are presented in Fig. 4.24. X-ray-diagram below shows the phase composition of the initial sored concrete – A1. Upper X-ray diagrams show phase composition in the end of all cascades. A general trend of phase formation or dissolution could not be identified. All phases of the unreacted sored concrete – A1 (Anhydrite, Brucite, Halite and 318-phase) could be also identified in each cascade.

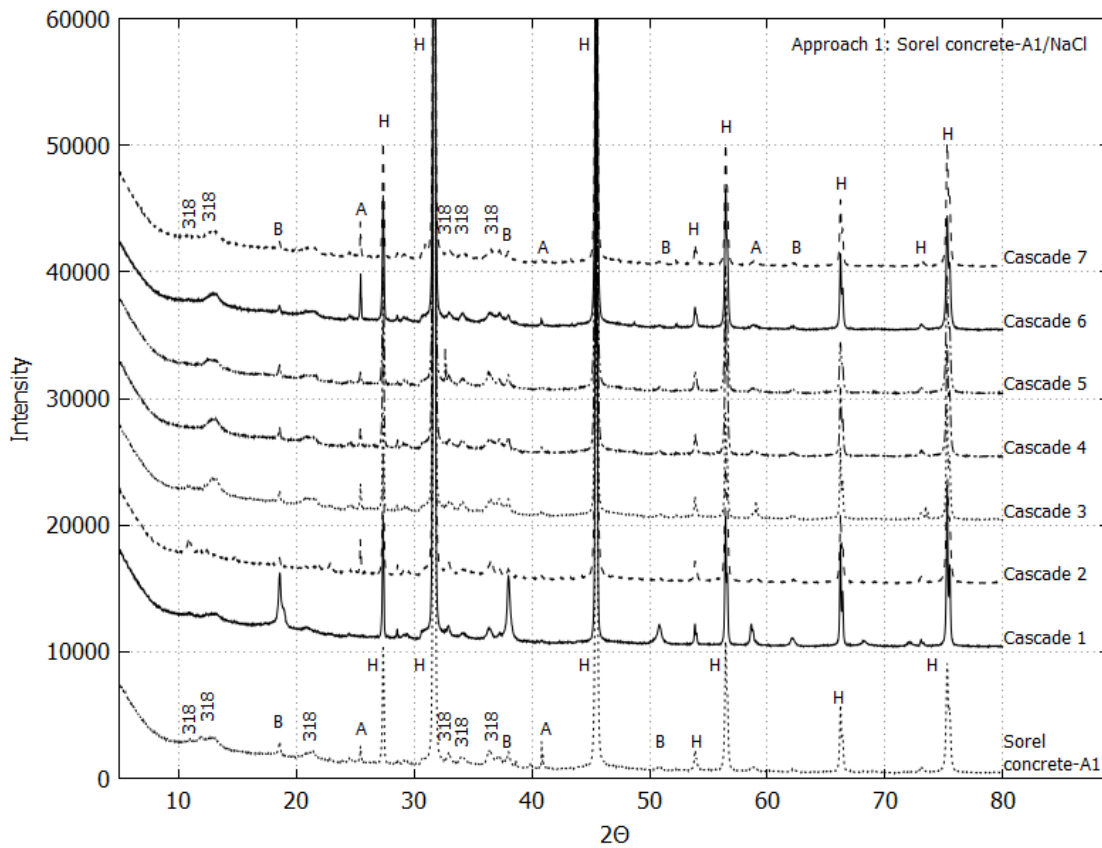


Fig. 4.24 Phase composition of sorel concrete – A1 after reaction with NaCl solution in approach 1; A – Anhydrite, B – Brucite, H – Halite, 318 – 318-phase (See appendix for X-ray diffraction analysis of approaches 2 and 3.)

The solution was analysed with regard to its content of calcium, chloride, magnesium, potassium, sodium and sulphate. Concentrations of chloride and sodium were stable near to its initial level of NaCl solution (Fig. 4.25).

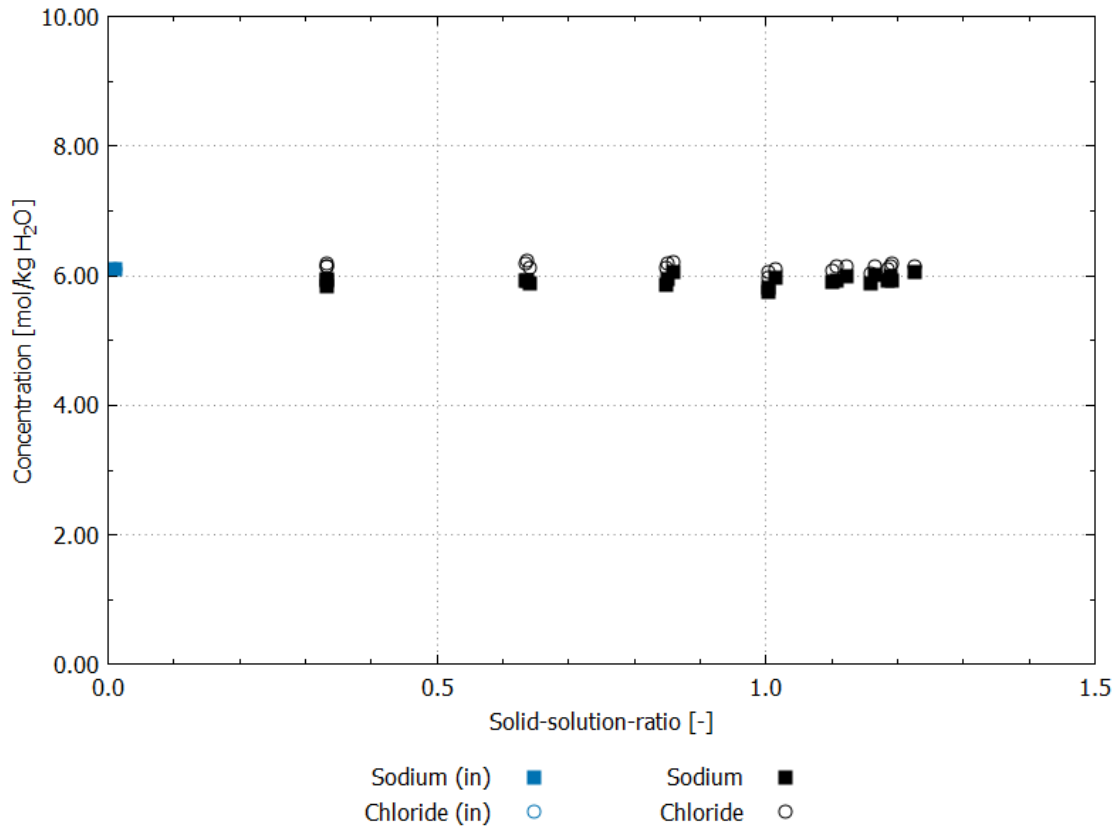


Fig. 4.25 Cascade experiment: Development of solution composition in the system sorrel concrete – A1 / NaCl solution for sodium and chloride concentrations. Blue data points describe solution composition of initial NaCl solution

Calcium and sulphate concentrations increased in the first cascade (SSR = 0.33) to 0.04 mol/kg H₂O (Fig. 4.26). Concentrations changed not significantly during the following cascades. Potassium concentration increased slowly from 0.000 mol/kg H₂O in the initial solution 0.004 - 0.005 mol/kg H₂O after cascade 7 (SSR = 1.2). The magnesium concentrations increased most significant from 0.000 mol/kg H₂O to circa 0.16 - 0.17 mol/kg H₂O at SSR = 0.33. But magnesium concentrations decreased with ongoing experiment again. Noticeable is the bent at SSR of 1.11 in development of magnesium concentrations. At this SSR value magnesium concentrations decreased faster than before. Finally, a value of about 0.10 mol/kg H₂O was attained at SSR 1.23.

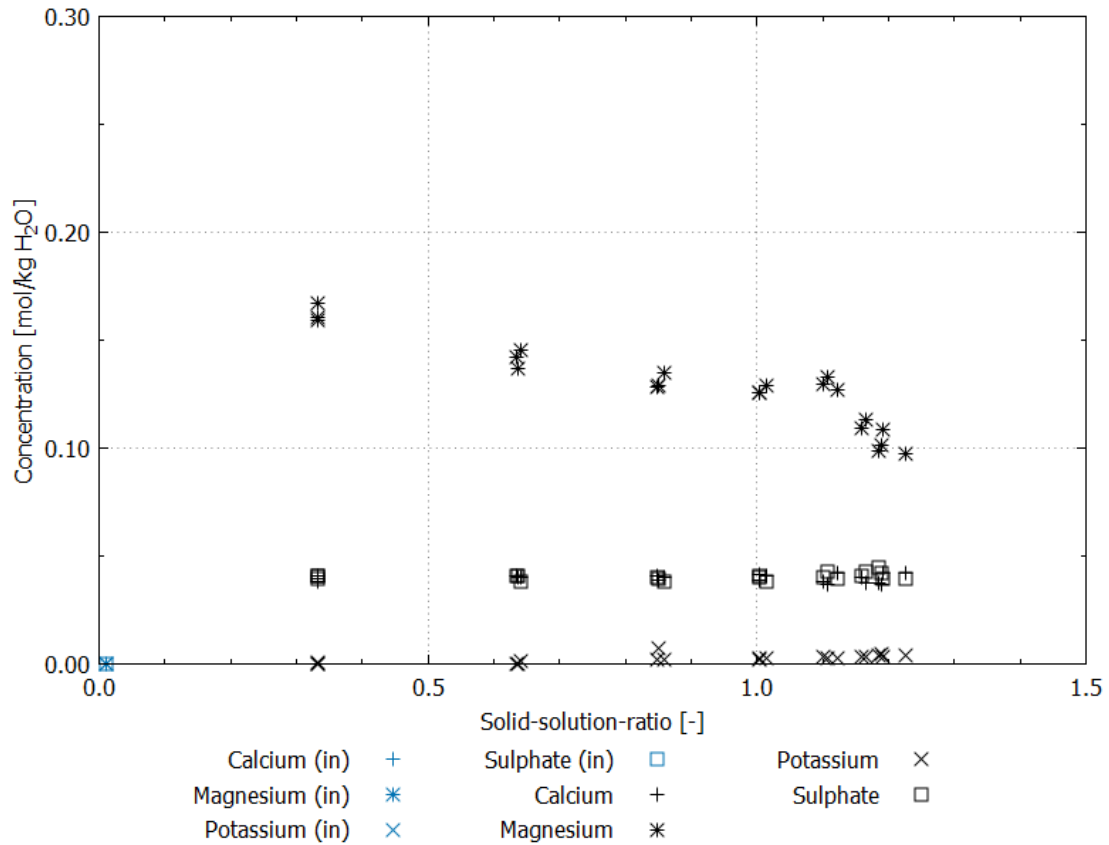


Fig. 4.26 Cascade experiment: Development of solution composition in the system sorel concrete – A1 / NaCl solution for calcium, magnesium, potassium and sulphate concentrations. Blue data points describe solution composition of initial NaCl solution

The initial density of NaCl solution was 1.20 g/cm³ and the initial pc_H-value was 6.75. Density changed not significantly during cascade experiments. The pc_H increased with increasing SSR to 7.83 – 9.13 in the last cascade (Fig. 4.27).

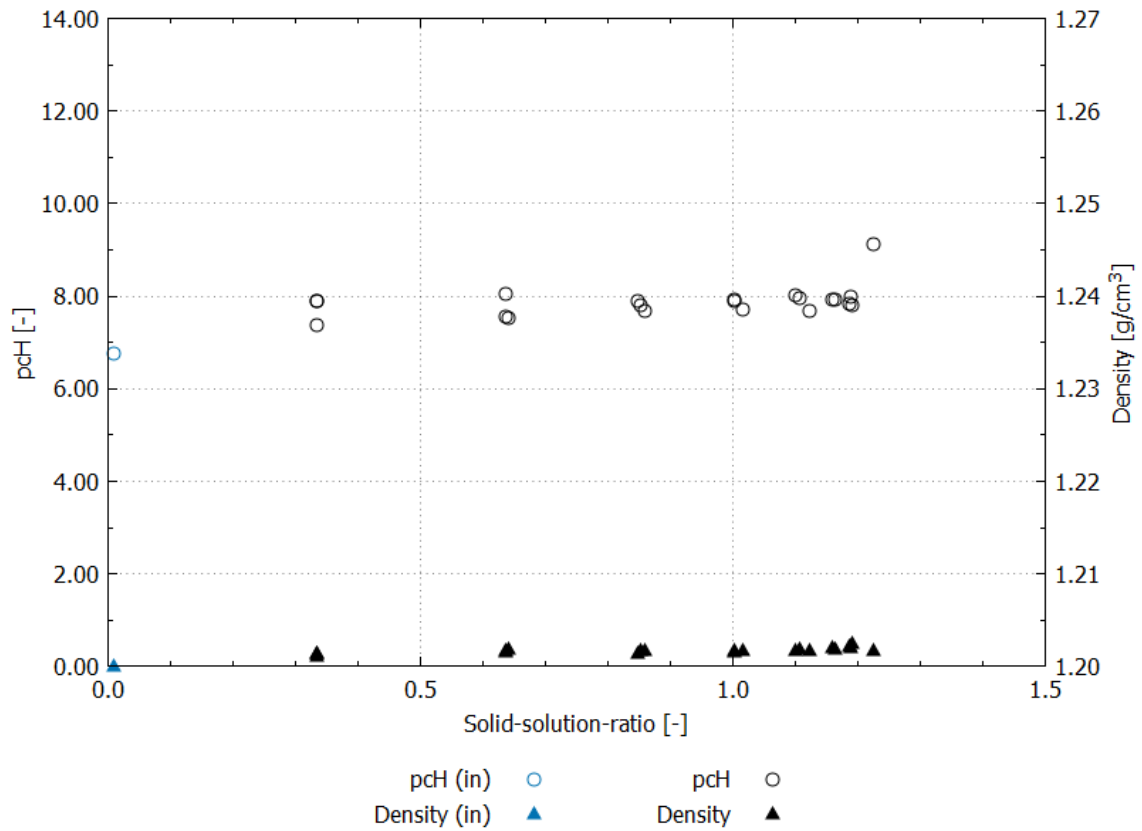


Fig. 4.27 Cascade experiment: Development of pc_H and density in the system sorel concrete – A1 / NaCl solution

4.2.2.2 System salt concrete / $MgCl_2$ solution

The cascade experiments in the system salt concrete / $MgCl_2$ solution were performed in three batches simultaneously too. The minimal equilibration time was determined to fifteen days based on experimental results of batch experiments. Tab. 4.2 summarizes the equilibration time per cascade and the temperature during the cascade experiments.

Tab. 4.2 Reaction time for each cascade and temperature during cascade experiments in the system salt concrete / $MgCl_2$ solution. Vessel 1 bled during pressure filtration. Hence, the experiment in this vessel had to be restarted

Cascade	Reaction time [days]	Temperature [°C]	Reaction time [days]	Temperature [°C]
	Vessel 1	Vessel 1	Vessel 2 + 3	Vessel 2 + 3
1	23	25.4	15	25.8
2	17	24.9	23	25.4
3	15	25.1	17	24.9
4	16	24.9	15	25.1
5	27	25.8	16	24.9
6	16	25.5	27	25.8
7	18	25.4	16	25.5
8	15	25.0	18	25.4
9	-	-	15	25.0

X-ray-diffraction analysis of salt concrete from cascade experiments showed the dissolution of Friedels' salt and Portlandite in all cascades compared to the initial phase composition of salt concrete (Tab. 3.5). The formation of new phases depends on the progress of reaction. Carnallite and Gypsum were formed in cascades one to four (Fig. 4.28). In cascades five to eight only Gypsum was formed.

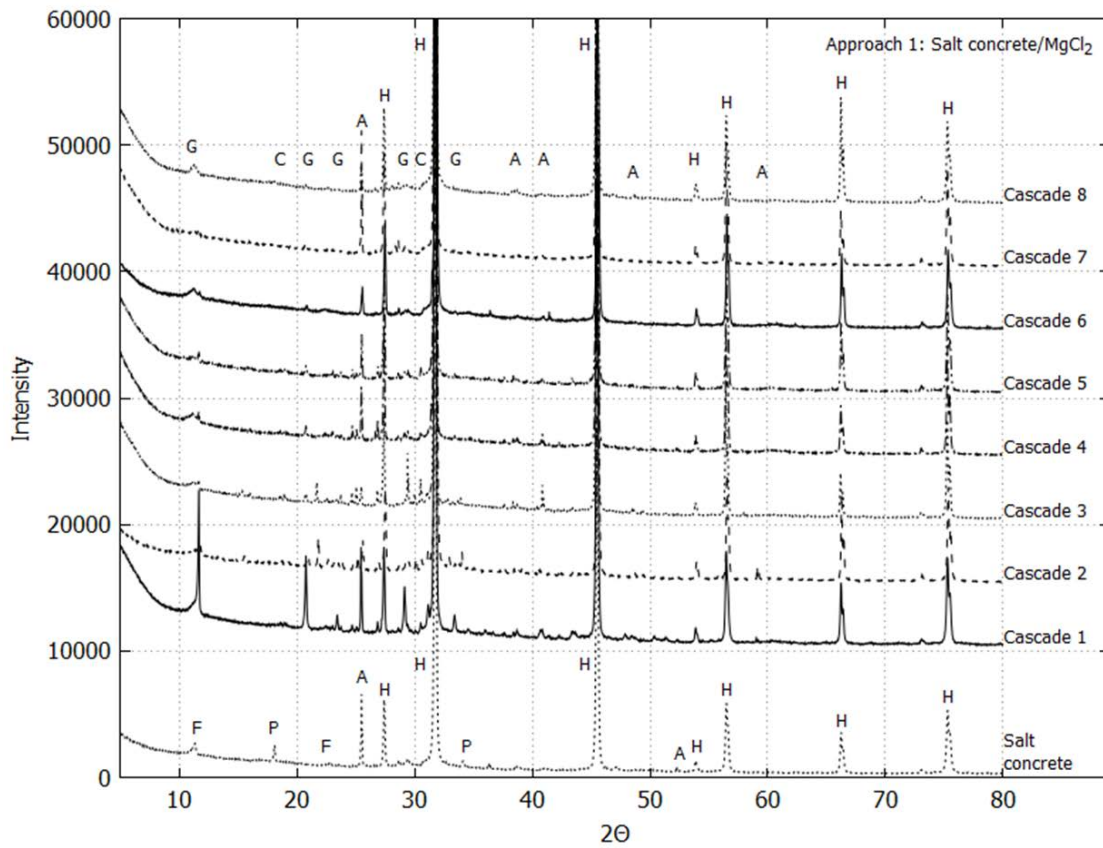


Fig. 4.28 Phase composition of salt concrete after reaction with MgCl₂ solution in approach 1; A – Anhydrite, C – Carnallite, F- Friedels' salt, G- Gypsum, H – Halite, P – Portlandite (See appendix for X-ray diffraction analysis of approaches 2 and 3.)

Note: Diffraction pattern of Gypsum around 11.0 2θ is displaced about 0.3 2θ to higher angles in comparison with Friedels' salt

Analysis of sodium and chloride concentrations is shown in Fig. 4.29. In the beginning of experiment concentrations were equal to initial concentrations in NaCl solution of 0.49 mol/kg H₂O sodium and 9.01 mol/kg H₂O chloride. With ongoing experiment and increasing SSR chloride concentrations decreased up to 7.05 mol/kg H₂O in single batch. In residual batches chloride concentrations decreased a little to 8.16 – 8.77 mol/kg H₂O. Sodium concentrations increased to 1.14 – 1.45 mol/kg H₂O in the last cascade.

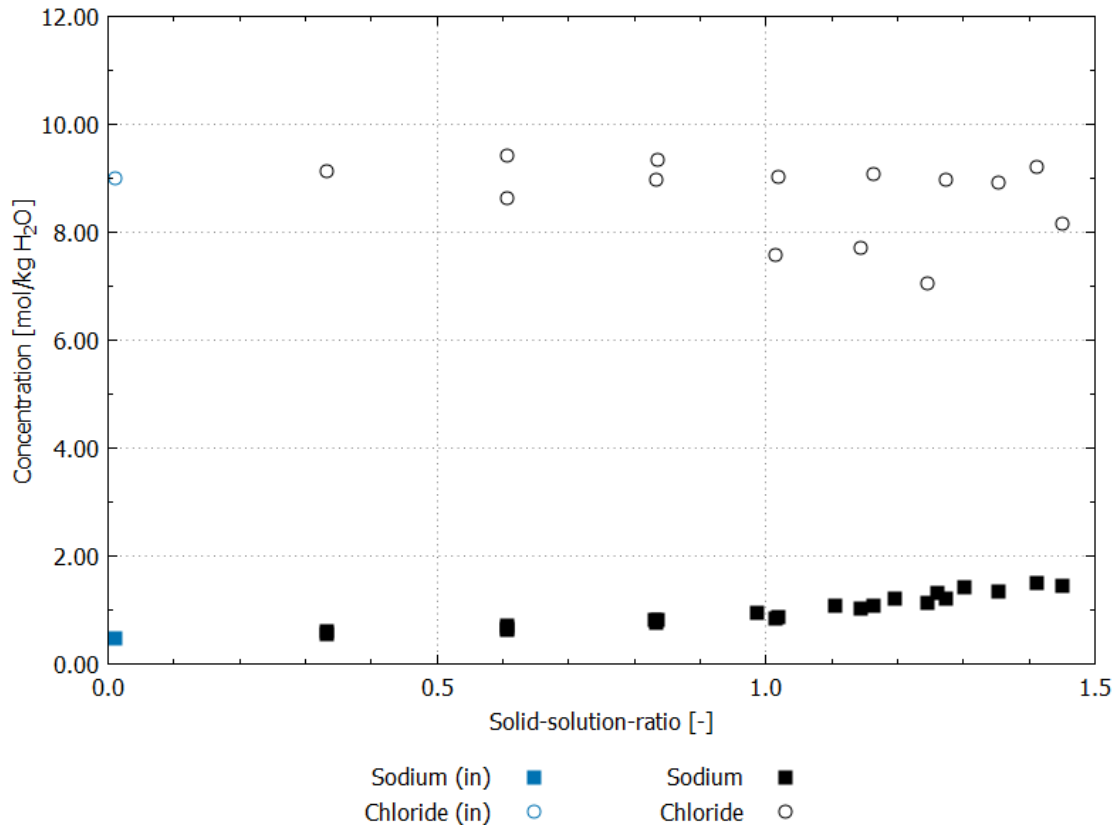


Fig. 4.29 Cascade experiment: Development of solution composition in the system salt concrete / MgCl_2 solution for sodium and chloride concentrations. Blue data points describe solution composition of initial NaCl solution

The potassium concentration changed less during the experiment. Concentrations decreased from 0.57 mol/kg H_2O in the initial solution to 0.50 – 0.52 mol/kg H_2O (Fig. 4.30) in the last cascade. Concentration of sulphate decreased from 0.29 mol/kg H_2O in the initial solution to about 0.03 mol/kg H_2O in the first cascade (SSR = 0.33). Concentration of sulphate increased again with ongoing experiment. In the last cascade (at a SSR of circa 1.45) it had its maximum value of 0.19 – 0.20 mol/kg H_2O . The initial concentration of calcium in the MgCl_2 solution was 0.001 mol/kg H_2O . Calcium concentration increased significantly to 3.64 – 3.76 mol/kg H_2O at SSR of circa 1.40. But calcium concentration decreased again when SSR was > 1.40. Concentration of magnesium in the initial solution was 4.36 mol/kg H_2O and decreased continuously with increasing SSR during cascade experiment. Finally, magnesium concentration was below the limit of quantification at SSR > 1.40.

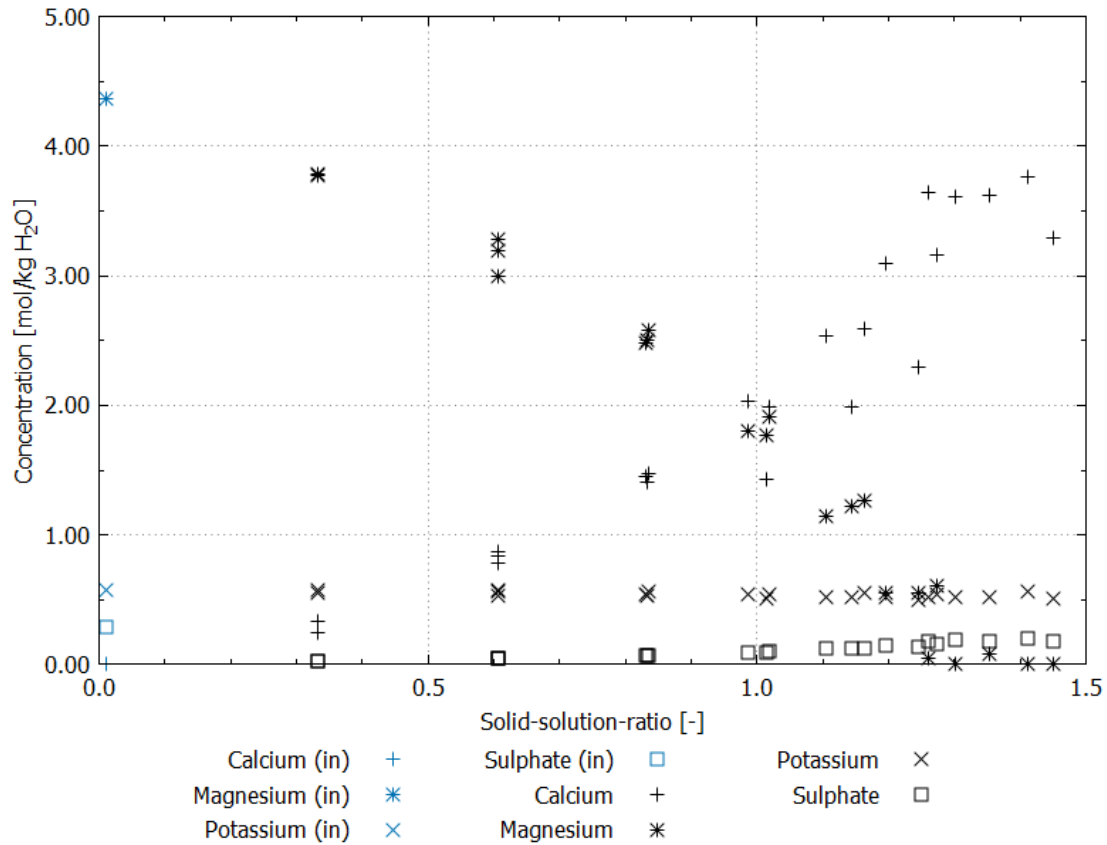


Fig. 4.30 Cascade experiment: Development of solution composition in the system salt concrete / MgCl₂ solution for calcium, magnesium, potassium and sulphate concentrations. Blue data points describe solution composition of initial NaCl solution

The initial density of the MgCl₂ solution was 1.29 g/m³ and the p_{cH}-value 7.15. The density increased during the execution of cascade experiments to 1.22 g/m³ at SSR > 1.26 (Fig. 4.31). At higher SSR density became nearly constant. The p_{cH}-value increased in first cascade (SSR = 0.33) to 8.26 – 8.29. With increasing SSR p_{cH} showed a decreasing trend to values about 8.00 in the end of cascade experiment.

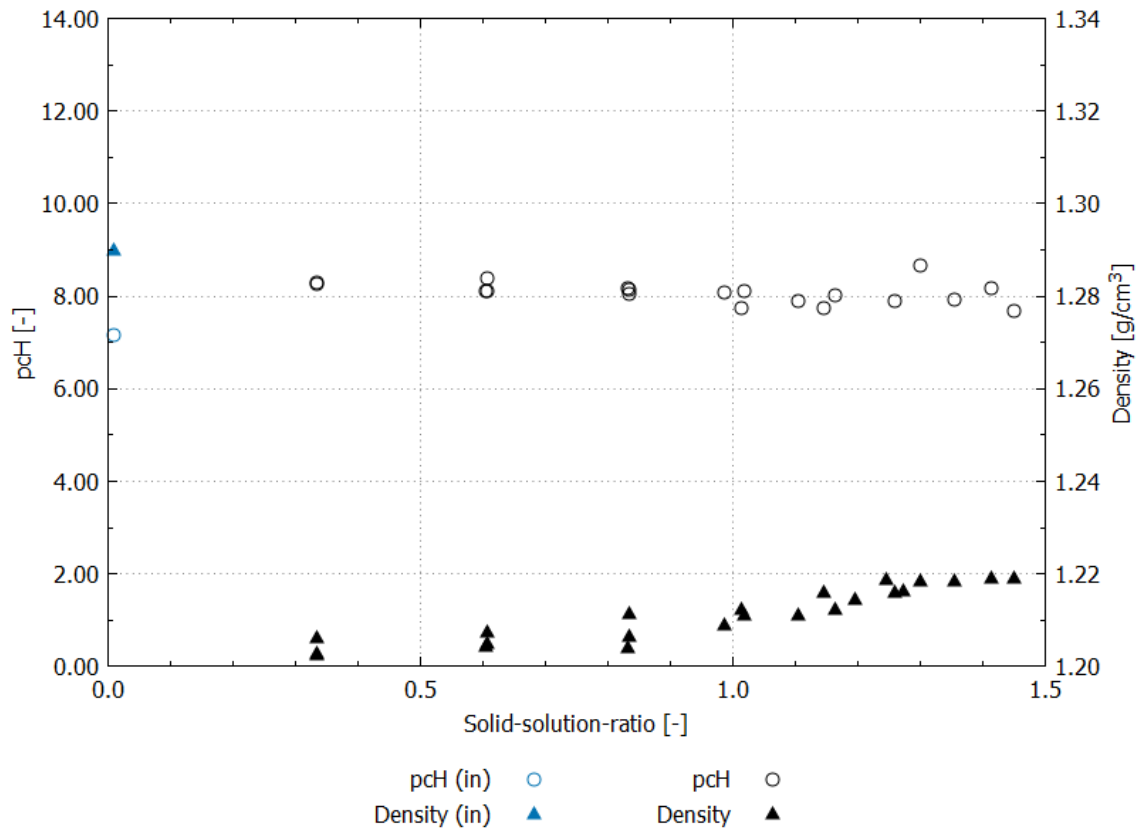


Fig. 4.31 Cascade experiment: Development of pc_H and density in the system salt concrete / $MgCl_2$ solution

4.2.3 Interpretation and discussion

4.2.3.1 Dissolution-precipitation processes in the system sored concrete – A1 / NaCl solution

System sored concrete / NaCl solution was known as thermodynamically unstable from batch experiments (chapters 4.1.2.1 and 4.1.3.1). But the X-ray analysis of the reacted sored concrete of cascade experiments was not in agreement with this finding of batch experiments because the initial mineral phases of sored concrete – A1, Anhydrite, Brucite, Halite and 318-phase, were still detectable in the end of each cascade by X-ray diffraction (Fig. 4.24).

Consideration of solution composition with increasing SSR showed the release of calcium, magnesium, potassium and sulphate into the NaCl solution (Fig. 4.25 and

Fig. 4.26). Calcium and sulphate ratio in the first cascade was 1:1. Hence, this concentration increase may be caused by dissolution of Anhydrite from the sorel concrete – A1. Because the concentrations of calcium and sulphate were constant with increasing SSR, it is expected that the saturation with respect to Anhydrite in the present solution was attained within the first cascade. This may explain the observation from X-ray-diffraction, that Anhydrite was detectable in all solid samples of cascade experiment, because in no cascade Anhydrite was dissolved completely from the sorel concrete – A1. Potassium increase in solution could be not explained based on the identified mineral phases of sorel concrete – A1 from X-ray-diffraction. But it is known from investigations of /GIE 1994/, that the crushed salt, which was available for the production of sorel concrete – A1, can also include Polyhalite. Hence, it may be assumed, that the content of Polyhalite in sorel concrete – A1 was too low for identification by X-ray-diffraction. But based on the development of solution composition it can also be explained with the Polyhalite content in sorel concrete – A1, which dissolved in NaCl solution. Probably, Polyhalite content is very low so that in each cascade the potassium was leached from the fresh sorel concrete – A1 and consequently potassium concentration in solution increased continuously with increasing SSR without attain saturation.

Development of magnesium content in solution was contrary to expectations. Based on data from /FRE 2015/ and /TEI 2009/ the dissolution of 318-phase and an increase of magnesium concentration up to 0.5 mol/ kg H₂O were expected. After magnesium concentration became > 0.5 mol/ kg H₂O, Brucite should become unstable. But X-ray-diffraction showed that both 318-phase and Brucite were detectable in solid samples during complete cascade experiment. Furthermore, magnesium concentration increased within first cascade (SSR = 0.33) compared with the pure NaCl solution. At this point a pronounced increase of slope is recorded reflecting an even more rapid decrease of Mg-concentration and indicating towards the formation of a new solid phase. The maximal concentration of magnesium was 0.16 mol/ kg H₂O. This means in consideration of solubility experiments of /FRE 2015/ in the system Mg(OH)₂-MgCl₂-NaCl-H₂O that 318-phase was never thermodynamically stable in the cascade experiment and dissolved during the whole time. Brucite should be stable during complete experiment at this magnesium content according to /FRE 2015/. The p_{cH} of measurements in the cascade experiments and the solubility experiments could not be compared because those data were not available by /FRE 2015/.

Calculation of SI of the reacted solution showed, that Anhydrite and Halite were supersaturated and thus were thermodynamically stable in this system, which is confirmed by X-ray diffraction analysis (Fig. 5.5). The supersaturation of Anhydrite is in agreement with the assumption of solution analysis that Anhydrite was only dissolved in first cascade because calcium and sulphate concentrations were constant with increasing SSR. In addition, Glauberite and Gypsum were supersaturated. But both phases were not detectable in mineral phase composition of reacted sorel concrete – A1 in cascade experiments. Polyhalite was undersaturated, which supports the assumption that traces of Polyhalite were dissolved only and may have caused the increase of potassium concentrations in the solution. Phases Brucite and 318-phase were undersaturated in the solution. Consequently, both phases should be dissolved in cascade experiments which are indicated in the model calculation.

The deviation between the calculated phase stability based on SI and solid phase composition in experiments could be explained by the process of production of sorel concrete – A1. Sorel concrete – A1 was produced in consideration of required boundary conditions (Tab. 3.1). This process aimed at receiving sorel concrete samples, which were produced with reproducible boundary conditions and at formation and crystallization of typical sorel phases. Hence, the crystallisation and percentage of 318-phase in sorel concrete – A1 is enhanced in comparison with sorel concrete – old. Furthermore, equilibration time for the system sorel concrete / NaCl was determined using sorel concrete – old. Probably, 318-phase of sorel concrete – old dissolved faster than in sorel concrete – A1. Consequently, the equilibration time of eleven days determined with the old material was not sufficient for sorel concrete – A1 caused by improved higher degree of crystallization of 318-phase. As a matter of fact, equilibration time was 17 days in cascade 5, at present 318-phase was still detectable at the end. That indicates that even longer equilibration time than 17 days per cascade had to be applied, which had been impractical for this work.

The deviation between development of magnesium concentrations which was expected according to /FRE 2015/ and the experimental results may be explained by different initial solutions. In solubility experiments of /FRE 2015/ various n-molar $MgCl_2$ solution were used, which were saturated with respect to NaCl. The magnesium-chloride content was at least 0.2 mol/kg H_2O . In cascade experiments a pure saturated NaCl was used and the magnesium content increased instantly. But the minimum concentration of magnesium for thermodynamic stability of the 318-phase was never

reached. It is therefore hypothesized, that new phase containing magnesium formed, and obviously, this phase is not present in the database used for the calculation.

4.2.3.2 Dissolution-precipitation processes in the system salt concrete / MgCl₂ solution

Results of cascade experiments verified that system salt concrete / MgCl₂ solution is thermodynamically not stable, as already indicated in the batch experiments. Anhydrite and Halite were detectable in accordance with batch experiments (Fig. 4.28). In addition, Carnallite and Gypsum were formed. But Carnallite was only formed in cascade 1 to 4. Formation of Bischofite could not be detected in comparison with batch experiments.

The increase of calcium concentrations in the solution can be explained by the dissolution of Portlandite and CSH phases from the salt concrete (Fig. 4.29 and Fig. 4.30). The corrosion process can be explained following /BIC 1968/ as combination of various corrosion processes: pH of initial MgCl₂ solution was about 5.0, whereas Portlandite, which is responsible for the high pH of 12-13 in cement, is not stable in neutral or acids milieus. Furthermore, MgCl₂ and MgSO₄ have the potential to dissolve Portlandite to Brucite and CaCl₂ and CaSO₄ respectively. Hence, combination of magnesia corrosion by MgCl₂ plus Gypsum corrosion by MgSO₄ induces dissolution of Portlandite. After complete dissolution of Portlandite pH usually decreases, and Brucite forms. However, in the experiments an increase of pH was detected because pH in the initial solution was low. This effect can be also explained by formation of Brucite, because dissolution of Brucite may also lead to an increase of pH. Usually, dissolution of Brucite causes a pH of 8.0 to 9.0 /HAG 2009/.

The low pH in solution resulted in destabilization and dissolution of CSH phases, because CSH phases are not thermodynamically stable in solutions with pH < 9.0 /HAG 2009/. CSH phase dissociate into SiO₂-gel and calcium-ions.

Based on the decrease of sulphate concentration in first cascade and the formation of Gypsum, which was detected by X-ray-diffraction, it can be concluded that calcium is released from CSH phase dissolution and subsequently precipitates as gypsum. As this reaction progresses, Anhydrite will react to Gypsum, thereby consuming free

water. This is supported by the results from X-ray diffraction, but only residual concentration of sulphate was measured in solution.

Saturation of Anhydrite, Gypsum and Halite were confirmed in calculations in agreement with results from X-ray diffraction (Fig. 5.6). Carnallite was also supersaturated in cascades 1 to 4 in agreement with experimental results of X-ray diffraction. The formation of Brucite was only assumed based on development of solution composition because of the decrease of magnesium concentrations. But results from calculation of the SI in the reacted solution of cascade experiments indicate that Brucite was only supersaturated in cascades 1 to 4. Indeed, according to /ZHA 2014/ MSH phases form by attack of sulphate and presence of magnesium from Brucite and silica gel. Hence, the decrease of magnesium concentration may be explained by formation of MSH and simultaneously consumption of Brucite. This is in agreement with decreasing SI of Brucite in the reacted solution. Calculation of SI also showed that reacted solution was saturated with respect to Glauberite, Pentasalt and Polyhalite and with 318-phase in cascades 1 to 4. Saturation with Polyhalite may be explained by the Polyhalite content in the crushed salt of salt concrete /GIE 1994/ and by the Polyhalite content in the initial $MgCl_2$ solution. Formation of Glauberite, Pentasalt and 318-phase could not be confirmed by X-ray diffraction.

4.3 Through-diffusion experiments

4.3.1 Setup of through-diffusion experiments

Diffusion coefficients of salt and sored concrete in NaCl and $MgCl_2$ solutions can be determined based on through-diffusion experiments. The through-diffusion experiments were performed in three phases:

- Phase 1: Cylindrical samples were placed in air-tight boxes with the downside face in contact with solution for saturation. To monitor the saturation of the samples the electrical conductivity on the surface of the opposite side was measured in time intervals of two weeks. When an electrical conductivity was measurable it was assumed that samples were saturated.

- Phase 2: Samples were placed in the diffusion-cells. Non-spiked saline solutions circulated both on the bottom and on the top of the diffusion-cell. Circulation of saline solution aimed at equilibration of saline solution and concrete because processes, which have an impact to the pore space, should be completed ideally before measurement of integral flux of tracer was started. A stationary diffusion flow through the concrete should be attained in this phase, too. It is assumed, that two times more is needed than for sample saturation.
- Phase 3: A spiked solution was circulated at the bottom of the diffusion-cell. Non-spiked solution was circulated at the top of the sample until a breakthrough of tracer was measureable. Afterwards, non-spiked solution passed the sample at the top. This solution was collected, weighted and analysed with regard to the tracer concentration. Based on the quantity of tracer in each solution sample the cumulated mass of tracer was calculated.

The concrete samples were placed in acrylic glass tubes before. The gap between concrete and acrylic glass tube were cast with araldite (Fig. 4.32). The enclosure of concrete samples in araldite and acrylic glass tubes was necessary to ensure that process of diffusion proceed from the lower to the upper part of the diffusion cell only. Fig. 4.33 shows a schematic depiction of a diffusion-cell.



Fig. 4.32 Concrete sample inserted in the lower part of a diffusion cell. Concrete sample was inserted in an acrylic glass tube and afterwards cast in araldite

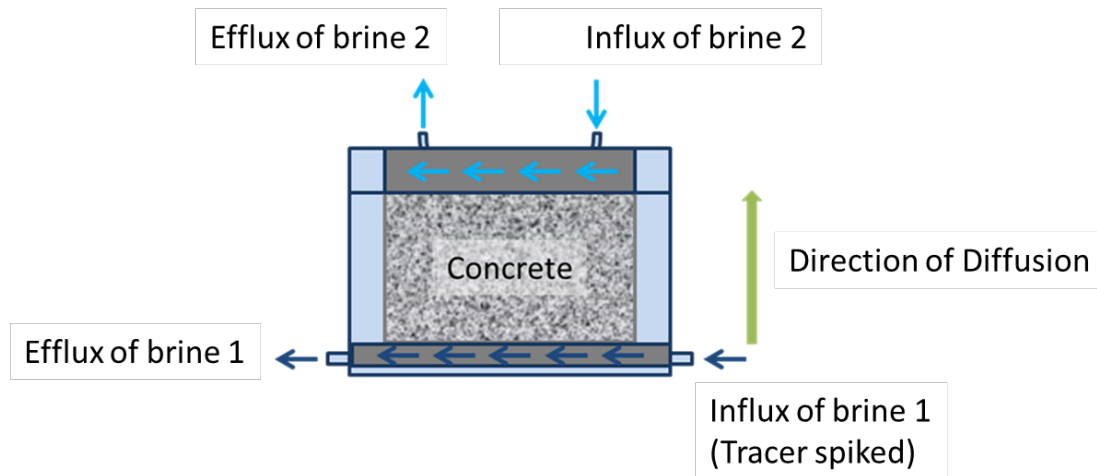


Fig. 4.33 Schematic depiction of a diffusion-cell

The diffusion flow \vec{j} is defined by the 1. Fick's law (Equation 4.2) /WED 1982/:

$$\vec{j} = \frac{dN}{A dt} = -D \frac{\delta c}{\delta z} \quad \text{Equation 4.2}$$

\vec{j} is the diffusion flow in [mol/(m²·s)], N the number of molecules in [mol], A the cross-section area in [m²], D is the diffusion coefficient in [m²/s], δc is the concentration of tracer at the lower part of the diffusion cell [mol/m³] and δz is the thickness of the sample [m]. The 1. Fick's law applies for following boundary conditions:

$$c_1 = \text{const.}$$

$$c_2 = \text{const.} = 0$$

c_1 describes the tracer concentration at the lower part of the diffusion cell, c_2 describes the initial concentration of tracer at the upper part of the diffusion cell, before the saline solution passed the sample.

The cumulated mass of tracer relating to the sample surface was calculated from laboratory results. The mass flux in [mol/m²] must be linear in time, if a stationary state is attained. The flux in [mol/(m²·s)] describes the left side of Equation 4.2 (1. Fick's law). The diffusion coefficient can be calculated by multiplying the flux F by the thickness of the sample (δz) and dividing the result by the tracer concentration (δc) in the initial solution at the bottom of the diffusion cell.

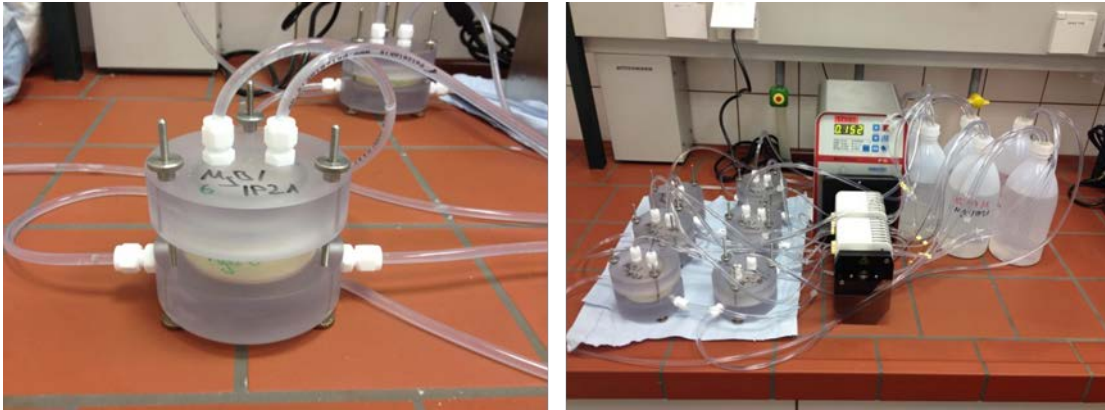


Fig. 4.34 Diffusion cell with insert concrete sample (left) and arrangement of through-diffusion experiments in laboratory (right)

Pilot test

Because diffusion in concrete is assumed to be a very slow process, the appropriate height of samples was determined in pilot tests. Furthermore, the procedure for through-diffusion experiments had to be checked before start of the main through-diffusion experiments. The setup of pilot test and main through-diffusion experiments was similar. But in pilot test the height of samples was varied between 1 cm, 2 cm and 3 cm. Variable sample thickness aimed at determining a practicable dimension of samples because if height is too small, transport processes may occur at the grain boundaries instead through the cement matrix. If the sample length is too big, through-diffusion experiments required very long time periods. Furthermore, in pilot test was checked if the contact surface between concrete and araldite and between araldite and acrylic glass tube respectively was tight. Results from pilot test are described in chapter 4.3.2.

4.3.2 Results of through-diffusion experiments

Pilot tests

Altogether twelve samples of salt and sorel concrete - old respectively were used for pilot tests of diffusion experiments. Three samples of each concrete with length of 1 cm, 2 cm and 3 cm were placed in phase 1 in NaCl and MgCl₂ solution respectively for saturation. A saturation of salt concrete samples was not detectable in both types of solution. Hence, phase 1 of through-diffusion experiments showed that salt concrete is

a very tight material, which did not saturate with saline solution within realistic experimental time periods. If salt concrete is not saturated, process of diffusion of radionuclides through the cement matrix can be excluded. Consequently, following results refer to sored concrete – old.

Fig. 4.35 shows cumulated mass of tracer caesium and lithium in diffusion experiments with NaCl solution and Fig. 4.36 from diffusion experiments with MgCl₂ solution. Below the comparison of through-diffusion experiments is referred to the integral flux of tracer because it is assumed, that process of diffusion is overlaid by transport of tracer at the grain boundaries. Hence, transport of tracer is not induced by diffusion only. Measurement results show, that the integral flux of caesium was faster compared to the integral flux of lithium in both saline solutions. In addition, the integral flux seemed to be influenced by the length of the sample. Integral flux proceeded most quickly in 1 cm samples and slowest in 3 cm samples. Furthermore, the integral flux depended from the saline solution itself: integral flux in NaCl solution was higher than in MgCl₂ solution for samples of sored concrete - old.

An increase of tracer concentrations was measureable in both systems near to time $t = 0$. This is caused by the general procedure of through-diffusion experiments, because in step 3 the tracer spiked solution at the bottom of the diffusion cell and the non-spiked solution at the top were both circulated until the breakthrough of tracer was measureable. Afterwards, non-spiked solution passed the sample, the solution was collected and the cumulated mass of tracers was calculated. Results below show only the last time interval of step 3 when non-spiked solution passed the sample and was collected.

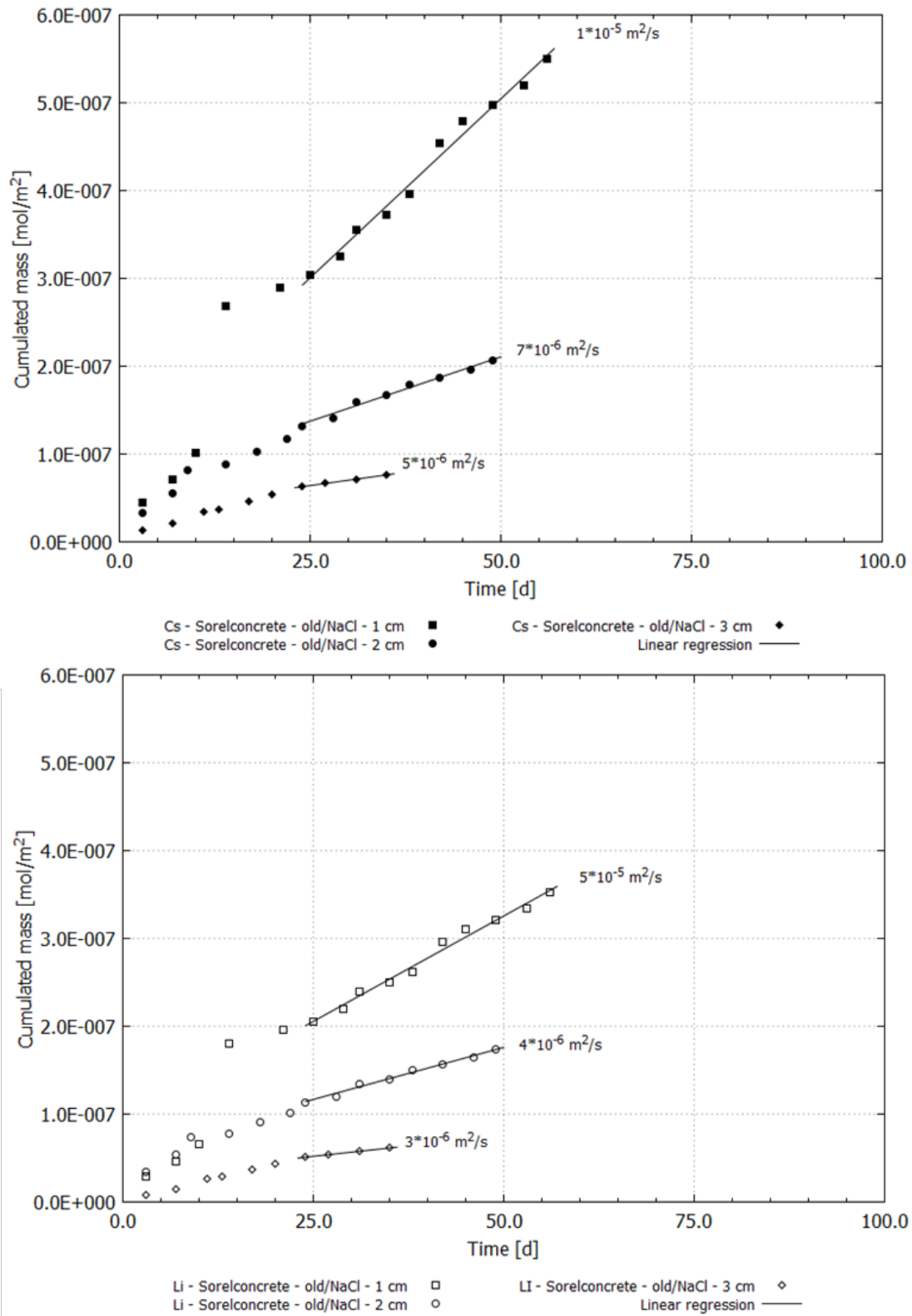


Fig. 4.35 Cumulated mass of tracer caesium (above) and lithium (below) in pilot tests of through-diffusion experiments with NaCl solution in samples of 1 cm, 2 cm and 3 cm in length

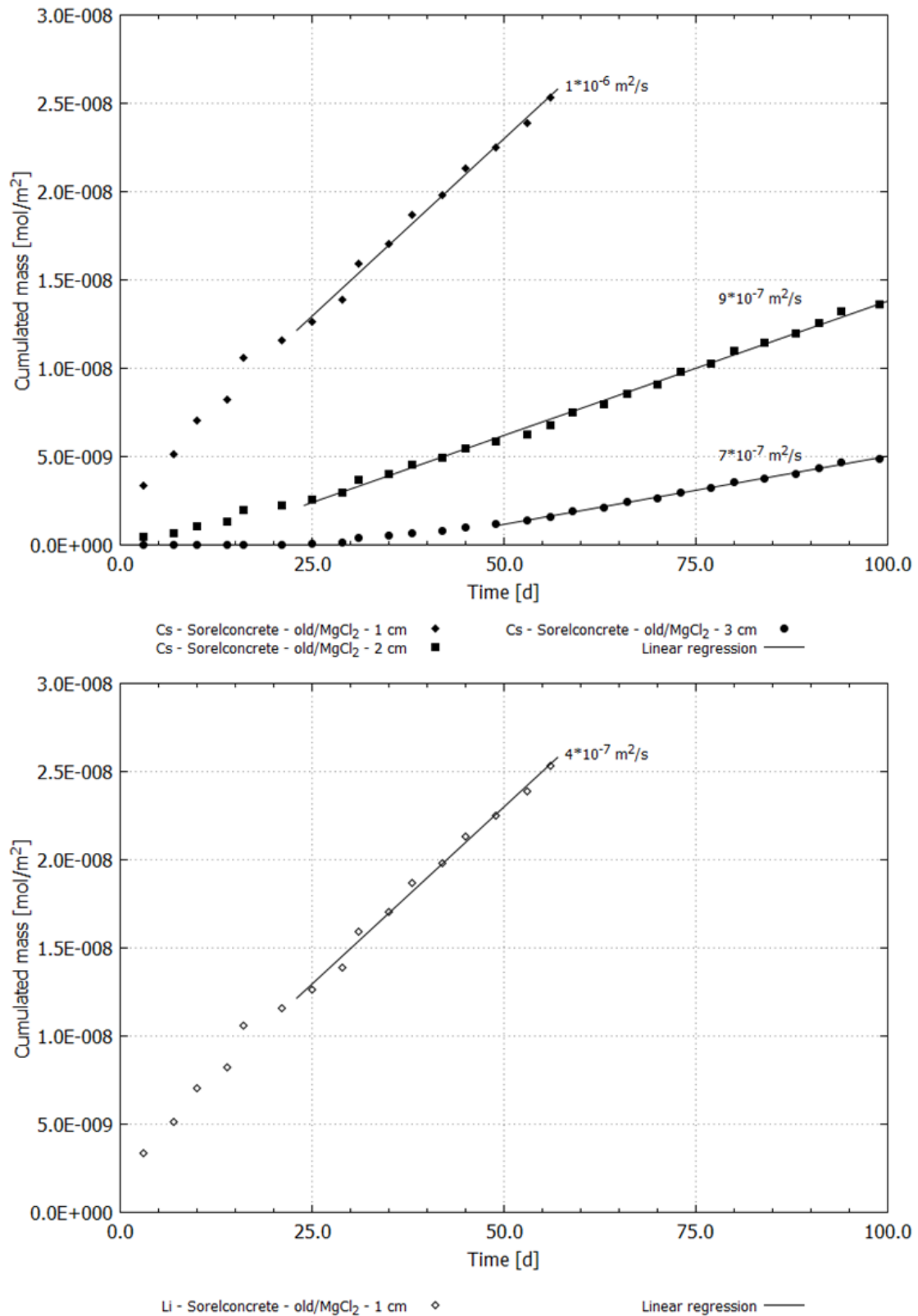


Fig. 4.36 Cumulated mass of tracer caesium (abv.) and lithium (bel.) in pilot tests of through-diffusion experiments with MgCl₂ solution in samples of 1,2,3 cm in length. Break through of lithium in 2,3 cm were not detectable

Finally, samples were dismantled from diffusion cells and put in coloured tracer solution of NaCl and MgCl₂ respectively. It aimed at verifying that integral flux of tracers occurred in the concrete sample instead of in the contact surface of sorel concrete and araldite. The test with coloured tracer solution confirmed that the method of through-diffusion experiments was successful because breakthrough of tracer was only visible at the concrete surface (Fig. 4.37).



Fig. 4.37 Sorel concrete sample from through-diffusion experiments in coloured tracer solution. The violet colour occurs in the middle of sample only verifying that diffusion occurred in the concrete matrix

Based on Equation 4.2 the apparent diffusion coefficients for caesium and lithium were calculated in the various systems taking into account the length of samples. Therefore Equation 4.2 was transposed to

$$-D = \frac{dN \cdot \delta_z}{A dt \cdot \delta_c} = \frac{\vec{j} \cdot \delta_z}{\delta_c} \quad \text{Equation 4.3}$$

The slope of the linear regressions (Fig. 4.35 and Fig. 4.36) corresponds to the flux \vec{j} of Equation 4.2. The slope was calculated by parameter fitting using Gnuplot Version 5.0. Therefore, the data points, which should be considered in the linear regression, were

defined before. In each sample, those data points were considered, which were most linear in time. The thickness of the sample (δ_z) and the initial concentration of tracers at the lower part of the diffusion cell (δ_c) were known from experiments. Calculated diffusion coefficients are shown in Tab. 4.3.

Tab. 4.3 Calculated diffusion coefficients in pilot through-diffusion experiments

System	Length of sample [m]	Apparent diffusion coefficient caesium [m ² /s]	Apparent diffusion coefficient lithium [m ² /s]
Sorel concrete - old/MgCl₂			
	0.01	1.14·10 ⁻⁰⁶	3.51·10 ⁻⁰⁷
	0.02	8.64·10 ⁻⁰⁷	-
	0.03	6.57·10 ⁻⁰⁷	-
Sorel concrete - old/NaCl			
	0.01	1.02·10 ⁻⁰⁵	4.50·10 ⁻⁰⁶
	0.02	7.32·10 ⁻⁰⁶	4.44·10 ⁻⁰⁶
	0.03	4.55·10 ⁻⁰⁶	2.65·10 ⁻⁰⁶

Based on results of pilot through-diffusion experiments the main through-diffusion experiment was performed to sorel concrete samples with a length of 3 cm. It is assumed that apparent diffusion coefficients of samples with larger length are more realistic: the pilot test showed a clear dependency of the calculated apparent diffusion coefficient from the length of the sample. But based on the fact, that all samples are composed of the same material all samples should lead to the same apparent diffusion coefficients. It is assumed that matrix diffusion is superimposed by a transport of tracer at the grain boundaries. Because of the inhomogeneity of sorel concrete, transport of tracers may be faster at the grain boundaries of the crushed salt than in the cement matrix. In samples with a length of 1 cm the contribution of transport along grain boundaries will be larger than in longer samples. Hence, calculated diffusion coefficients for samples with larger length are smaller but also more realistic.

Main through-diffusion experiment

The main through-diffusion experiment was performed with six sorel concrete samples. In this experiment the sorel concrete – A1 was used. Three samples were saturated with NaCl solution and three with MgCl₂ solution.

In the system with NaCl solution only results of two cores are available, because in the third sample a flux of solution from the upper part of the diffusion cell to the lower part was detected. Hence, a measurement of the integral flux was not possible anymore. Fig. 4.38 shows the cumulated mass of tracers caesium and lithium in core 4 and core 5. In core 4, no tracer could be detected within the first ten days. After ten days both caesium and lithium were measureable. A decrease of slope in the cumulated mass of tracer concentration was measured after 25 days. After 40 and 45 days a significant step in the cumulated mass of tracer was detectable. This phenomenon will be discussed in chapter 4.3.3. The cumulated mass of tracers in core 5 increased continuously up to 60 days. But it is assumed that the integral flux of tracer was not constant in time at the beginning of through-diffusion experiments. Hence, only time period from 25 to 40 days in core 4 and of 25 to 60 days in core 5 was considered in linear regression to determine the apparent diffusion coefficient.

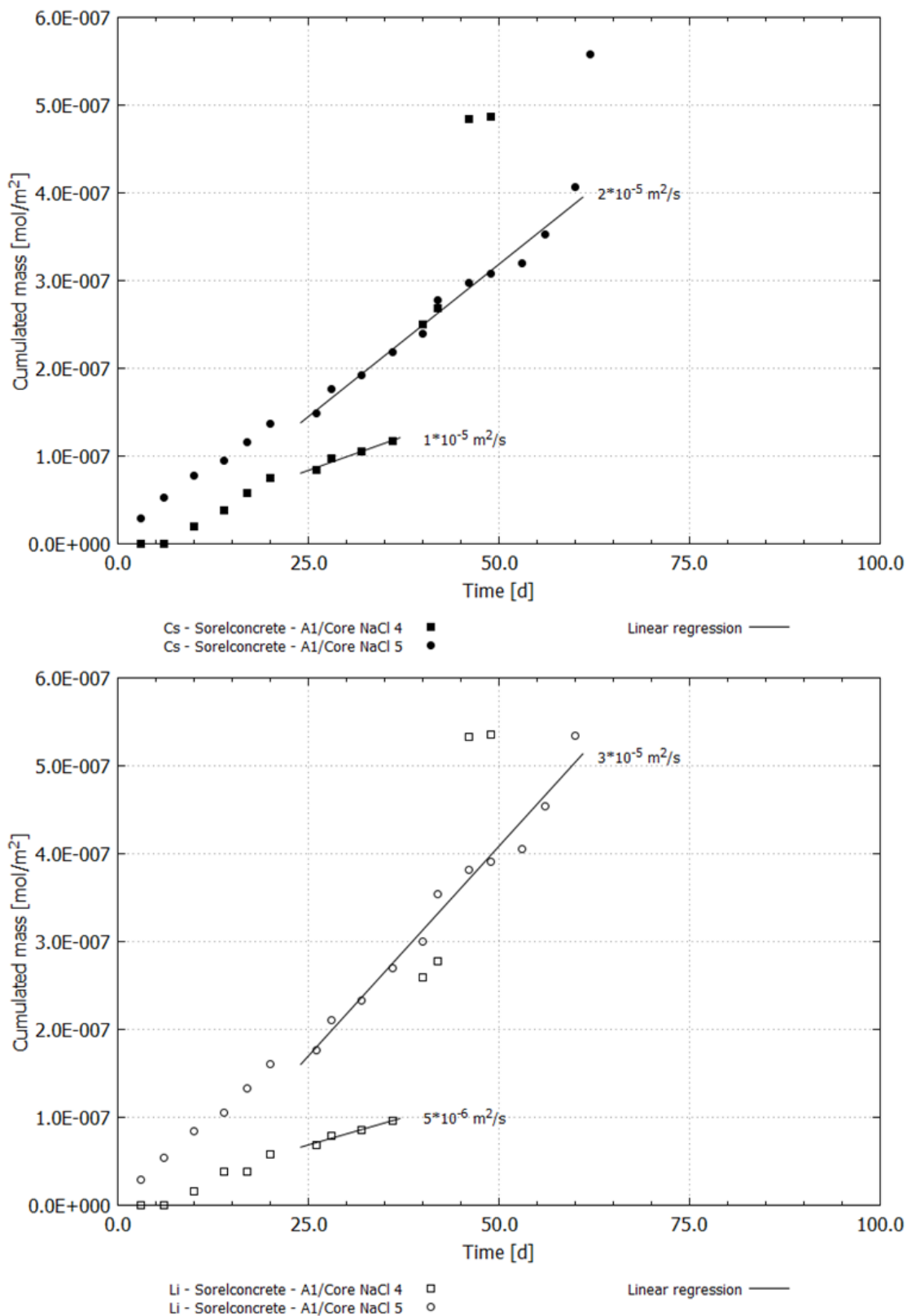


Fig. 4.38 Cumulated mass of tracer caesium (abv.) and lithium (bel.) in main through-diffusion experiments with NaCl solution in samples with 3 cm in length

Fig. 4.39 shows the cumulated mass of tracer caesium in through-diffusion experiments with $MgCl_2$ solution. A break-through of lithium was not detected within the experimental time. The development of cumulated mass of tracer shows that integral flux of tracer occurred very similar in core 1 and core 3, but was less in core 5. The linear regression for calculation of the slope was adapted in core 1 and core 3 to the time period of 40 days to 70 days because of the small step and increase of the slope after 40 days. The development of cumulated mass of core 2 showed a small change in its slope after 25 days. Hence, the linear regression was adapted to the time period of 25 days to 70 days.

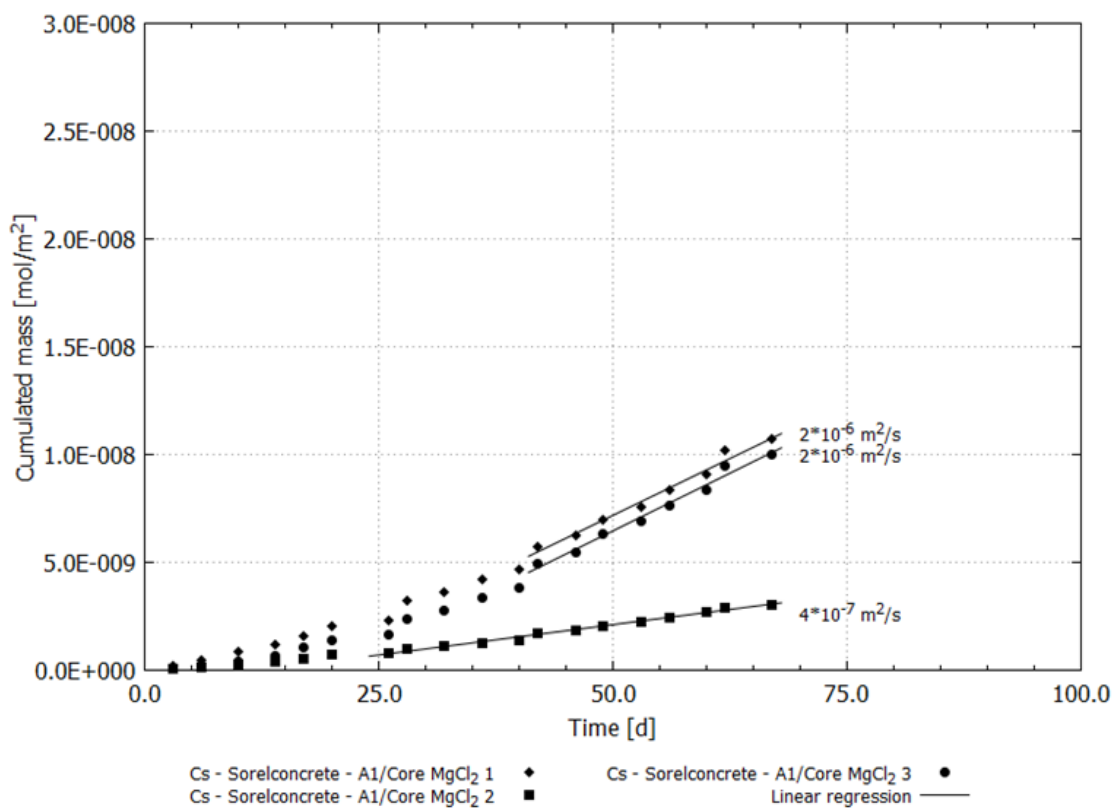


Fig. 4.39 Cumulated mass of tracer caesium in main through-diffusion experiments with $MgCl_2$ solution in samples with 3 cm in length

The calculated apparent diffusion coefficients are listed in Tab. 4.4 based on Equation 4.3. Results confirmed results of pilot tests: The apparent diffusion coefficient in system sorel concrete / $NaCl$ solution was higher than in the system sorel concrete / $MgCl_2$ solution. They varied about circa one order of magnitude for caesium. The apparent diffusion coefficients of caesium and lithium varied, too. Apparent diffusion coefficient

of lithium was smaller in sorel concrete than apparent diffusion coefficient of caesium. They vary about circa a half order in system with NaCl solution. An apparent diffusion coefficient for lithium in system sorel concrete / MgCl₂ solution could not be determined.

Tab. 4.4 Calculated diffusion coefficients in main through-diffusion experiments

System	Length of sample [m]	Apparent diffusion coefficient caesium [m ² /s]	Apparent diffusion coefficient lithium [m ² /s]
Sorel concrete - A1 / MgCl₂			
Core 1	0.03	1.63·10 ⁻⁰⁶	-
Core 2	0.03	4.36·10 ⁻⁰⁷	-
Core 3	0.03	1.66·10 ⁻⁰⁶	-
Sorel concrete - A1 / NaCl			
Core 4	0.03	1.04·10 ⁻⁰⁵	6.47·10 ⁻⁰⁶
Core 5	0.03	2.33·10 ⁻⁰⁵	2.48·10 ⁻⁰⁵
Core 6	0.03	-	-

4.3.3 Interpretation and discussion

Through-diffusion experiments were planned to be done with salt and sorel concrete samples. Ideally, concrete samples should be uniformly and completely saturated with solution. To accomplish this, prior to the actual measurement of diffusion concrete samples were exposed to NaCl and MgCl₂ solution. But measurements of electrical conductivity of salt concrete samples indicated no saturation of the samples, even after samples were placed in saline solution for more than one and a half year. In contrast, samples of sorel concrete – old and – A1 saturated within two to three months. According to /HAG 2009/ the available salt concrete exhibited a very small degree of cross-linked pores due to the fast hardening process resulting from the low w/c-ratio of 0.38. The small degree of cross-linked pores affected permeability, too. Permeability measurements from advection experiments showed, that permeability for gas was not measureable in most salt concrete samples. In contrast, sorel concrete samples showed permeability to gas between 10⁻¹⁶ m² and 10⁻²⁰ m². Furthermore, the proportion between MgCl₂ solution and MgO, which is assumed here as correspondent value to w/c-ratio, was > 2.0 for sorel concrete. According to the model of Powers 1958/59, cited in /HAG 2009/, sorel concrete has to be a concrete with very slow hardening process and high degree of cross-linked pores caused by the high w/c-ratio.

Permeability measurement confirmed this assumption. Therefore, through-diffusion experiments could be only performed with sorel concrete. Saturation of salt concrete samples with ongoing time is not finished yet. But saturation of salt concrete is very slowly. Hence, the performance of through-diffusion experiments with salt concrete was not to realize. But the slow process of saturation in salt concrete seems to be in accordance with a very slow integral flux in the concrete.

Pilot through-diffusion test aimed at testing the through-diffusion cells and adaptation of the procedure. It was estimated at the beginning, which lengths of sample were practicable in terms of time required and the determination of realistic diffusion coefficients. Results of pilot tests showed a clear dependence of the tracer flux from the length of the sample (Fig. 4.35 and Fig. 4.36). In general, flux of tracer was higher in samples with 1 cm in length than in samples with 3 cm in length. Very probably, this results from the inhomogeneity of sorel concrete caused by the crushed salt inclusions. The integral flux occurs faster along the grain boundaries and is not retarded by diffusion in the cement matrix. With increasing sample length percentage of integral flux in the cement matrix increases and consequently the whole diffusion process is slower. Related to the diffusion through an in situ sealing element, the integral flux determined in samples with higher length seems to be more realistic. Clearly, for through-diffusion experiments to yield meaningful results, sample size (length, cross sectional area) must be in a certain relation to the grain size and homogeneity of the material investigated (Fig. 3.2). Hence, main through-diffusion experiments were performed with samples of 3 cm in length.

At the end of pilot through-diffusion experiments sorel concrete samples were dismantled and put in coloured tracer solution (Fig 4.37). In that way was checked that integral flux of tracer occurred through the concrete instead of at the surface between sorel concrete and araldite. This check showed additionally, that tracers did not diffuse homogenously through the samples but had preferred pathways. As the value of calculated apparent diffusion coefficients are related to the cross sectional area of the samples, diffusion coefficients in homogenously saturated material could in fact be higher.

Both results of pilot through-diffusion and main through-diffusion experiments demonstrated that the integral flux depends on the present saline solution. The visual inspection after saturation of the samples indicated, that all samples were consistent

saturated. Apparent diffusion coefficients for caesium in NaCl solutions were in average one order of magnitude higher than in $MgCl_2$ solution and apparent diffusion coefficient of lithium was circa half an order higher than for caesium. Determination of apparent diffusion coefficient for lithium in $MgCl_2$ solution was not possible, because there was no break-through of tracer in experimental time. Higher apparent diffusion coefficients in NaCl solution may be caused by corrosion of sorel concrete. Batch and cascade experiments before confirmed that sorel concrete is not thermodynamically stable in the presence of NaCl solution, especially the stabilizing 318-phase. When sorel concrete samples of the system sorel concrete / NaCl solution were dismantled from diffusion cells, spots of corrosion at the faces of the samples could be clearly discerned (Fig. 4.40).

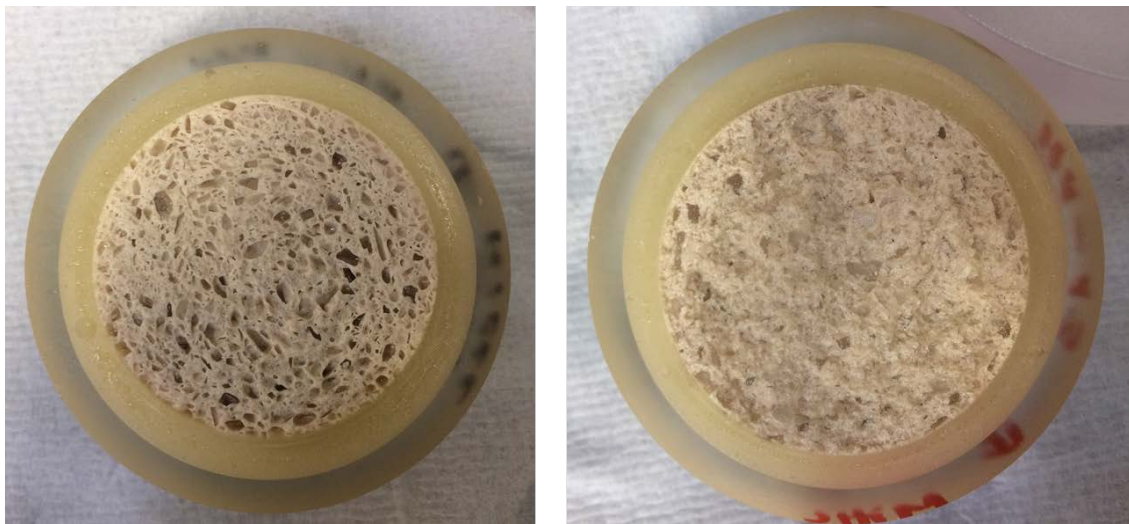


Fig. 4.40 Sorel concrete samples after dismantling from through-diffusion cells. Left: $MgCl_2$ solution; Right: NaCl solution

Progressive damaging of the sample due to corrosive processes is further supported by clearly visible steps in the development of cumulated mass of tracer (Fig. 4.38). Hence, it is concluded that NaCl solution corroded the sorel concrete and created additional pathways for tracers. Dependent on the current state of phase formation, it is assumed that pathways were temporarily clogged so that integral flux of tracer was slower for a short time. When mineral phases were flushed out, tracer was transported much faster which results in a step in the slope of the cumulated mass of tracer. Samples in system sorel concrete / $MgCl_2$ solution were not corroded based on results of geochemical experiments before. This statement was supported in through-diffusion

experiments by the continuous increase of tracer concentration without steps in its development of cumulated mass (Fig. 4.39).

Differences between lithium and caesium may be interpreted in terms of ionic mobilities: the ionic mobility is affected by the size of an ion, its charge and the hydration number. The hydration number describes the number of water molecules, which are bound within the hydration sphere of an ion. In general, smaller ions can bind higher numbers of water molecules because of their higher charge density. This results in a bigger hydrate-sphere. Ions with large hydrate-spheres have lower ionic mobility, which may result in the lower diffusion of lithium in comparison to caesium /APP 2005/.

In the system sorel concrete / $MgCl_2$ solution significant higher apparent diffusion coefficients of caesium was measured. This effect may be induced by the lower ionic mobility of lithium in comparison to caesium as discussed in section before.

Furthermore, it was expected that diffusion occurred simultaneously in the same system in the main through-diffusion experiment. But results showed, that in system sorel concrete – A1 / NaCl solution diffusion in core 4 was lower than in core 5 and in system sorel concrete - A1 / $MgCl_2$ solution diffusion was lower in core 2 than in core 1 and 3. Samples for through-diffusion experiments were prepared from three sorel concrete samples with a length of 10 cm by partition. Hence, half of smaller samples in through-diffusion experiments were produced from the upper part and second half of samples from the lower part of the 10 cm sorel concrete samples. Cores 2 and 4, which showed lower diffusion, were produced from the lower part. Probably, effects of decomposition and compaction during the hardening process influenced the integral flux significantly: components with higher density sagged down before sample was hardened and the higher axial pressure in the lower part of the sample results in an improved compaction of the lower part. The effect of compaction seems to be much more relevant in sealing element with a size of a couple of meters. This may positively affect the sealing capacity of a sealing element: if solution enters a sealing element, solution starts to saturate the sealing element primarily from the bottom before upper parts of the sealing become saturated (Fig. 4.41). The effect of decomposition seems to be not relevant in-situ, because sealing elements are constructed by concreting in layers to prevent effects of decomposition.

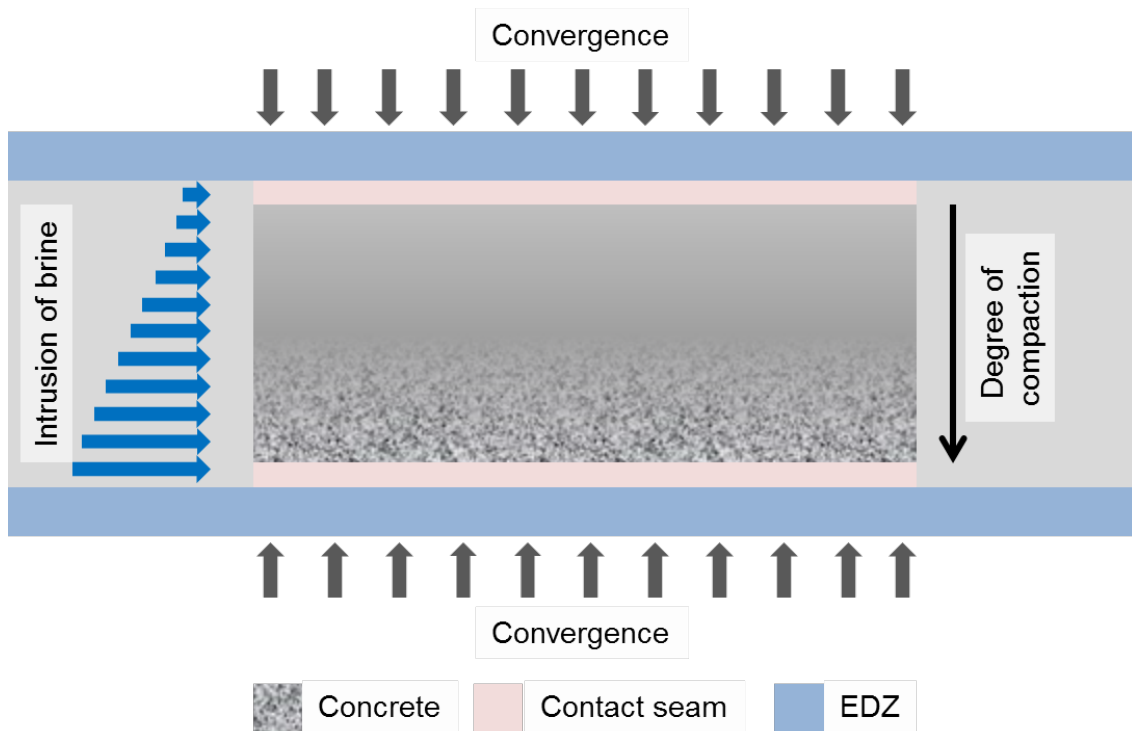


Fig. 4.41 Schematic depiction of a concrete sealing: saturation of solution starts in the lower part of a sealing element. Affected by the higher degree of compaction in the lower part of a sealing an improved sealing capacity in this section of a sealing is assumed

Obtained apparent diffusion coefficients should only be considered as approximate values, because they depend on various boundary conditions:

- Properties of the sored concrete sample are affected by the point of installation in the complete sealing element. Hence, diffusion in the upper part of a sealing element differs from diffusion in the lower part.
- Diffusion depends on the composition and potential corrosion effects of solution which saturates the sealing element before (chapter 4.3.2).
- Diffusion velocity depends on the chemical element which is transported through a sealing element.
- Determination of diffusion coefficients was based on the subjective perception at which point of time diffusion was stationary in time.

- Calculation of diffusion coefficient was referred to the complete cross-section area of sored concrete samples, but investigations with coloured tracer showed, that diffusion occurred only partly. Visual inspection of coloured samples could not show whether pathways for tracer were even smaller than the coloured surface because tracer spread after breakthrough at the surface. For this reason it was desist from calculations with smaller cross-section areas.

4.4 Advection experiments

4.4.1 Setup of advectons experiments

Advection experiments aim at investigating the advective flow and its impact on the corrosions processes and development of permeability. Fig. 4.42 shows a sketch for the experimental set-up of an advection experiment. The sample is placed in an advection cell from steel and the gap between steel tube and concrete is cast with araldite. Both faces are closed by messing casings with an opening for the influx respectively outflows of solution. Solution enters the sample with defined fluid injection pressure. Outflowing solution is collected at the opposite face of the sample.

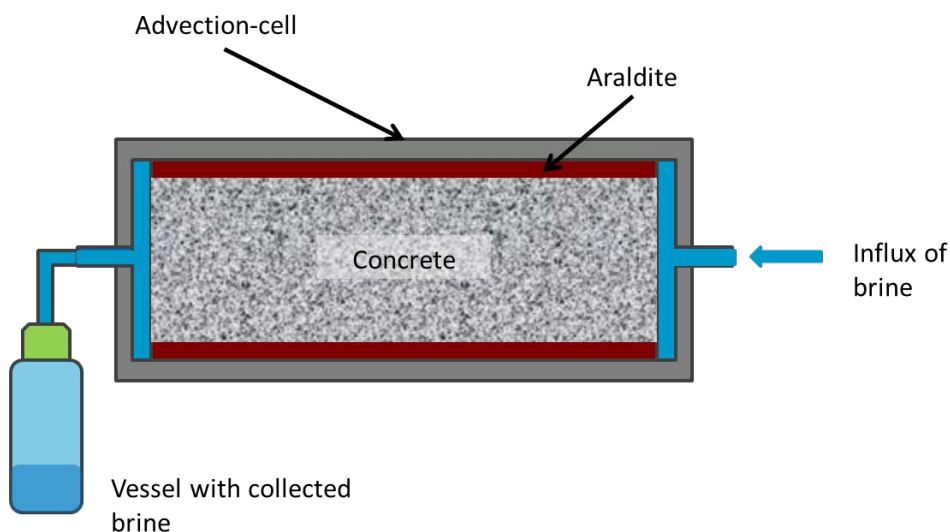


Fig. 4.42 Functional principle of an advection cell

Based on the Darcy's law for compressible fluids the permeability K can be calculated according to

$$k = \frac{Q \cdot n \cdot p_1 \cdot L}{\Delta p \cdot p^* \cdot A} \quad \text{Equation 4.4}$$

k is the permeability in [m^2], q the volume flow in [m^3/s], η the dynamic viscosity of the solution in [$\text{kg}/(\text{m}\cdot\text{s})$], p_1 the gas pressure at the outflowing surface in [$\text{kg}/(\text{m}\cdot\text{s}^2)$], p_2 the gas pressure at the inflowing surface in [$\text{kg}/(\text{m}\cdot\text{s}^2)$], L the length of the sample in [m], Δp the difference pressure (p_2-p_1) in [$\text{kg}/(\text{m}\cdot\text{s}^2)$], p^* the average internal pressure in the pores ($(p_1+p_2)/2$) in [$\text{kg}/(\text{m}\cdot\text{s}^2)$] and A the cross section area of the sample in [m^2]. Additionally, the collected solution is analysed with regard to its composition, development of density and pH-value.

The advection experiments are divided in two types of samples:

- a) pure sorel concrete samples
- b) combined samples of salt concrete fitted into hollow cylinders of rock salt

Pure sorel concrete samples

The pure sorel concrete samples were 10.0 cm in length and 5.0 cm in external diameter. Altogether ten samples of sorel concrete were investigated. Five samples were exposed to NaCl solution and five to MgCl_2 solution. The experiments were performed in three steps:

- Step 1: Continuous percolation of solution through the concrete samples – exchange of the pure solution of the concrete sample to defined saline solution and determination of initial permeability.
- Step 2: “Stop-and-flow” experiments – “Stop-and-flow” experiments aimed at investigating of kinetic effects because it was assumed, that equilibration between saline solution and concrete adjust not instantaneous. Hence, the flux of solution was stopped for 12, 23, 34 and 83 days in all concrete samples, which were exposed to NaCl solution and for 18, 28, 45 and 76 days in all concrete samples, which were exposed to MgCl_2 solution simultaneously. Two solution samples were taken from all concrete samples at the end of each stop (without stop after 83/76 days). The first solution sample was taken at some

5 ml. The volume of this solution sample was chosen to be very small to avoid dilution with unreacted fresh solution. It was assumed that this volume of solution was enclosed in the samples while flux of solution was stopped. Hence, this solution had more time to equilibrate with the concrete than solution which percolated the samples continuously. The second sample was taken at some 25 ml. It aimed at determining permeability after solution was enclosed in the samples and to compare solution compositions between solutions, which was enclosed in the sample for a while and had more time for equilibration consequently and those solutions, which percolated the samples continuously with very short equilibration times. After enclosure of 83/76 days 25 ml sample were taken only.

- Step 3: Continuous percolation of solution through the concrete samples – three to four solutions samples of 25 ml were produced. In this experimental phase it was checked if there is a difference in development of solution composition and permeability between phase of “stop-and-flow” experiments and continuously percolation of solution through the samples.

Combined samples of salt concrete fitted into hollow cylinders of rock salt

In a second part of experiments combined samples of concrete and rock salt were investigated. Therefore a salt concrete core was coated with salt slurry and inserted in a hollow rock salt cylinder. This special construction offers the possibility to investigate the development at the contact seam, which is to be assumed to be the weak point of a sealing element.



Fig. 4.43 Combined sample of salt concrete and rock salt

Sample preparation of combined samples was very complex: Dimensions of the hollow rock salt cylinder and the salt concrete core were first cut at the turning machine. The combined samples had a length of 10.0 cm and a diameter of 7.0 cm. The diameter of the concrete core was 3.5 cm. Afterwards, the concrete core was coated with salt slurry (powdered rock salt left over from turning plus water) and inserted in the hollow rock salt cylinder. The combined samples were dried in vacuum with P_4O_{10} in an exsiccator.

Advection experiments with combined samples were performed in advection cells without confining stress, corresponding to the advection experiments with pure soerel concrete samples described in section before and in isostatic cells with confining stress. The main difference is that in isostatic cells a confining pressure influenced the development of permeability in addition to hydraulic and chemical influences. Samples in advection cells were only exposed to hydraulic and chemical influences. Both results will be shown in chapter 4.4.2.



Fig. 4.44 Installation of the combined sample in the isostatic cell with rubber jacket

In contrast to advections experiments on pure sored concrete samples the combined samples were all exposed to NaCl solution in the beginning of experiments. The presence of NaCl solution results in a reduction of the integral permeability. If the permeability was reduced to a level $< 1 \cdot 10^{-18} \text{ m}^2$, the solution were changed to MgCl_2 solution. Another succession during percolation of saline solutions was not useful: in pre-experiments the combined samples were primary percolated with MgCl_2 solution. In that case the MgCl_2 solution percolated the samples at the contact seam very fast and the storage bottles with saline solution would be evacuated in a couple of minutes. Meaningful results of the development of permeability could not be produced. Therefore, the positive effect of NaCl solution was exploited for reduction of the integral permeability and combined samples were firstly exposed to MgCl_2 solution after permeability was low. In this way the impact of corrosive MgCl_2 solution on a combined sealing element of salt concrete and rock salt could be reasonable investigated.

Advection experiments were performed as “stop-and-flow” during experiments with NaCl solution and with continuous percolation during samples were exposed to MgCl_2 solution. In “stop-and-flow” experiments flux of NaCl solution was enclosed in the samples between permeability measurements. “Stop-and-flow” experiments were conducted because it could not be expected, that equilibrium between saline solution and concrete is attained instantaneously. In addition, percolation of NaCl solution in the beginning of advection experiments may result in flushing out of the salt slurry from the contact seam. Hence, the NaCl solution was only injected at the contact seam between salt concrete and rock salt so that there was more equilibration time for reaction between NaCl solution and salt concrete. Once a week NaCl solution was percolated

short time to determine permeability and to substitute the reacted versus fresh NaCl solution.

4.4.2 Laboratory results of advection experiments

4.4.2.1 Advection experiments with sorel concrete – A1

Permeability of sorel concrete cores to gas was determined before start of advection experiments with saline solutions. Gas permeability was between 10^{-16} m^2 and 10^{-18} m^2 . Afterwards, advection experiments were commenced. The gas permeability measured before was considered so that samples with higher and lower gas permeability were investigated both in advection experiments with NaCl and MgCl_2 solution. Permeability to gas in each sample and its application in advection experiments with NaCl or MgCl_2 solution is given in appendix A 1.9 Tab. A 1.22.

Sorel concrete – A1 / NaCl solution

The initial permeability to NaCl solution was in the range of $2 - 3 \cdot 10^{-17} \text{ m}^2$ in all five sorel concrete samples. During determination of initial permeability samples were percolated continuously about ten days (Fig. 4.45). A small increase of permeability was already detectable to all samples within these ten days. After ten days “stop-and-flow” experiments were started and the percolation of NaCl solution was stopped for twelve days. At the end of this time period a new permeability was measured. Permeability increased to $4 - 5 \cdot 10^{-17} \text{ m}^2$ in all samples. With ongoing “stop-and-flow” experiments permeability increased to $8 \cdot 10^{-17} \text{ m}^2 - 1 \cdot 10^{-16} \text{ m}^2$ after solution was enclosed for 23 days and to $1 - 3 \cdot 10^{-16} \text{ m}^2$ after solution was enclosed for 34 days. After enclosure of solution for 34 days the velocity of development of permeability became different between the various sorel concrete samples. Especially, the permeability of core A1-10 was clearly higher than of the cores A1-3/-5/-7 and -9. Afterwards, NaCl solution was enclosed for 83 days. Permeability increased to $4 - 7 \cdot 10^{-16} \text{ m}^2$ in cores A1-3/-5/-7 and -9 and to $1 \cdot 10^{-15} \text{ m}^2$ in core A1-10. Finally, NaCl solution was percolated through the samples continuously again. With continuous percolation a small increase of permeability was measured. But this procedure aimed especially at comparing solution composition of solution, which was enclosed in the samples for a while and

solution, which percolated the samples continuously. These results will be presented below.

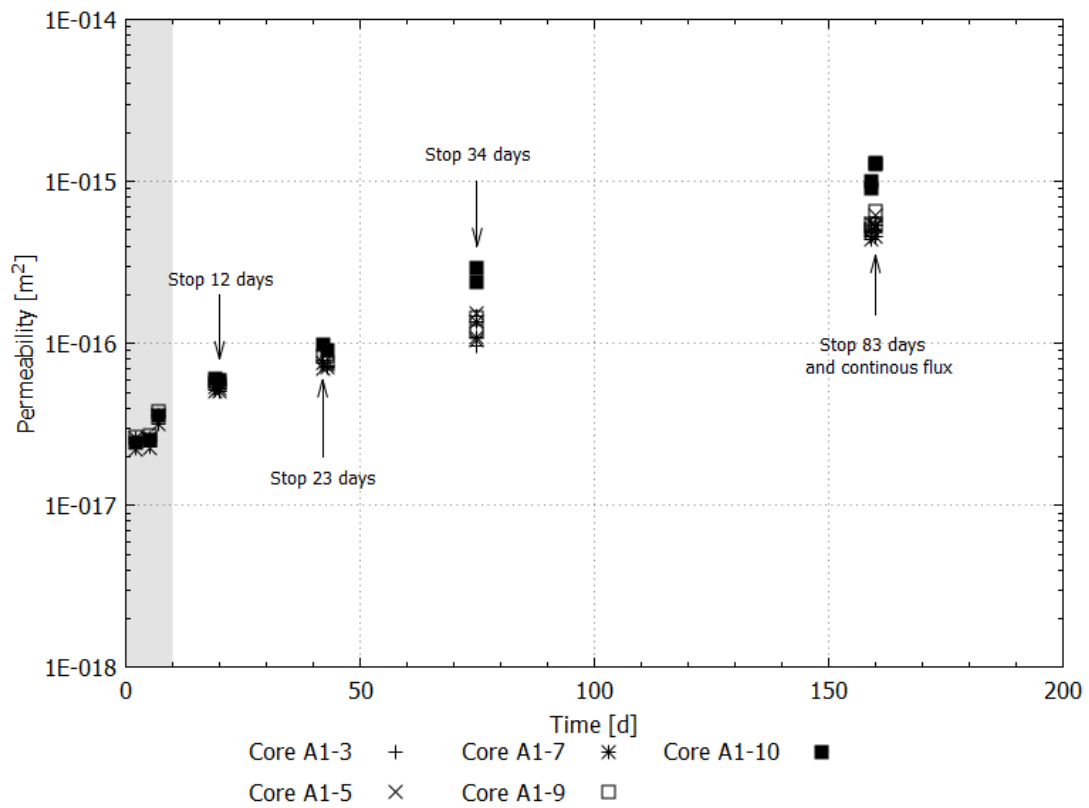


Fig. 4.45 Permeability development in advection experiments with sorel concrete – A1 and NaCl solution. Light grey rectangle marks time of continuous percolation in the beginning of experiments. Percolation was also continuous in the end of experiments (days 159/160). Blue data points describe solution composition of initial NaCl solution

Tab. 4.5 gives an overview of the volume of NaCl solution, which percolated the samples and the development of permeability at the various points of time at sampling. Results show, that permeability increase was higher if a small volume of solution was enclosed in the samples than if a five to six times higher volume of NaCl solution percolated the samples. This effect is also showed in Fig. 4.45: permeability differed less between the primary and second measurement of permeability after solution was enclosed in the samples but increased significantly when percolation was stopped and solution was enclosed.

Tab. 4.5 Overview of volume of passed through solution in [ml] and measured permeability in [m^2] in various cores during percolation of NaCl solution. Blue marked measurements present time periods of continuous percolation

Time	A1-3		A1-5		A1-7		A1-9		A1-10	
[d]	[ml]	[m^2]	[ml]	[m^2]						
2	16	2.3E ⁻¹⁷	16	2.2E ⁻¹⁷	19	2.6E ⁻¹⁷	19	2.7E ⁻¹⁷	17	2.4E ⁻¹⁷
5	59	2.3E ⁻¹⁷	59	2.2E ⁻¹⁷	68	2.6E ⁻¹⁷	68	2.7E ⁻¹⁷	64	2.5E ⁻¹⁷
7	97	3.2E ⁻¹⁷	97	3.2E ⁻¹⁷	111	3.6E ⁻¹⁷	112	3.8E ⁻¹⁷	107	3.6E ⁻¹⁷
19*	100	5.1E ⁻¹⁷	100	5.1E ⁻¹⁷	114	5.4E ⁻¹⁷	115	5.7E ⁻¹⁷	111	6.0E ⁻¹⁷
20	125	5.0E ⁻¹⁷	126	5.0E ⁻¹⁷	141	5.3E ⁻¹⁷	115	5.6E ⁻¹⁷	141	5.9E ⁻¹⁷
42*	130	7.9E ⁻¹⁷	131	7.0E ⁻¹⁷	146	7.6E ⁻¹⁷	148	8.4E ⁻¹⁷	147	9.8E ⁻¹⁷
43	171	7.2E ⁻¹⁷	173	7.4E ⁻¹⁷	187	7.1E ⁻¹⁷	189	7.5E ⁻¹⁷	189	9.1E ⁻¹⁷
75*	173	9.7E ⁻¹⁷	176	1.0E ⁻¹⁶	189	1.1E ⁻¹⁶	192	1.2E ⁻¹⁶	202	2.9E ⁻¹⁶
75	196	1.5E ⁻¹⁶	200	1.5E ⁻¹⁶	211	1.3E ⁻¹⁶	214	1.5E ⁻¹⁶	229	2.4E ⁻¹⁶
159*	221	5.0E ⁻¹⁶	227	5.5E ⁻¹⁶	235	4.9E ⁻¹⁶	241	5.5E ⁻¹⁶	277	1.0E ⁻¹⁵
159	238	4.6E ⁻¹⁶	253	5.0E ⁻¹⁶	258	4.4E ⁻¹⁶	266	5.1E ⁻¹⁶	313	9.1E ⁻¹⁶
160	256	4.6E ⁻¹⁶	273	5.2E ⁻¹⁶	274	4.5E ⁻¹⁶	286	5.4E ⁻¹⁶	344	1.3E ⁻¹⁵
160	282	5.4E ⁻¹⁶	304	6.2E ⁻¹⁶	301	5.3E ⁻¹⁶	317	6.5E ⁻¹⁶	381	1.3E ⁻¹⁵

* signed lines give measurement values after stop of percolation

Subsequent figures show the development of solution compositions with regard to their concentrations of sodium and chloride (Fig. 4.46), magnesium and sulphate (Fig. 4.47) and calcium and potassium (Fig. 4.48). The blue data points in each graphic present the initial concentration of elements in NaCl solution before reaction with sored concrete.

The initial concentrations of sodium and chloride were 6.13 - 6.45 mol/kg H₂O in the NaCl solution. Concentration of sodium was 2.69 - 3.00 mol/kg H₂O and of chloride 6.60 - 6.89 mol/kg H₂O in the first measurement of outflowing solution from advection experiments. But concentrations converged fast to initial concentrations of NaCl solution within the time period of continuous percolation of ten days. Sodium concentrations were 5.20 - 5.90 mol/kg H₂O and chloride 6.25 - 6.40 mol/kg H₂O in following measurements of "stop-and-flow" experiments. Sodium concentration increased again to circa 6.10 - 6.27 mol/kg H₂O if solution was percolated continuously again.

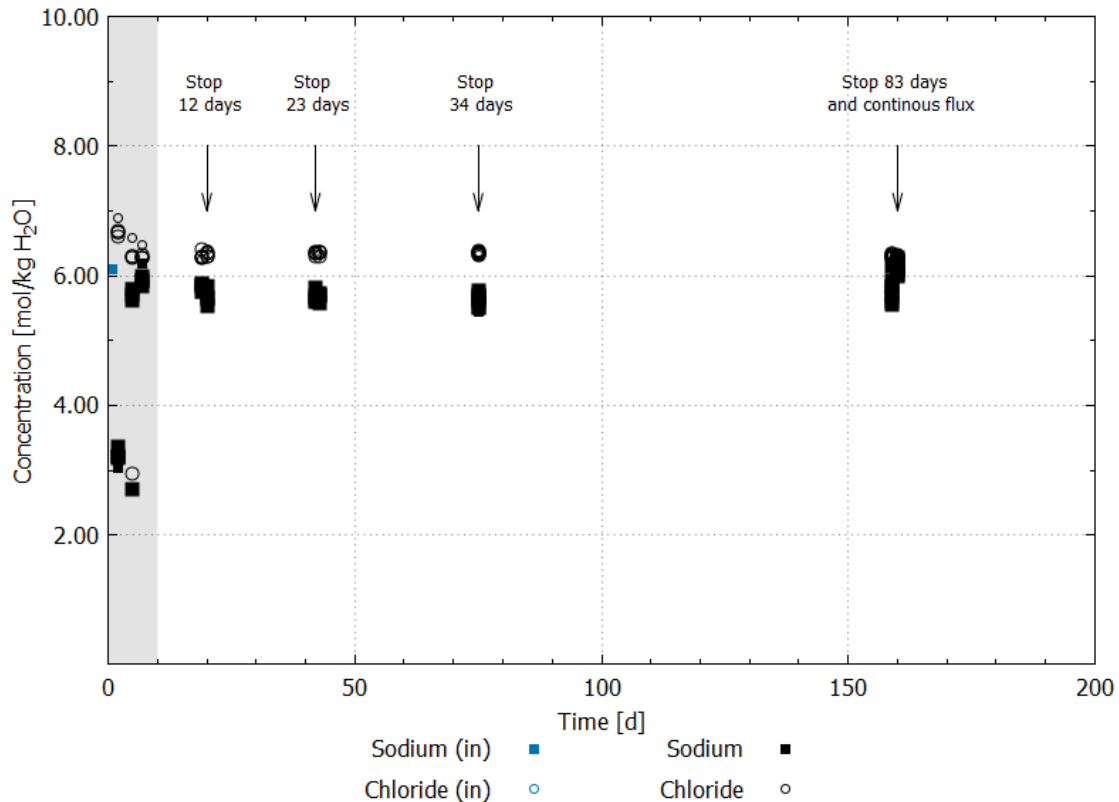


Fig. 4.46 Development of sodium and chloride concentrations in advection experiment with sorrel concrete – A1 and NaCl solution. Light grey rectangle marks time of continuous percolation in the beginning of experiments. Percolation was also continuous at the end of experiments (days 159/160). Blue data points describe solution composition of initial NaCl solution

The concentrations of magnesium and sulphate in the NaCl solution were below the detection limit. The first measurements of outflowing solutions showed a significant increase of magnesium concentrations to 1.58 - 1.87 mol/kg H₂O. But concentrations decreased fast within ten days to circa 0.17 - 0.20 mol/kg H₂O. An increase of magnesium concentrations was measurable again with start of “stop-and-flow” experiments: After solution was enclosed for twelve days concentration was 0.21 - 0.26 mol/kg H₂O ($x_t = 19$ days in Fig. 4.47) in first solution sample and 0.32 - 0.36 mol/kg H₂O in the second solution sample ($x_t = 20$ days). Analyzation of solutions after solution was enclosed for 23 days showed concentrations of 0.25 - 0.29 mol/kg H₂O ($x_t = 42$ and 43 days). The difference between concentrations of enclosed and percolated solution was not significant. Magnesium concentrations was

Laboratory investigations

0.31 – 0.39 mol/kg H₂O after solution was enclosed for 34 days ($x_t = 75$ days) and increased further during NaCl solution was percolated again. Because of the higher permeability both solution samples (5 ml and 25 ml) were taken at the same day ($x_t = 75$ days), hence, the difference of concentrations between the first and second solution sample is only to identify in the absolute concentrations in appendix A 1.4 . After solution was enclosed for 83 days the magnesium concentration was 0.30 - 0.39 mol/kg H₂O ($x_t = 159$ days). In the last experimental phase of continuously percolation about two days the magnesium concentration decreased to values < 0.16 mol/kg H₂O ($x_t = 160$ days).

The sulphate concentrations were below the detection limit in the initial solution and increased to about 0.04 mol/kg H₂O within five days. The concentration of sulphate was changed not significantly with ongoing advection experiment.

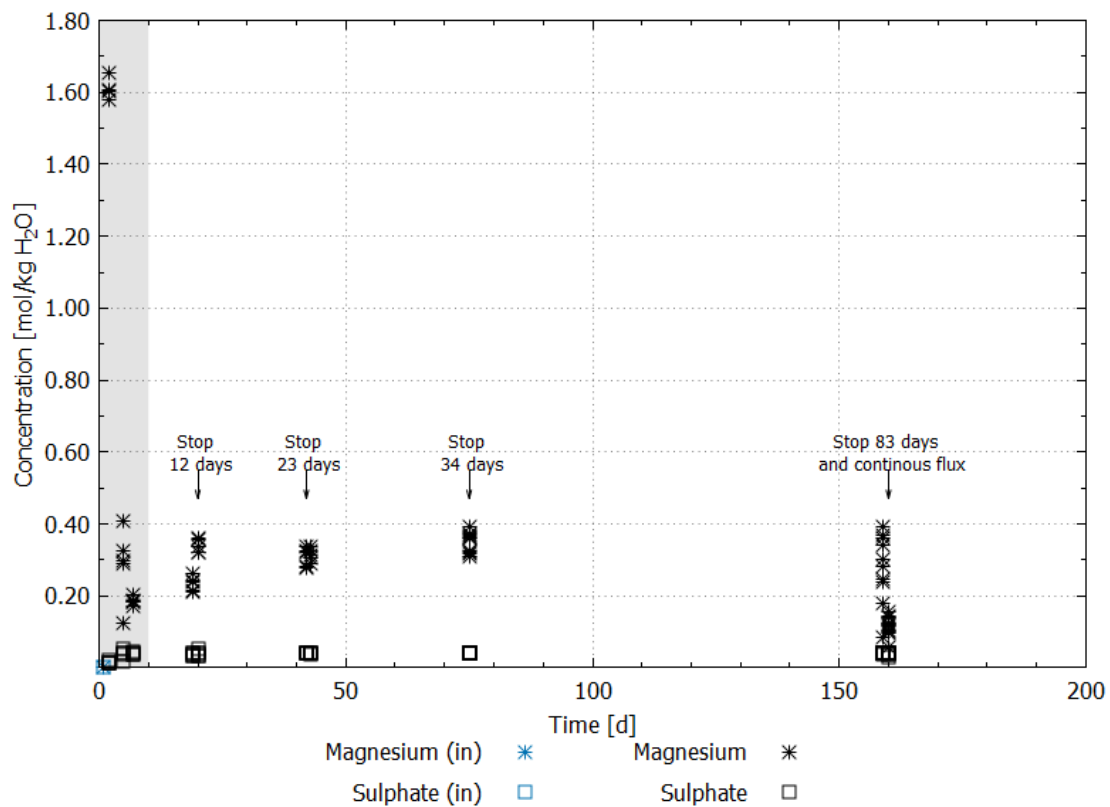


Fig. 4.47 Development of magnesium and sulphate concentrations in advection experiment with sored concrete – A1 and NaCl solution. Light grey rectangle marks time of continuous percolation at the beginning of experiments. Percolation was also continuous in the end of experiments (days 159/160). Blue data points describe solution composition of initial NaCl solution

Concentrations of calcium and potassium were below the detection limit in the initial NaCl solution. Potassium concentration increased in the first solution sample to 0.01 mol/kg H₂O but decreased direct within the second sample below the detection limit again. Concentration did not change with ongoing experiment.

The calcium concentration increased to circa 0.10 – 0.13 mol/kg H₂O in the beginning of advection experiment and decreased again within ten days to 0.04 mol/kg H₂O. This concentration changed not significantly during further “stop-and-flow” experiment in all samples and decreased finally a little to 0.03 mol/kg H₂O during percolation of NaCl solution.

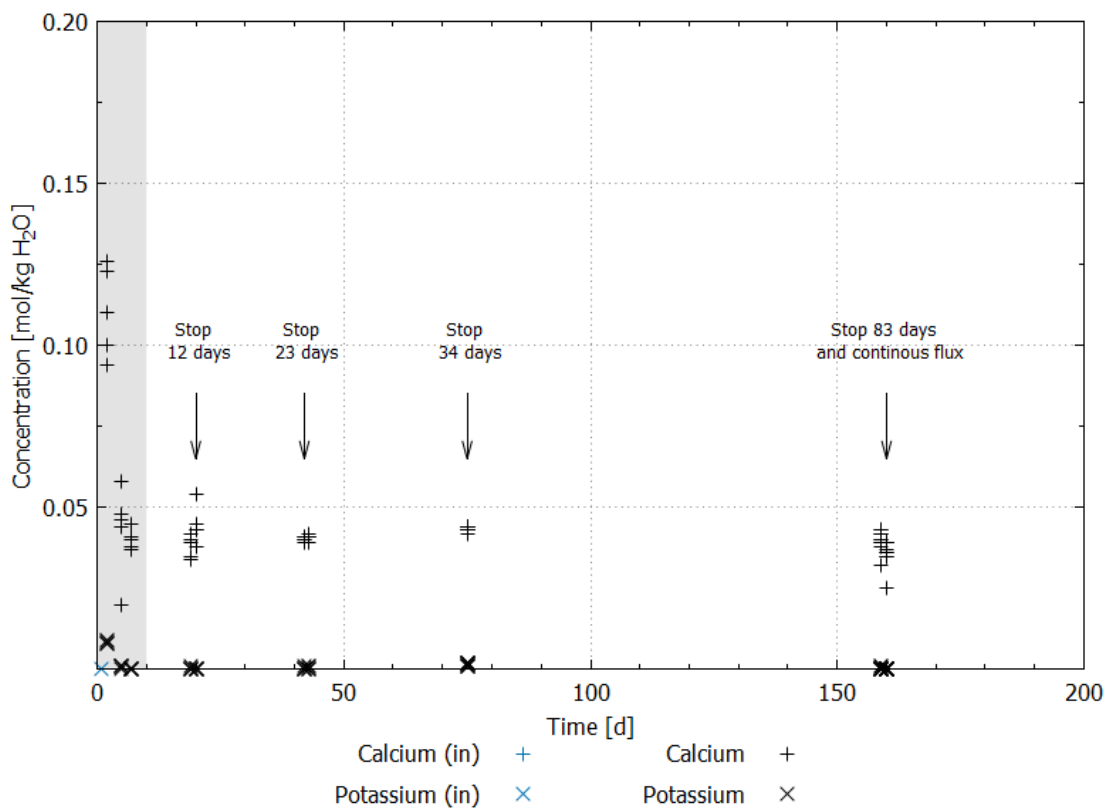


Fig. 4.48 Development of calcium and potassium concentrations in advection experiment with sorel concrete – A1 and NaCl solution. Light grey rectangle marks time of continuous percolation at the beginning of experiments. Percolation was also continuous at the end of experiments (days 159/160). Blue data points describe solution composition of initial NaCl solution

The p_{cH} of the outflowing solution increased in advection experiments to circa 7.42 - 8.41. In the initial NaCl solution p_{cH} was 6.75. The density changed not significantly in comparison to the initial density of NaCl solution (1.20 g/cm^3).

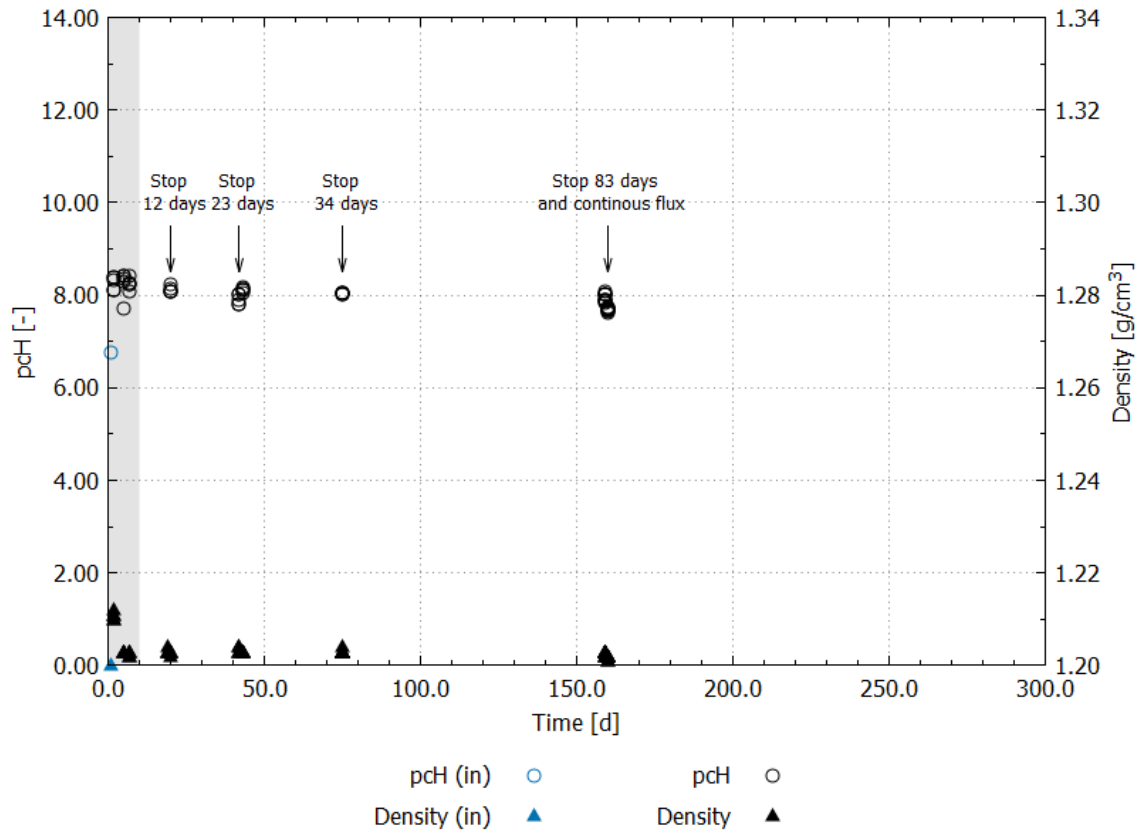


Fig. 4.49 Development of p_{cH} and density in advection experiment with sorel concrete – A1 and NaCl solution. Light grey rectangle marks time of continuous percolation at the beginning of experiments. Percolation was also continuous at the end of experiments (days 159/160). Blue data points describe p_{cH} and density of initial NaCl solution

Sorel concrete- A1 / $MgCl_2$ solution

The initial permeability between $5 \cdot 10^{-18} \text{ m}^2$ and $7 \cdot 10^{-18} \text{ m}^2$ to $MgCl_2$ solution was determined by continuous percolation of solution through the sorel concrete samples. No significant change in permeability was measureable within the time period of ten days during continuous percolation. Development of permeability during phase of “stop-and-flow” experiments is described below. Two solution samples were taken after every stop corresponding to advection experiments with NaCl solution: primary a small

sample of 5 ml for analysis of solution, which was enclosed in the samples and second a solution sample of 25 ml to receive a comparison between the composition of enclosed and percolated solution. Permeability was determined simultaneously and is described as first and second permeability measurement below. After $MgCl_2$ solution was enclosed for 18 days ($x_t = 40$ days in Fig. 4.50) permeability decreased a little and became lower in the second permeability measurement ($x_t = 43$ days). The enclosure of solution for 28 days induced decrease of permeability to $2 \cdot 10^{-18} m^2$ ($x_t = 54$ days). But permeability decreased further during 25 ml $MgCl_2$ solution percolated the samples unless in core A1-2. After solution enclosure of 45 days permeability decreased to values of $2 \cdot 3 \cdot 10^{-18} m^2$ ($x_t = 84$ days) and was reduced further during the second permeability measurement afterwards. Last stop of 76 days reduced permeability to values $< 2 \cdot 10^{-18} m^2$. In the following time period $MgCl_2$ solution percolated the samples continuously again. No further significant change in permeability was measurable in this time period anymore.

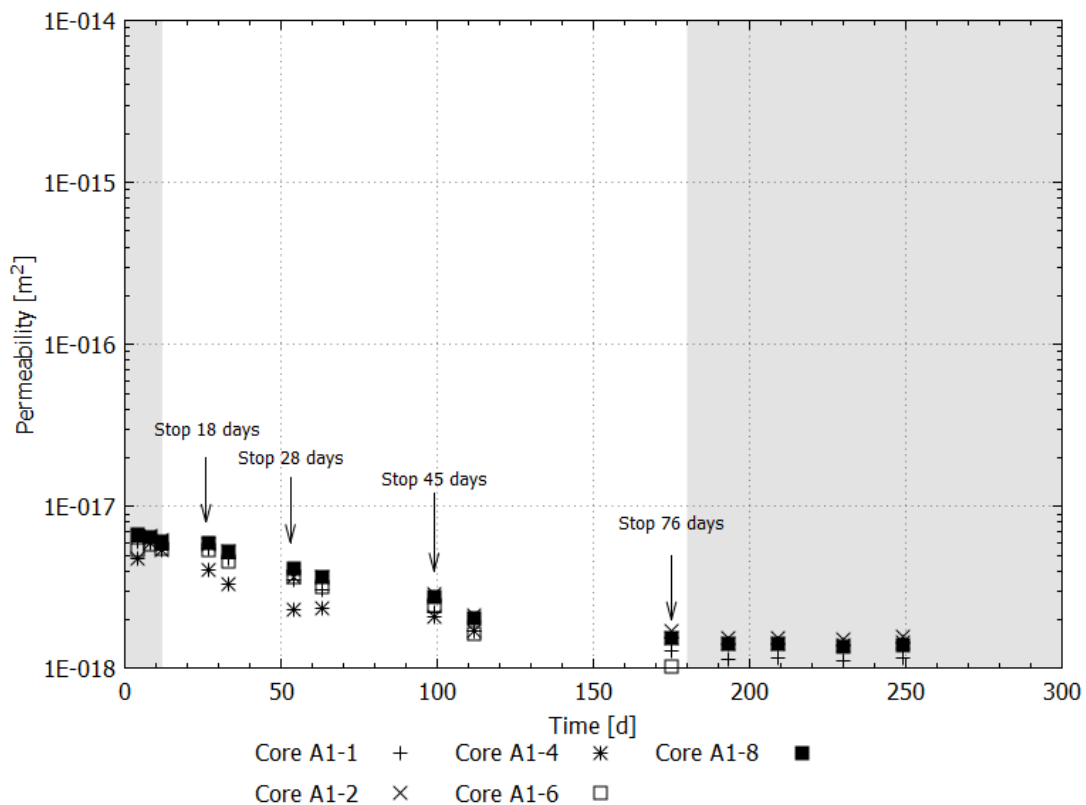


Fig. 4.50 Permeability development in advection experiments with sorrel concrete – A1 and $MgCl_2$ solution. Light grey rectangles mark time of continuous percolation at the beginning and end of experiments. Time period between is characterized by “Stop and flow” experiments

An overview of the volume of MgCl_2 solution, which percolated the cores at various points of time, and the measured permeability, is given in Tab. 4.6 in addition to Fig. 4.50. Results showed that a stop of 18 days caused no significant impact on change of the permeability, but stops of 28, 45 and 76 days. The percolation of MgCl_2 solution direct after the stops of 18 and 28 days showed no significant impact on permeability during more volume of MgCl_2 solution percolated the core than during the stops was enclosed in the samples. But permeability decreased during percolation of solution for second permeability measurement after stop of 45 days too. Because of the low permeability time of percolation was longer after 45 days to receive the defined volume of outflowing solution. Finally, MgCl_2 solution was percolated continuously again. An impact on permeability was not detected even though solution percolated very slowly caused by the low permeability.

Tab. 4.6 Overview to volume of passed through solution in [ml] and measured permeability in [m^2] in various cores during percolation of $MgCl_2$ solution. Blue marked measurements present time periods of continuous percolation. With * signed lines give measurement values after stop of percolation.

Time	A1-1		A1-2		A1-4		A1-6		A1-8	
[d]	[ml]	[m^2]								
4	11	$6.1E^{-18}$	11	$6.4E^{-18}$	8	$4.7E^{-18}$	9	$5.4E^{-18}$	12	$6.7E^{-18}$
8	26	$6.2E^{-18}$	27	$6.6E^{-18}$	23	$6.0E^{-18}$	23	$5.8E^{-18}$	28	$6.5E^{-18}$
12	40	$5.5E^{-18}$	43	$6.2E^{-18}$	36	$5.4E^{-18}$	37	$5.5E^{-18}$	43	$6.1E^{-18}$
27*	43	$5.5E^{-18}$	46	$5.8E^{-18}$	39	$4.1E^{-18}$	41	$5.4E^{-18}$	47	$6.0E^{-18}$
33	62	$4.8E^{-18}$	66	$5.2E^{-18}$	51	$3.3E^{-18}$	58	$4.6E^{-18}$	68	$5.3E^{-18}$
54*	64	$3.5E^{-18}$	69	$3.6E^{-18}$	54	$2.3E^{-18}$	60	$3.6E^{-18}$	70	$4.2E^{-18}$
63	81	$3.1E^{-18}$	89	$3.7E^{-18}$	66	$2.4E^{-18}$	78	$3.2E^{-18}$	91	$3.7E^{-18}$
99*	84	$2.2E^{-18}$	93	$2.9E^{-18}$	68	$2.1E^{-18}$	81	$2.4E^{-18}$	95	$2.8E^{-18}$
112	98	$1.7E^{-18}$	110	$2.1E^{-18}$	82	$1.7E^{-18}$	95	$1.6E^{-18}$	112	$2.1E^{-18}$
175*	109	$1.3E^{-18}$	124	$1.7E^{-18}$	94	$1.5E^{-18}$	103	$1.0E^{-18}$	125	$1.5E^{-18}$
193	122	$1.1E^{-18}$	142	$1.5E^{-18}$	111	$1.4E^{-18}$	114	$9.4E^{-19}$	142	$1.4E^{-18}$
209	135	$1.2E^{-18}$	158	$1.5E^{-18}$	125	$1.4E^{-18}$	124	$9.3E^{-19}$	156	$1.4E^{-18}$
230	151	$1.1E^{-18}$	179	$1.5E^{-18}$	144	$1.4E^{-18}$	137	$8.9E^{-19}$	176	$1.4E^{-18}$
249	165	$1.2E^{-18}$	199	$1.6E^{-18}$	162	$1.5E^{-18}$	148	$9.5E^{-19}$	193	$1.4E^{-18}$

In the following the results of solution analysis are showed. Blue data points describe concentrations of initial $MgCl_2$ solution. Initial sodium concentration was $0.49 \text{ mol/kg H}_2\text{O}$. First measurement of outflowing solution in advection experiments had a concentration between to $2.55 \text{ mol/kg H}_2\text{O}$ and $2.96 \text{ mol/kg H}_2\text{O}$, but concentrations decreased with ongoing experiment to $0.49 - 0.53 \text{ mol/kg H}_2\text{O}$. In the last phase of the advection experiment (continuous percolation) approximately the initial sodium concentration of $MgCl_2$ solution was measured. Chloride concentration of initial $MgCl_2$ solution was $9.01 \text{ mol/kg H}_2\text{O}$. Concentration decreased clearly during percolation of $MgCl_2$ solution in the beginning of experiments (up to twelve days) to circa $6.68 - 7.71 \text{ mol/kg H}_2\text{O}$ respectively. In the following time period of “stop-and-flow” experiments concentrations varied between $7.80 - 8.68 \text{ mol/kg H}_2\text{O}$. The initial concentration of chloride is finally approximately achieved in the last phase of continuously percolation (from 180 days).

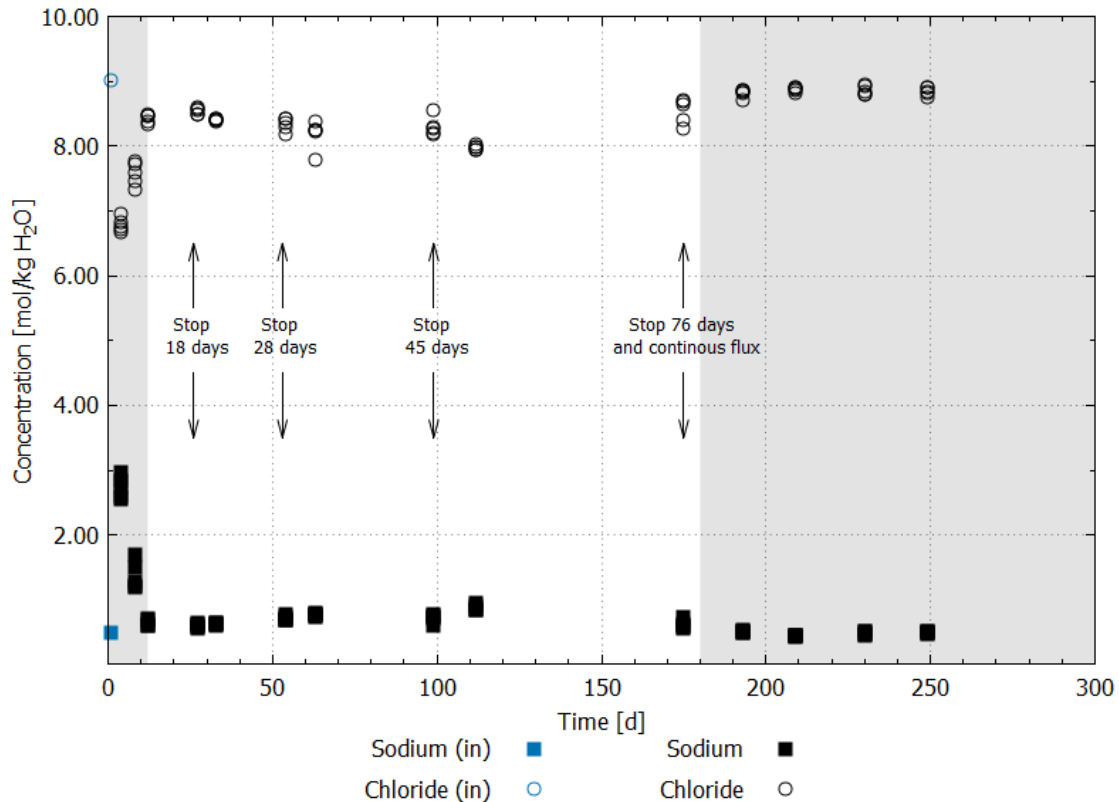


Fig. 4.51 Development of sodium and chloride concentrations in advection experiment with sored concrete – A1 and MgCl₂ solution. Light grey rectangles mark time of continuous percolation at the beginning and end of experiments. Time period between is characterized by “Stop and flow” experiments. Blue data points describe solution composition of initial MgCl₂ solution

Initial magnesium concentration of MgCl₂ solution was 4.36 mol/kg H₂O in average. Within the first experimental phase (up to ten days) concentration was clearly lower: 1.75 - 2.02 mol/kg H₂O after four days and 2.71 - 3.17 mol/kg H₂O after eight days. In the phase of “stop-and-flow” magnesium concentration increased to values between 3.49 - 4.13 mol/kg H₂O. In the sample, which was taken for second permeability measurements after solution was enclosed for 45 days ($x_t = 112$ days) the magnesium concentrations was lower in comparison to samples taken before. In the last phase of the advection experiment (continuous percolation) the magnesium concentrations approximates to the initial concentrations of magnesium in MgCl₂ solution again.

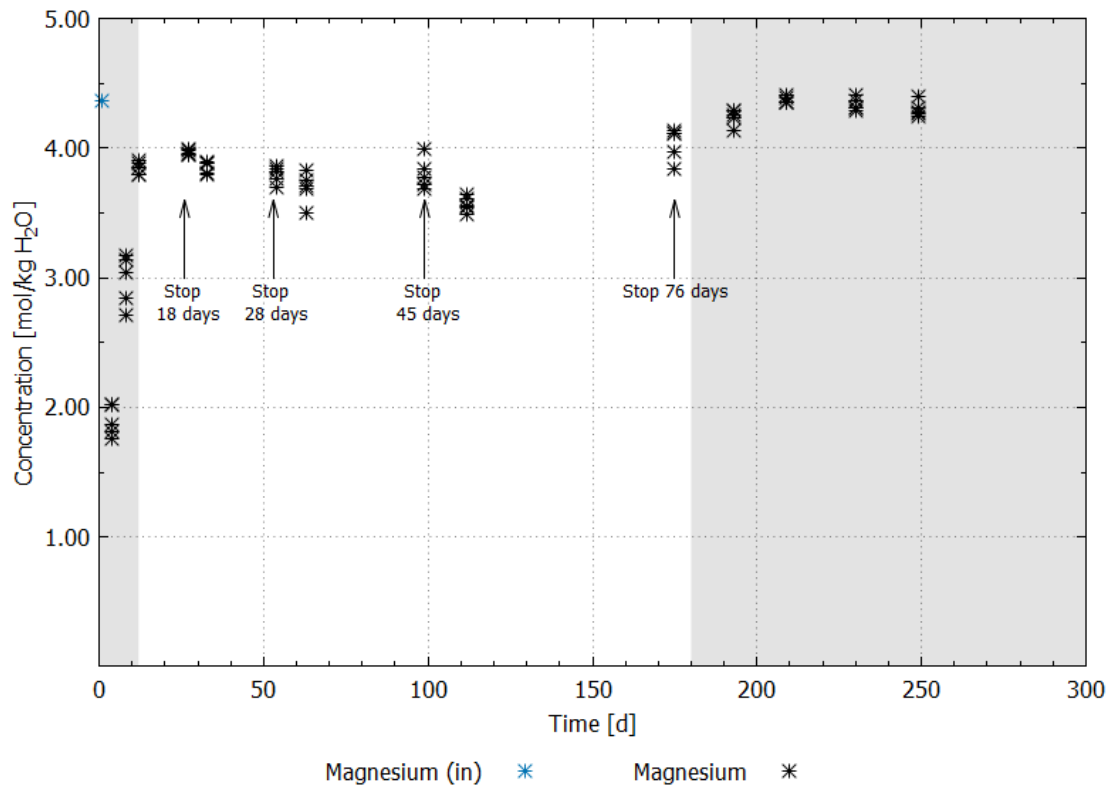


Fig. 4.52 Development of magnesium concentrations in advection experiment with sorrel concrete – A1 and MgCl₂ solution. Light grey rectangles mark time of continuous percolation at the beginning and end of experiments. Time period between is characterized by “Stop and flow” experiments. Blue data points describe solution composition of initial MgCl₂ solution

Fig. 4.53 shows calcium, potassium and sulphate concentrations during the advection experiment. The calcium concentration was 0.001 mol/kg H₂O in initial MgCl₂ solution. Calcium concentration increased short time in the first solution sample during continuous percolation in the beginning to 0.11 - 0.13 mol/kg H₂O but decreased afterwards to its initial concentration. Initial potassium concentration was about 0.57 mol/kg H₂O. Potassium concentration decreased interim to concentrations of 0.01 - 0.03 mol/kg H₂O ($x_t = 4$ days) but increased significantly with start of “stop-and-flow” experiments. During time period of “stop-and-flow” potassium concentration increased continuously from stop to stop up to 0.80 – 0.83 mol/kg H₂O. After solution was enclosed for 76 days, potassium concentration decreased to concentrations of

0.68 - 0.74 mol/kg H₂O. During time period of continuous percolation at the end of experiment nearly the initial concentration of potassium was achieved. The development of sulphate concentrations was similar to the potassium concentrations: The initial concentration was about 0.29 mol/kg H₂O. Concentrations decreased in the first solution sample during continuous percolation to values of 0.01 - 0.02 mol/kg H₂O but increased with ongoing experiment and start of “stop-and-flow” experiments up to 0.34 - 0.42 mol/kg H₂O after solution was enclosed for 45 days ($x_t = 99$ days). Concentration after enclosure of solution for 76 days is less low. If solution percolated continuously again, concentrations decrease to the initial level of MgCl₂ solution.

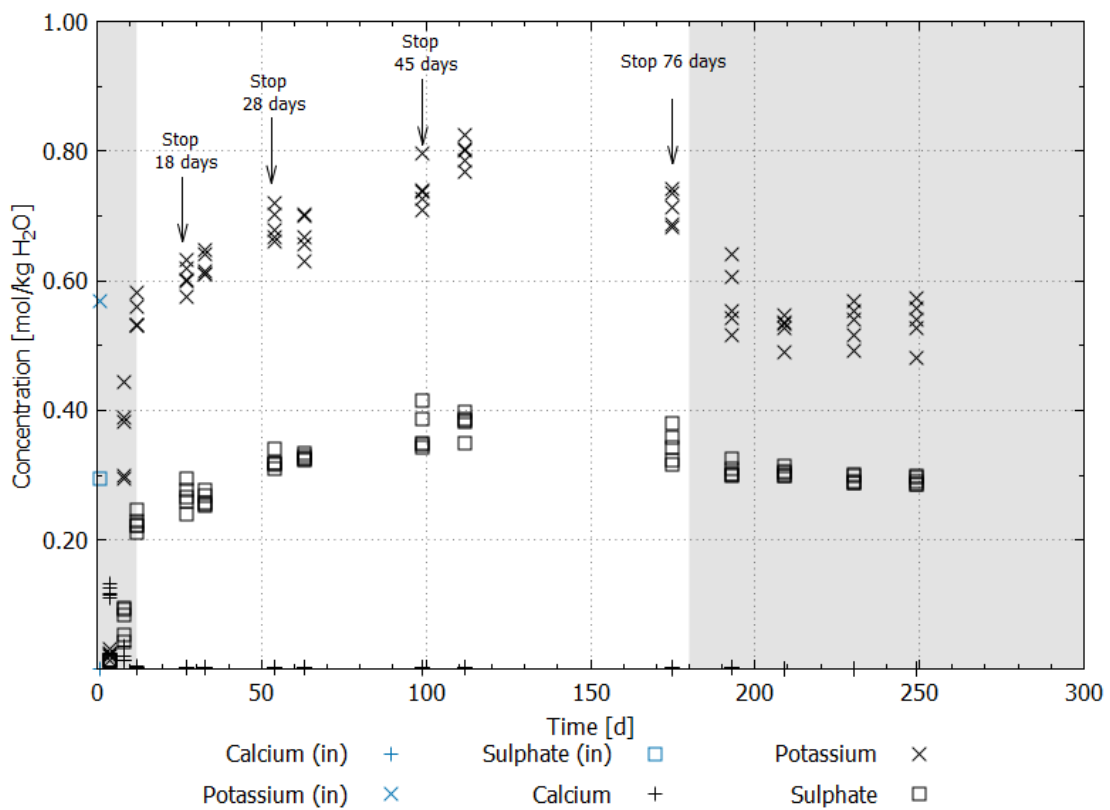


Fig. 4.53 Development of calcium, potassium and sulphate concentrations in advection experiment with sored concrete – A1 and MgCl₂ solution. Light grey rectangles mark time of continuous percolation at the beginning and end of experiments. Time period between is characterized by “Stop and flow” experiments. Blue data points describe solution composition of initial MgCl₂ solution

The p_{cH} increased from 7.15 in the initial solution to circa 8.36 to 8.77 in the outflowing solution. This value changed not significantly with time. Density decreased in comparison to initial solution from 1.29 g/cm^3 to 1.21 g/cm^3 in the first sample of outflowing solution. Afterwards, density increased to 1.28 g/cm^3 during phase of “stop-and-flow”. Finally, density corresponded to its initial value of 1.29 g/cm^3 in last phase of continuous flux.

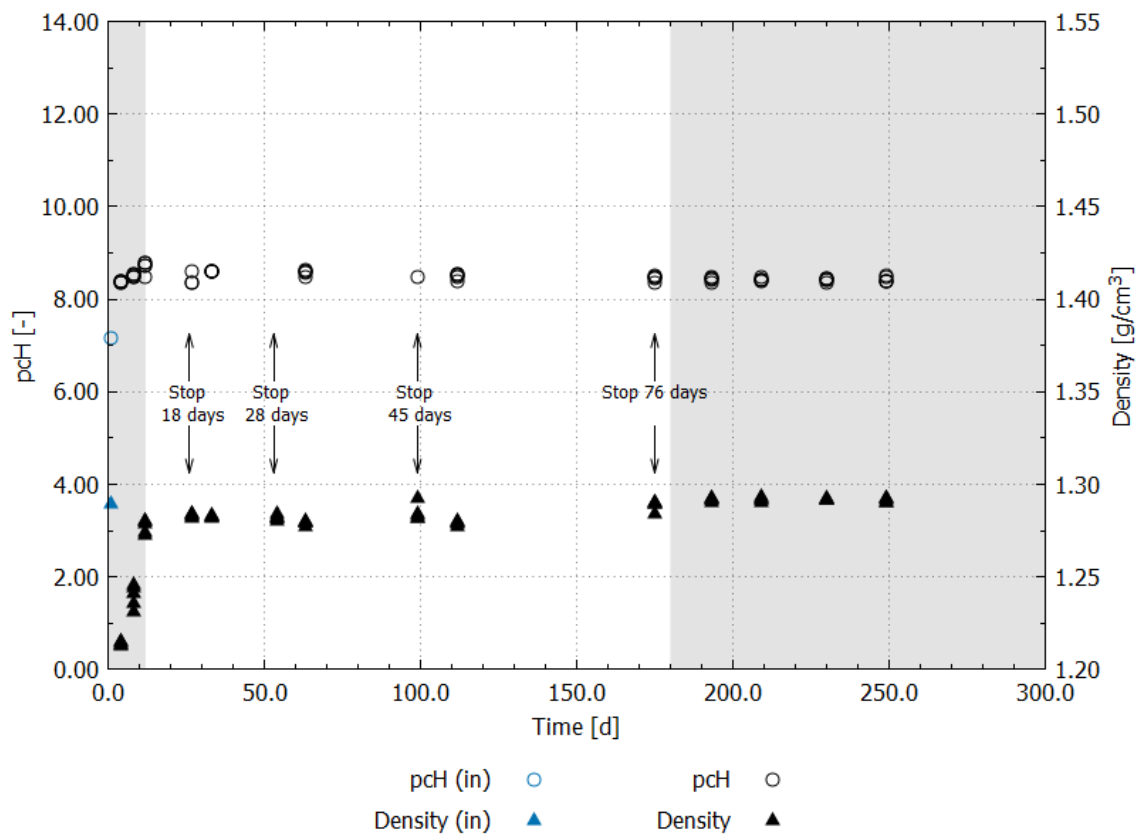


Fig. 4.54 Development of p_{cH} and density in advection experiment with sorel concrete – A1 and MgCl_2 solution. Light grey rectangles mark time of continuous percolation at the beginning and end of experiments. Time period between is characterized by “Stop and flow” experiments. Blue data points describe p_{cH} and density of initial MgCl_2 solution

4.4.2.2 Advection experiments with combined samples of rock salt and salt concrete

Based on permeability measurements to gas in salt concrete cores, advection experiments with salt concrete corresponding to equivalent experiments with sored concrete did not seem to be meaningful because permeability was very low ($< 10^{-19} \text{ m}^2$) or samples were even gas tight. Hence, a method was developed to investigate the integral permeability of a complete sealing element at laboratory scale as described in chapter 4.3.2. Permeability to gas of rock salt cores was also measured before combined samples were produced. Rock salt cores had also very low permeability or were gas tight. Measured permeability of salt concrete and rock salt cores are listed in appendix A 1.10 Tab. A.1.26 and Tab. A.1.27. In addition these Tables (Tab. A.1.26 and Tab. A.1.27) give an overview which core was plugged in which combined sample.

a) Pilot test

The pilot test refers to first laboratory test with a combined core of salt concrete in a hollow rock salt cylinder, which was exposed to MgCl_2 solution. In phase 1 the combined sample was exposed to a confining stress of 10 MPa to simulate the convergence of the host rock. In addition saturated NaCl solution was injected. The combination of confining stress and NaCl solution resulted in a decrease of permeability to $8 \cdot 10^{-18} \text{ m}^2$. The previous history of this combined sample is especially interesting for investigations on the influence of confining stress and is not representative for the following investigations. How the previous history is related to geomechanic properties is for this reason not discussed in this thesis, but is in detail reported in /JAN 2016c/.

In second experimental phase the confining stress was reduced to 2 MPa and afterwards the injected solution were changed to MgCl_2 solution. The fluid injection pressure was increased from 0.1 MPa to circa 0.7 MPa at the same time. This resulted in an increase of permeability to MgCl_2 solution to $5 \cdot 10^{-17} \text{ m}^2$. After solution injection pressure was reduced to 0.1 MPa again a decrease of permeability was measured. After circa 1500 hours reaction with MgCl_2 solution ($x_t = 3400$ hours in Fig. 4.55) permeability was decreased some one order to $5 \cdot 10^{-17} \text{ m}^2$. But with ongoing experimental time permeability increased again and was some $2 \cdot 10^{-16} \text{ m}^2$ at the end of experiment after 3000 hours of reaction with MgCl_2 solution ($x_t = 5250$ hours).

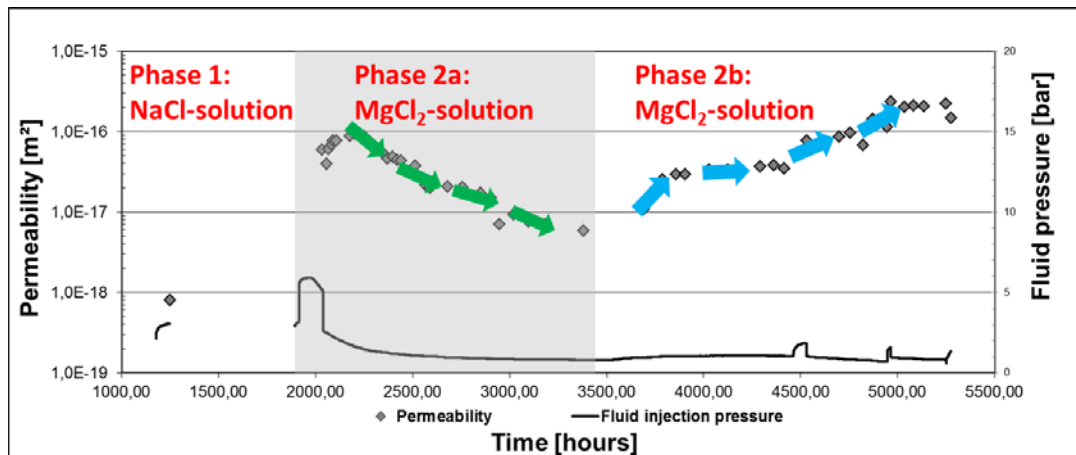


Fig. 4.55 Pilot test of advection experiment in isostatic cell with combined samples of salt concrete and rock salt

In Fig. 4.56 the development of outflowing solution in the pilot test is shown. The measured concentrations of sodium, chloride, calcium, potassium, magnesium and sulphate showed no significant deviation to the concentrations of initial $MgCl_2$ solution.

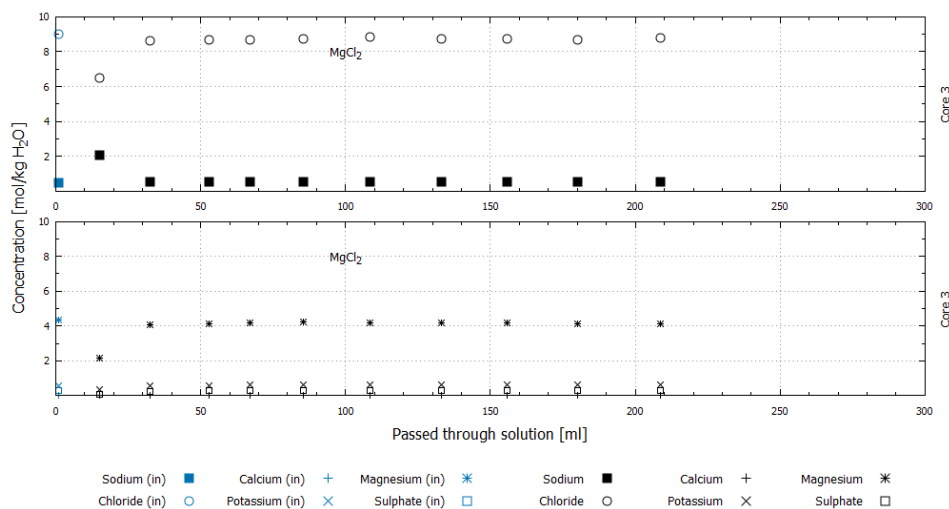


Fig. 4.56 Development of solution composition in pilot test of advection experiments in isostatic cell with combined samples of salt concrete and rock salt. Blue data points describe solution composition of initial $MgCl_2$ solution

This test was the pilot test for experiments with combined samples of salt concrete inserted in hollow rock salt cylinders in isostatic cells. For further investigations of the process a comprehensive laboratory program with combined samples was carried out.

In this program the influence of NaCl solution to the process of permeability reduction was investigated too before the influence of MgCl₂ solution was researched. The results are shown below.

b) Experiments in isostatic cells

“Stop-and-flow” experiments with NaCl solution

Comparison of combined samples showed an initial permeability to NaCl solution between 10^{-13} m^2 and 10^{-16} m^2 after installation in isostatic cells. Initial permeability was measured with a confining stress of 1.0 to 1.5 MPa, a solution injection pressure of 0.1 MPa, and refers to the integral permeability of the complete sealing element consisting of EDZ, contact seam and sealing of salt concrete. The small variation of confining stress is due to the experimental set up in laboratory, which is influenced by small variations in temperature. A significant effect on permeability was not assumed.

The initial permeability depended significantly from the fitting accuracy of the internal salt concrete core in the hollow rock salt cylinder. Hence, it may be assumed that the contact seam is the primary pathway for solutions. The experimental results in Fig. 4.57 show that the rate of reduction of the permeability of the contact seam depends on the initial permeability and consequently on the fitting accuracy of salt concrete core and rock salt cylinder.

In core 1 the initial permeability was around 10^{-13} m^2 and decreased very slowly. After circa 80 days confining stress was increased to 5 MPa for acceleration of the minimizing process. After 200 days permeability was around 10^{-18} m^2 and the confining stress was reduced to 1 MPa again. Afterwards, the permeability increased to 10^{-17} m^2 .

Initial permeability in core 2 was 10^{-14} m^2 at the beginning. The confining stress was increased to 5 MPa within a time period of 40 to 50 days. But an impact on the permeability was not detectable. Permeability reduced to 10^{-18} m^2 within circa 120 days. After 150 days no permeability was measureable anymore.

Core 3, 4, 5 and 8 developed very similar with the main difference in the initial permeability: core 3 had the highest initial permeability near 10^{-13} m^2 and core 5 and 8 the lowest near 10^{-15} m^2 . Permeability in each core was minimized with a constant confining stress of 1 MPa and the target permeability of 10^{-18} m^2 was achieved in circa

Laboratory investigations

50 days (core 3 and 4), in core 5 and 8 even after 25 days. Permeability in core 4 was further minimized until no flux was measurable anymore after circa 80 days.

Initial permeability of core 6 was 10^{-13} m^2 and permeability was reduced to 10^{-15} m^2 within the next 30 days. Afterwards, permeability minimizing to core 6 was stopped.

Core 7 finally had the lowest initial permeability of 10^{-17} m^2 . The confining stress was directly increased to 3 MPa for three days. Permeability decreased very fast to 10^{-18} m^2 and afterwards the confining stress was reduced to 1 MPa. However, permeability decreased further to 10^{-20} m^2 .

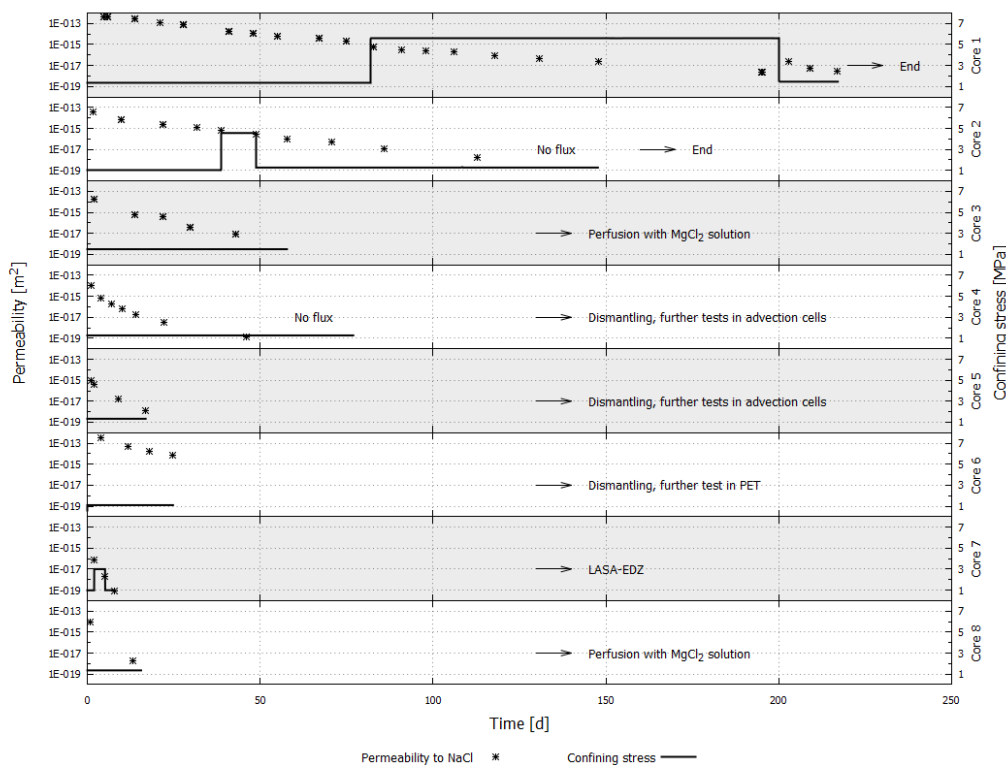


Fig. 4.57 Development of permeability in combined samples in isostatic cells with influence of saturated NaCl solution and confining stress

Afterwards, various tests were performed with the various cores. Core 1 was dismantled without further investigation. Because of the long process of permeability reduction core 1 did not seem to be representative. The permeability of core 3 and core 8 was further investigated in isostatic cells, but solution was changed to MgCl_2

solution (Fig. 4.58 and Fig. 4.59). Core 4 and 5 were dismantled and permeability was further investigated in advection cells without a confining stress. Results of cores 4 and 5 are shown in the next section “Experiments in advection cells”. Core 7 was dismantled too but was not further investigated with regard to chemical-hydraulic effects. Core 6 finally was dismantled very early, because this core served for investigations of the contact seam and diffusion using positron emission tomography (PET) at HZDR.

Percolation with $MgCl_2$ solution

Permeability to $MgCl_2$ solution in core 3 decreased further to $3 \cdot 10^{-19} \text{ m}^2$ after change of solution. But with ongoing experiment permeability increased to about $2 \cdot 10^{-18} \text{ m}^2$. This order of permeability was constant during the remaining experimental time. Permeability in core 8 was about $1 \cdot 10^{-19} \text{ m}^2$ after change to $MgCl_2$ solution, increased slowly to $3 \cdot 10^{-19} \text{ m}^2$ and seemed to be approximately constant afterwards. Because of the small permeability solution passed the sample very slowly and no further measurements of permeability could be conducted anymore during experimental time.

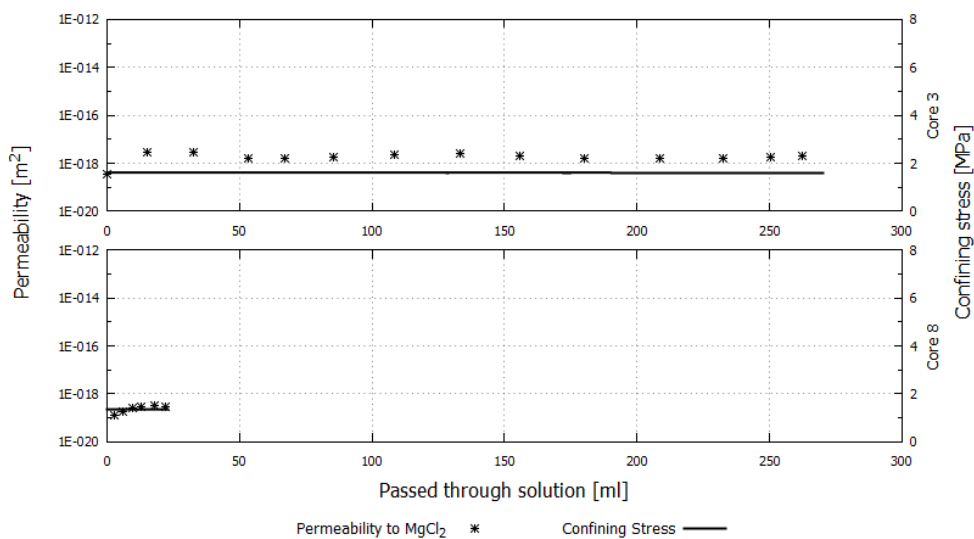


Fig. 4.58 Development of permeability of core 3 and core 8 in isostatic cells after changing to $MgCl_2$ solution

Because of the small permeability in core 8 the volume of outflowing solution was too small for analysis. Hence, only solution analysis of core 3 is shown below (Fig. 4.59). As in earlier presentations of solution analysis, concentrations of initial $MgCl_2$ solution

are shown in comparison with concentrations of outflowing solution. The solution of the first permeability measurement ($x = 0.02$ ml in Fig. 4.58) could not be analysed because of its small volume. Hence, first solution was analysed after flow through of 15 ml $MgCl_2$ solution. This solution had increased concentration of sodium of some 1.5 mol/kg H_2O and chloride concentration was decreased by some 2.5 mol/kg H_2O in comparison to initial solution. Magnesium concentration also decreased to 2.13 mol/kg H_2O in the first sample but increased to magnesium concentration of initial solution with ongoing percolation of $MgCl_2$ solution. Concentrations of calcium, potassium and sulphate did not change significantly compared to initial concentration. After percolation of circa 30 ml $MgCl_2$ solution all concentrations of outflowing solution corresponded to concentrations of initial (inflowing) solution. There were no further significant changes in solution concentrations with ongoing percolation.

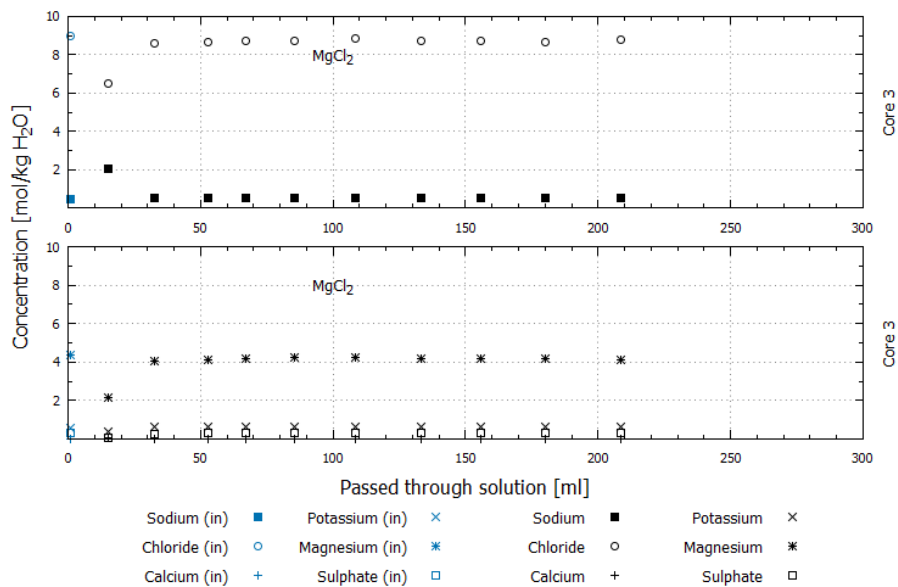


Fig. 4.59 Development of solution composition during flowing through of $MgCl_2$ solution in core 3 in isostatic cells. Blue data points describe solution composition of initial $MgCl_2$ solution

Experiments in advection cells

This section presents results of permeability measurements to combined samples, which were pressure less cast in advection cells. The previous history of core 4 and 5 was described in section “Experiments in isostatic cells” before. Both samples were afterwards dismantled from isostatic cells and inserted in advection cells as described

in chapter 4.3.2. First both samples were percolated with $MgCl_2$ solution. But solution passed both samples directly very fast, hence, a measurement of permeability was not meaningful. Thus, both advection cells were opened again and the contact seam was investigated by compressed air, which was injected at the lower surface and leakage spray, which was applied at the upper surface (Fig. 4.60). This proceeding visualized the preferred pathway of solution at the contact seam by the wet areas and blistering. Additionally, it is assumed that the contact seam opened a little after samples were dismantled from isostatic cells.



Fig. 4.60 Verification of the contact seam between salt concrete and rock salt after dismantling from isostatic cells. Left: Saline solution pathed the samples driven by compressed air (Core 4). Right: Visualization of path ways using leakage spray (Core 5)

Because percolation of $MgCl_2$ solution was therefore not meaningful, both samples were again exposed to NaCl solution in the advection cells. NaCl solution was injected at one samples surface and flux of NaCl solution was stopped afterwards. In comparison to last permeability measurements with NaCl solution in the isostatic cells (with confining pressure), permeability in both samples increased about circa one order (Fig. 4.61). With ongoing time, in which samples were exposed to NaCl solution, a decrease of permeability was measured again. After both samples showed permeability to NaCl $\leq 1 \cdot 10^{-18} m^2$, solution was changed once more to $MgCl_2$ solution. In both samples an increase of permeability was measured. In core 4 the permeability increased slowly about circa a half order to $5 \cdot 10^{-18} m^2$ within the next four measurements. Permeability in core 5 increased directly about one order to $1 \cdot 10^{-17} m^2$. The ongoing percolation with $MgCl_2$ solution did not change the permeability significantly.

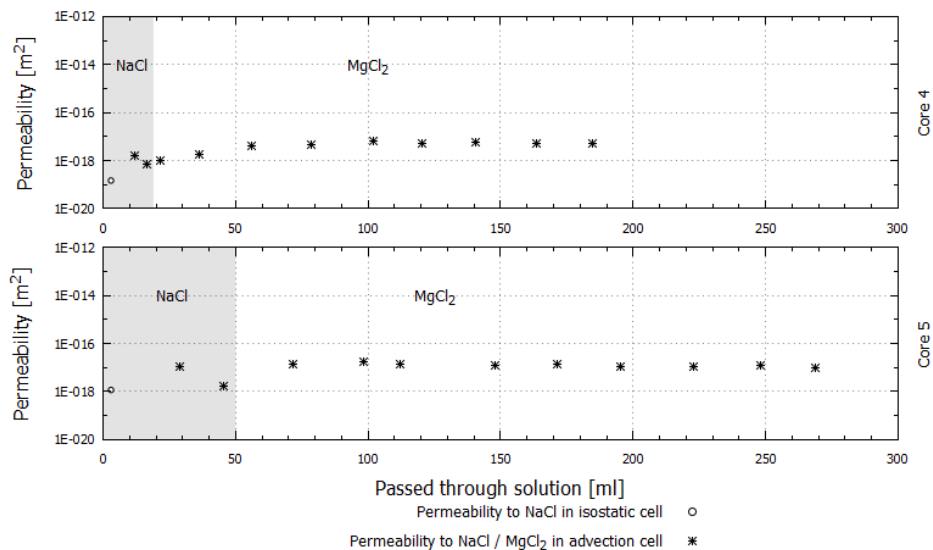


Fig. 4.61 Development of permeability after dismantling of combined samples (core 4 and core 5) from isostatic cells and pressure less cast in advection cells. Samples were first percolated with NaCl solution and afterwards with $MgCl_2$ solution

Fig. 4.62 shows the development of solution composition during percolation of MgCl_2 solution in core 4 and 5. The solution composition during percolation with NaCl solution is not included. The sodium and chloride concentrations were between 5.0 mol/kg H_2O and 6.0 mol/kg H_2O in the first measurement with MgCl_2 solution in core 4. This composition was very close to sodium and chloride concentrations in saturated NaCl solution. With ongoing percolation of MgCl_2 solution both concentrations converged to the initial concentrations of sodium and chloride in MgCl_2 solution. After percolation of 60 ml MgCl_2 solution the initial concentrations of sodium and chloride were achieved. Concentrations of calcium, potassium, magnesium and sulphate were closed to 0.0 ml/kg H_2O in the first solution sample of core 4. With ongoing experiment the magnesium concentration increased. After percolation of 60 ml MgCl_2 solution the magnesium concentration of outflowing solution corresponded to concentration in the initial MgCl_2 solution. Also concentrations of potassium and sulphate increased and approximated to initial concentrations. The development of solution composition in core 5 was very similar to those in core 4. The first solution sample was taken after percolation of 25 ml MgCl_2 solution, hence, concentrations were nearly to concentrations of the second sample of core 4. After percolation of 60 ml MgCl_2 solution all concentrations were in agreement with initial MgCl_2 solution concentrations too. Because of the higher permeability of core 5, more solution could pass the sample in the same time. Hence, a higher volume of outflowing solution was analysed. Following, solution composition did not show further changes in its composition anymore.

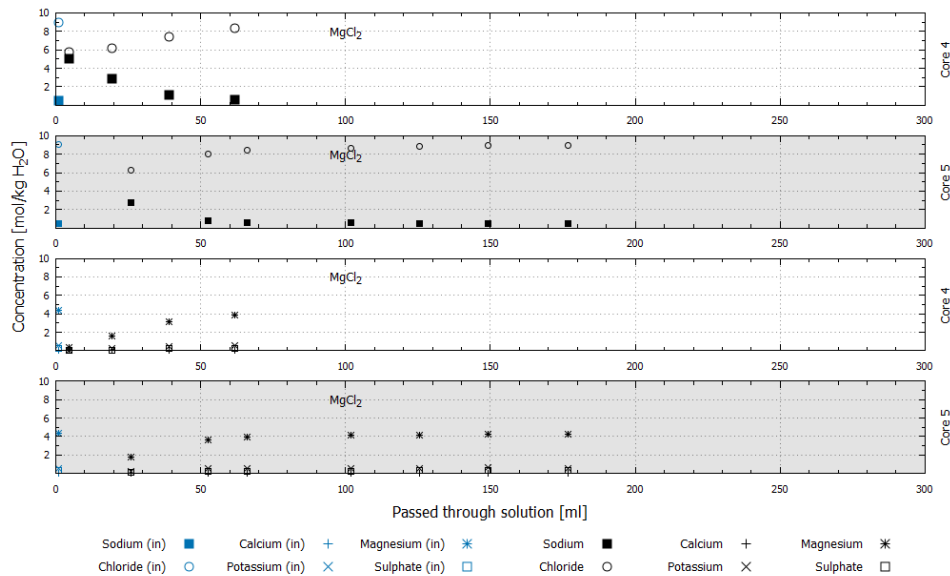


Fig. 4.62 Development of solution composition during flowing through of MgCl₂ solution in core 4 and core 5 in advection cells. Blue data points describe solution composition of initial MgCl₂ solution

4.4.3 Interpretation and discussion

4.4.3.1 Development of the permeability of sorel concrete during percolation with saline solutions and its influence to the sealing capacity

Sorel concrete – A1 / NaCl solution

Development of permeability in advection experiments with sorel concrete with NaCl solution showed a significant increase of permeability about two orders of magnitude. At the end of advection experiments samples were percolated by 300 ± 20 ml of NaCl solution, depending on the permeability of the sorel concrete cores, excluded core A1-10. In core A1-10 permeability increased faster compared to residual cores; altogether 380 ml NaCl solution percolated it.

Development of solution compositions was very similar in all samples. Significant differences of solution composition has been observed between the continuous percolations in the beginning of advection experiments (ten days), the “stop-and-flow” experiments and finally in the second phase of continuous percolation before

experiments were finished. Solution compositions, which were measured within the first ten days, are assumed to reflect the composition of the pore solution of the sored concrete before replacement by NaCl solution.

At the beginning of “stop-and-flow” experiments, solution composition changed significantly and magnesium, calcium and sulphate concentrations were significantly increased. During “stop-and-flow” experiments two solution samples were taken after every time period of stop. In first solution sample solution was collected, which was enclosed in the core for the defined period of time. Sample includes only 3.0 – 5.0 ml solution. The second solution sample includes around 25.0 ml solution, which was percolated after solution was enclosed in the samples. Before start of advection experiments it was assumed, that the composition of solutions, which were enclosed in the samples for a while, will be differ from percolated solutions. But analysis showed that there were no significant differences in solution compositions during “stop-and-flow” experiments (Fig. 4.46 to Fig. 4.48). Probably, phases were dissolved during the stop of percolation, but all dissolved elements were instantly replaced by percolation. After resuming the flow concentrations of magnesium, calcium and sulphate were also increased.

Calculation of SI showed, that the reacted solution was supersaturated with respect to Anhydrite, Glauberite, Gypsum, Halite and $\text{Na}_2\text{Ca}_5(\text{SO}_4)_6 \cdot 6\text{H}_2\text{O}$ and undersaturated with respect to Brucite, Dansite and 318-phase (Fig. 5.7). Percolated cores were not inspected using XRD because it is assumed that the solution passed the samples along preferential pathways and not integral through the whole cross-sectional area. Hence, it seemed to be necessary to identify the exact course of the pathways in order to take solid samples out of these pathways. But currently no method is available for identification of the pathways. However, calculated saturation compares well with batch and cascade experiments in the system sored concrete / NaCl solution. Hence, it can be assumed that Anhydrite and Halite were thermodynamically stable. Phases Glauberite, Gypsum and $\text{Na}_2\text{Ca}_5(\text{SO}_4)_6 \cdot 6\text{H}_2\text{O}$ should be present in the samples because of supersaturation. Brucite and 318-phase are expected to dissolve because of undersaturation.

Dissolution of phases is supported by the increase of magnesium concentrations in comparison with initial solution. Dansite was continuous undersaturated in advection experiments in agreement with cascade experiments. In batch experiments Dansite

was temporarily supersaturated and dissolved finally. Hence, it can be assumed that Dansite formed only temporarily by corrosion of sorel concrete with NaCl solution and dissolved again during equilibration. It is supposed that Dansite was only formed in sorel concrete – old and is negligible for sorel concrete – A1.

Solution composition during the phase of “stop-and-flow” (Fig. 4.45) showed that progress of corrosion depends significantly from elapsed time: if a small volume of NaCl solution was enclosed in the sample at least for ten days, permeability increased significantly more than if volume, which was five to six times higher, percolated the sample continuously. Effects of various reaction times, induced by the various time periods of solution enclosure, could not be identified. That indicates that reaction time of ten days was sufficient to attain local equilibrium within the sample. This is in agreement with determined reaction time of eleven days in batch experiments.

The last step of advection experiments showed, that concentrations of calcium, magnesium and sulphate decreased, if samples were percolated continuously by NaCl solution in comparison to “stop-and-flow” experiments. Hence, under the flow velocity applied no local equilibrium can be assumed: the percolating solution passes the sample more rapid than its solid constituents can equilibrate with it. This confirms results of permeability measurement discussed in section before.

Summarizing, the corrosion effect has to be most significant, if NaCl solution percolates a sealing element of sorel concrete very slowly or solution is enclosed in the sealing for a while. But when the local equilibrium between solution and sealing is attained, no ongoing corrosion and increase of permeability is expected anymore.

/KRA 2008/ required an initial permeability $< 10^{-18} \text{ m}^2$ for sealing elements. Sorel concrete – A1 samples produced in GRS laboratory did not satisfy this requirement. Indeed, in situ sealings will be compacted by the convergence of the host rock, which may result in an ongoing decrease of permeability. Additionally, /KRA 2008/ assume that permeability may increase about four order of magnitude to 10^{-14} m^2 resulting from corrosion effects. In experiments permeability increased only to 10^{-15} m^2 although solution was enclosed in the cores several times. Hence, the impact of corrosion was less in experiments than expected according to /KRA 2008/. Indeed, an ongoing corrosion and resulting increase of permeability can not be excluded, if samples would be further exposed to corrosive solution.

Laboratory investigations

In Tab. 4.7 the theoretical volume flow of solution through a sealing element was calculated according to the boundary conditions of /KRA 2008/. Calculations were based on Equation 4.4 in consideration of the permeability of sored concrete – A1 in laboratory, the required permeability of $< 10^{-18} \text{ m}^2$ and the assumption, that the required permeability increase about four orders of magnitude to 10^{-14} m^2 .

Tab. 4.7 Calculated volume flow through a sealing element

General boundary conditions			
Length [m]	150		
Cross section area [m ²]	22.5		
Viscosity (NaCl) [g/m ³ ·s]	0.0057		
Pressure (outflowing surface) (p ₁) [kg/m·s ²]	100 000		
Fluid pressure* (p ₂) [kg/m·s ²]	600 000		
Volume flow according to various permeability			
Permeability	10 ⁻¹⁷ m ²	10 ⁻¹⁸ m ²	10 ⁻¹⁴ m ²
Volume flow	2.85·10 ⁻⁵ m ³ /d / 0.01 m ³ /a	2.85·10 ⁻⁶ m ³ /d / 0.001 m ³ /a	0.03 m ³ /d / 10.39 m ³ /a
* Corresponding to a hydrostatic head of around 51.0 m			

The calculated volume flow was $< 1.0 \text{ m}^3/\text{a}$ both permeability is 10^{-17} m^2 and 10^{-18} m^2 . Hence, the intrusion of $0.001 \text{ m}^3/\text{a}$ and $0.01 \text{ m}^3/\text{a}$ solution may have no significant impact to the failure of the sealing function of a sealing element. More significant seems to be the intrusion of $10.39 \text{ m}^3/\text{a}$ when permeability increased to $> 10^{-14} \text{ m}^2$. Indeed, to evaluate if the safety requirements of a repository are met the type and mass of radionuclides which may be released from the repository has to be considered in addition to the development of permeability of the sealing element.

Sored concrete – A1 / MgCl₂ solution

Initial permeability of sored concrete cores, which was exposed to MgCl₂ solution was between $5 \cdot 10^{-18} \text{ m}^2$ to $7 \cdot 10^{-18} \text{ m}^2$. During percolation and “stop-and-flow” experiments, respectively, permeability decreased in all samples to circa $1 \cdot 10^{-18} \text{ m}^2$.

Solution analyses showed that similar to advection experiments with NaCl solution, composition changed significantly between time of percolation of solution in the beginning (up to twelve days) and start of “stop-and-flow” experiments (Fig. 4.51 to

Fig. 4.53). It is also assumed that this time was needed to replace pore solution of sorel concrete by NaCl solution. Composition of solution showed increased concentrations of calcium and sulphate and decreased concentrations of calcium and magnesium in comparison with initial $MgCl_2$ solution. Concentration of potassium and sulphate was most increased after solution was enclosed in the cores for 30 days. Hence, reactions proceeded, which were clearly time dependent. But both potassium and calcium concentration decreased again after solution was enclosed for 76 days. It can be assumed that primary potassium and sulphate were dissolved from concrete and if equilibration time is sufficient, new potassium and sulphate containing phases were formed, when the solution had 76 days to equilibrate. On the other hand potassium and sulphate containing phases may be consumed to the point of complete dissolution causing a drop of their concentrations in the analysed solution after 76 days. Because of decrease of permeability it can be assumed that pores are clogged by formation of new phases which impeded dissolution of primary phases. Decreased concentrations of calcium and magnesium can be interpreted in terms of formation of new calcium and magnesium containing phases. Solution analyses in the last phase of advection experiments (continuous percolation) showed that element concentrations corresponded to concentration of initial concentration essentially. Hence, it can be assumed that no further reaction proceeds because contact surface of the pathway was in equilibrium with $MgCl_2$ solution. This is in accordance with development of permeability which became also constant during continuous percolation.

Consideration of phase saturation in the outflowing solution showed that all phases, which were known from initial composition of sorel concrete, were saturated or supersaturated during “stop-and-flow” experiments (Fig. 5.8). Hence, dissolution of potassium and sulphate could not be explained with the used database. Consumption of magnesium may results from the formation of Dansite, Kainite, Loewite or 318-phase. All phases include magnesium and showed increase of SI. Calcium could be consumed by formation of Glauberite. But all these phases (without 318-phase) also include sulphate. Consequently, for these reactions to be possible, another phase containing sulphate had to dissolve. Additionally, development of SI showed, that there was no phase, which became undersaturated during “stop-and-flow” experiments. Hence, it can be assumed that THEREDA database release 6.0 is not adequate for this system. At least one phase is missing.

Results of solution analysis and permeability measurements showed, that equilibration between sorel concrete and MgCl_2 solution was affected by time. Reactions in this system seemed to be more slowly than in system with NaCl solution because this effect became primarily significant if solution was enclosed in the cores for at least 20 days. The enclosure of a small volume of solution in the cores had a higher impact on the development of solution composition and permeability than the percolation of a five to six time larger volume of MgCl_2 solution. Especially, if permeability became very low (close to $1 \cdot 10^{-18} \text{ m}^2$) and solution percolated samples very slowly, percolation of solution had an impact on the permeability. However, percolation of solution in the end of experiment (from 180 days) showed no effect to solution composition and permeability, although percolation of solution was very slow caused by the less permeability. It is hypothesized, that along percolated sections within the sample local equilibria prevented further corrosion.

Summarizing, MgCl_2 solution showed, compared to NaCl solution, a beneficial impact on the sealing capacity on sorel concrete. This effect was also described by /FRE 2015/, with regard to sorel concrete compositions C3 and C4.

However, it is assumed, that the contact seam between sealing element and EDZ is the preferred pathway for solutions. In present advection experiments with sorel concrete only the sealing capacity of the pure sorel concrete in contact with NaCl and MgCl_2 solution, respectively, was investigated. Hence, it is necessary to perform advection experiments with combined samples of sorel concrete and rock salt. But based on the very complex sample preparation of combined samples, it was not possible to develop the procedure for the fabrication. Furthermore, sorel concrete cores were fabricated in laboratory. So hardening time was much less than for the investigated salt concrete. Moreover, sorel concrete samples were not compacted during hardening. This may result in higher pore volumes and higher permeability compared to compacted samples of sorel concrete. Contrary to this procedure, a real in situ sealing element will have time to harden for years and will be subject to increasing pressure due to convergence of host rock. In that case sorel concrete had much more time for hardening than in presented laboratory experiments and additionally sorel concrete would also be compacted by the convergence from the host rock. This may result in improved sealing properties.

4.4.3.2 Development of the contact seam between sealing element and host rock during percolation with saline solutions and its influence to the sealing capacity

Salt concrete / NaCl solution

Advection experiments with combined samples of salt concrete were all started in isostatic cells with confining stress of 1.0 MPa in minimum. Procedure of sample preparation with regard to the initial permeability, which was measured directly after installation of the combined sample in isostatic cells showed, that there was a significant dependence between accuracy of sample preparation with the turning machine and permeability. If the salt concrete core fitted smoothly into the hollow rock salt cylinder, the initial permeability was higher than in case of emplacement of salt concrete core went along with some friction. The assumption that the contact seam is the primary pathway for solution is supported by this finding.

All samples showed that permeability decreased with time when saturated NaCl solution was enclosed in the samples (Fig. 4.57). Permeability decrease depended on the initial permeability: If initial permeability was around 10^{-13} m^2 , permeability decreased very slowly. To reach the required end permeability $< 10^{-18} \text{ m}^2$ more than 100 days were needed. If initial permeability was $< 10^{-14} \text{ m}^2$, permeability decreased much faster within 25 to 50 days. Based on the knowledge of batch experiments in the system salt concrete / NaCl solution, corrosion of salt concrete was not expected. But calculation of SI in solution from leaching experiments showed, that various phases, which could be not detected in pure salt concrete, were supersaturated. Especially, Glauberite and Gypsum were initially supersaturated and became saturated with ongoing reaction. Hence, it can be speculated that both phases form if salt concrete is in contact with NaCl solution. From /BIC 1968/ it is known, that formation of Gypsum is associated with an increase of volume. This may result in a progressive plugging of the contact seam by crystallisation processes. Further crystallisation processes may result from reaction of the rock salt with NaCl solution. In addition exchange reactions proceed in local equilibrium between solid sample and solution and may result in a temporary clogging of pathways too. These dissolution-precipitation processes within in the contact seam might result in a gradual decrease of the hydraulic conductivity.

In addition, the impact of confining stress was investigated both in three isostatic cells and in advection cells. Increase of confining stress up to 5 MPa within time periods of ten days in maximum, showed no impact on the development of permeability. But in core 1 confining stress was increased for more than 100 days. When stress was decreased finally, permeability increased about one order of magnitude again. A similar phenomenon was observed when dismantling the cores from isostatic cells. When applying leakage spray and pressure air on the contact seam, the gap became clearly visible (Fig. 4.60). Following, measurement of permeability for NaCl solution in the same cores in advection cells confirmed this finding by increased permeability of one order of magnitude in comparison with last determined permeability to NaCl solution in isostatic cells (Fig. 4.61). Hence, permeability decrease in combined samples seemed to be induced by combined influence of dissolution-precipitation processes plus confining pressure.

But further investigations in pressure less advection cells showed additionally that permeability could also be reduced by enclosure of NaCl solution only. It can be assumed, based on laboratory results, that presence of NaCl solution in a sealing element of rock salt is sufficient to reduce permeability at the contact seam. Based on current results it cannot be concluded, how the velocity of permeability decrease is influenced by confining stress. Therefore more comprehensive and systematic experiments with regard to confining stress are needed. However, this was not the goal of chemical-hydraulic investigations in this work. But based on the experimental layout of advection experiments in isostatic cells, performing of mechanical dictated experiments is realizable.

Salt concrete / MgCl₂ solution

Substitution of NaCl solution by MgCl₂ solution showed in all samples both in isostatic and advection cells that permeability was increased by about one order of magnitude and became constant during ongoing percolation with MgCl₂ solution (Fig. 4.58 and Fig. 4.61). This effect may result from the different wettability of concrete and rock salt with respect to NaCl und MgCl₂ solution. Handling of both solutions in laboratory showed that the wettability of NaCl solution is higher than of MgCl₂ solution. It may be assumed that the adhesion of MgCl₂ solution to the surface of salt concrete and rock salt at the contact seam is lower than of NaCl solution. Hence, MgCl₂ solution percolated the samples faster, induced by injection pressure.

Observation of solution composition showed that concentrations were close to concentrations of NaCl solution after NaCl solution was substituted by MgCl₂ solution (Fig. 4.59 and Fig. 4.62). During percolation of MgCl₂ solution composition gradually approached concentrations of initial MgCl₂ solution. After 50 ml MgCl₂ solution passed the concentrations equalled those from the inflowing MgCl₂ solution. Probably, NaCl solution, which was injected before to the samples, was replaced in the beginning. During ongoing percolation with MgCl₂ solution no effects of corrosion could be identified in solution composition. This finding agrees well with the constant permeability. Hence, corrosion was not detected although the contact seam was percolated with corrosive solution.

But development of permeability in the pilot test showed divergent results (Fig. 4.55 and Fig. 4.56): permeability decreased again after the first permeability increase, which resulted from solution change and increase of injection pressure. Afterwards, permeability became constant for a while and increased finally significantly. In the pilot test the decrease of permeability was explained by the formation of Brucite and Gypsum as result of corrosion effects by MgCl₂ solution. The pores were plugged by formation of new phases because of the higher volume in comparison with Portlandite and permeability was reduced. Because especially Brucite induced decrease of pH at the contact face of salt concrete and solution, CSH phases became thermodynamically unstable and dissolved. Because CSH phases are important for the stability of salt concrete, the concrete lost its stability, pores could no longer be clogged and permeability started to increase again. But effects of corrosion could not be determined in the percolated solution although batch and cascade experiments before showed that the system salt concrete / MgCl₂ solution is thermodynamically unstable. Similar results as to the development of permeability of salt concrete in the presence of MgCl₂ solution showed earlier investigations from /MEY 2003a/.

Deviation of experimental results between pilot test, investigation of /MEY 2003a/ and current results of advection experiments may be explained by the properties and conditions of the various samples. In percolation experiments of /MEY 2003a/ a mixture of salt concrete with an increased porosity was used. The combined sample of pilot test (chapter 4.4.2.2) was submitted to an increased confining stress in comparison with residual combined samples in advection experiments. Hence, a bulking of concrete structure could not be excluded. Supposedly sample from pilot test and samples investigated by /MEY 2003a/ showed a higher pore volume and consequently increased

surface compared to other combined samples, which were investigated afterwards. Based on the higher surface of salt concrete samples with increased porosity and of the pilot test an effect of corrosion effected by percolation of MgCl_2 solution, could be observed. Thus, missing effect of corrosion in the advection experiments can be ascribed to the low surface of salt concrete in comparison to leaching experiments and percolation experiments before. If there were corrosion effects in present advection experiments, these effects were too small to induce significant effects to solution composition and permeability.

These results are important for the construction of sealing elements from salt concrete and their integral performance with regard to their sealing capacity. Contrary to former investigations, the stability of salt concrete sealing element in the presence of MgCl_2 solution might be higher than hitherto assumed. The effective surface area of concrete will progressively decrease during convergence of the host rock. The available pore space, which is necessary to exchange local equilibrium solution and essentially to trigger further corrosion, is also reduced by convergence. This sum of these effects improves sealing capacity of salt concrete sealing elements significantly.

4.5 PET-measurements on salt concrete – halite contact zone

4.5.1 Set up of PET-measurements

Aim of PET-measurements were

- Monitoring of the diffusion process from the surface into the specimen with a salt concrete – halite contact.
- Demonstration and evaluation of the PET-method for diffusion studies
- Evaluation of the preparation method.

The sample “Halit_Zement_1” (Fig. 4.63) was produced at and delivered by GRS. It was produced from a cylindrical halite drill core, diameter 70 mm. This specimen was bored out and a salt concrete core with a diameter of 35 mm was inserted into the bore. The joint between salt and salt concrete was flushed with concentrated NaCl-solution, until permeability fell below 10^{-17} m^2 . This combined sample was glued into an acrylic glass cylinder. The length of the sample was 118 mm.

End caps with two Luer fluid ports were machined at HZDR. The gap between sample and end cap was minimized (spacing about 0.1 mm). The gap volume was gauged with concentrated salt solution (0.5 mL).

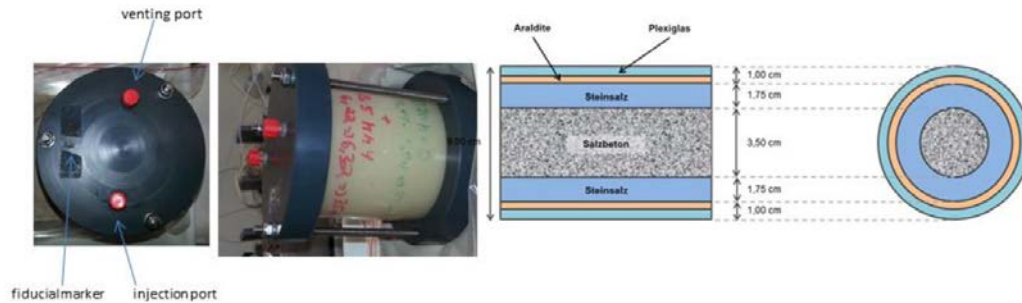


Fig. 4.63 Sample “Halit_Zement_1”

The long-lived positron-emitting radionuclide ^{22}Na (decay time 2.6018 y) was applied as PET-tracer. A volume of 0.6 mL of concentrated NaCl-solution was labelled with ^{22}Na and then slowly injected through the fluid port into the gap volume. The second port served as purge connector. The total injected activity was calculated from the delivery note of the producer of the radionuclide (Perkin-Elmer) to be 3.16 MBq. This is a low activity for PET-studies, with typical activities around 100 MBq. However, the long decay time allows long recording periods and thus recording of a sufficient number of events for image reconstruction.

A fiducial marker was fixed to the sample casing for activity calibration and for positioning control.

The measuring method is described in /KUL 2016a/. We apply a high-resolution PET-scanner (ClearPET by Raytest) with a spatial resolution in the order of 1 mm. The diameter of the field of view (FOV) was adjusted to 130 mm, the length is 100 mm. We shifted the sample three times in order to cover the complete sample and to avoid image deterioration at the margin of the FOV.

In order to simplify the positioning and the data processing it is recommendable to reduce the sample length to about 90 mm, which would fit into the FOV.

23 frames were recorded, each with 3 - 4 bed positions, making a total number of 78 records. The duration of the single recordings was initially 20 min and at last 120

minutes, which means a frame length of 6 h. Unfortunately, a number of detectors intermittently failed in the course of the measurements, which affects mainly the calibration and the signal-to-noise ratio of the images. In order to improve the signal-to-noise ratio, the initial frames with short durations were joined, obtaining 16 frames.

The image reconstruction was conducted with our improved method which is based on the reconstruction method supplied by the producer which applies procedures from the STIR-library, an open-source “Software for Tomographic Image Reconstruction” (<http://stir.sourceforge.net/>). It comprises random correction, dead-time correction, attenuation correction, normalization (equalization of in-homogeneous sensitivity), and scatter. The scatter correction is a tedious and time-consuming step. The scattered radiation is computed from an initial image of the activity distribution (usually an uncorrected image) as radiation source, and a rough model of the Compton scatter cross section. Without scatter correction, Compton scatter would produce somewhat blurred images, where the blur-ring is inseparable from real tracer diffusion effects. Thus, this correction is inevitable, when diffusion effects are investigated.

After reconstruction, the images were calibrated, considering both the total injected activity and the known activity of the fiducial marker, yielding 16 frames with increasing lapse-time (0.20, 0.34, 0.89, 1.35, 1.76, 2.18, 2.6, 3.23, 4.02, 4.89, 5.72, 6.9, 15.9, 21.8, 34.8, 70.8 days after injection).

4.5.2 Results of PET-measurements

The images are shown in Fig. 4.64 and as movie in the supplement. The underlying data are stored in the Interfile-format (a nuclear-medical imaging format with a header file (*.hv) in ASCII-format and a binary data file (*.v) which is defined in the header file. The header file format was partially modified in order to consider non-medical information. The binary data file is in 32-bit float field (little endian), with a dimension of 145×145×95 voxels with isotropic size of 1.15 mm. These images can be viewed with any software for volumetric image processing, like Amide (<http://amide.sourceforge.net/>), ImageJ (<https://imagej.nih.gov/ij/>), or Paraview (<http://www.paraview.org/>).

Fig. 4.64 is a compiled 3D-presentation of all 16 frames. The data is decay corrected; therefore the color scale of all frames is comparable. An iso-surface at 30 Bq/voxel is shown in brown-beige colour. It is depicting the input volume at the inlet-endplate and the joint between salt and cement, where the tracer effectively entered. The actual tracer distribution is illustrated by two ortho-slices. Low levels below 5 Bq/voxel (light blue) are erroneous and near the noise threshold. Therefore, the apparent increase of activity in the outer zone (salt) is insignificant, whereas the increase in the central cement zone during the last frames is real.

Laboratory investigations

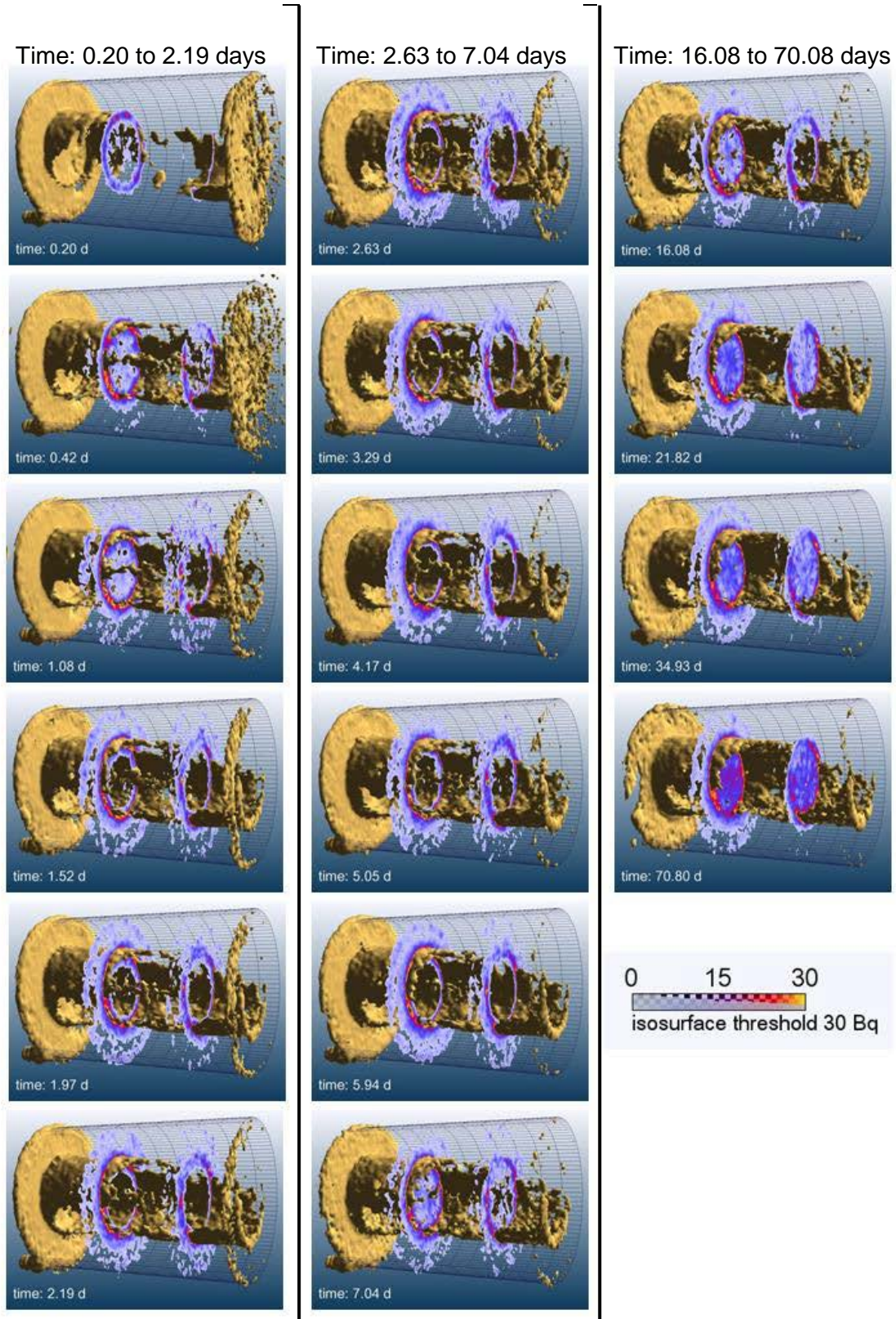


Fig. 4.64 Compiled 3D-presentation of all 16 PET time frames

4.5.3 Interpretation and discussion

It was anticipated before, that the solution should remain in the gap between the endplate and the solid material, and that the radionuclide would diffuse from this front face into the material. In contrast, we observed an instantaneous infiltration of the tracer into the joint between halite and salt concrete. Beyond that, there is no significant infiltration, which could be presumed also into the contact between halite and glue at the surface, or directly into the halite or rock salt. We therefore conclude that the sealing of the joint was not completely successful. The joint probably contained air, which caused capillary suction. The transport pathway has a demerging structure, which causes a highly heterogeneous tracer distribution in the cylindrical joint. This pattern is rather stationary.

The activity concentration is a measure of the total tracer volume V that entered one voxel with an edge length of dx and a total volume of $V_x = d_x^3$, because the initial activity concentration a_0 of the fluid is fixed. Assuming a surface area corresponding to the lateral face of one voxel, we can estimate the thickness of the layer (s. Fig. 4.65).

$$\delta = \frac{a}{a_0} \cdot \frac{V_x}{d_x^2} = \frac{a}{a_0} \cdot d_x$$

Equation 4.5

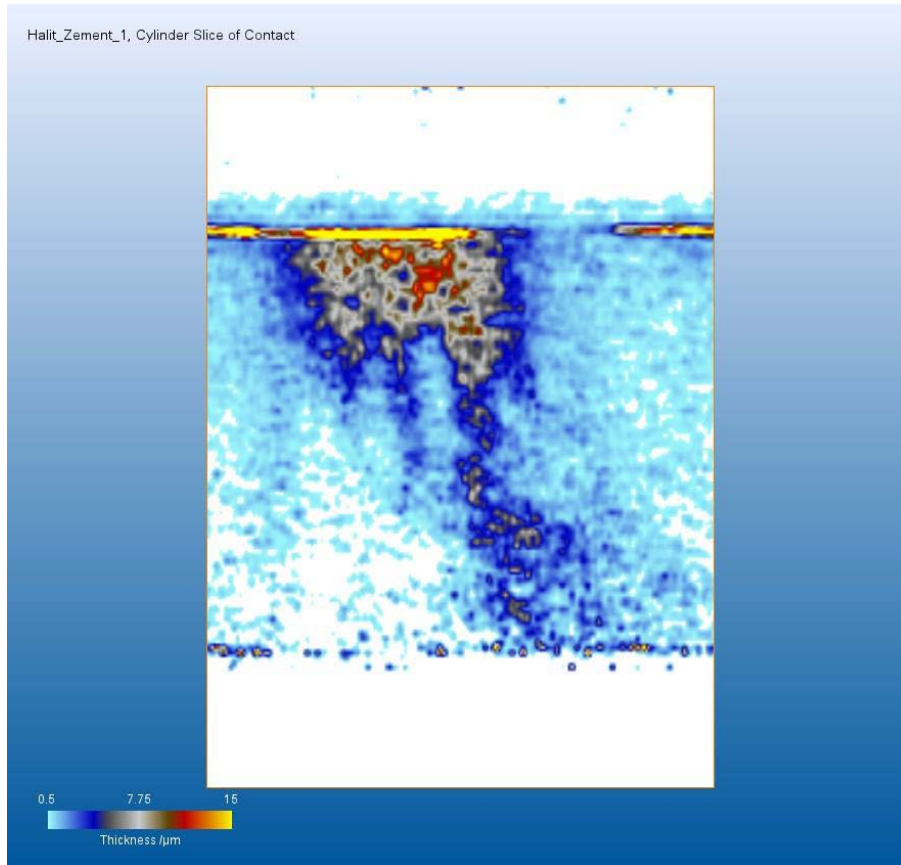


Fig. 4.65 Estimation of the layer thickness δ from the activity concentration a on the joint surface (as cylinder slice)

It has to be noted, that this thickness δ is far below the spatial resolution of the PET scanner. However, it is derived from the concentration, and not directly visualized as structural image, and therefore is a mean value over the voxel size.

With longer times (larger than 10 days), we observe significant spreading of the tracer distribution into the cement. This is observable in the four last frames of Fig. 4.64 (Time 16.08 to 70.08 days) by the increasing blue to red coloring of the central zone of the slices. In principle, local diffusion parameters could be estimated from this spatiotemporal pattern by inverse modelling /KUL 2016b/ and /LIP 2017/. However, it is not sensible here to derive local diffusion properties from the tracer propagation out of this zone of the joint, because the signal is dominated by noise, and the computation is too involved.

Instead, we computed the effective tracer propagation as mean value over the complete sample volume. We take advantage from the axial symmetric geometry and computed circular mean values of activity $a_{mean}(r, z)$ (r : radius of the integration circle, $N(r)$: number of voxels on the integration circle), at first for each slice z (grey lines in Fig. 4.66), according to

$$a_{mean}(r, z) = \frac{1}{N(r)} \sum_r a(x_r, y_r, z) \Big|_{\sqrt{x_r^2 + y_r^2} = r} \quad \text{Equation 4.6}$$

From these circular means we computed the mean radial activity a_r (red lines in Fig. 4.66).

According to Crank (The mathematics of Diffusion, Clarendon, 1975, p. 75) molecular diffusion from a cylindrical shell into a cylinder is described by

$$c(r) = \frac{2D}{R} \sum_{n=1}^{\infty} \exp(-Da_n^2 t) \frac{\alpha_n J_0(r a_n)}{J_1(R a_n)} \int_0^1 \exp(Da_n^2 \lambda) c_0(\lambda) d\lambda \quad \text{Equation 4.7}$$

with concentration c , diffusion coefficient D , cylinder radius R , concentration at the surface c_0 , Bessel functions J_0 , J_1 , and α_n root of Bessel function J_0 . This – somewhat intricate - equation can serve as a basis for approximating the mean diffusion coefficient. This is valid for homogeneous material on the drill core scale.

Here, we derived the increase of penetration depth of the tracer with time as qualitative measure of diffusion with the help of robust descriptive statistical methods, i. e. quantiles. As measure of the penetration depth we identified the interquartile range. Taking the radial concentration as a distribution density function, we estimated the interval between the positions of the median and the first quartile as penetration depth into the cement, and the interval between third quartile and the median as that of the salt. The positions of the quartiles are marked in Fig. 4.66 as vertical lines. One drawback of this method has to be observed: The position of the median is not fixed at the material joint, but moves with time towards the cement, because of the higher diffusion coefficient in this zone. However, the method yields a reasonable estimate of the penetration depth without relying on supplementary data. These penetration depths are shown in Fig. 4.67.

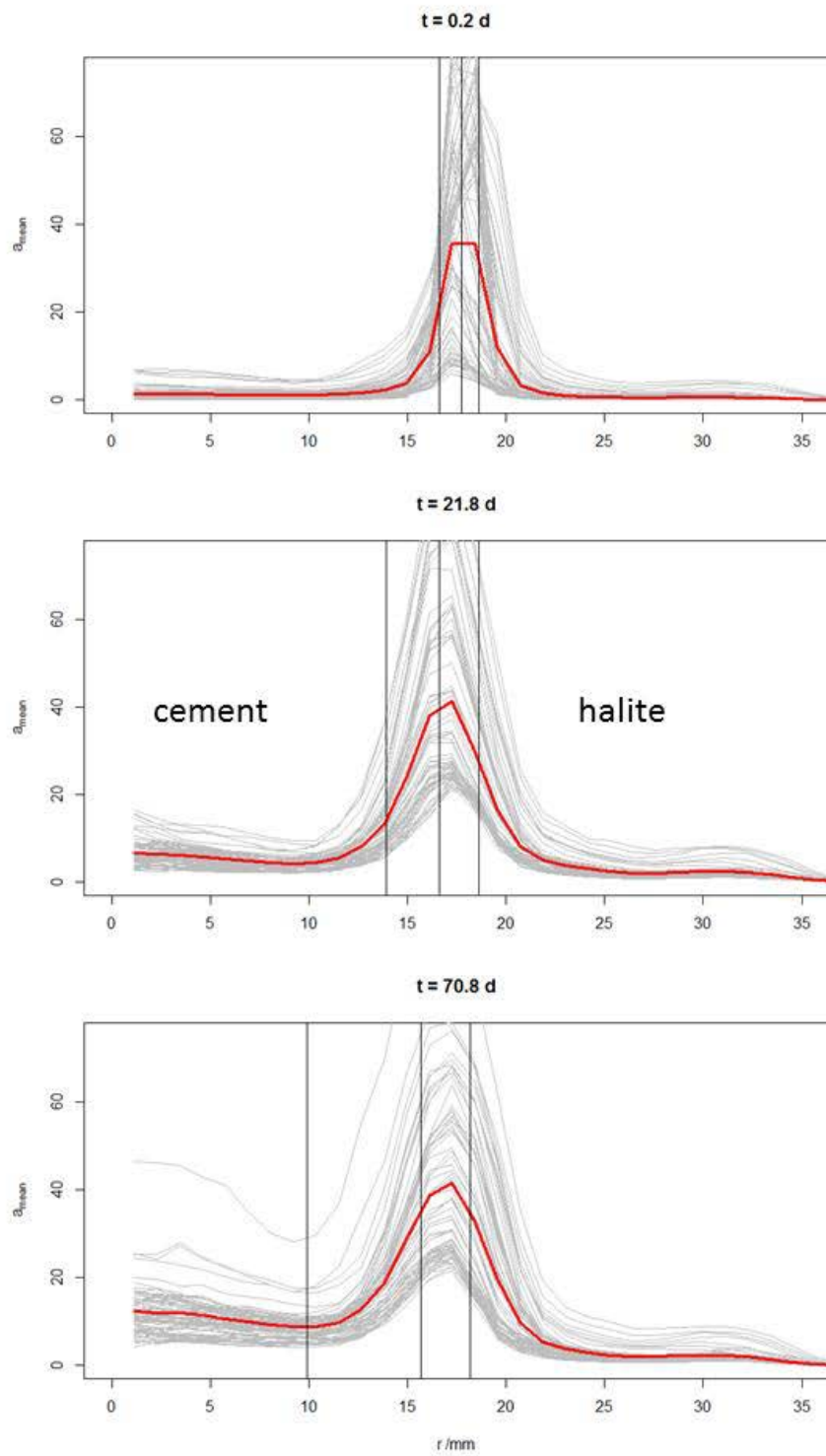


Fig. 4.66 Circular mean values of the activity a_{mean} for three frames (0.2, 21.8, 70.8 days) in grey. The mean radial activity a_r is plotted in red. The sample axis is at 0 mm, the joint zone is clearly visible in the top profile at

17.5 mm, and the halite mantle extends to 35 mm (scaling in voxel sizes (1.15 mm)). The spreading on the left hand side from the joint is significant, whereas the variations on the right hand side are not exceeding statistical variations. The vertical lines are the first, second (median), and third quartiles of the radial tracer concentration profile, interpreted as a distribution density function

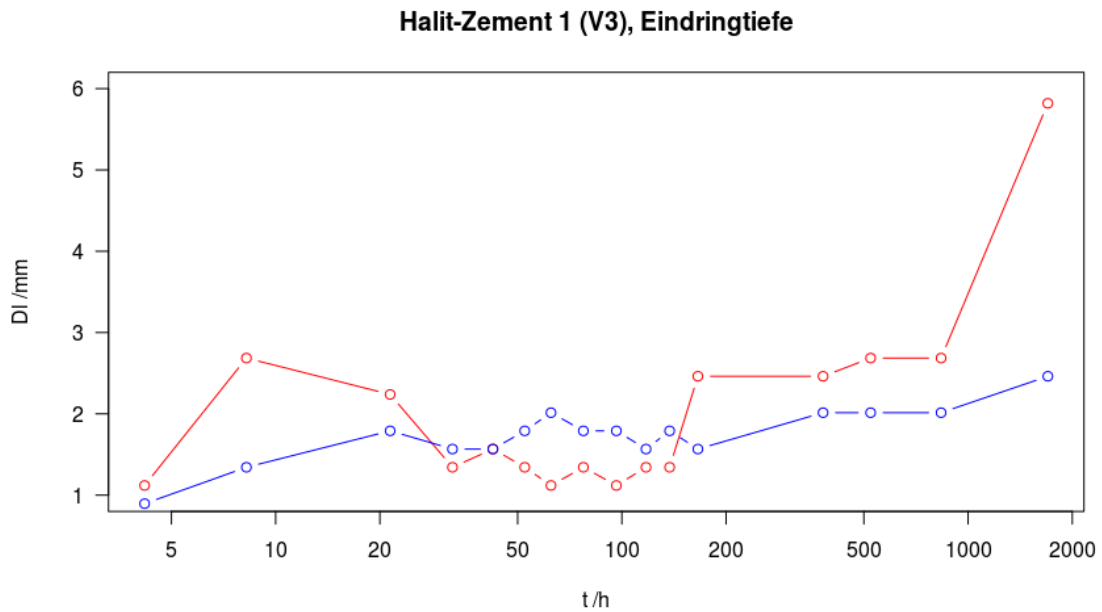


Fig. 4.67 The interquartile ranges (interval length of the 50 % – 25 % (cement, red) and 75 % – 50 % (halite, blue) values of the circular distribution in Fig. 4.66) was interpreted as penetration depth of the tracer (applying the interquartile range as robust measure of the standard deviation). The error range is in the order of the voxel dimension of 1.15 mm, therefore, the increase becomes significant after about 150 h

In this particular case, the situation at the contact between host rock and cement is complicated. Here, we could visualize the invasion of the labelled fluid into the joint zone. It could be shown, that the fluid distribution follows a very heterogeneous patchy structure, and that the thickness of the moist layer is in the order of 10 μm .

It is also possible to derive diffusion parameters of the material. Here, we visualized the distribution of $^{22}\text{Na}^+$ -ions. During the first 10 days the diffusional spreading was below resolution and sensitivity of the method. After 50 days we found significant spreading into the cement (about 5 mm in 70 days) and a slight penetration into the salt. From this penetration rate, it is possible to estimate a mean diffusion coefficient of the cement. It should be noted, that the asymmetry of the mean activity is not only due to different material properties, but to some part a geometrical effect: The diffusional spreading in the cement is convergent, and in the salt divergent.

In this particular case, the initial spreading of the tracer over the contact zone reduced the initial tracer concentration and localization. The method would be more sensitive and more exact, when the initial tracer concentration was higher – i. e. without suction into the joint, when majority of the tracer diffuses from the gap at the endplate, and not from a widely distributed source zone.

We estimate the PET method as unique for studying such a complex situation. There is virtually no other method available for detecting and quantifying intrusions of smallest quantities of brine in a large volume. Also, GeoPET is the only method for dealing with complex diffusion processes. In principle, also destructive methods could be applied, but these would only represent one final situation of a time dependent process, which is insufficient information for process understanding and parameterization.

In particular, all aims could be achieved. We could

- Monitor the tracer distribution at the cement – host rock contact zone
- Demonstrate the feasibility of deriving diffusion properties from repeated PET measurements
- Derive a minimum observation period (ca. 20 days, recommendation: up to ca. 1 year) and a minimum activity (3 MBq of ^{22}Na is sufficient)
- Evaluate the preparation method (found an open joint with fluid penetration between cement and host rock, but good sealing between salt and plexiglass mantle)
- Estimate the distribution and width of the water film in the joint

We recommend improvement the preparation method, in order to avoid open joints. The sample length should not exceed 80 – 90 mm. Prior to PET-measurements, the sample should be characterized with μCT . A μCT -image would also serve as start model for PET-reconstruction and improve the quality of the PET-images. Then, the fixing rods should be made of lighter material (PEEK, CFK...) to improve CT imaging. The injection should be conducted under “visual” control of PET-Imaging for better understanding of the injection process (initial distribution of the tracer). The injection ports should be improved (e.g. use of septa) to reduce the contamination risk (the endplate was slightly contaminated). To simplify mantling and reduce the impact of confining pressure unload, materials with higher strength probably could be used instead of plexiglass as mantle (thin steel tube, aluminum, PEEK), but then image quality of PET and CT should be tested before.

5 Model investigations

5.1 Model methods

The program “PHREEQC Interactive”, version 3.3.5-10806 was used to model the chemical reactions taking place between concrete and solution. PHREEQC is free software for calculation of thermodynamically equilibrium and has been continuously developed by the US Geological Survey /PAR 2013/. The program is able to handle the Pitzer formalism, which is widely used for modelling in high saline solutions /PIT 1991/.

5.2 Database

THEREDA database release 6.0

For modelling of the reaction path between sorel and salt concrete respectively and high saline solutions the THEREDA database release 6.0 from 4th July, 2013 was used. This parameter file was designed to model dissolution and precipitation reactions of cementitious material in aqueous solutions. It is valid for temperatures of 298.15 K.

CEMDATA 07

CEMDATA 07 is a database developed for Portland cement hydrates in the system CaO-Al₂O₃-SiO₂-CaSO₄-CaCO₃-H₂O by EMPA, Switzerland /MAT 2007/. It is valid for temperatures of 0 °C – 50 °C. Temperature dependence is described by the three-term analytical model. The used version 07.02 of CEMDATA 07 is from 14th August, 2008.

5.3 Calculation and adjustments

5.3.1 Calculation of saturation indices from the composition of experimental solutions

PHREEQC was used to calculate saturation indices (SI) of experimental solutions from batch and cascade experiments. SI of each mineral phase describes the status of saturation of this phase in the solution. SI is defined by Equation 5.1.

$$SI = \log \frac{Q}{K} = \log \frac{a_A \cdot a_B}{a_A^{Eq} \cdot a_B^{Eq}} \quad \text{Equation 5.1}$$

Q describes the Ionic activity product and K the solubility constant of the considered mineral phase. Q is defined by the activity of element A of the mineral phase multiplied with the activity of element B of the mineral phase. K describes the product of the activity of the elements A and B in equilibrium of the considered mineral phase. The calculated SI describes the status of saturation as below:

SI < 0 → undersaturation

SI = 0 → saturation

SI > 0 → supersaturation

This procedure aimed at verifying formation and dissolution of phases, which were determined by X-ray diffraction and to identify phases, which may be formed but could not be detected by X-ray diffraction.

5.3.2 Calculations and adjustments in the system sorel concrete / NaCl solution

The adjustment of modelling to laboratory results from cascade experiments was performed by stepwise adaption of modelling parameters. All calculations were performed imposing a reaction temperature of 25°C and a reaction pressure of 0.1 MPa. Kinetic effects which may influence the reaction process in laboratory were not considered in the calculations, because no such data were available for the phases under consideration. In fact, experimental results of advection experiments indicate, that kinetic effects indeed played a role to the reaction of salt and sorel concrete with saline solutions.

Primary the mineral phase composition of sorel concrete was calculated by oxygen balance based on the elemental composition from decomposition in laboratory (Tab. 5.1).

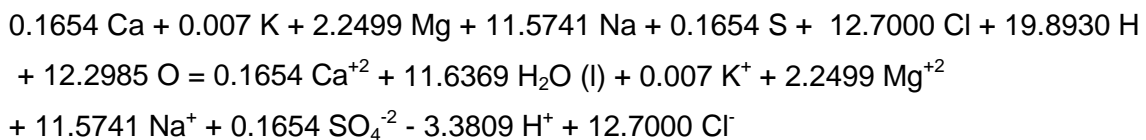
Tab. 5.1 Composition of sorel concrete for PHREEQC based on laboratory decomposition

Element composition of sorel concrete (decomposition in laboratory)		Mineral phases of sorel concrete (assumption, based on decomposition)	
Element	Concentration [mol/kg]	Mineral phase	Concentration [mol/kg]
Ca	0.1654	CaSO ₄	0.1654
S	0.0944		
K	0.0070	K ₂ O	0.0035
Mg	2.2499	MgCl ₂	0.5630
		Mg(OH) ₂	1.6870
Na	11.5741	NaCl	11.5741
Cl	12.7000*		

*Chloride concentration was calculated based on the percentage 3:1 of Mg(OH)₂ : MgCl₂ related to composition of 318-phase (3 Mg(OH)₂·MgCl₂·8H₂O)

Afterwards, the hydroxide and hydronium ion concentrations were calculated by charge balance. Because the mass of formula was smaller 1000 g/kg, 8.260 mol/kg H₂O was added to receive a formula weight of 1000 g/kg.

Finally, the equation for definition of sorel concrete as special reactant in PHREEQC was determined by consideration of charge balance:



The relevant boundary conditions during stepwise adaption of modelling parameters are summarized below.

Step 1 (sorel concrete / NaCl solution)

This step of calculation aimed at determining all mineral phases, which may be considered in the dissolution-precipitation processes during reaction of sorel concrete with NaCl solution. Considered phases only refer to phases included currently in the THEREDA database release 6.0. The complete phases, which should be considered in this system, are listed in appendix A 2.4

Tab. 5.2 Boundary conditions of calculation step 1 (sorel concrete / NaCl solution)

Step 1 (sorel concrete / NaCl solution) – Boundary conditions		
Ambient conditions		
	Reaction temperature	25°C
	Reaction pressure	0.1 MPa
Reacting agent		
	NaCl solution (saturated)	Saturated to Halite
	Sorel concrete	0.1654 mol/kg CaSO ₄ , 0.0035 mol/kg K ₂ O, 0.5630 mol/kg MgCl ₂ , 1.6870 mol/kg Mg(OH) ₂ , 11.5741 mol/kg NaCl, 8.260 mol/kg H ₂ O
Phases, which are allowed to precipitate		
	No limitation	
Reaction		
	Titration of sorel concrete to NaCl solution	0.5 mol in 5 steps

Step 2 (sorel concrete / NaCl solution)**Tab. 5.3** Boundary conditions of calculation step 2 (sorel concrete / NaCl solution)

Step 2 (sorel concrete / NaCl solution) – Boundary conditions		
Ambient conditions		
	Reaction temperature	25 °C
	Reaction pressure	0.1 MPa
Reacting agent		
	NaCl solution (saturated)	Saturated to Halite
	Sorel concrete	0.1654 mol/kg CaSO ₄ , 0.0035 mol/kg K ₂ O, 0.5630 mol/kg MgCl ₂ , 1.6870 mol/kg Mg(OH) ₂ , 11.5741 mol/kg NaCl, 8.260 mol/kg H ₂ O
Phases, which are allowed to precipitate		
	Anhydrite	Based on knowledge of X-ray diffraction (<i>Step 2a</i>)
	Brucite	Based on knowledge of X-ray diffraction (<i>Step 2a</i>)
	Halite	Based on knowledge of X-ray diffraction (<i>Step 2a</i>)
	318-Phase	Based on knowledge of X-ray diffraction (<i>Step 2a</i>)
Reaction		
	Titration of sorel concrete to NaCl solution	0.5 mol in 5 steps

Step 3 (sorel concrete / NaCl solution)

To improve the agreement between experimental and modelling results, more magnesium phases were considered, which are not included in the THEREDA database release 6.0 at present.

Tab. 5.4 Boundary conditions of calculation step 3 (sorel concrete / NaCl solution)

Step 3 (sorel concrete / NaCl solution) – Boundary conditions		
Ambient conditions		
	Reaction temperature	25°C
	Reaction pressure	0.1 MPa
Reacting agent		
	NaCl solution (saturated)	Saturated to Halite
	Sorel concrete	0.1654 mol/kg CaSO ₄ , 0.0035 mol/kg K ₂ O, 0.5630 mol/kg MgCl ₂ , 1.6870 mol/kg Mg(OH) ₂ , 11.5741 mol/kg NaCl, 8.260 mol/kg H ₂ O
Phases, which are allowed to precipitate		
	Anhydrite	Based on knowledge of X-ray diffraction
	Brucite	Based on knowledge of X-ray diffraction
	Halite	Based on knowledge of X-ray diffraction
	318-Phase	Based on knowledge of X-ray diffraction
	further magnesium phases	
Reaction		
	Titration of sorel concrete to NaCl solution	0.5 mol in 5 steps

5.3.4 Calculations and adjustments in the system salt concrete / MgCl_2 solution

In agreement with modelling activities of sorel concrete, calculations in the system salt concrete / MgCl_2 solution was performed by stepwise adaption of modelling parameters. Calculations were also performed imposing a reaction temperature of 25°C and a reaction pressure of 0.1 MPa. Kinetic effects could not be considered because such data were not available for phases under consideration as well as in calculations with sorel concrete before.

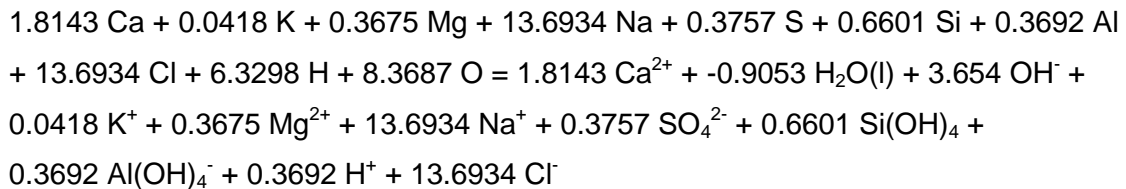
The composition of salt concrete was defined as special reactant based on laboratory decomposition. Firstly, the potential formation of mineral phases was balanced with element composition from laboratory decomposition (Tab. 5.5). Afterwards, the equation for describing the salt concrete in PHREEQC was determined at oxygen balance.

Tab. 5.5 Composition of salt concrete for PHREEQC based on laboratory decomposition

Element composition of salt concrete (decomposition in laboratory)		Mineral phases of salt concrete (assumption, based on decomposition)	
Element	Concentration [mol/kg]	Mineral phase	Concentration [mol/kg]
Ca	1.8143	CaO	1.4386
S	0.3757	CaSO ₄	0.3757
K	0.0418	K ₂ O	0.0209
Mg	0.3675	MgO	0.3675
Si	0.6601	SiO ₂	0.6601
Al	0.3692	Al ₂ O ₃	0.1846
Na	13.6934	NaCl	13.6934
Cl	13.6934		

Model investigations

The mass of included water was calculated based on information of /BER 1990/. Thus in silicon-rich concretes (calcium:silicon > 1) the formation of CSH 1.1 is preferred. CSH 1.1 includes 2.2 times more water than calcium. Afterwards, the equation for definition of salt concrete was charged balanced:



Formally, a recalculation of the formula weight yields 1059 g/kg salt concrete. The deviation from exactly 1000 g/kg salt concrete is due to a combination of the combined error of lab analysis and the fact that the assignment of elements to phases is of course an oversimplification of the real conditions. As the proportional contribution of each element remains the same it is expected that the impact on PHREEQC calculations is negligible because the progress of reaction is normalized with respect to the unit mass.

Step 1 (salt concrete)

In this calculation step all phases were determined, which should be considered in the system salt concrete / $MgCl_2$ solution in consideration of the THEREDA database release 6.0. Potential equilibrium phases in this system are listed in appendix Tab. A.1.46.

Tab. 5.6 Boundary conditions of calculation step 1 (salt concrete)

Step 1 (salt concrete) – Boundary conditions		
Ambient conditions		
	Reaction temperature	25°C
	Reaction pressure	0.1 MPa
Reacting agent		
	MgCl ₂ solution	0.486 mol/kg H ₂ O Na, 0.569 mol/kg H ₂ O K, 4.362 mol/kg H ₂ O Mg, 0.001 mol/kg H ₂ O Ca, 9.013 mol/kg H ₂ O Cl, 0.294 mol/kg H ₂ O SO ₄
	Salt concrete	1.4386 mol/kg CaO, 0.3757 mol/kg CaSO ₄ , 0.0209 mol/kg K ₂ O, 0.3675 mol/kg MgO, 0.6601 mol/kg SiO ₂ , 0.1846 mol/kg Al ₂ O ₃ , 13.6934 mol/kg NaCl
Phases, which are allowed to precipitate		
	No limitation	
Reaction		
	Titration of salt concrete to NaCl solution	0.5 mol in 5 steps

Step 2 (salt concrete / MgCl₂ solution)**Tab. 5.7** Boundary conditions of calculation step 2a and 2b (salt concrete) - I

Step 2 (salt concrete / MgCl₂ solution) – Boundary conditions		
Ambient conditions		
	Reaction temperature	25°C
	Reaction pressure	0.1 MPa
Reacting agent		
	MgCl ₂ solution	0.486 mol/kg H ₂ O Na, 0.569 mol/kg H ₂ O K, 4.362 mol/kg H ₂ O Mg, 0.001 mol/kg H ₂ O Ca, 9.013 mol/kg H ₂ O Cl, 0.294 mol/kg H ₂ O SO ₄
	Salt concrete	1.4386 mol/kg CaO, 0.3757 mol/kg CaSO ₄ , 0.0209 mol/kg K ₂ O, 0.3675 mol/kg MgO, 0.6601 mol/kg SiO ₂ , 0.1846 mol/kg Al ₂ O ₃ , 13.6934 mol/kg NaCl
Phases, which are allowed to precipitate (2a)		
	Anhydrite	Based on knowledge of X-ray diffraction (<i>Step 2a</i>)
	Bischofite	Based on knowledge of X-ray diffraction (<i>Step 2a</i>)
	Carnallite	Based on knowledge of X-ray diffraction (<i>Step 2a</i>)
	CSH	Based on knowledge of X-ray diffraction (<i>Step 2a</i>)
	Friedels' salt	Based on knowledge of X-ray diffraction (<i>Step 2a</i>)
	Gypsum	Based on knowledge of X-ray diffraction (<i>Step 2a</i>)
	Halite	Based on knowledge of X-ray diffraction (<i>Step 2a</i>)
	Portlandite	Based on knowledge of X-ray diffraction (<i>Step 2a</i>)

Tab. 5.8 Boundary conditions of calculation step 2a and 2b (salt concrete) - II

Step 2 (salt concrete / MgCl₂ solution) – Boundary conditions		
Phases, which are allowed to precipitate (2b)		
	Brucite	Based on supersaturation in calculation (<i>Step 2b</i>)
	Gibbsite	Based on supersaturation in calculation (<i>Step 2b</i>)
	Hydrotalcite	Based on supersaturation in calculation (<i>Step 2b</i>)
	Kerolite	Based on supersaturation in calculation (<i>Step 2b</i>)
	Oxychloride-Mg (318-phase)	Based on supersaturation in calculation (<i>Step 2b</i>)
	Polyhalite	Based on supersaturation in calculation (<i>Step 2b</i>)
	Sepiolite	Based on supersaturation in calculation (<i>Step 2b</i>)
	SiO ₂ (amorphous)	Based on supersaturation in calculation (<i>Step 2b</i>)
	SiO ₂ (crystalline)	Based on supersaturation in calculation (<i>Step 2b</i>)
	Strätlingite	Based on supersaturation in calculation (<i>Step 2b</i>)
Reaction		
	Titration of salt concrete to NaCl solution	0.5 mol in 5 steps

Step 3 (salt concrete / MgCl₂ solution)

In this step the THEREDA database release 6.0 were completed to four solid solutions corresponding to the CEMDATA 07 database /MAT 2007/. It should be tested if addition of potential concrete phases from CEMDATA 07 draw a conclusion to phase formation of experimental results. The conversion of input data from CEMDATA 07 database to THEREDA database release 6.0 is listed in Appendix A 1 .

Tab. 5.9 Boundary conditions of calculation step 3 (salt concrete / MgCl₂ solution) - I

Step 3 (salt concrete / MgCl₂ solution) – Boundary conditions		
Ambient conditions		
	Reaction temperature	25°C
	Reaction pressure	0.1 MPa
Reacting agent		
	MgCl ₂ solution	0.486 mol/kg H ₂ O Na, 0.569 mol/kg H ₂ O K, 4.362 mol/kg H ₂ O Mg, 0.001 mol/kg H ₂ O Ca, 9.013 mol/kg H ₂ O Cl, 0.294 mol/kg H ₂ O SO ₄
	Salt concrete	1.4386 mol/kg CaO, 0.3757 mol/kg CaSO ₄ , 0.0209 mol/kg K ₂ O, 0.3675 mol/kg MgO, 0.6601 mol/kg SiO ₂ , 0.1846 mol/kg Al ₂ O ₃ , 13.6934 mol/kg NaCl
Phases, which are allowed to precipitate (2a)		
	Anhydrite	Based on knowledge of X-ray diffraction (<i>Step 2a</i>)
	Bischofite	Based on knowledge of X-ray diffraction (<i>Step 2a</i>)
	Carnallite	Based on knowledge of X-ray diffraction (<i>Step 2a</i>)
	CSH	Based on knowledge of X-ray diffraction (<i>Step 2a</i>)
	Friedels' salt	Based on knowledge of X-ray diffraction (<i>Step 2a</i>)
	Gypsum	Based on knowledge of X-ray diffraction (<i>Step 2a</i>)
	Halite	Based on knowledge of X-ray diffraction (<i>Step 2a</i>)
	Portlandite	Based on knowledge of X-ray diffraction (<i>Step 2a</i>)

Tab. 5.10 Boundary conditions of calculation step 3 (salt concrete /MgCl₂ solution) - II

Step 3 (salt concrete / MgCl₂ solution) – Boundary conditions		
Phases, which are allowed to precipitate (2b)		
	Brucite	Based on supersaturation in calculation (<i>Step 2b</i>)
	Gibbsite	Based on supersaturation in calculation (<i>Step 2b</i>)
	Hydrotalcite	Based on supersaturation in calculation (<i>Step 2b</i>)
	Kerolite	Based on supersaturation in calculation (<i>Step 2b</i>)
	Oxychloride-Mg	Based on supersaturation in calculation (<i>Step 2b</i>)
	Polyhalite	Based on supersaturation in calculation (<i>Step 2b</i>)
	Sepiolite	Based on supersaturation in calculation (<i>Step 2b</i>)
	SiO ₂ (amorphous)	Based on supersaturation in calculation (<i>Step 2b</i>)
	SiO ₂ (crystalline)	Based on supersaturation in calculation (<i>Step 2b</i>)
	Strätlingite	Based on supersaturation in calculation (<i>Step 2b</i>)
Solid solutions		
	Hydrogarnet	C ₃ AH ₆
		Si-Hydrogarnet
	AFt	Ettringite
		Tricarbonate
	AFm	Monosulphate
		Monocarbonate
		Hemicarbonate
		C ₄ AH ₁₃
		C ₂ AH ₈
		Strätlingite
	CSH	Jennite-type
		Tobermorite-type
Reaction		
	Titration of salt concrete to NaCl solution	0.5 mol in 5 steps

5.4 Modelling results

Subsequent model investigations refer to laboratory results of leaching experiments as described in chapters 4.1.2 and 4.2.2 and are based on the current available THEREDA database release 6.0. In description of the modelling results the following findings should be considered:

Aluminium and silicon were below the quantification limit in batch experiments as well as in the cascade experiment although the initial salt concrete contained both elements (Tab. 3.4). Consequently, aluminium and silicon containing phases could not be considered in these systems by calculation of the SI from composition of experimental solutions. However, a formation of aluminium and silicon containing phases cannot be excluded based on this model investigation because analyzation of colloids in high saline solution is not trivial: colloidal dissolved elements may coagulate and sediments. Deposit phases cannot be analysed with the present methods used in context of phase analysis in laboratory. Hence, it is conceivable that aluminium and silicon were included in the reacted solutions and aluminium and silicon containing phases may be formed indeed formation was not detectable by laboratory or modelling investigations.

The theoretical calculation of SI both from the compositions of the reacted solutions in laboratory experiments (chapters 5.4.1 to 5.4.2) and from the complete modelling of the cascade experiments (chapters 5.4.4 and 5.4.5) refers only to the available phases in the THEREDA database release 6.0. Mineral phases included in the THEREDA database release 6.0 make no claim to be complete. Hence, if there are no phases which may explain the development of dissolution-precipitation processes in experiments, this statement refers only to the current available THEREDA database release 6.0. In fact, the THEREDA database release 6.0 may be incomplete or there are current unknown phases in the investigated reaction processes.

5.4.1 Calculation of saturation indices from experimental solutions in batch experiments

Sorel concrete – old / NaCl solution

Calculation of SI of the experimental solution of batch experiments in the system sorel concrete – old / NaCl solution showed, that only Halite was supersaturated during whole experimental time (Fig. 5.1). This agrees with observation of X-ray diffraction that Halite was detectable during complete experiment (chapter 4.1.2.1). But calculation of SI showed that the degree of supersaturation of Halite decreased over the experimental time of 88 days. Because there was no solution analysis after 200 days anymore, saturation with ongoing experiment could not be calculated. Anhydrite, Dansite ($\text{Na}_{21}\text{MgCl}_3(\text{SO}_4)_{10}$) and Glauberite ($\text{Na}_2\text{Ca}(\text{SO}_4)_2$) were supersaturated up to 88 days. Thereafter, they became undersaturated. But Anhydrite, Dansite and Glauberite was not detected in solid phase by X-ray-diffraction. The 318-phase was undersaturated during complete experiment, which is in accordance with X-ray diffraction. After 18 days the SI of all phases decreased simultaneously.

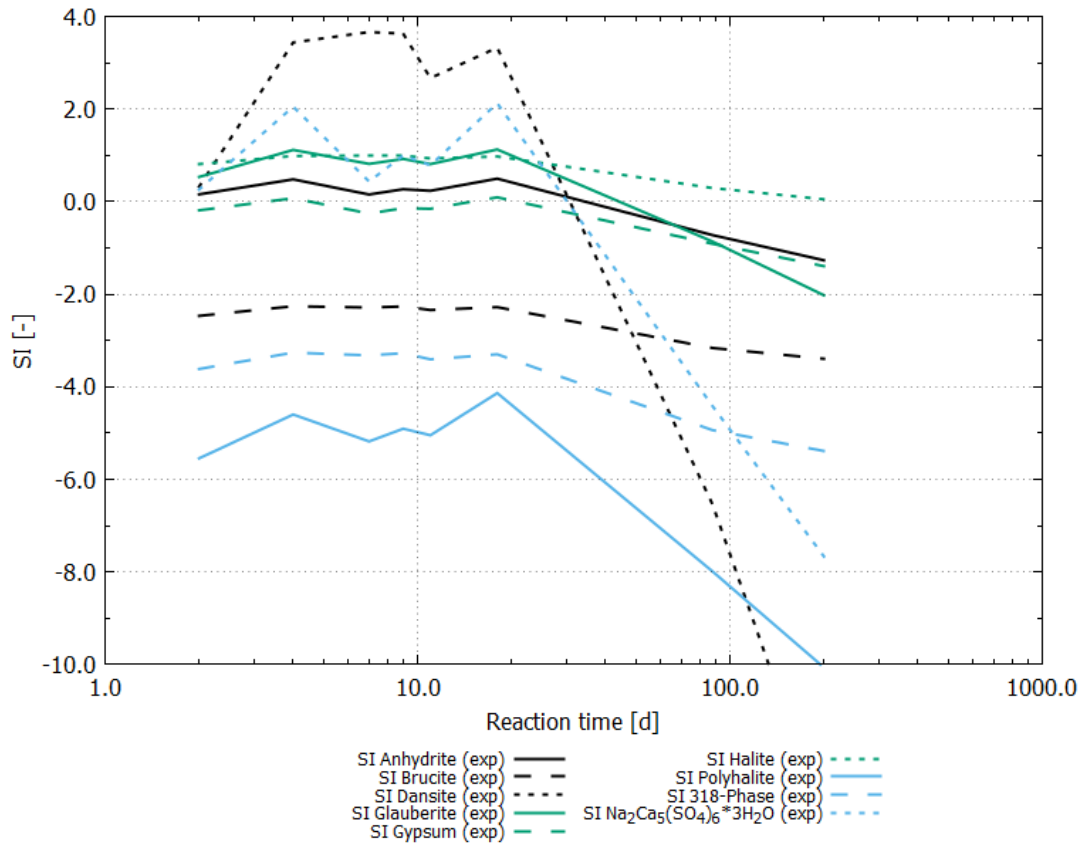


Fig. 5.1 Calculated SI of experimental solution in batch experiment in system sorel concrete - old / NaCl solution

Sorel concrete – old / MgCl₂ solution

Calculated SI of the reacted solution of batch experiments in system sorel concrete – old / MgCl₂ solution showed in agreement with results from X-ray-diffraction, that Anhydrite, Bischofite, Carnallite, Halite and the 318-phase were supersaturated during complete batch experiment (Fig. 5.2). Calculation showed supersaturation of additional phases, which were not identified by X-ray-diffraction. Noticeable is supersaturation of Brucite and Polyhalite. The SI of Gypsum alternated around 0.0 during total experimental time. Consequently, Gypsum was closed to saturation whole time.

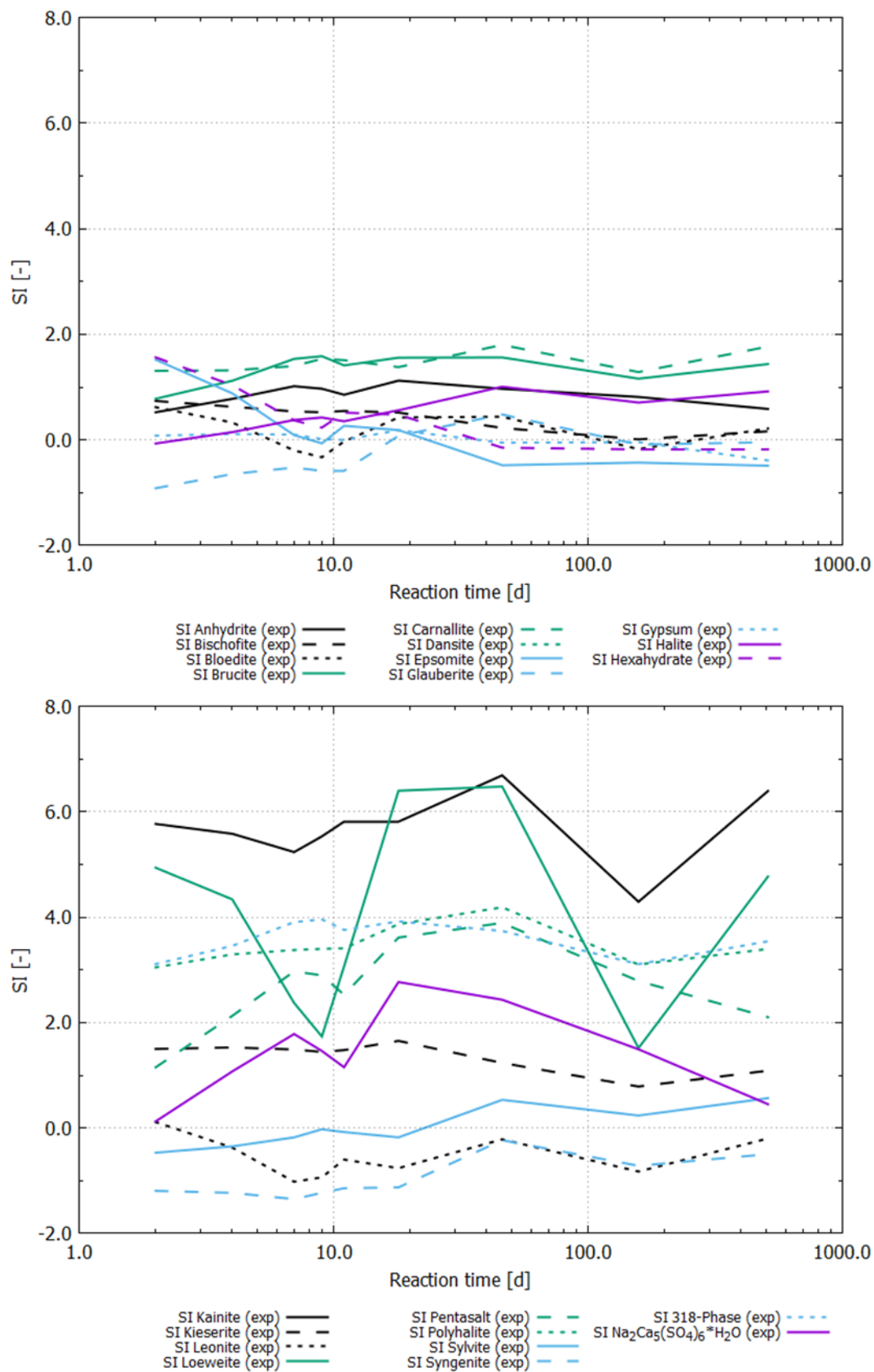


Fig. 5.2 Calculated SI of experimental solution in batch experiment in system sorel concrete - old / MgCl₂ solution

Salt concrete / NaCl solution

In reacted solution in the system salt concrete / NaCl solution among other phases Anhydrite, Gypsum and Halite, were supersaturated up to eleven days. Afterwards, SI decreased to ≈ 0.0 . Portlandite was continuously undersaturated. In addition calculation of SI showed supersaturation to amorphous and crystalline SiO. Detection by X-ray diffraction was not possible. CSH phases were continuously undersaturated. Supersaturation of Anhydrite and Halite accords with experimental results of X-ray diffraction. Portlandite could be detected by X-ray diffraction although saturation in the reacted solution was not verified. SI of Friedel's salt could not be calculated because aluminium was not quantifiable in the reacted solution from batch experiment.

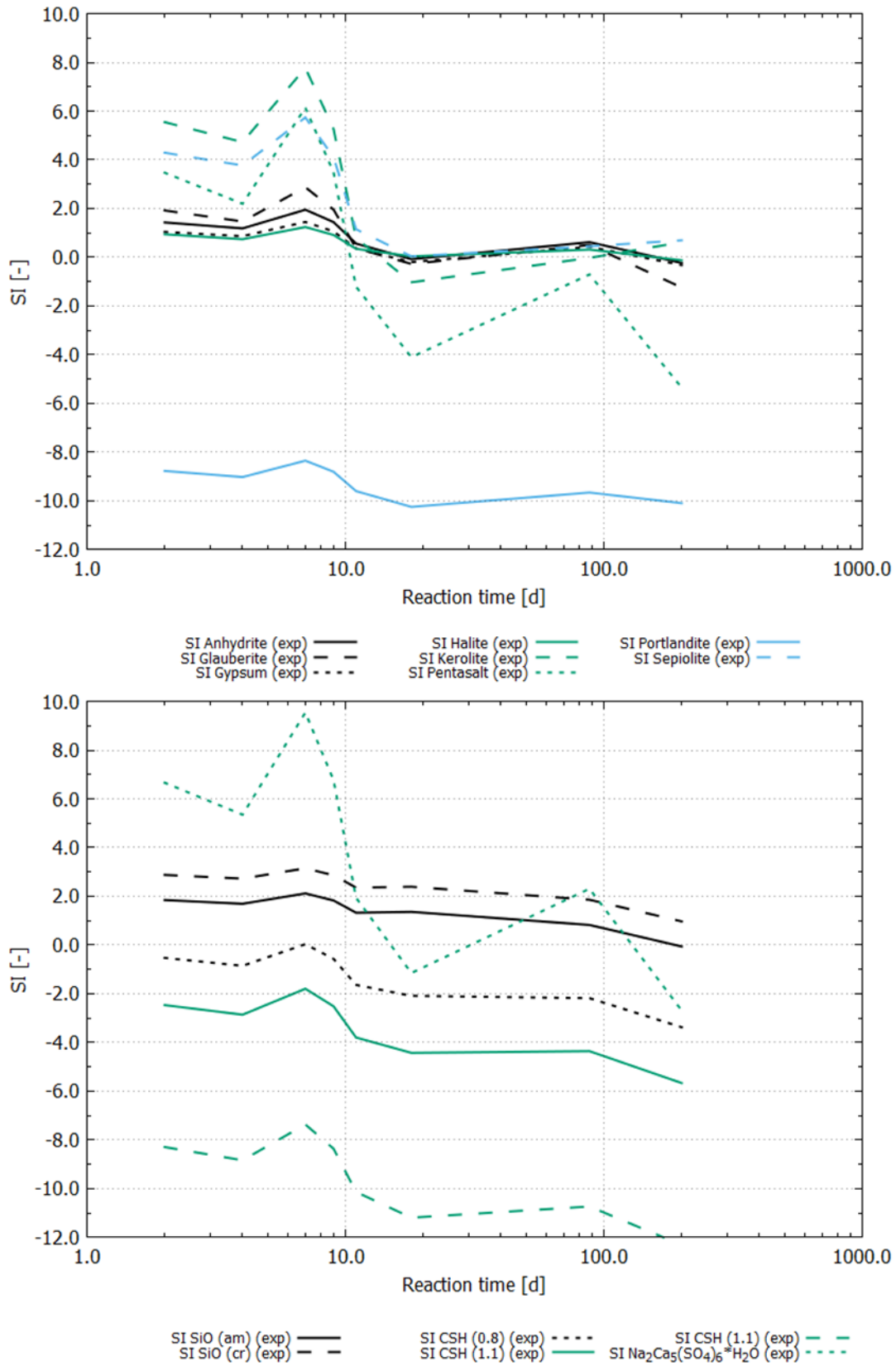


Fig. 5.3 Calculated SI of experimental solution in batch experiment in system salt concrete / NaCl solution

Salt concrete / MgCl₂ solution

Reacted solution in the system salt concrete / MgCl₂ solution was supersaturated to Anhydrite, Carnallite, Gypsum and Halite. Bischofite was supersaturated up to 46 days. Afterwards, SI of Bischofite was around 0.0. Portlandite was undersaturated. SI of Friedel's salt as well as CSH phases, SiO and MSH phases could not be calculated corresponding to system salt concrete / NaCl solution because aluminium and silicon were below the quantification limit in the reacted solution.

Among other phases (Fig. 5.4) Brucite, Polyhalite and 318-phase were supersaturated during total experimental time although saturation of these phases were not expected based on laboratory investigations.

Thus presence of phases Anhydrite, Bischofite, Carnallite, Gypsum and Halite in solid samples of reacted salt concrete, detected by X-ray diffraction, could be confirmed by saturation of those phases in the reacted solution. Dissolution of Portlandite from salt concrete could also be verified by undersaturation in the reacted solution.

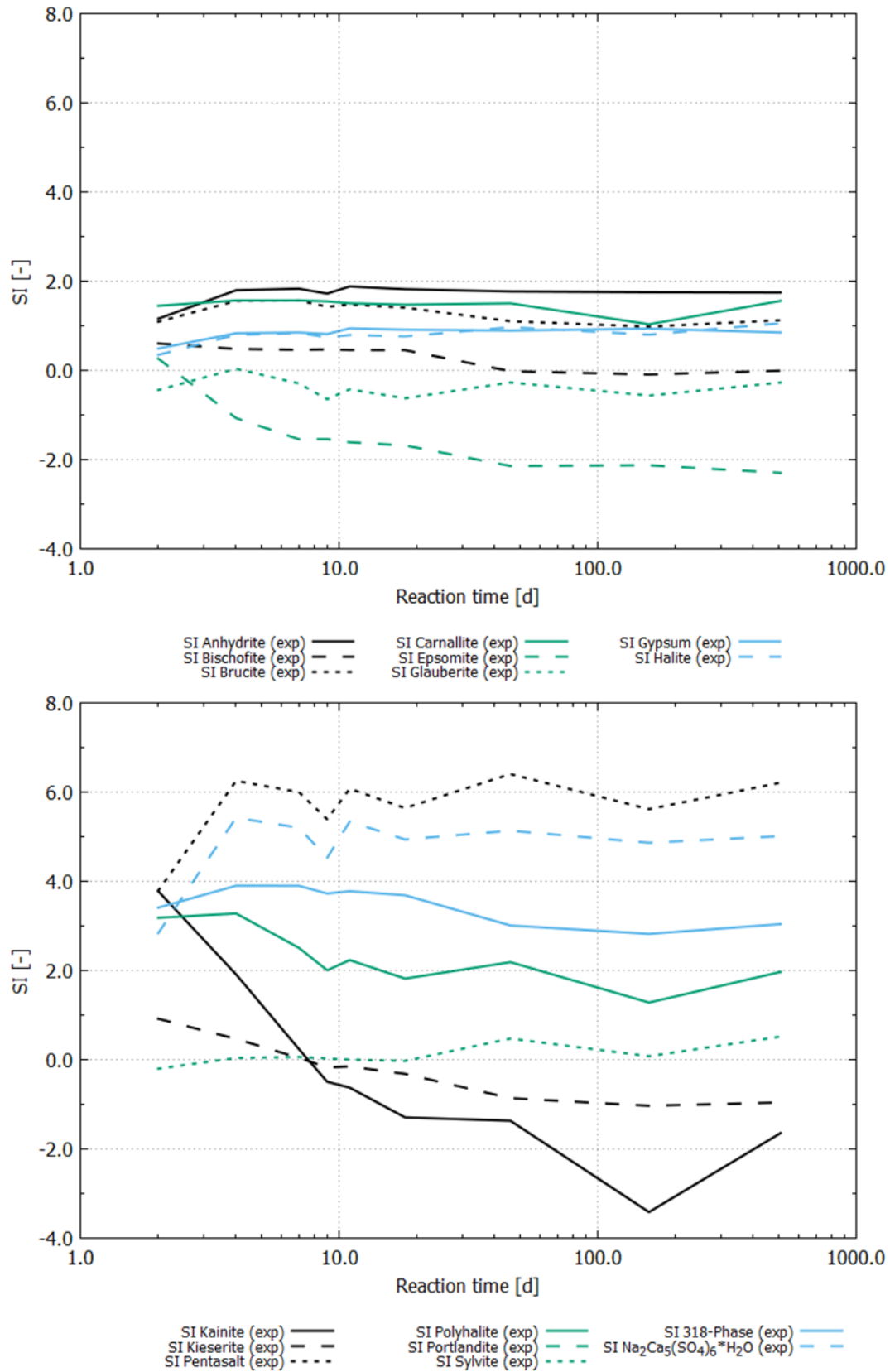


Fig. 5.4 Calculated SI of experimental solution in batch experiment in system salt concrete / MgCl₂ solution

5.4.2 Calculation of saturation indices from experimental solutions in cascade experiments

Sorel concrete – A1 / NaCl solution

The reacted solution of cascade experiments in the system sorel concrete – A1 / NaCl solution was supersaturated to Anhydrite, Glauberite, Gypsum and Halite. Brucite, Polyhalite, 318-Phase and $\text{Na}_2\text{Ca}_5(\text{SO}_4)_6 \cdot \text{H}_2\text{O}$ were undersaturated in solution during complete cascade experiment. In agreement with results of X-ray diffraction thermodynamic stability of Anhydrite and Halite could be verified by saturation of these phases in the reacted solution. But Glauberite and Gypsum, which were supersaturated in the solution, could not be detected in solid phase by X-ray diffraction. On the other hand Brucite and 318-phase were detected by X-ray diffraction in the end of each cascade but both were not (super) saturated in solution and consequently should be dissolved during cascade experiment.

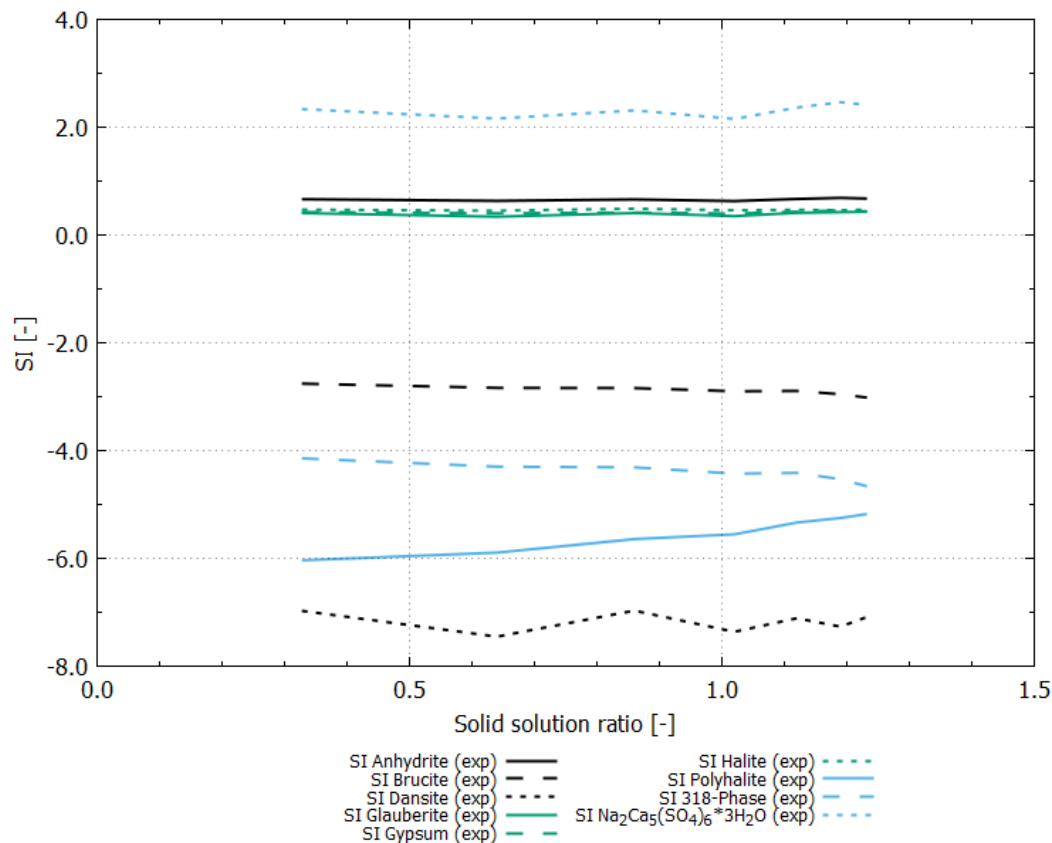


Fig. 5.5 Calculated SI of experimental solution in cascade experiment in system sorel concrete – A1 / NaCl solution

Salt concrete / MgCl₂ solution

In the reacted solution of cascade experiment in the system salt concrete / MgCl₂ solution Anhydrite, Gypsum and Halite were supersaturated. This is in agreement with X-ray diffraction of the reacted salt concrete because all phases were detected during the complete cascade experiment. Carnallite was only supersaturated until SSR \approx 1.0 was reached. In cascade experiments formation of Carnallite was detected in cascades 1 to 4, which corresponds to an SSR \approx 1.0. Hence, formation of Carnallite was verified by SI of Carnallite in solution. Bischofite was nearly saturated at low SSR but became clearly undersaturated with increased SSR. Formation of Bischofite was not detected by X-ray diffraction in cascade experiments, but before in batch experiments in the system salt concrete / MgCl₂ solution. Thus SI of Bischofite in reacted solution verified that it was not formed in cascade experiments as it did in batch experiments. Dissolution of Portlandite was verified by calculated saturations of the solution, because it was undersaturated.

Calculated SI showed additionally that reacted solution was supersaturated to Polyhalite up to SSR \approx 1.25, afterwards SI decreased significantly. 318-phase was supersaturated too and became undersaturated at SSR \approx 1.1. Brucite were supersaturated in the beginning but became undersaturated at SSR \approx 1.0. Supersaturated phases Brucite, Polyhalite and 318-phase were not detected by X-ray diffraction.

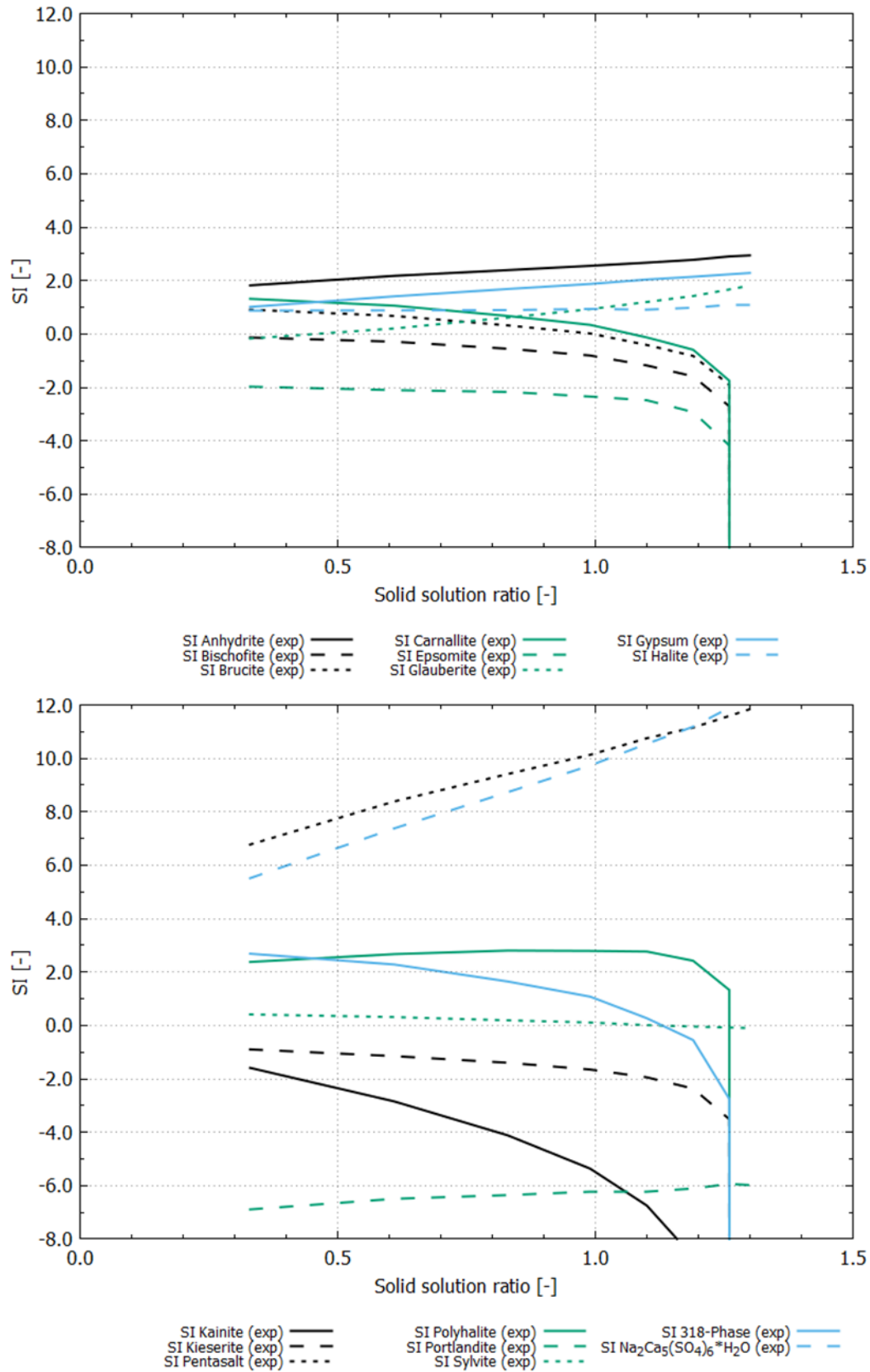


Fig. 5.6 Calculated SI of experimental solution in cascade experiment in system salt concrete/MgCl₂ solution. As to the sudden drop of SI, s. chap, 4.2.3.2.

5.4.3 Calculation of saturation indices from experimental solutions in advection experiments with sorel concrete

Sorel concrete – A1 / NaCl solution

Calculation with PHREEQC of the SI in advection experiments with sorel concrete – A1 / NaCl solution showed that Anhydrite, Gypsum and Halite were continuously supersaturated. But SI of Anhydrite, Gypsum and Halite were higher during phase of percolation than in time period of “stop-and-flow” experiments. SI decreased further by percolation of NaCl solution in the end of advection experiments at 159 and 160 days. Brucite and 318-phase were undersaturated whole time. But SI of Brucite and 318-phase decreased in phase of continuous percolation by start of experiments and became nearly constant during “stop- and-flow” experiments. After NaCl solution was percolated again, SI decreased further.

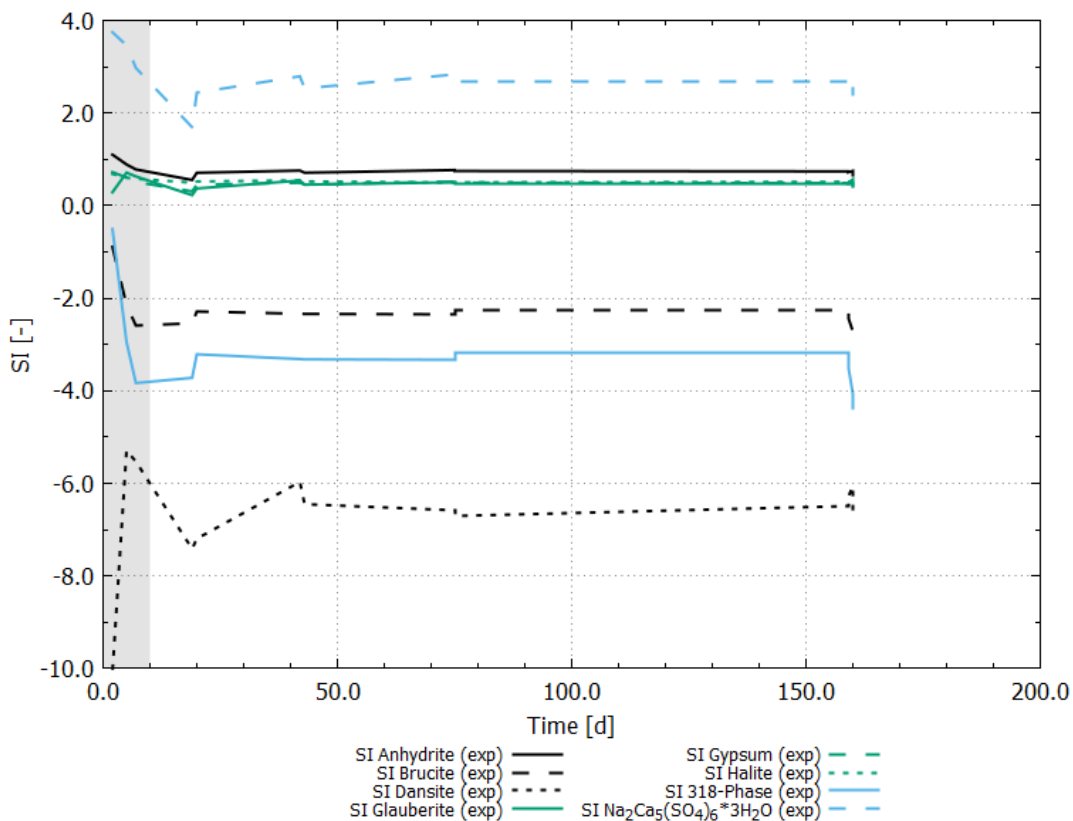


Fig. 5.7 Calculated SI of experimental solution in advection experiment in system sorel concrete – A1 / NaCl solution. Light grey rectangle marks time of continuous percolation at the beginning of experiments. Percolation was also continuous at the end of experiments (days 159/160)

Sorel concrete – A1 / MgCl₂ solution

During continuous percolation of MgCl₂ solution at the beginning of advection experiments Anhydrite and Halite were supersaturated. Saturation of all other phases increased significantly within ten to twelve days. Among other phases Brucite, Carnallite, Polyhalite and 318-phase became supersaturated within this time period. SI of Bischofite and Gypsum increased simultaneously, but SI was around 0.0 during “stop- and-flow” experiments.

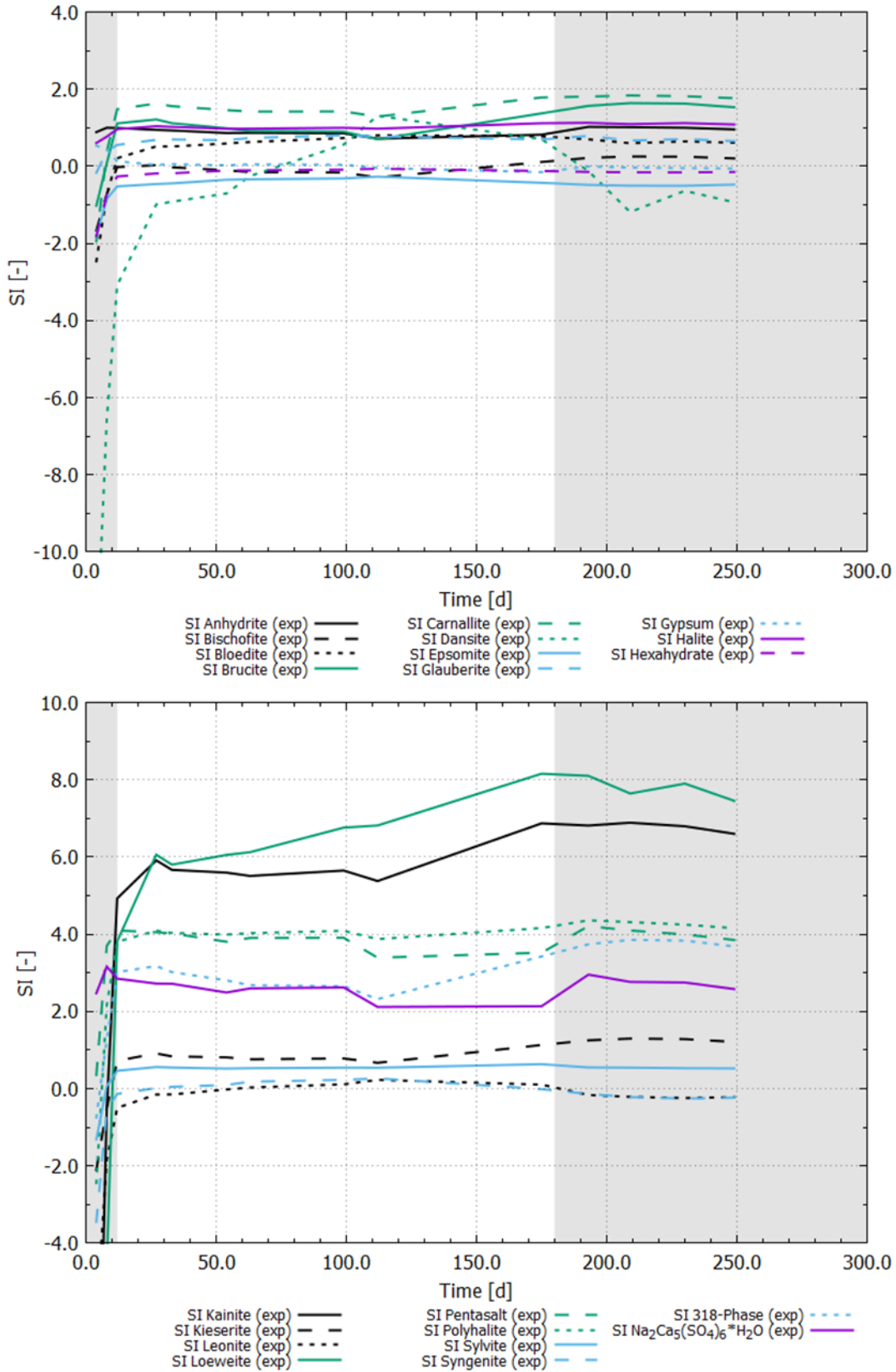


Fig. 5.8 Calculated SI of experimental solution in advection experiment in system sorrel concrete – A1 / MgCl₂ solution

5.4.4 Modelling of the reaction of sorel concrete with NaCl solution

Within this chapter four various data will be compared: Primary the concentrations of the relevant elements and compounds (calcium, chloride, magnesium, potassium, sodium and sulphate) calculated by modelling of the cascade experiments using PHREEQC are compared to experimental determined concentrations. Concentrations of modelling are signed by (X_{cal} / element name_{cal}) and concentrations of experimental results by (X_{exp} / element name_{exp}) below. In addition the SI are considered: SI, which were calculated from the experimental solutions in chapter 5.4.2 are shown as coloured lines in the figures (Fig. 5.9 and Fig. 5.10) and are signed as (SI_{exp} / phase name_{exp}). The SI, which are based on modelling of the cascade experiments, are shown in Tab. 5.11 are signed as (SI_{cal} / phase name_{cal}).

Step 1 (sorel concrete / NaCl solution)

In this step the general reaction of sorel concrete - A1 and saturated NaCl solution was calculated. The calculated element concentrations are shown by lines in Fig. 5.9 and Fig. 5.10 in comparison with experimental determined concentrations from cascade experiments (as data points) relating to the mass of reacted sorel concrete. In addition the SI of reacted solution of cascade experiments are given, which were calculated before in chapter 5.4.2 (marked with coloured lines).

The calculated chloride concentrations (Cl_{cal}) corresponding with experimental concentrations (Cl_{exp}) over the whole reaction path. Sodium concentrations (Na_{cal} and Na_{exp}) fitted well up to 0.3 kg reacted sorel concrete. But calculated concentrations (Na_{cal}) became too low in comparison to experimental concentrations (Na_{exp}) with increasing mass of reacted sorel concrete.

Glauberite_{exp}, Halite_{exp} and $\text{Na}_2\text{Ca}_5(\text{SO}_4)_6 \cdot 3\text{H}_2\text{O}_{\text{exp}}$ were supersaturated during whole experimental reaction and SI changed not significant. Dansite, which was considered based on calculated SI of batch experiments, was undersaturated whole time. Polyhalite_{exp} was also undersaturated.

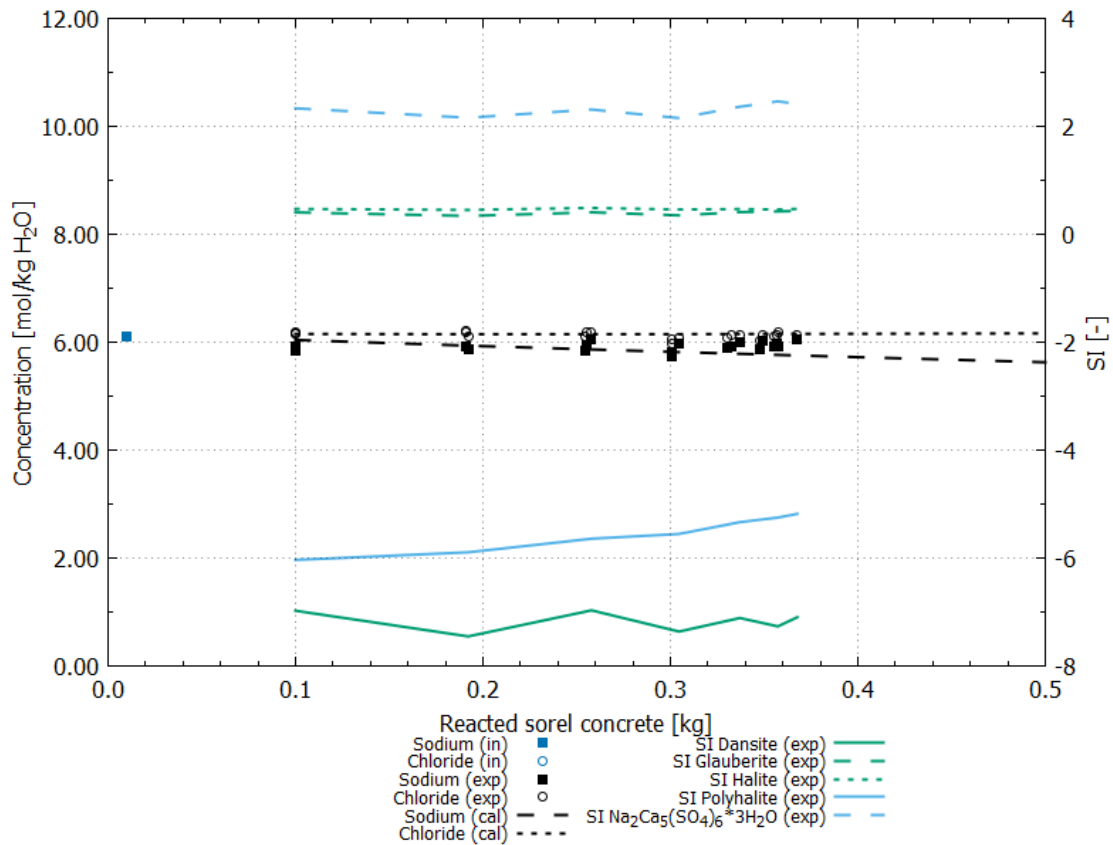


Fig. 5.9 Step 1 (sorel concrete / NaCl solution): Comparison of calculated (cal) and experimental (exp) concentrations of sodium and chloride. Additionally, the initial (in) concentrations of elements in NaCl solution and the saturation index of chloride and sodium containing phases in cascade experiment are given

The ratio of concentrations for calcium (Fig. 5.11) and sulphate (Fig. 5.10) was 1:1 both in experiment and modelling. But in experiment calcium (Ca_{exp}) and sulphate ($SO_4^{2-}_{exp}$) dissolved directly and concentrations in solution were about 0.04 mol/kg H_2O during whole experiment. In modelling concentrations of calcium (Ca_{cal}) and sulphate ($SO_4^{2-}_{cal}$) were lower in the beginning (0.02 mol/kg H_2O at 0.10 kg reacted sorel concrete) and increased with ongoing reaction. After reaction of 0.3 kg sorel concrete, the concentration (Ca_{cal} and $SO_4^{2-}_{cal}$) of 0.04 mol/kg H_2O was in agreement with the experiment. Experimental determined and calculated concentrations of potassium (K_{exp} and K_{cal}) were in good agreement. The small increase of potassium (K_{exp}) in solution could be reproduced with PHREEQC.

Model investigations

A significant deviation was noticed in the development in magnesium concentration (Fig. 5.10). A decrease of magnesium (Mg_{exp}) from 0.16 – 0.17 mol/kg H_2O to 0.10 mol/kg H_2O was measured in experiments. Additional concentrations decreased faster after 0.33 kg sorel concrete reacted. The concentration of magnesium (Mg_{cal}) in first reaction step in modelling was only 0.05 mol/kg H_2O and afterwards the magnesium (Mg_{cal}) concentration increased significantly. When circa 0.36 kg sorel concrete reacted (this mass is in agreement with the mass of reacted concrete at the end of cascade experiments) the magnesium (Mg_{cal}) concentration was calculated to circa 0.18 mol/kg H_2O . This value is higher than the maximum magnesium concentration in experiments.

Anhydrite_{exp}, Glauberite_{exp}, Gypsum_{exp} and $Na_2Ca_5(SO_4)_6 \cdot 3H_2O_{exp}$ were supersaturated during whole reaction time of experiments without significant changes in SI. Brucite_{exp}, Dansite_{exp}, Polyhalite_{exp} and 318-phase_{exp} were undersaturated. SI of Brucite_{exp} and 318-phase_{exp} became a low decreasing trend when 0.33 kg sorel concrete reacted. That is in accordance with the point of time when magnesium (Mg_{exp}) concentrations decreased faster.

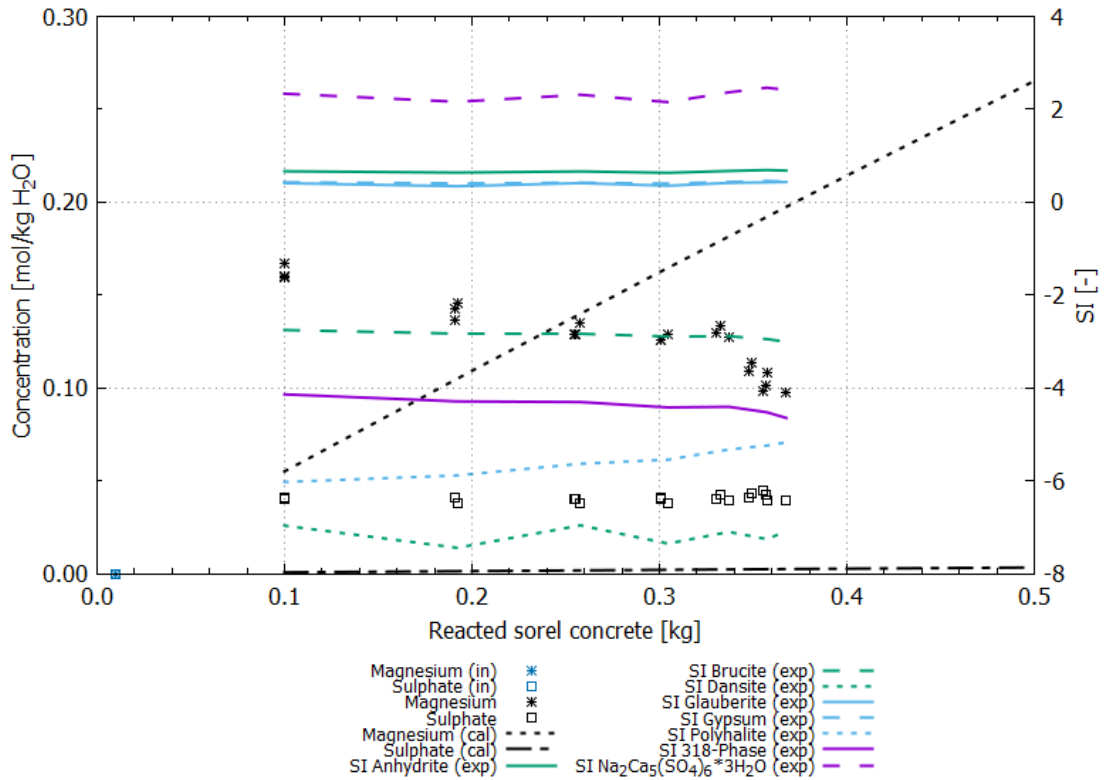


Fig. 5.10 Step 1 (sorel concrete / NaCl solution): Comparison of calculated (cal) and experimental (exp) concentrations of magnesium and sulphate. Additionally, the initial (in) concentration of elements in NaCl solution and the saturation index of calcium, magnesium, potassium and sulphate containing phases in cascade experiments are given

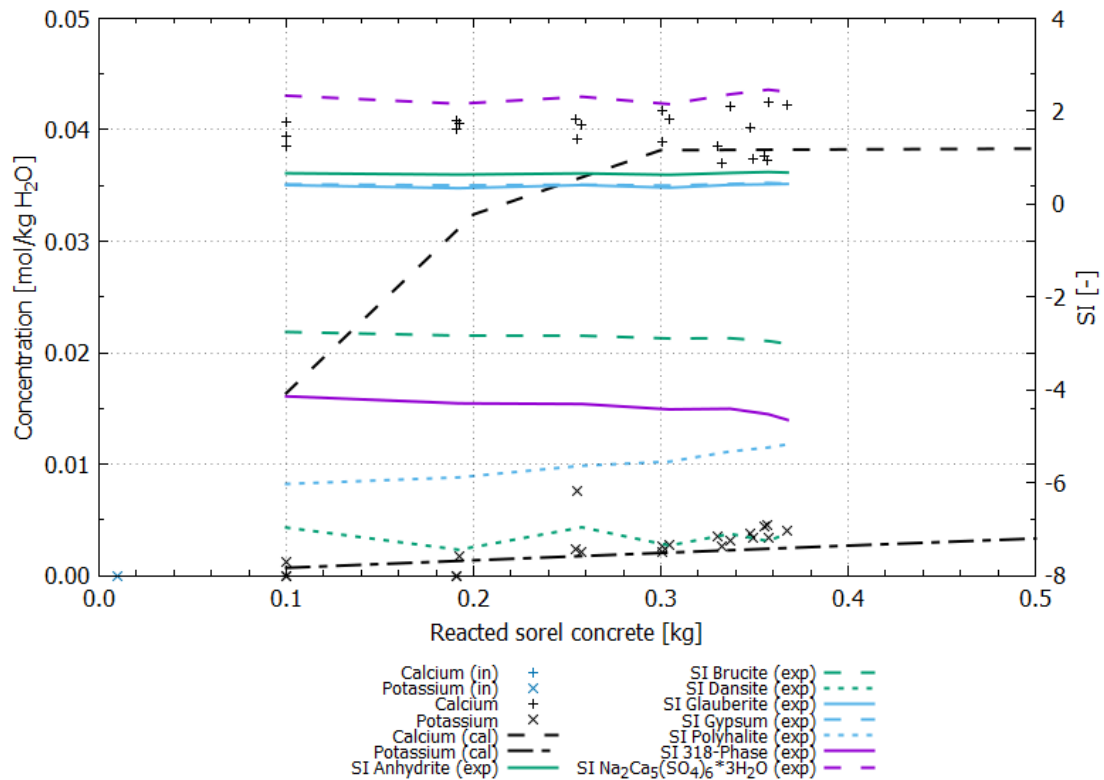


Fig. 5.11 Step 1 (sorel concrete / NaCl solution): Comparison of calculated (cal) and experimental (exp) concentrations of calcium and potassium. Additionally, the initial (in) concentration of elements in NaCl solution and the saturation index of calcium, magnesium, potassium and sulphate containing phases in cascade experiments are given

Tab. 5.11 shows SI_{cal} of relevant phases in modelling of cascade experiments. Phases, which are not presented, were undersaturated. Saturation of Anhydrite_{cal} and Halite_{cal} is consistent with experimental results of cascade experiments. Also, the undersaturation of 318-phase_{cal} is correctly predicted. In contrast, saturation of Brucite_{exp} was not calculated in the reacted solution of cascade experiments but Brucite was saturated in modelling.

Tab. 5.11 Saturation index in step 1 (sorel concrete / NaCl solution). Phases, which are not listed, were undersaturated during complete reaction

Reaction step	Anhydrite SI	Brucite SI	Halite SI	318-Phase SI
1	-0.725	0.000	0.000	-0.527
2	-0.145	0.000	0.000	-0.374
3	0.000	0.000	0.000	-0.284
4	0.000	0.000	0.000	-0.219
5	0.000	0.000	0.000	-0.168

Step 2 (sorel concrete / NaCl solution)

Mineral phases, which may form during the reaction of sorel concrete with NaCl solution were limited to those phases, which were determined by X-ray diffraction in laboratory on (reacted) sorel concrete A1: Anhydrite, Brucite, Halite and 318-phase. This approach did not result in an improvement of calculation.

Because calculated reaction path of step 2 (sorel concrete / NaCl solution) closely resembles results of step 1 (sorel concrete / NaCl solution), results are not represented separately.

Step 3 (sorel concrete / NaCl solution)

Other attempts to reproduce results from the cascade experiments included the consideration of more magnesium phases, which are not part of the THEREDA database release 6.0. Yet, in neither case an accordance of model calculation and experiments could be achieved.

5.4.5 Modelling of the reaction of salt concrete with MgCl₂ solution

In agreement with chapter 5.4.4 concentrations of experimental and modelling results are compared in Fig. 5.12 to Fig. 5.20. In addition, SI_{exp} , which were calculated from the

composition of the reacted solution in experiments are compared to SI_{cal} calculated by modelling of the cascade experiments. SI_{exp} , based on experiments are shown in Fig. 5.12 to Fig. 5.20 and SI_{cal} , based on modelling of cascade experiments are shown in Tab. 5.12 to Tab. 5.14.

Step 1 (salt concrete / $MgCl_2$ solution)

Fig. 5.12 to Fig. 5.14 show results from modelling compared to experimental results. Modelling results of the general reaction of salt concrete with $MgCl_2$ solution are shown by lines. The experimental results from the cascade experiment are shown by points. In addition the SI_{exp} of selected phases of the reacted solution of cascade experiments, which were calculated in chapter 5.4.2, are shown by coloured lines. Because of clear arrangement not all phases, which are known from calculation of SI_{exp} of cascade experiments using PHREEQC are shown.

The concentrations of chloride and sodium were in good agreement between modelling and experimental results in beginning of reaction (0.1 kg reacted salt concrete). The high spread of chloride (Cl_{exp}) concentrations with ongoing experiment was conspicuous. Values were between 7.05 mol/kg H_2O and 9.41 mol/kg H_2O . This spread was not depicted by modelling. Calculated concentrations (Cl_{cal}) increased from 8.87 mol/kg H_2O to 8.89 mol/kg H_2O . Modelled sodium (Na_{cal}) concentrations increased from 0.55 mol/kg H_2O to 0.63 mol/kg H_2O . In experiment concentrations (Na_{exp}) increased twice as much to 1.43 – 1.45 mol/kg H_2O . Calculation of SI_{exp} of Halite from experimental solutions shown that Halite was supersaturated during the whole experiment. SI_{exp} was < 1 up to 0.3 kg of reacted concrete and increased to values > 1 afterwards. If more than 0.4 kg concrete had reacted, SI_{exp} increased further up to $SI \approx 1.5$.

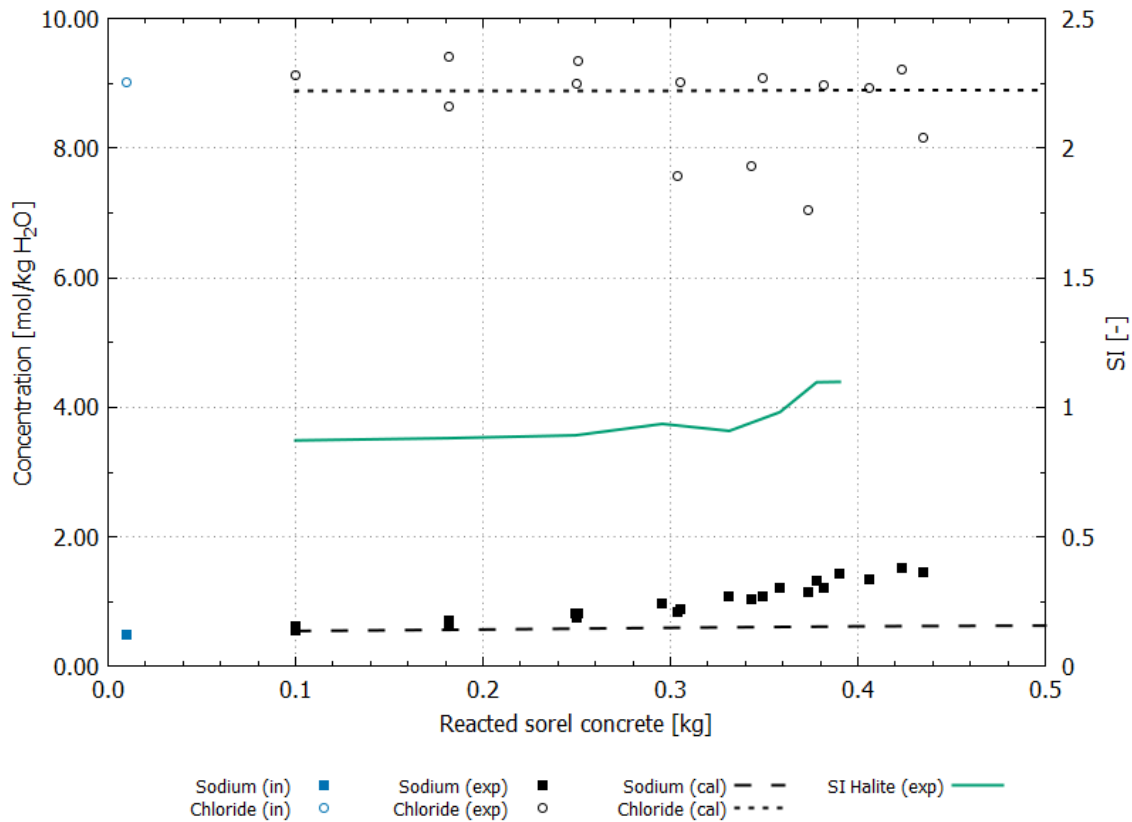


Fig. 5.12 Step 1 (salt concrete / MgCl₂ solution): Comparison of calculated (cal) and experimental (exp) concentrations of sodium and chloride. Additionally, the initial (in) concentrations of elements in MgCl₂ solution and the saturation index of Halite are given

Fig. 5.13 shows the development of calcium and magnesium concentrations. Calcium (Ca_{exp}) concentrations increased significantly in the cascade experiment from 0.001 mol/kg H₂O in the initial MgCl₂ solution to 3.29 – 3.61 mol/kg H₂O. Calculated concentrations (Ca_{cal}) showed only a small amount to 0.11 mol/kg H₂O. Magnesium concentrations developed contrary: concentrations (Mg_{exp}) decreased from 4.36 mol/kg H₂O in the initial solution to below the detection limit. But modelling results (Mg_{cal}) showed only a decrease to 3.72 mol/kg H₂O.

Calculation of SI showed that Anhydrite_{exp} and Gypsum_{exp} were supersaturated all time. SI of Gypsum_{exp} increased from ≈ 1.0 to ≈ 2.3, of Anhydrite_{exp} from ≈ 1.8 to ≈ 3.0. When more than 0.42 kg concrete had reacted, both SI decreased a little. In modelling both Anhydrite_{cal} and Halite_{cal} were saturated during whole reaction. The SI of Brucite_{exp} was circa 0.8 in the first cascade and decreased with ongoing experiment. When about

0.3 kg concrete had reacted, SI of Brucite_{exp} became < 0.0, hence, the solution was undersaturated. With ongoing reaction SI_{exp} decreased to ≈ -2.0. Brucite_{cal} was undersaturated in modelling during whole reaction time.

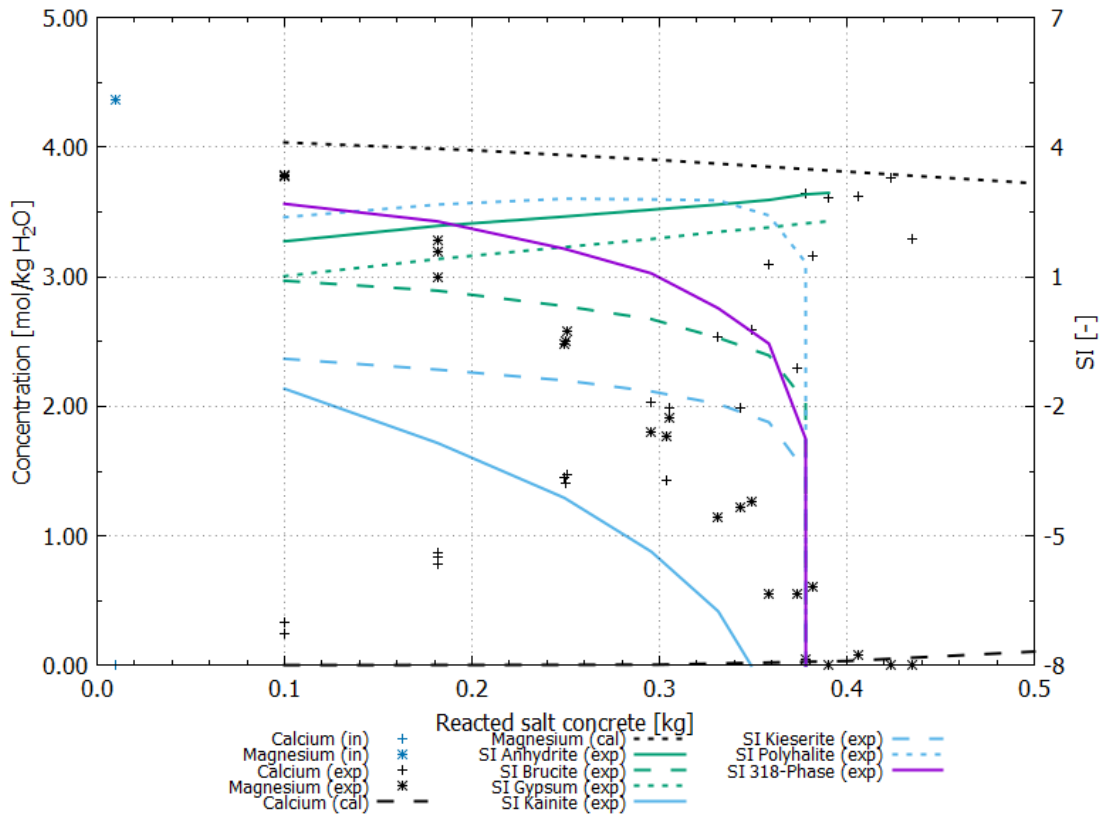


Fig. 5.13 Step 1 (salt concrete / MgCl₂ solution): Comparison of calculated (cal) and experimental (exp) concentrations of calcium and magnesium. Additionally, the initial (in) concentrations of elements in MgCl₂ solution and the saturation index of selected phases are given

Concentrations of potassium (K_{exp}) changed less in the experiment in comparison with the initial concentration of 0.57 mol/kg H₂O and decreased to 0.50 – 0.52 mol/kg H₂O. Modelling results showed that potassium (K_{cal}) concentrations increased from 0.50 mol/kg H₂O to 0.61 mol/kg H₂O. Sulphate concentrations developed contrary in experiments and calculation. In experiments concentrations ($SO_4^{2-}_{exp}$) increased from 0.03 mol/kg H₂O to 0.19 mol/kg H₂O. In calculations concentrations ($SO_4^{2-}_{cal}$) decreased from 0.13 mol/kg H₂O to 0.005 mol/kg H₂O.

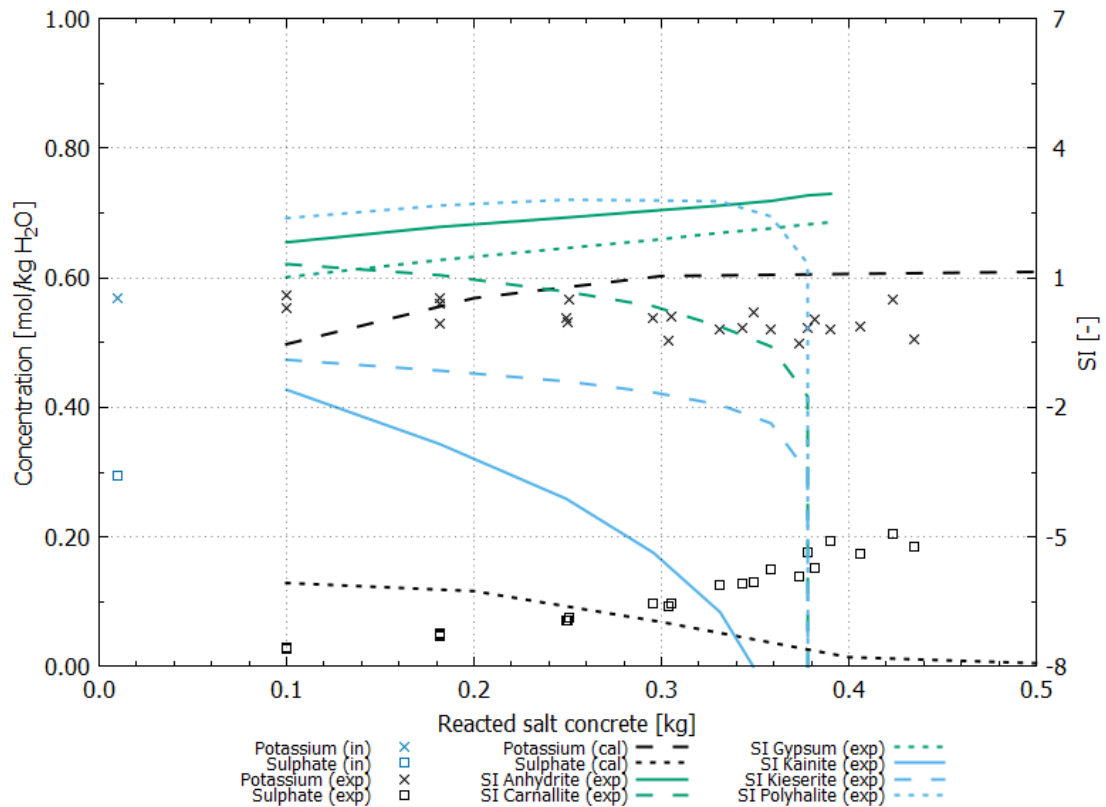


Fig. 5.14 Step 1 (salt concrete / MgCl₂ solution): Comparison of calculated (cal) and experimental (exp) concentrations of potassium and sulphate. Additionally, the initial (in) concentrations of elements in MgCl₂ solution and the saturation index of selected phases are given

Compared to the reacted solution of cascade experiments solution in modelling was saturated to Hydrotalcite_{cal} and Kerolite_{cal}. Saturation with Anhydrite_{cal} and Halite_{cal} is in agreement with saturation in experiments. Polyhalite_{cal} was saturated only in first two reaction steps of modelling and became undersaturated with increasing SSR. In experiments Polyhalite_{exp} was continuously undersaturated but SI also decreased with increasing SSR. Saturation of 318-phase differs in experiments and modelling, because 318-phase_{cal} was saturated in modelling but in cascade experiments 318-phase_{exp} was only supersaturated in the beginning and became undersaturated after reaction of 0.3 kg salt concrete.

Tab. 5.12 Saturation index in step 1 (salt concrete / MgCl₂ solution). Phases, which are not listed, were undersaturated during complete reaction

Reaction step	Anhydrite SI	Halite SI	Hydrotalcite SI	Kerolite SI	318-Phase SI	Polyhalite SI
1	0.000	0.000	0.000	0.000	0.000	0.000
2	0.000	0.000	0.000	0.000	0.000	0.000
3	0.000	0.000	0.000	0.000	0.000	-0.430
4	0.000	0.000	0.000	0.000	0.000	-1.835
5	0.000	0.000	0.000	0.000	0.000	-2.836

Step 2 (salt concrete / MgCl₂ solution)

This step was executed in two steps. First, phases, which are allowed to precipitate, were limited to those phases, which were known from X-ray-diffraction of laboratory salt concrete samples and amorphous phases (Tab. 5.7). Because calculation did not agree with laboratory results, the formation of those phases was tolerated, which were supersaturated after first calculation of step 2a (salt concrete / MgCl₂ solution).

The calculated concentrations of Chloride (Cl_{cal}) and Sodium (Na_{cal}) showed no significant change in its development of concentrations compared to step 1 (salt concrete / MgCl₂ solution) (Fig. 5.15).

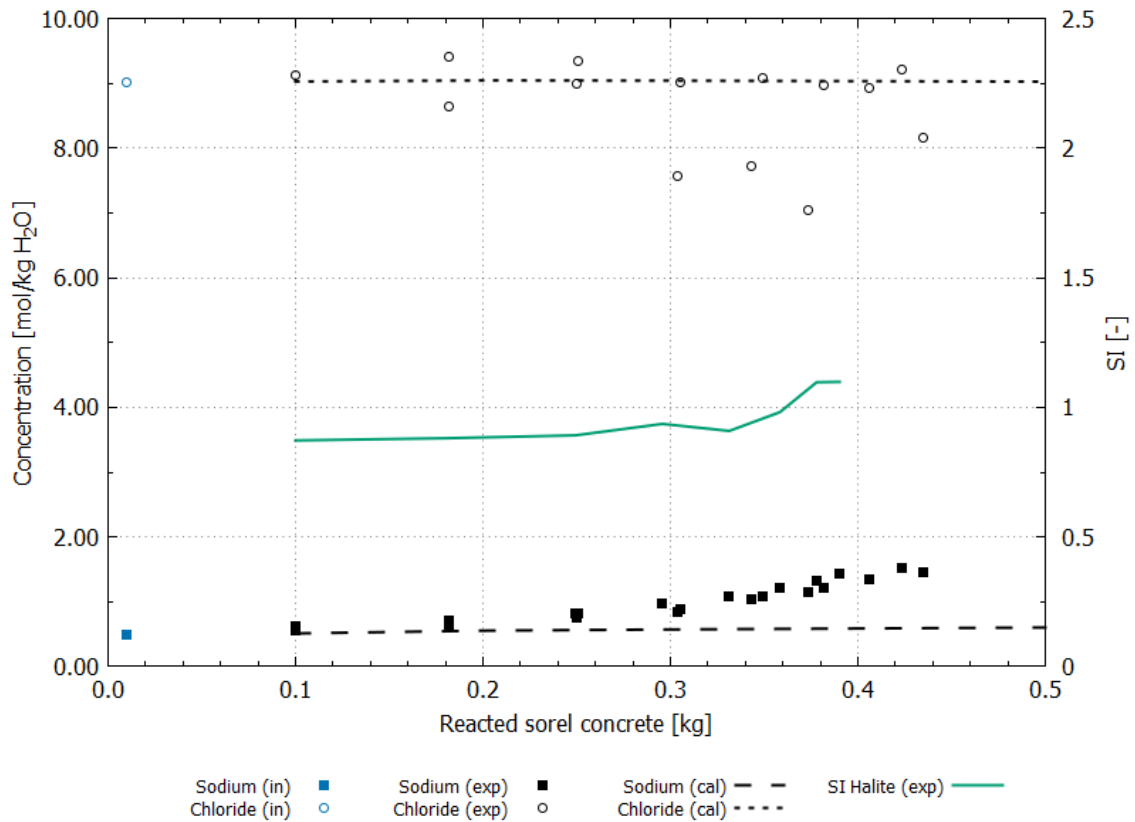


Fig. 5.15 Step 2 (salt concrete / $MgCl_2$ solution): Comparison of calculated (cal) and experimental (exp) concentrations of sodium and chloride. Additionally, the initial (in) concentrations of elements in $MgCl_2$ solution and the saturation index of Halite are given

The calculated calcium (Ca_{cal}) concentrations increased already at 0.2 kg reacted concrete in step 2 (salt concrete / $MgCl_2$ solution). Calcium (Ca_{cal}) concentrations of 0.44 mol/kg H_2O were also higher at the end in comparison to step 1 (salt concrete / $MgCl_2$ solution). The change in magnesium (Mg_{cal}) concentrations was also higher compared to step 1 (salt concrete / $MgCl_2$ solution). Concentrations decreased up to 3.47 mol/kg H_2O . But development of calcium (Ca_{cal}) and magnesium (Mg_{cal}) concentrations did not fit to experimental concentrations too.

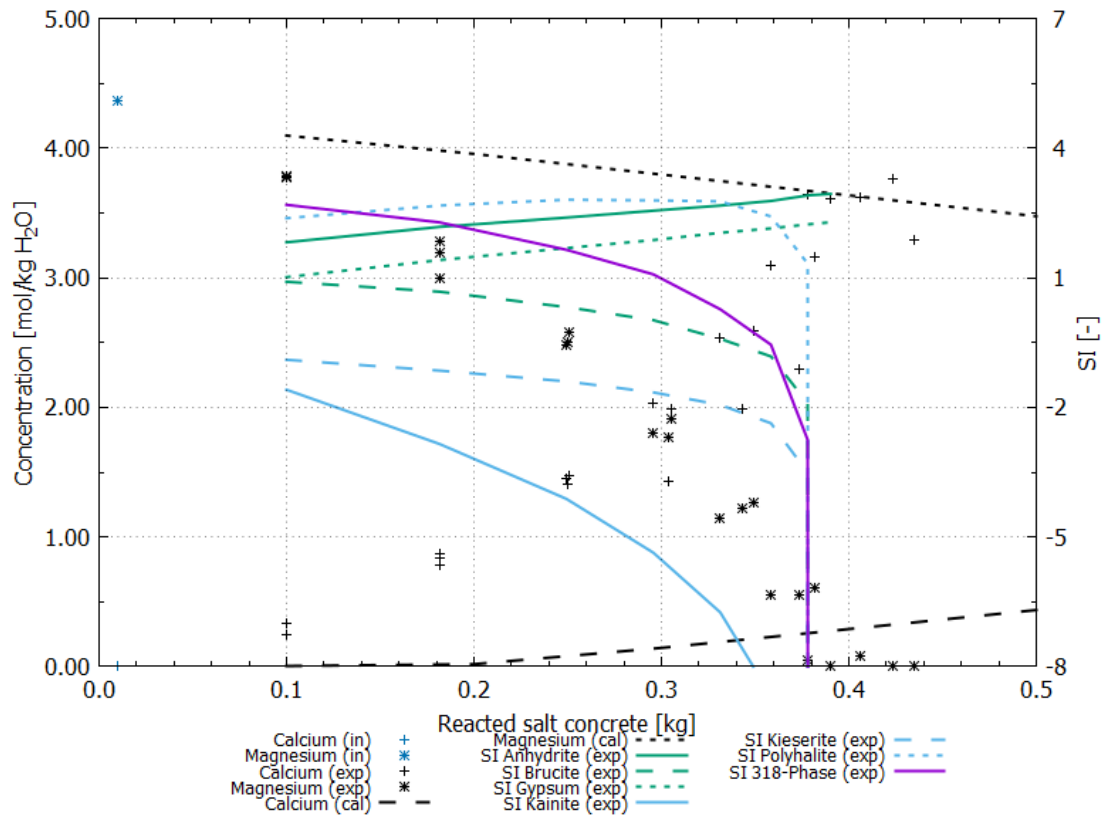


Fig. 5.16 Step 2 (salt concrete / MgCl₂ solution): Comparison of calculated (cal) and experimental (exp) concentrations of calcium and magnesium. Additionally, the initial (in) concentrations of elements in MgCl₂ solution and the saturation index of selected phases are given

In comparison to step 1 (salt concrete / MgCl₂ solution) calculated potassium (K_{cal}) concentrations agreed with experimental concentrations in the beginning of experiments. But potassium (K_{cal}) concentrations increased with increasing mass of reacted salt concrete in agreement with calculation before. This development was not in accordance with experiments, too. Sulphate ($SO_4^{2-}_{cal}$) concentrations developed also contrary to experimental results. In comparison to step 1 (salt concrete / MgCl₂ solution) sulphate ($SO_4^{2-}_{cal}$) concentrations were at 0.12 mol/kg H₂O but they decreased much faster.

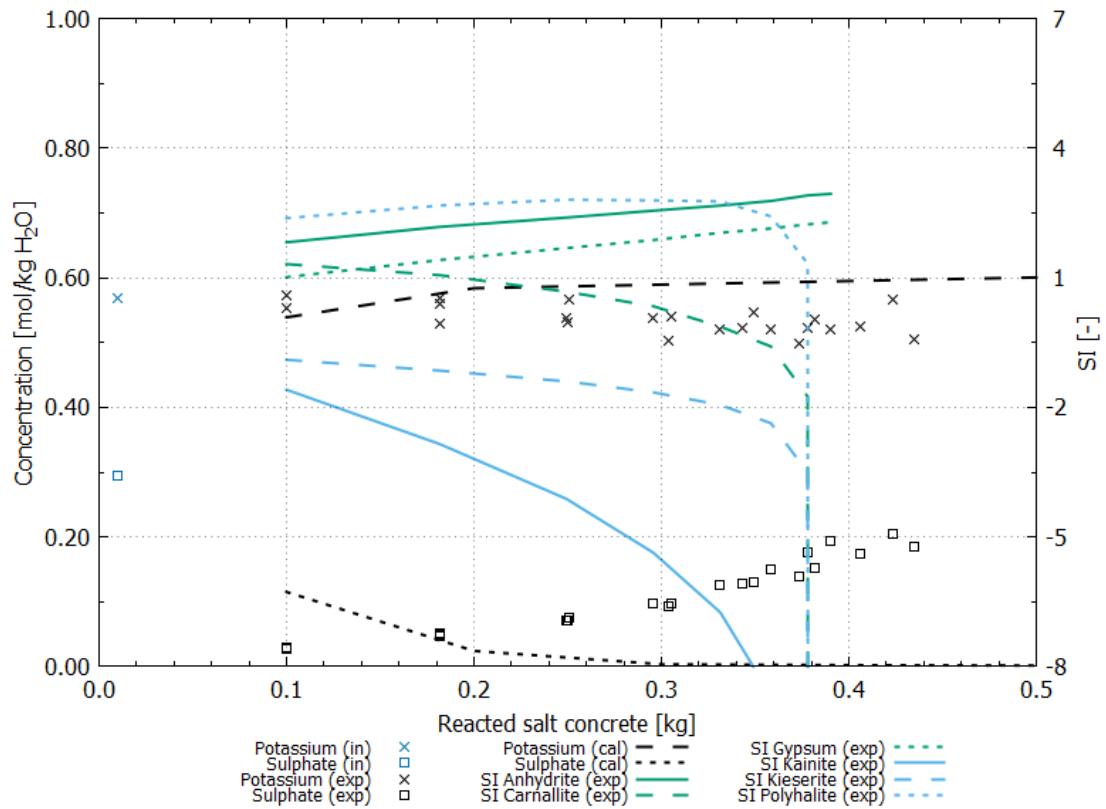


Fig. 5.17 Step 2 (salt concrete / MgCl₂ solution): Comparison of calculated (cal) and experimental (exp) concentrations of potassium and sulphate. Additionally, the initial (in) concentrations of elements in MgCl₂ solution and the saturation index of selected phases are given

Calculation of SI in modelling of step 2 (salt concrete / MgCl₂ solution) did not differ significantly from saturation of phases from step 1 (salt concrete / MgCl₂ solution) before: Phases Anhydrite_{cal}, Halite_{cal}, Hydrotalcite_{cal}, Kerolite_{cal} and 318-phase_{cal} were still saturated. Polyhalite_{cal} was also saturated in the beginning, but became undersaturated earlier in second step of reaction as in step 1.

Tab. 5.13 Saturation index in step 2 (salt concrete / MgCl_2 solution). Phases, which are not listed, were undersaturated during complete reaction

Reaction step	Anhydrite SI	Halite SI	Hydrotalcite SI	Kerolite SI	318-Phase SI	Polyhalite SI
1	0.000	0.000	0.000	0.000	0.000	0.000
2	0.000	0.000	0.000	0.000	0.000	-1.346
3	0.000	0.000	0.000	0.000	0.000	-3.161
4	0.000	0.000	0.000	0.000	0.000	-3.792
5	0.000	0.000	0.000	0.000	0.000	-4.175

Step 3 (salt concrete / MgCl_2 solution)

The calculated chloride (Cl_{cal}) concentrations were at 5.96 mol/kg H_2O after reaction of 0.1 kg salt concrete and increased with increasing mass of reacted concrete to 6.61 mol/kg H_2O . In comparison to experimental results calculated chloride (Cl_{cal}) concentrations were too low. Sodium (Na_{cal}) concentrations were at 1.39 mol/kg H_2O in calculation and increased to 4.03 mol/kg H_2O after 0.5 kg concrete reacted. This concentration is more than twice as much as in laboratory experiments. In comparison to steps before an increase of sodium concentration could be calculated in step 3 (salt concrete / MgCl_2 solution) in agreement with laboratory results. But concentration (Na_{cal}) was too high.

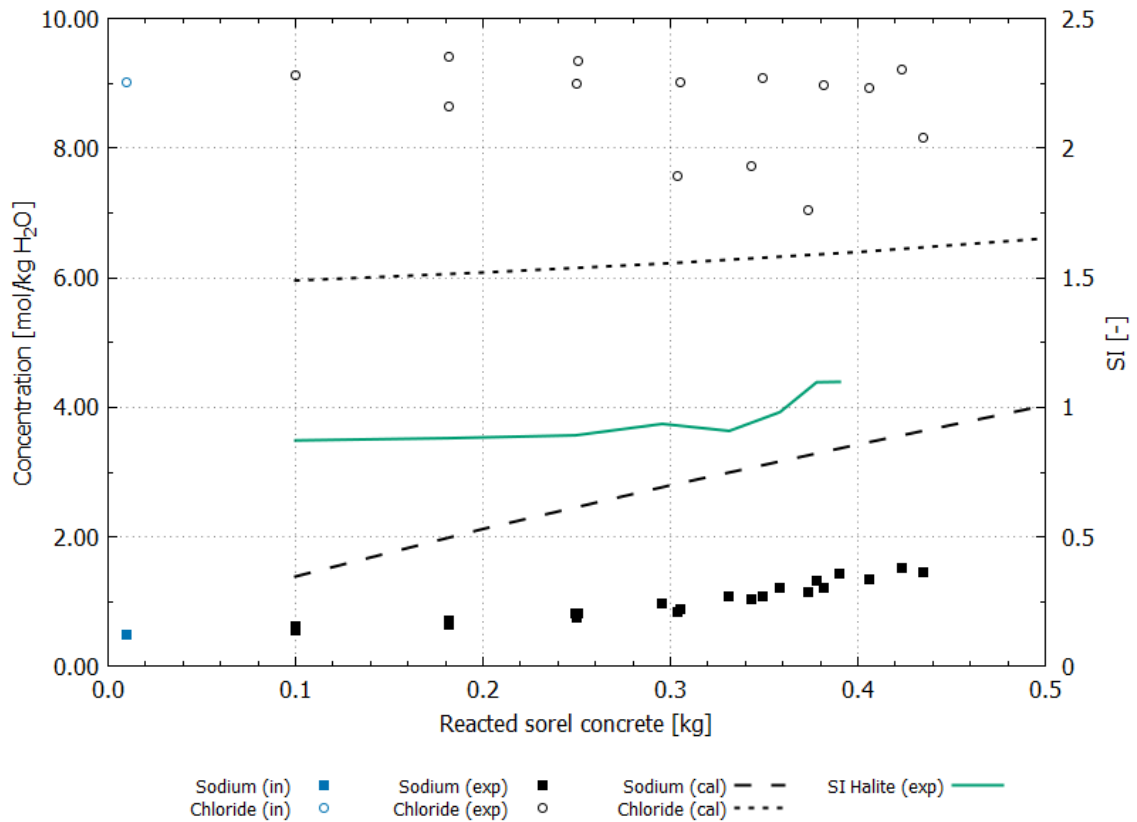


Fig. 5.18 Step 3 (salt concrete / MgCl₂ solution): Comparison of calculated (cal) and experimental (exp) concentrations of sodium and chloride. Additionally, the initial (in) concentrations of elements in MgCl₂ solution and the saturation index of Halite are given

The concentration of calcium (Ca_{cal}) decreased in step 3 (salt concrete / MgCl₂ solution) from 1.97 mol/kg H₂O to 1.04 mol/kg H₂O. This did not conform to laboratory results, because calcium (Ca_{exp}) concentrations in experiments increased. Calculated magnesium (Mg_{cal}) concentration was continuously 0.00 mol/kg H₂O. The decrease of experimental magnesium (Mg_{exp}) concentration could not be calculated in this step.

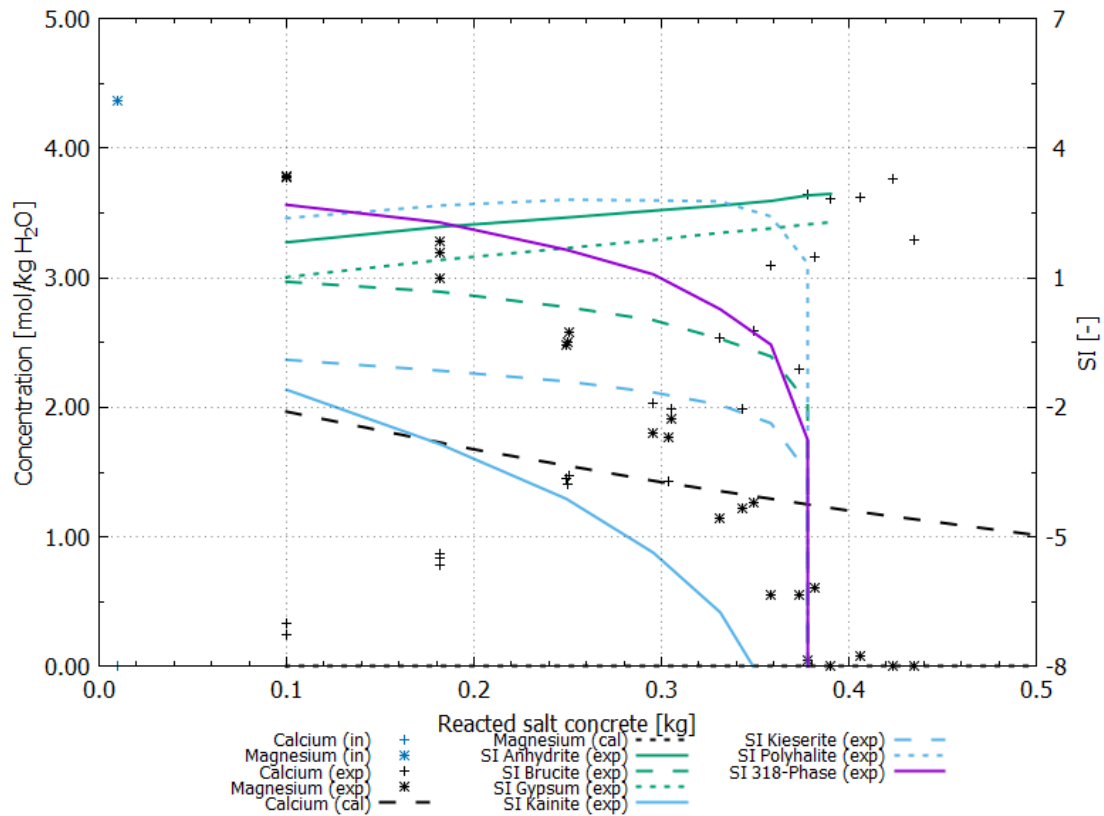


Fig. 5.19 Step 3 (salt concrete / MgCl_2 solution): Comparison of calculated (cal) and experimental (exp) concentrations of calcium and magnesium. Additionally, the initial (in) concentrations of elements in MgCl_2 solution and the saturation index of selected phases are given

Potassium (K_{cal}) concentrations decreased in calculation from 0.64 mol/kg H_2O to 0.56 mol/kg H_2O . In comparison to laboratory results the trend was in agreement with experimental potassium (K_{exp}) concentrations. But experimental concentrations (K_{exp}) were 0.05 mol/kg H_2O smaller in average than calculated concentrations. The development of sulphate concentration could not be calculated. Calculated concentration ($\text{SO}_4^{2-}_{\text{cal}}$) was constant at 0.00 mol/kg H_2O but in experiments concentrations ($\text{SO}_4^{2-}_{\text{exp}}$) increased.

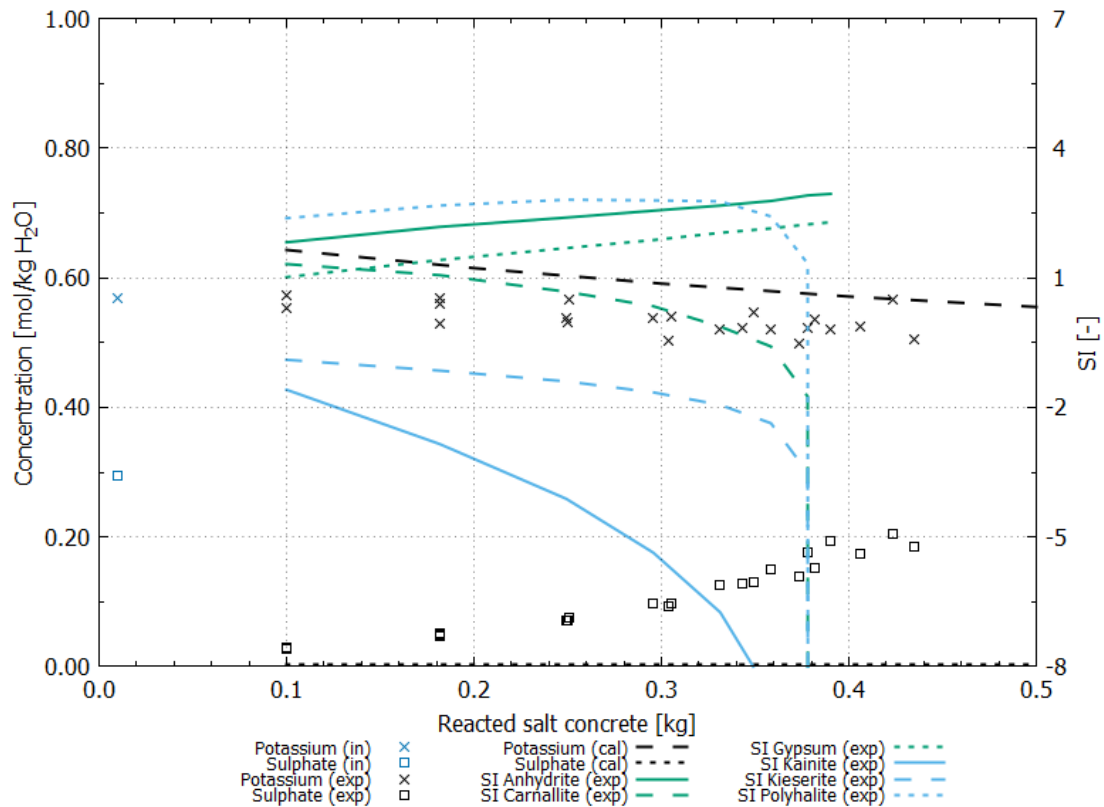


Fig. 5.20 Step 3 (salt concrete / MgCl₂ solution): Comparison of calculated (cal) and experimental (exp) concentrations of potassium and sulphate. Additionally, the initial (in) concentrations of elements in MgCl₂ solution and the saturation index of selected phases are given

Saturation of phases changed compared to earlier steps: now Anhydrite_{cal}, Friedels' salt_{cal}, Hydrotalcite_{cal}, Hydrogarnet_{cal} (C₃AH₆ / Ca₃Al₂(OH)₁₂) and Tobermorite_{cal} (Ca_{2.5}(SiO)₃(OH)₅·1.5H₂O) were saturated. In experiments only Anhydrite_{exp} was supersaturated. In comparison to steps before Halite_{cal}, Kerolite_{cal} and 318-phase_{cal} were undersaturated in step 3 (salt concrete / MgCl₂ solution) and Polyhalite_{cal} became now undersaturated direct in first step of reaction. Undersaturation of Halite_{cal} and 318-phase_{cal} is not in accordance with experimental results. Kerolite_{exp} was not considered in calculation of SI_{exp} because Kerolite contents silicon and silicon as well as aluminium were below the quantification limit in experiments. Hence, calculation of SI_{exp} for silicon and aluminium containing phases was not realizable.

Tab. 5.14 Saturation index in Step 3 (salt concrete / MgCl₂ solution). Phases, which are not listed, were undersaturated during complete reaction

Reaction step	Anhydrite SI	Friedels' salt SI	Halite SI	Hydro talcrite SI	Kerolite SI	318-Phase SI	Polyhalite SI	Si-Hydrogarnet SI	Tobermorite SI
1	0.000	0.000	-0.518	0.000	-45.055	-4.353	-9.834	0.000	0.000
2	0.000	0.000	-0.339	0.000	-45.168	-4.317	-9.895	0.000	0.000
3	0.000	0.000	-0.217	0.000	-45.260	-4.285	-9.946	0.000	0.000
4	0.000	0.000	-0.119	0.000	-45.325	-4.256	-9.988	0.000	0.000
5	0.000	0.000	-0.028	0.000	-45.353	-4.232	-10.022	0.000	0.000

5.5 Interpretation and discussion

5.5.1 Comparison between modelling and experimental results in the system sorel concrete – A1 / NaCl solution

Comparison between experimental and modelling results showed good agreement in chloride, sodium and potassium concentrations. Both in modelling and in cascade experiments Halite, which is assumed to be the main chloride and sodium containing phase, was supersaturated. Halite was also detectable in solid samples by X-ray diffraction. Hence, Halite is thermodynamically stable in sorel concrete with NaCl solution. Glauberite and $\text{Na}_2\text{Ca}_5(\text{SO}_4)_6 \cdot 3\text{H}_2\text{O}$ was supersaturated in cascade experiments, but in modelling both phases were undersaturated. In addition both phases could not be detected by X-ray diffraction. It can be assumed, however, that both phases were formed in cascade experiments, but their masses in comparison to the total mass of concrete samples was too low for detection or their degree of crystallisation was too low. Furthermore, experimental solution was supersaturated with respect to Glauberite and $\text{Na}_2\text{Ca}_5(\text{SO}_4)_6 \cdot 3\text{H}_2\text{O}$. However, in modelling both phases did not form because of undersaturation.

Increase of potassium concentrations may result from dissolution of Polyhalite from the crushed salt in sorel concrete, because from /GIE 1994/ it is known, that crushed salt contains low mass of Polyhalite and Polyhalite was undersaturated in experiments and modelling. Probably, Polyhalite was dissolved with increasing SSR and results in a slow but continuous increase of potassium concentrations in solution.

Calcium and sulphate concentrations increased in proportion 1:1 both in cascade experiments and in modelling. But in experiments concentrations increased in first reaction step and were constant with ongoing increase of SSR while in modelling concentrations increased more slowly. At SSR of 0.3 calcium and sulphate concentrations between experiments and modelling fit well. Both solution in experiments and solution in modelling were supersaturated with respect to Anhydrite and Anhydrite was also detectable in solid phases of experiments. Hence, it can be supposed that Anhydrite was in equilibrium.

Calcium and sulphate containing phases Glauberite, Gypsum and $\text{Na}_2\text{Ca}_5(\text{SO}_4)_6 \cdot 3\text{H}_2\text{O}$ were supersaturated in experiments although all phases could not be detected by X-ray

diffraction. But phases may also be included in the reacted sores concrete in low amounts or with an amorphous structure so that they could not be detected by X-ray diffraction. The saturation of these phases in experiment was not in agreement with modelling results because all phases were continuously undersaturated in modelling. Hence, it can be hypothesised that Glauberite, Gypsum and $\text{Na}_2\text{Ca}_5(\text{SO}_4)_6 \cdot 3\text{H}_2\text{O}$ were dissolved partly in experiments within the first cascade. In the following cascades equilibration between the calcium and sulphate content of solution and solid phases was attained, so no further Glauberite, Gypsum and $\text{Na}_2\text{Ca}_5(\text{SO}_4)_6 \cdot 3\text{H}_2\text{O}$ was dissolved. Based on experimental data it cannot be stated, which phases were dissolved. Glauberite, Gypsum and $\text{Na}_2\text{Ca}_5(\text{SO}_4)_6 \cdot 3\text{H}_2\text{O}$ were undersaturated in modelling, hence, these phases may dissolve when the reacted solution was subjected to fresh concrete.

The most pronounced deviation was observed between magnesium concentrations in experiments and modelling because in experiments concentrations increased significantly within first cascade and decreased with increasing SSR while magnesium concentrations in modelling increased continuously. Calculation of SI in experiments showed undersaturation with respect to Brucite and 318-phase, while both phases were detectable by X-ray diffraction. An equilibrium of Brucite and 318-phase between solution and solid did consequently not exist, hence, in the calculation of SI both phases dissolved continuously with increasing SSR (Fig. 5.6). This finding is shown by modelling results because magnesium concentrations increase while 318-phase is undersaturated. Contrary to experimental results, Brucite was saturated in modelling, hence only 318-phase was thermodynamically instable. But in experiments magnesium concentrations decreased with ongoing experiment. Thus Brucite and 318-phase were dissolved. Consequently, another magnesium containing phase formed. But based on calculation of SI from experimental solutions with the THEREDA database release 6.0 no phase could be identified which was formed in experiments.

Summarizing the results indicate, that in the used database at least one magnesium containing phase is missing, the nature of which is currently unknown. For a better representation of the cascade leaching experiment this phase has to be identified in laboratory experiments.

In a final attempt to model the results from cascade leaching experiments the used THEREDA database release 6.0 was supplemented by adding a special magnesium

phase according to internal communication /FRE 2015a/. However, that phase was defined for the system $\text{MgO-MgCl}_2\text{-H}_2\text{O}$ at 25°C while the system in cascade experiments also includes calcium, potassium and sulphate. Consequently, model results still did not match the experiment.

A more fundamental problem is that no data of reaction kinetic are available for the key solid phases in the systems under consideration. Hence, in modelling equilibrium between solid phases and solution is calculated instantly while in experiments time dependent dissolution-precipitation processes can be expected. Furthermore, formation of colloids and amorphous phases could be a problem in modelling. These phases become crystalline within very long time periods only and can have low solubility. Hence, due to an incomplete understanding of processes, the modelling of cascade experiments is not possible at present.

5.5.2 Comparison between modelling and experimental results in the system salt concrete / MgCl_2 solution

Calculated concentrations of chloride and sodium in step 1 (salt concrete / MgCl_2 solution) and their concentrations in cascade experiments (Fig. 5.12) agreed well up to 180 g of reacted salt concrete. Concentrations of both elements were constant with increasing SSR in modelling but in experiments chloride concentrations varied between 7.05 mol/kg H_2O and 8.77 mol/kg H_2O and sodium concentrations increased with ongoing addition of salt concrete. Both in modelling and experiments solution was saturated with respect to Halite and it was also detectable in X-ray-diffraction. Consideration of SI in the reacted solution of experiments and X-ray diffraction showed, that there was no sodium containing phase in the THEREDA database release 6.0, which dissolved significantly and may induce the increase of sodium in solution. Because increase of sodium concentration could not be calculated and in experiments there was no sodium containing and dissolving phase to identify, it can be assumed that there is a phase which is currently unknown and consequently is not considered in the THEREDA database release 6.0.

Discrepancy between modelling and experimental results of calcium and magnesium concentrations was very significant, because the increase of calcium concentration in experiments started directly within the first cascade and concentration became several times higher than calculated concentrations. Magnesium concentrations in experiments

decreased to 0.0 mol/kg H₂O while in modelling concentrations decreased only about 0.05 mol/ kg H₂O.

CSH and MSH phases are low crystalline or amorphous. Consequently, detection by X-ray diffraction was not realizable. Hence, dissolution and formation could not be identified by available experimental methods. In addition the content of silicon in reacted solution was smaller than the quantification limit. The low silicon content may be induced by coagulation of the colloidal dissolved elements in high saline solutions. The clot sediments and is not detectable by solution analysis. Consequently, the measured concentrations of silicon in solution may be lower than the effectively reactive content of silicon. Because of the low measured silicon content, calculation of SI in the reacted solution occurred without consideration of CSH and MSH phases and a reconstruction of phase dissolution and formation of these phases based on SI was not possible. On the other hand, CSH phases were considered in modelling by a simplified model according to /BER 1990/ as CSH (0.8), CSH (1.1) and CSH (1.8) for CSH, which indicate compositions of various calcium-silicon ratios. Kerolite and Sepiolite are potential MSH phases, which are included in THEREDA database release 6.0. The composition of MSH phases with respect to magnesium and silicon may be largely variable. This variability is currently not covered in the THEREDA database release 6.0. Furthermore, their characterization in cement systems is not researched sufficiently /ALT 2011/. Contrary to findings with XRD, Kerolite was saturated in model calculations. Kerolite may be formed in experiments, silicon thereby being removed from solution. This may result in silicon concentration below the quantification limit. But Kerolite is amorphous, hence verification by X-ray diffraction was not possible. Based on the complete consumption of magnesium in cascade experiments it can be assumed that also another phase was formed in which magnesium was bound. Also in that case, THEREDA database release 6.0 seems not to be complete with regard to MSH phases. Based on the significant deviation between calculated and experimental determined concentrations of calcium, there seem to be difficulties in modelling of CSH phases too. This may result from theoretical calcium-silicon ratios of CSH which are not equal to real ratios or from incorrect solubility of CSH phases.

Development of potassium concentration also showed deviations. In experiments potassium concentrations decreased a little up to 0.3 kg reacted salt concrete and changed not significantly with ongoing increase of SSR. Contrary, in modelling potassium concentrations increased within this reaction period and became constant

afterwards. Calculated SI in the reacted solution showed supersaturation with respect to Carnallite within this period of time and Carnallite was also detectable by X-ray diffraction. Afterwards, when potassium concentration changed not significantly anymore, Carnallite was undersaturated and also not detectable in X-ray-diffraction. Hence, it can be assumed that potassium was not consumed anymore by formation of Carnallite. On the other hand Carnallite was permanent undersaturated in modelling hence, consumption of potassium by formation of Carnallite, as seen in experiments, can be excluded. But increase of potassium concentrations indicated dissolution of an unknown potassium containing phase. Based on development of saturation in modelling increase of potassium concentrations may be induced by dissolution of Polyhalite, which became undersaturated with increasing reacted mass of salt concrete. The dissolution of Polyhalite in modelling is not in agreement with the saturation of Polyhalite in the reacted solution in experiments: in experiments Polyhalite was continuously supersaturated and became primary undersaturated in the last cascade.

Sulphate concentrations developed differently, too. While in experiments sulphate concentrations increased, concentrations in modelling decreased. Increase of sulphate concentrations in experiments may be induced by dissolution of Kainite and Kieserite because the SI in reacted solution decreased. But this is speculative, because both phases were not detected by X-ray diffraction in solid sample before. Otherwise sulphate containing phases such as Anhydrite, Glauberite, Gypsum, Pentasalt and $\text{Na}_2\text{Ca}_5(\text{SO}_4)_6 \cdot 3\text{H}_2\text{O}$ showed an increase of SI, hence sulphate had to be consumed simultaneously. Consequently, more sulphate had to be dissolved than was consumed for phase formation. Currently it cannot be clarified, if there is another sulphate containing phase, which induced the increase of sulphate concentrations.

Kainite and Kieserite were also undersaturated in modelling. However, decrease of sulphate concentration indicated its precipitation in a new phase. Compared to experimental results, only Anhydrite was saturated hence, sulphate had to be consumed by formation of Anhydrite in modelling.

Adaption of phases which are allowed to precipitate in step 2 (salt concrete / MgCl_2 solution) resulted in small changes of concentrations of calcium, magnesium, potassium and sulphate in comparison with step 1 (salt concrete / MgCl_2 solution). Solution was saturated to Anhydrite, Halite, Hydrotalcite, Kerolite and 318-phase and

became also undersaturated with respect to Polyhalite during reaction. Hence, adaption in step 2 (salt concrete / MgCl_2 solution) resulted only in small changes of solubility of phases, which did not result in an improvement of modelling results.

As already explained in chapter 5.3.3 the addition solid solutions of the CEMDATA 07 database in step 3 (salt concrete / MgCl_2 solution) showed significant deviations to modelled development of concentrations to steps before. Furthermore, the saturation of phases deviated: only Anhydrite and Hydrotalcite was still saturated. In addition phases of solid solutions (Si-Hydrogarnet and Tobermorite) became saturated. In comparison to experimental results, Anhydrite was the only phase, which was (super) saturated both in experiments and modelling. But saturation of other phases in experiments could not be calculated by PHREEQC because those phases all include aluminium or silicon and both concentrations were below the quantification limit in experiments (compare explanation in chapter 5.4).

The increase of chloride and sodium concentrations in step 3 (salt concrete / MgCl_2 solution) may be induced by thermodynamic instability of Halite. Simultaneously Friedels' salt was formed because it was continuously saturated in modelling and part of chloride, which was dissolved from Halite, was consumed. Hence, sodium concentrations increased more than chloride concentrations. But this did not conform to observations in experiments, because in experiments Halite was thermodynamically stable, based on supersaturation and detection in X-ray-diffraction and second, Friedels' salt was dissolved as detected by X-ray diffraction.

The magnesium content of the initial solution was consumed directly in step 3 (salt concrete / MgCl_2 solution). This may result from the absence of kinetic data in THEREDA database release 6.0: in laboratory magnesium was consumed time dependent because the measured magnesium content in the solution decreased slowly within seven cascades. But this effect of time dependent consumption of magnesium can currently not be modelled. With the database in use, magnesium had to be consumed by formation of Hydrotalcite, because this is the only magnesium containing phase which was saturated in modelling and could be formed consequently. Formation of Hydrotalcite was not detected in experiments. But this may result from the composition of reacted solution in which aluminium was below the quantification limit as explained before. Hence, formation of Hydrotalcite in experiments can neither be verified nor excluded.

Model investigations

Concentration of calcium increased significantly in comparison with initial concentrations in the first step of modelling but decreased in following steps again. The initial increase of calcium concentration may result from dissolution of CSH phases from salt concrete: CSH phases were thermodynamically instable in modelling, which is in agreement with experimental results. But calcium was consumed simultaneously to dissolution of CSH phases. This may have occurred by formation of Anhydrite, Friedels' salt, Si-Hydrogarnet and Tobermorite. Consumption of calcium, which results in decrease of calcium concentration, did not conform to experimental results. Hence, formation of those phases in significant percentages can be excluded. Additionally, Anhydrite could only be formed in first step of calculation because all sulphate from initial solution was consumed within this step. But in experiments sulphate concentrations increased with ongoing SSR, hence complete consumption of sulphate by formation of Anhydrite is excluded.

In comparison to steps before development of potassium concentrations in modelling matched better with experimental results. Both in modelling and experiments potassium concentrations decreased and development occurred nearly simultaneously. But modelled potassium concentrations were around 0.1 mol kg/H₂O higher than experimental determined concentrations. In experiments potassium concentrations decreased slowly from concentration of initial MgCl₂ solution but in modelling potassium concentrations increased in the first reaction step in comparison with the initial concentrations and only then decreased in following reactions steps. In experiments consumption of potassium was explained by formation of Carnallite. But this phase was not thermodynamically stable in modelling. An initial increase of potassium concentrations in comparison with initial solution may result from dissolution of Polyhalite from the crushed salt of salt concrete, as it was assumed in leaching experiments before. But potassium had to be consumed by formation of another potassium containing phase. Indeed no saturated phase in the database used potassium. Hence, consumption of potassium in modelling in step 3 (salt concrete / MgCl₂ solution) cannot be explained currently.

Summarizing, none of the aforementioned modelling approaches resulted in a satisfactory agreement with cascade experiments. This may be caused by an incomplete knowledge of phase dissolution-precipitation processes in experiments and an incomplete database. Especially, the knowledge of formation and composition of

Model investigations

MSH phases is not sufficient. Thus, the existing database must be adapted and extended for high-saline conditions.

6 Evaluation of cement based sealing materials

Model investigations and comparison to experiments showed, that corrosion processes of sorel and salt concrete are not completely understood currently. There are still deficits in identification of corrosion products in experiments and consequently in adaption of the database. Hence, the evaluation of the geochemical long-term stability of the cement based sealing materials refers to the experimental results.

6.1 Evaluation of sorel concrete with respect to its geo-chemical material behaviour and its sealing capacity

The corrosion behaviour of sorel concrete was investigated in a comprehensive laboratory program of leaching and transport experiments. Leaching experiments with sorel concrete supported the assumption, that sorel concrete is thermodynamically stable in presence of MgCl_2 solutions, which have magnesium contents $\geq 0.5 \text{ mol/kg H}_2\text{O}$. Formation of new phases Carnallite and Bischofite could be detected both in X-ray diffraction and are confirmed by respective saturation indices in reacted solution. Indeed, a negative impact on the sealing capacity was not expected because the stabilizing 318-phases of sorel concrete were still stable, even after more than 500 days of reaction with MgCl_2 solution. The impact to the sealing capacity was investigated in advection experiments.

Investigation of sorel concrete in presence of NaCl solution showed both in batch and in cascade experiments, that sorel concrete is thermodynamically not stable in this system. Based on calculated SI of the reacted solution it could be verified that the stabilizing 318-phase is thermodynamically not stable. In batch experiments this was also verified by X-ray diffraction. In cascade experiments dissolution of 318-phase could not be verified by X-ray diffraction. Based on experiments with sorel concrete produced under reproducible conditions it is assumed that equilibration time in cascade experiments was not sufficient for the complete dissolution of 318-phases. This was attributed to a higher percentage of 318-phase and higher degree of crystallization in the sorel concrete – A1 samples. But the increase of magnesium concentrations in the NaCl solution may be affected by the dissolution of 318-phases.

Both systems sorel concrete / MgCl_2 solution and sorel concrete / NaCl solution were investigated further in transport experiments. Through-diffusion experiments with sorel concrete confirmed findings from experiments before: diffusion coefficient was around one order of magnitude higher in the thermodynamically instable system with NaCl solution compared to MgCl_2 solution. This may be caused by the corrosion of sorel concrete by NaCl solution simultaneously to the diffusion process. Calculation of the cumulated mass of tracer showed in sorel concrete samples with NaCl solution that flux of tracer was not linear in time during complete diffusion experiments. Probably, the steps in the slope were induced by the corrosion of sorel concrete which result in a generation of pathways through the samples which enables an overlay of advective transport to the diffusive transport of tracer. Those pathways may be plugged temporary by dissolution-precipitation processes which induced a slower transport of tracers again. Consequently, advective transport seems to be the controlling process, if NaCl solution enters to a sealing element of sorel concrete.

Advection experiments with MgCl_2 solution verified, that MgCl_2 solution did not have a negative impact to the sealing capacity of sorel concrete. Percolation with MgCl_2 solution even resulted in improvement of the sealing capacity. Probably, this effect is caused by the formation of additional phases as Bischofite and Carnallite, which formation could be verified in leaching experiments before and which may plugged the pores of sorel concrete in advection experiments.

Percolation of sorel concrete with NaCl solution resulted, correspondent to findings from leaching experiments, in significant corrosion of sorel concrete. Based on the saturation of the reacted solution it was found, that stabilizing 318-phase was not stable. Probably, the dissolution of 318-phase resulted in significant increase of permeability.

Additionally, comparison of “stop-and-flow” experiments to continuous percolation of solutions in advection experiments showed, that precipitation-dissolutions processes are time-dependent. Hence, the impact on chemical processes and in consequence to development of permeability was more significant if solution was enclosed in the sealing for a while. Related to an in situ sealing element the impact of saline solution depends much more from the time of reaction than from the volume of solution.

Based on these results it cannot be assumed that sorel concrete, fabricated under laboratory conditions, maintains its sealing function if saturated NaCl solution approaches the sealing element. However, it should be considered, that the investigated sorel concrete was only hardening for 200 days without influence of compaction. But in situ sealing elements will be constructed a couple of years before intrusion of brine to the disposal site is expected. Hence, sorel concrete would be hardening for longer time periods and in addition the compaction of sorel concrete by the convergence from the host rock can be assumed. This may result in a decrease of pore volume and increase of density of sorel concrete. Thus, an improved resistance in comparison with intrusion of saline solution would be expected.

In comparison to laboratory program with salt concrete no advection experiments with combined samples were conducted at present. Based on the findings discussed before, it seems to be necessary to perform advection experiments with combined samples of sorel concrete and rock salt, too. Caused by the higher compaction of sorel concrete resulting from the confining stress, an improvement of the sealing capacity is conceivable. However, compaction of the combined sample should be performed while $MgCl_2$ solution is enclosed in the samples, because the advection experiments with the pure sorel concrete showed, that the presence $MgCl_2$ solution induced a decrease of permeability. The effect of $MgCl_2$ solution to the rock salt is still to be investigated.

6.2 Evaluation of salt concrete with respect to its geo-chemical material behaviour and its sealing capacity

Corresponding to sorel concrete the corrosion behaviour of salt concrete was also investigated by leaching and transport experiments. Leaching experiments with salt concrete showed that salt concrete did not corrode in presence of NaCl solution. Indeed consideration of the calculated SI of the reacted solution of experiments showed that additional phases were saturated, which could not be detected by X-ray diffraction before. Hence, formation of further phases can be expected. Probably, some of these phases need longer time periods for crystallization so that detection by X-ray diffraction is also possible.

In batch and cascade experiments with salt concrete and $MgCl_2$ solution the corrosion of salt concrete could be clearly verified. Especially, the development of the composition of the reacted solution showed, that stabilizing CSH phases from the salt

concrete were dissolved. A drop in magnesium concentration indicated the formation of MSH phases. Hence, salt concrete was not thermodynamically stable in presence of MgCl_2 solution.

Further investigations in advection experiments with combined samples of salt concrete showed, that presence of NaCl solution resulted in a decrease of the integral permeability of the combined sample. The decrease of permeability could be detected both while combined samples were inserted in isostatic cells and confining stress was applied and while samples were placed in advection cells without confining stress. This may result from findings of leaching experiments, that additional phases were formed which resulted in reduction of permeability by plugging the pores and contact seam. Investigations showed that the confining stress influenced the development of permeability too, because if confining stress was reduced, for example by dismantling of combined samples from isostatic cells, an opening of the contact seam between salt concrete and rock salt could be detected both by visualizing with leakage spray and by ongoing permeability measurements in advection cells. But re-enclosure of NaCl solution in the sample without confining stress resulted in decrease of permeability again.

Considering an in situ sealing element it can be concluded, that the sealing capacity of a sealing from salt concrete is influenced advantageously by intrusion of saturated NaCl solution. The convergence from the host rock, which may induce further closure of gaps and fissures, probably accelerates this process. Measurements of the confining stress in an in situ sealing element showed that after ten years of convergence from the host rock confining stresses of 5 MPa were measured. In contrast, in laboratory experiments confining stress of 1 MPa was sufficient to induce acceleration of permeability decrease. Thus, in situ an influence of confining stress resulting from the convergence of the host rock may also be expected.

Both in isostatic cells and in advection cells NaCl solution was substituted by MgCl_2 solution during experiments. Based on leaching experiments corrosion of salt concrete and in addition an increase of permeability were expected. But advection experiments showed that permeability increased about circa one order of magnitude and became constant with ongoing percolation of MgCl_2 solution. Analysis of percolated solution showed no significant changes in its composition in comparison to the initial MgCl_2

solution. Hence, an impairment of the sealing function could not be determined in advection experiments.

Summarizing it can be assumed, that a sealing of salt concrete may also satisfy its sealing function versus MgCl_2 solution. Therefore it is needed that permeability is low: Permeability by percolation with NaCl solution should be at least one order of magnitude smaller than permeability should be by percolation with MgCl_2 solution because in experiments permeability to MgCl_2 solution was in average one order of magnitude higher than to NaCl solution. Additionally a decrease of confining stress should not occur if MgCl_2 solution percolates a sealing element, because investigations with NaCl solution showed that a reduction of confining stress may result in an increase of permeability. This effect may occur with MgCl_2 solution, too. Furthermore, the surface of potential pathways has to be very low to limit effects of corrosion: Earlier investigations of /MEY 2003a/ and the pilot test (chapter 4.4.2.2 a) showed that the effect of corrosion was higher to damaged cores. The damage of the cores resulted in micro-cracks and an increased volume of pores which induces higher reactive surfaces. In this damaged samples percolation of MgCl_2 solution resulted in significant increase of permeability.

Discrepancy of corrosion effects of leaching elements and advection experiments may be explained by the difference of the specific surface: the powdered concrete, which was used in leaching experiments, has a significant higher surface than the compacted salt concrete samples in advection experiments. Because of the lower specific surface, corrosion processes occurred more slowly or were even inhibited.

In further investigations it is recommended to perform advection experiments with combined samples and MgCl_2 solution, which was not exposed to NaCl solution before. It is expected, that in a repository salt concrete may be only exposed to confining stress without having any contact with NaCl solution. The pure presence of confining stress is sufficient to reduce the contact seam to a level of permeability which limits the percolation of MgCl_2 solution similar to currently performed advection experiments. Indeed, the time periods which are required for a sufficient reduction of the contact seam will depend from the repository location and should be quantified with respect to the ambient conditions as salt composition, temperature and convergence rate.

7 Conclusions

The leaching experiments with sorel concrete and saline solutions verified previous investigations of the corrosion behaviour of sorel concrete. In general, sorel concrete corrodes in presence of saturated NaCl solution and is thermodynamically stable in presence of MgCl₂ solution. The dissolution of the stabilizing 318-phase from sorel concrete is the most significant process during corrosion. The comparison between samples of sorel concrete – old and sorel concrete – A1 showed that the properties of the raw material as well as the boundary conditions during hardening have a significant impact to the thermodynamically stability of sorel concrete.

Through-diffusion and advection experiments confirmed the corrosive impact of NaCl solution. The apparent diffusion-coefficients in samples saturated with NaCl solution were in average one order higher than in samples saturated with MgCl₂ solution. Additionally, after dismantling of the samples from the through-diffusion cells a significant damage of the samples could be identified. Permeability measurements in advection experiments showed that percolation of NaCl solution resulted in an increase of permeability while percolation of MgCl₂ solution resulted in decrease of permeability. Hence, percolation of MgCl₂ solution even improved the sealing function of sorel concrete in the experiments.

A satisfactory modelling of the reaction of sorel concrete with NaCl solution was not possible. Problems are the missing of kinetic effects in the THEREDA database release 6.0 and the incomplete understanding of dissolution-precipitation processes in experiments.

Salt concrete shows opposed corrosion behaviour: it is thermodynamically stable in NaCl solution and corrodes in MgCl₂ solutions. Corrosion results in dissolution of stabilizing CSH phases.

Permeability measurements with gas to salt concrete showed that salt concrete is a very tight material. Percolation of solution through salt concrete did not occur. Advection experiments to combined samples of salt concrete inserted in a hollow rock salt cylinder showed that NaCl solution combined with a confining stress resulted in a decrease of the integral permeability. Subsequent percolation with MgCl₂ solution

Conclusions

induced an increase of permeability of some one order of magnitude. Further increase of permeability with ongoing percolation of MgCl_2 solution was not observed.

Modelling of leaching experiments with salt concrete was not possible at present caused by the incomplete database and the missing knowledge of formation of MSH phases.

8 Summary and outlook

Purpose of the research projects LAVA (FKZ: 02 E 11122) and LAVA-2 (FKZ: 02 E 11324) was the investigation of salt and sored concrete with respect to their chemical-hydraulic properties in presence of saline solution and implications for the sealing function.

At the beginning the material properties of salt and sored concrete were described. Part of the information derived from an extensive literature research, another part from laboratory investigations of the materials based on decomposition and X-ray diffraction. Corrosion processes in salt and sored concrete, which are currently known, were also summarized. Because it was necessary to produce new sored concrete of composition A1 under specified boundary conditions related to the material properties of raw material and conditions during hardening, the process of sored concrete sample production was also described.

In the next chapter, the laboratory experiments were described. The laboratory program comprised leaching experiments, divided into batch and cascade experiments, through-diffusion experiments and advection experiments.

Batch experiments aimed at verifying of corrosive systems and the determination of equilibration times. Batch experiments were performed in four systems: sored concrete / NaCl solution, sored concrete / $MgCl_2$ solution, salt concrete / NaCl solution and salt concrete / $MgCl_2$ solution. Additionally, it was tested, if tracers caesium and lithium are sorbed by concrete. Based on batch experiments systems sored concrete / NaCl solution and salt concrete / $MgCl_2$ solution were identified as corrosive systems. This was in accordance with literature research. Hence, cascade experiments were only performed in these systems.

Sorption of lithium was located in both systems with $MgCl_2$ solution by decrease of lithium concentration in solution. In batch experiments with NaCl solution no sorption of lithium was detected. Caesium was not sorbed both in NaCl and in $MgCl_2$ solution.

Investigation of the reaction path of the powdered sored concrete with NaCl solution in cascade experiments showed most significant changes in solution composition by the development of magnesium concentrations. In comparison with calculated SI of the

reacted solution could be verified that characteristic and stabilizing 318-phase of sorel concrete was thermodynamically not stable. Experiments also showed, that another magnesium containing phase had to be formed, because the dissolved magnesium was consumed simultaneously. Composition of this new phase could currently not be determined, nor based on experimental neither on modelling results.

In cascade experiments with salt concrete and $MgCl_2$ solution the dissolution of stabilizing CSH phases was indicated by a continuous increase of calcium concentration in solution. In addition magnesium was consumed from solution. One possible explanation for this finding is the formation of MSH phases. However, due to their amorphous structure it was not possible to detect dissolution and formation of CSH or MSH phases by X-ray diffraction. However, significant corrosion of salt concrete was verified.

Both through-diffusion and advection experiments aimed at determining the integral permeability of sealing material being imposed to defined mechanical and chemical stress.

Through-diffusion experiments were only conducted with sorel concrete samples. Salt concrete samples proved to be very tight and did not allow any flux of tracer. The stationary diffusion flow, which was needed for the measurement of diffusion, could be realized with sorel concrete only. Hence, it can be hypothesized that the sealing capacity of salt concrete versus diffusive transport processes is well. In pilot tests the potential impact of the sample length, hence the impact of the heterogeneity of the material, was explored. The main through-diffusion experiment was performed with sorel concrete samples with 3 cm in length. Apparent diffusion coefficients were determined for caesium and lithium with sorel concrete in presence of NaCl and $MgCl_2$ solution. Experimental results showed significant dependence of the integral flux on the present solution and on the tracer. Based on results it was assumed, that especially in the corrosive system of sorel concrete with NaCl solution an interaction of various transport processes occurred. The NaCl solution corroded the sorel concrete as showed in leaching experiments before. Corrosion affected the creation of new pathways for tracers, which resulted in an accelerated flux of tracers. But flux of tracer was not linear in time. Hence, it is assumed, that pathways for tracers were clogged temporarily. The temporarily clogging of pathways was not observed in through-diffusion experiments with $MgCl_2$ solution. Adapted from this finding an overlay of

advective transport to the diffusive transport of tracer is assumed in system sorel concrete / NaCl solution.

Advection experiments were divided in two types of advection experiments: experiments, which were performed to pure sorel concrete samples with periods of continuously percolation and periods with “stop-and-flow” experiments and advection experiments which were performed to combined samples of salt concrete and rock salt. These experiments aimed at investigating the development of integral permeability of sealing, contact seam (between sealing and rock salt) and the EDZ. Advection experiments with sorel concrete were conducted with NaCl and MgCl₂ solution, too. Comparison of the effect of continuous percolation and “stop-and-flow” experiments indicated kinetically controlled reactions in both solutions. The impact on development of permeability and on solution composition was more pronounced if a small volume of solution was in contact with the concrete for longer period of time than if a bigger volume of solution percolated the samples continuously. With NaCl solution reaction processes resulted in an increase of permeability, in MgCl₂ solution permeability even decreased. In consequence the volume of solution, which attacks a sealing element, is less important than the rate at which it penetrates the concrete.

Investigation of the permeability of combined samples of salt concrete and rock salt showed that NaCl solution in combination with confining stress has the potential to reduce the integral permeability of a sealing element. This may be induced by crystallization processes, especially at the contact seam and reduction of the contact seam, caused by the confining stress. Permeability could be reduced down to levels $< 1 \cdot 10^{-19} \text{ m}^2$ which marks the detection limit of the method applied. Dismantling a combined sample resulted in an opening of the contact seam. This was detected by visual inspection and by permeability measurement without confining stress. Unexpectedly, contact with NaCl solution without confining pressure also resulted in a reduction of permeability.

In a second step NaCl solution was substituted by MgCl₂ solution in part of the samples. This resulted in an increase of permeability over nearly one order of magnitude. Permeability increased both in isostatic and advection cells. Contrary to earlier investigations, no further increase of permeability could be determined with ongoing percolation of MgCl₂ solution. The composition of the outflowing solution did not indicate significant corrosion because it corresponded to that of the initial solution.

It is concluded that under the experimental boundary conditions imposed (reduction of the permeability by NaCl solution and by reduction of the contact seam by confining stress before, low integral permeability and no decrease of the confining stress during percolation of MgCl₂ solution), MgCl₂ solution did not generate significant corrosion processes.

In next section, the modelling activities were described. Modelling activities referred to calculation of SI from reacted solutions of experiments to review dissolution-precipitation processes and to modelling of cascade experiments. The various steps of modelling for systems with sorel concrete and NaCl solution and salt concrete with MgCl₂ solution respectively were described. Modelling of the cascade experiments resulted in both systems (sorel concrete / NaCl solution and salt concrete / MgCl₂ solution) in significant deviations between experimental and modelling results. Further adjustments of the model did not result in an improvement of results. Most likely, this can be attributed to significant deficits of the applied THEREDA database release 6.0.

The report concluded with an evaluation of salt and sorel concrete with regard to its sealing function and future requirements of research.

9 Zusammenfassung und Ausblick

Ziel der Forschungsvorhaben LAVA (FKZ: 02 E 11122) und LAVA-2 (FKZ: 02 E 11324) war die Untersuchung der chemisch-hydraulischen Eigenschaften von Salz- und Sorelbeton in Gegenwart salinärer Lösungen und der Einfluss potentieller Korrosionsprozesse auf die Abdichtungsfunktion.

Zu Beginn der Arbeiten wurde zunächst der aktuelle Stand von Wissenschaft und Technik zu Eigenschaften und dem Korrosionsverhalten von Salz- und Sorelbeton zusammengestellt. Dazu erfolgte eine umfassende Literaturrecherche. Ergänzend wurden die Ausgangsmaterialien im Labor analysiert und deren Analyseergebnisse dargestellt. Allerdings war es notwendig neuen Sorelbeton der Rezeptur A1 herzustellen, weil der bislang verfügbare Sorelbeton zwar der Zusammensetzung des A1 entsprach, jedoch die Randbedingungen an die Materialeigenschaften der Ausgangsmaterialien sowie während der Produktion und des Abbindesprozesses nicht eingehalten worden waren. Das Verfahren zur Herstellung des neuen Sorelbetons A1 unter definierten Randbedingungen wurde innerhalb des Berichtes dargestellt.

Im folgenden Kapitel wurden die Laborexperimente beschrieben. Die Experimente umfassten Auslaugversuche, unterteilt in Batch- und Kaskadenversuche, Through-Diffusion-Versuche und Advektionsversuche. Ergänzend wurde im Unterauftrag eine Untersuchung im Geo-PET (Positronen-Emissions-Tomograph) durchgeführt.

In den Batchexperimenten sollten zunächst die verschiedenen Systeme aus Beton und salinärer Lösung untersucht werden, um das potentielle Korrosionspotential und die damit verbundenen Equilibrierungszeiten zu ermitteln. Die Versuche wurden in den vier Systemen Sorelbeton / NaCl Lösung, Sorelbeton / MgCl₂ Lösung, Salzbeton / NaCl Lösung und Salzbeton / MgCl₂ Lösung durchgeführt. Ergänzend wurden in den Batchversuchen parallel die Sorptionseigenschaften der Tracer Cäsium und Lithium untersucht. Die Tracer sollten später in den Through-Diffusion-Versuchen zum Einsatz kommen. Die Ergebnisse zeigten in Übereinstimmung mit der Literatur, dass in den Systemen Sorelbeton / NaCl Lösung und Salzbeton / MgCl₂ Lösung mit einer Korrosion zu rechnen ist. Aus diesem Grund wurden die anschließenden Kaskadenversuche auch nur in diesen Systemen durchgeführt.

Die Untersuchung der Sorptionseigenschaften von Cäsium und Lithium ergab, dass in beiden Systemen mit $MgCl_2$ Lösung eine Sorption von Lithium erfolgte, da die Tracerkonzentration in Lösung abnahm. In den Systemen mit NaCl Lösung wurde Lithium nicht sorbiert. Eine Sorption von Cäsium erfolgte weder in den System mit NaCl noch mit $MgCl_2$ Lösung.

Bei der Untersuchung des Reaktionspfades zwischen gemahlenem Sorelbeton und NaCl Lösung in den Kaskadenversuchen zeigte sich die Entwicklung der Magnesiumkonzentration in der Reaktionslösung als die signifikanteste Veränderung. Verantwortlich hierfür ist, dass die charakteristische und stabilitätsbestimmende 318-Phase des Sorelbetons thermodynamisch nicht stabil ist. Die thermodynamische Instabilität der 318-Phase im Versuch konnte basierend auf den berechneten Sättigungsindizes aus der Reaktionslösung bestätigt werden. Zudem zeigten die Untersuchungen, dass sich gleichzeitig eine andere Phase bilden muss. Allerdings konnte diese neue Phase derzeit weder anhand von Laboruntersuchungen noch anhand von Modellrechnungen benannt werden.

In den Kaskadenversuchen mit Salzbeton und $MgCl_2$ Lösung zeigte sich, dass die Calciumkonzentration in Lösung kontinuierlich anstieg. Dies lässt sich durch die Auflösung der CSH-Phase aus dem Salzbeton erklären. Gleichzeitig wurde Magnesium verbraucht, was auf die Bildung der sogenannten MSH-Phasen schließen lässt. Da diese Phasen zumeist als amorphe Phasen auftreten, war eine Identifizierung der Phasen mittels Röntgendiffraktometrie jedoch nicht möglich.

In Through-Diffusion- und Advektionsexperimenten sollte die Entwicklung der integralen Durchlässigkeit der Spezialbetone unter Einwirkung sowohl chemischer als auch mechanischer Einflüsse ermittelt werden.

Die Through-Diffusion-Experimente konnten nur mit Sorelbeton durchgeführt werden, da Salzbeton sich als extrem dichtes Material erwies, was eine Diffusion des Tracers innerhalb der möglichen Versuchslaufzeit nicht möglich machte. Daher kann angenommen werden, dass der diffusive Transport von Tracern auf die Abdichtungsfunktion von Salzbeton keinen signifikanten Einfluss hat. In Vorversuchen mit Sorelbeton konnte ermittelt werden, dass die Länge der Diffusionsstrecke einen signifikanten Einfluss auf die Diffusionsgeschwindigkeit hat. Die Beobachtung lässt sich auf die Heterogenität des Materials zurückführen. Für die Hauptversuche wurde,

basierend auf den Vorversuchen, eine Probenlänge von 3 cm festgelegt. Die Versuche zeigten eine signifikante Abhängigkeit des integralen Flusses von der gegenwärtigen Lösung und von dem verwendeten Tracer. Anhand der Ergebnisse ist anzunehmen, dass insbesondere in dem korrosiven System aus Sorelbeton mit NaCl Lösung mit einer Interaktion verschiedener Transportprozesse zu rechnen ist, da kein gleichmäßiger Anstieg der Tracerkonzentration ermittelt werden konnte. Die Auslaugexperimente zuvor hatten gezeigt, dass NaCl Lösung den Sorelbeton korrodiert, sodass mit einer Bildung neuer Fließwege für den Tracer gerechnet werden kann. Der Tracerfluss war jedoch nicht linear über die Zeit. Daher wird angenommen, dass die Porenräume zeitweise durch Phasenumbildungen immer wieder verengt wurden. Dem gegenüber entwickelte sich der Tracerfluss in den Versuchen mit $MgCl_2$ Lösung linear, sodass hier von keiner zeitweiligen Verengung der Porenräume ausgegangen wird. Basierend auf diesen Versuchsergebnissen wird angenommen, dass in den Through-Diffusion-Versuchen mit NaCl Lösung eine Überlagerung von advektivem und diffusivem Transport stattfand.

Die Advektionsversuche können in zwei unterschiedliche Arten der Durchführung unterteilt werden. Versuche, die an reinem Sorelbetonprüfkörpern durchgeführt wurden, wurden zeitweise mit einer kontinuierlichen Durchströmung und zeitweise als „Stop-and-Flow“ Experimente durchgeführt. Die Versuche an kombinierten Prüfkörpern aus Salzbeton, der in einen Steinsalzzylinder eingesetzt wurde, wurden alle als „Stop-and-flow“ Versuche durchgeführt. Die Versuche an den kombinierten Prüfkörpern dienten zur Untersuchung der Entwicklung der integralen Permeabilität im Salzbeton selbst, der Kontaktfuge zwischen Salzbeton und Steinsalz und der Auflockerungszone.

Die Advektionsversuche mit Sorelbeton wurden mit NaCl und $MgCl_2$ Lösung durchgeführt. Der Vergleich zwischen kontinuierlicher Durchströmung und „Stop-and-flow“ Experimenten zeigte, dass die chemischen Reaktionen zwischen Sorelbeton und Lösung in beiden Systemen kinetisch beeinflusst sind. Die Permeabilitätsentwicklung wurde deutlich mehr beeinflusst, wenn ein kleines Lösungsvolumen für einen gewissen Zeitraum in der Probe eingeschlossen war, als wenn ein größeres Lösungsvolumen die Probe in kürzerer Zeit durchströmte. Die Reaktion mit NaCl Lösung führte zu einem Permeabilitätsanstieg während die Reaktion mit $MgCl_2$ Lösung zu einer Senkung der Permeabilität führte.

Die Untersuchungen an den kombinierten Prüfkörpern aus Salzbeton und Steinsalz zeigten, dass die Kombination aus Manteldruck und NaCl Lösung zu einer Abnahme der integralen Permeabilität führt. Dies lässt sich auf Kristallationsprozesse auf der Kontaktfuge sowie auf einer Minimierung der Kontaktfuge durch den Manteldruck zurückführen. Die Permeabilität konnte auf Werte $< 1 \cdot 10^{-19} \text{ m}^2$ reduziert werden. Dieser Wert stellt die Bestimmungsgrenze der angewendeten Messmethode dar. Bei einem Ausbau der Prüfkörper aus der Versuchsanordnung konnte eine Öffnung der Kontaktfuge durch die Abnahme des Manteldrucks festgestellt werden. Allerdings zeigten die Versuche, dass die NaCl Lösung auch ohne Manteldruck das Potential hat die Permeabilität auf der Kontaktfuge zu reduzieren.

Im Anschluss wurde die NaCl Lösung in den Advektionsversuchen an den kombinierten Prüfkörpern durch MgCl_2 Lösung ersetzt. Die Permeabilität stieg gegenüber der Permeabilität mit NaCl Lösung in allen Prüfkörpern um eine halbe bis eine ganze Größenordnung an. Gegenüber früheren Untersuchungen konnte jedoch keine weitere Permeabilitätssteigerung bei weiterer Durchströmung mit MgCl_2 Lösung festgestellt werden. Auch anhand der Analyse der auströmenden Lösung gegenüber der Ausgangslösung konnten keine signifikanten Korrosionsprozesse festgestellt werden. Daher kann, basierend auf den Laborergebnissen und den angewendeten Randbedingungen (Reduktion der Permeabilität durch NaCl Lösung und der Kontaktfuge durch Manteldruck, geringe integrale Permeabilität und keine Abnahme des Manteldrucks während der Durchströmung mit MgCl_2 Lösung) angenommen werden, dass die Durchströmung mit MgCl_2 Lösung zu keinen signifikanten Korrosionsprozessen führt.

Die Modellierung bezieht sich zum einen auf die Berechnung der Sättigungsindizes basierend auf den Lösungszusammensetzungen aus den experimentellen Lösungen als auch auf die Modellierung der Kaskadenexperimente. Die verschiedenen Schritte zur Anpassung der Modellrechnungen an die Kaskadenversuche für beide System (Sorelbeton / NaCl Lösung und Salzbeton / MgCl_2 Lösung) wurden dargestellt. Allerdings führten die Modellrechnungen zu keiner zufriedenstellenden Übereinstimmung zwischen den experimentellen und berechneten Ergebnissen. Diese Schwierigkeiten lassen sich vor allem auf Defizite in der THEREDA Datenbank Release 6.0 sowie auf unzureichende Kenntnisse der Phasenum- und Neubildung in den Laborversuchen zurückführen.

Zusammenfassung und Ausblick

Abschließend erfolgte eine Bewertung der Baustoffe Salz- und Sorelbeton basierend auf den experimentellen und modelltheoretischen Ergebnissen.

References

- /ALT 2011/ Altmaier, M., Brendler, V., Bube, C., Neck, V., Marquardt, C., Moog, H.C., Richter, A., Scharge, T., Voigt, W., Wilhelm, S., Willms, T. and Wollmann, G.: *THEREDA - Thermodynamische Referenz-Datenbasis*. ISBN 978-3-939355-41-0, Karlsruhe Institut für Technologie – Institut für Nukleare Entsorgung (KIT-INE), HZDR-IRC, Gesellschaft für Anlagen- und Reaktorsicherheit (GRS) mbH, TU-BAF, AF-Colenco AG, GRS-Bericht, 265, 2011.
- /APP 2005/ Appelo, C.A.J. and Postma, D.: *Geochemistry, groundwater and pollution*. ISBN 978-0-415-36428-7, CRC Press, Amsterdam, 649 p., 2005.
- /BER 1990/ Berner, U. *A Thermodynamic Description of the Evolution of Pore Water Chemistry and Uranium Speciation During the Degradation of Cement*. Nagra, Technical Report, 90 (12), 1990.
- /BIC 1968/ Biczók, I.: *Betonkorrosion – Betonschutz*. Bauverlag GmbH, Wiesbaden - Berlin, Wiesbaden, 659 p., 1968.
- /BMU 2010/ Federal Ministry for the Environment, Nature Conservation, Building and Nuclear Safety (BMU): *Safety Requirements Governing the Final Disposal of Heat-Generating Radioactive Waste*. Technical Report, <http://www.bmub.bund.de/en/topics/nuclear-safety-radiological-protection/nuclear-safety/details-nuclear-safety/artikel/safety-requirements-governing-the-final-disposal-of-heat-generating-radioactive-waste/>, 2010.
- /BRA 2008/ Brassler, T., Herbert, H.-J., Mische, R. and Schmidt-Döhl, F. *Endlagerung radioaktiver Abfälle in Deutschland, Anhang Wirtsgesteine*. ISBN 978-3-939355-22-9, Technical Report, Braunschweig / Darmstadt, 2008.

References

- /DBE 2004/ Deutsche Gesellschaft zum Bau und Betrieb von Endlagern für Abfallstoffe mbH (DBE): *Verfüllmaterial für Strecken mit hohen Anforderungen - Materialeigenschaften und Materialkennwerte Salzbeton M2*. P192, Technical Report, BfS, Deutschland, 2004.
- /DIN 2013/ Dinnebier, R.E., Pannach, M. und Freyer, D. *3Mg(OH)₂·MgSO₄·8H₂O: A Metastable Phase in the System Mg(OH)₂-MgSO₄-H₂O*. 10.1002/zaac.201300128, Zeitschrift für anorganische und allgemeine Chemie, 639 (10) S. 1827-1833, 2013.
- /ENG 2006/ Engelhardt, H.-J. *Salzbeton - Zusammenstellung der Eigenschaften und Materialkennwerte (Referenzmaterial M3)*. P221, Technical Report, BfS, 2006.
- /ENG 2008/ Engelhardt, H.-J. *Mikroskopische Untersuchungen des Kontaktbereichs von Steinsalz und Salzbeton – ASSE Vordamm*. Technical Report, 2008. (Unpublished)
- /FRE 2007/ Freyer, D. and Voigt, W. *Zur Problematik des MgO-Betons*. ISBN 3-936028-50-8, In: Band 37 *Bauchemie: Tagung der GDCh-Fachgruppe Bauchemie*, 27./28. September 2007 in Siegen. GDCh-Fachgruppe Bauchemie, 2007.
- /FRE 2009/ Freyer, D. and Voigt, W. *Anforderungen an Baustoffe im Salinar: Bindemittelphasen des MgO-Baustoffe für den Einsatz im Kalisalz*. ISBN 978-3-936028-61-4, In: Band 41: *Bauchemie: Tagung der GDCh-Fachgruppe Bauchemie*, 8./9. Oktober 2009 in Freiberg. Gesellschaft Deutscher Chemiker, 2009.

References

- /FRE 2015/ Freyer, D., Gruner, M. and Popp, T. *Zusammenhang von Chemismus und mechanischen Eigenschaften des MgO-Baustoffs*. TU Bergakademie Freiberg, E15 Naturwissenschaften, ISBN 978-3-86012-516-8, Technical Report, Freiburger Forschungshefte, Freiberg, Sachsen, 2015.
- /FRE 2015a/ Freyer, D. (2015): Instiut für anorganische Chemie, TU Bergakademie Freiberg, personal communication (05.06.2015)
- /FRE 2015b/ Freyer, D. *Laboruntersuchungen am Magnesiabaustoffsystem – Fragestellungen und Vorgehensweise*. In: Fachgespräch "Verschlussysteme – In-situ-Bauwerke aus Magnesiabaustoff und dessen chemisch-mechanische Eigenschaften im Hinblick auf HAW-Endlager“, 28.-29. April 2015, Freiberg, http://www.ptka.kit.edu/downloads/ptka-wte-e/FG_Verschluss_2015_Vortraege_Web-Version.pdf (January 2018), 2015.
- /GIE 1994/ Gies, H., Gresner, H., Herbert, H.-J., Jockwer, N. and Mittelstädt, R. *Das HAW-Projekt Stoffbestand und Petrophysik des Steinsalzes im HAW-Feld (Asse, 800-m-Sohle)*. GSF-Bericht, 1994.
- /HAG 2009/ Hagemann, S., Xie, M. and Herbert, H.-J. *Unsicherheits- und Sensitivitätsanalyse zur Korrosion von Salzbeton durch salinare Lösungen*. GRS-Bericht, A (3458), 2009.
- /HAG 2014/ Hagemann, S., Bischofer, B. and Scharge, T. *Entwicklung von Methoden und Modellen zur Bestimmung des Redoxpotentials salinärer Lösungen*. GRS-Bericht, 260, 2014.

References

- /HER 1996/ Herbert, H.-J. and Mönig, J. *Exemplarische Untersuchungen von Wechselwirkungsreaktionen UTD-relevanter chemisch-toxischer Abfälle mit hochsalinaren Lösungen*. GRS 126, ISBN 3-923875-79-7, Project Report, 1996.
- /HER 2000/ Herbert, H.-J. *Zur Geochemie und geochemischen Modellierung hochsalinärer Lösungen mineralischer Rohstoffe*. Geologisches Jahrbuch Reihe D, Heft SD 1, ISBN 3-510-95845-4 (2000)
- /LEA 1998/ Lea, F.M. and Hewlett, P.C.: *Lea's chemistry of cement and concrete, 4th ed.* ISBN 0-340-56589-6, Arnold, London, 1053 p., 1998.
- /HEY 2015/ Heydorn, M., Teichmann, L., Schneefuß, J. and Meyer, T. *Schachtanlage Asse II – Anwendungsversuch Pilotströmungsbarriere PSB A1*. In: Fachgespräch "Verschlusssysteme – In-situ-Bauwerke aus Magnesiabaustoff und dessen chemisch-mechanische Eigenschaften im Hinblick auf HAW-Endlager“, 28.-29. April 2015, Freiberg, http://www.ptka.kit.edu/downloads/ptka-wte-e/FG_Verschluss_2015_Vortraege_Web-Version.pdf (January 2018), 2015.
- /JAN 2016a/ Jantschik, K., Czaikowski, O., Moog, H.C. and Wieczorek, K. *Investigating the sealing capacity of a seal system in rock salt (DOPAS project)*. 10.3139/124.110721, ISSN 0932-3902, In: EUROSAFE 2015, 2.-3. November 2015, Köln, <http://www.hanser-elibrary.com/loi/kt> (17 January 2018), 2016.

References

- /JAN2016b/ Jantschik, K., Hertes, U., Meyer, T. and Moog, H.C. *Development of chemical-hydraulic models for the prediction of the long-term sealing capacity of concrete based sealing materials in rock salt*. GRS-A-3869, Project Report, 2016. (Unpublished)
- /JAN 2016c/ Jantschik, K. and Moog, H.C. *Final technical report on ELSA related testing on chemical-hydraulic behaviour – LAVA*. DOPAS Contract Number: FP7 – 323273, Deliverable n°3.29, Project Report, <http://www.posiva.fi/en/dopas/deliverables> (January 2018), 2016.
- /JAN 2011/ Jantschik, K., Czaikowski, O., Moog, H.C. and Wieczorek, K. *CHM-coupled long-term evolution of seals in rock salt repositories*. 19660, ISBN 978-1-5108-4654-8, In: 16th International High-Level Conference (IHLRWM 2017), 9.-13. April 2017, Charlotte, North Carolina, USA, 2017.
- /KUD 2009/ Kudla, W., Gruner, M., Voigt, W. and Finder, M. *Magnesiabeton bei der Errichtung von geotechnischen Verschlussbauwerken für Untertagedeponien und Endlager für radioaktive Abfälle im Salzgestein*. ISBN 978-3-936028-61-4, In: Band 41: Bauchemie: Tagung der GDCh-Fachgruppe Bauchemie, 8./9. Oktober 2009 in Freiberg. Gesellschaft Deutscher Chemiker, 2009.
- /KUL 2016a/ Kulenkampff J., Gründig M., Zakhnini A., Lippmann-Pipke J. *Geoscientific process monitoring with positron emission tomography (GeoPET)*. Solid Earth 7, 1217-2031, 2016
- /KUL 2016b/ Kulenkampff, J., Zakhnini, A., Gründig, M., Lippmann-Pipke, J. *Quantitative experimental monitoring of molecular diffusion in clay with positron emission tomography*. Solid Earth, 7, 1207-1216, 2016b

References

- /KRA 2008/ Krauke, W. and Fliß, T. *Konzeptplanung und Nachweisführung für ein Abdichtungsbauwerk im Hauptanhydrit aus Magnesiabinder*. P266, Technical Report, BfS, 2008.
- /LIP 2017/ Lippmann-Pipke, J., Gerasch, R., Schikora, J., Kulenkampff, J. *Benchmarking PET for geoscientific applications: 3D quantitative diffusion coefficient determination in clay roc*. Computers & Geosciences, 101, 21-27, 10.1016/j.cageo.2017.01.00, 2017
- /MAT 2007/ Matschei, T., Lothenbach, B. and Glasser, F.P. *Thermodynamic properties of Portland cement hydrates in the system CaO-Al₂O₃-SiO₂-CaSO₄-CaCO₃-H₂O*. ISSN 0008-8846, Cement and Concrete Research, 37, S. 1379-1410, 2007.
- /MEY 2003a/ Meyer, T., Herbert, H.-J. and Schmidt-Döhl, F. *Korrosion von Salzbeton durch saline Lösungen*. Gesellschaft für Anlagen- und Reaktorsicherheit (GRS) mbH, Institut für Baustoffe, Massivbau und Brandschutz (iBMB), Materialprüfanstalt für das Bauwesen (MPA BS), P180, Technical Report, 2003.
- /MEY 2003b/ Meyer, T., Herbert, H.-J. and Schmidt-Döhl, F. *Korrosion zementhaltiger Materialien bei Mehrfachdurchströmung mit salinaren Lösungen*. Gesellschaft für Anlagen- und Reaktorsicherheit (GRS) mbH, Institut für Baustoffe, Massivbau und Brandschutz (iBMB), Materialprüfanstalt für das Bauwesen (MPA BS), GRS-A-3150, Project Report, 2003. (Unpublished)
- /MOO 2013/ Moog, H.C. *THEREDA R-06 Release notes*. https://www.thereda.de/de/datenabfrage/ready-to-use-datenbasen?task=downloaddb&format=raw&filename=THEREDA_Release_notes_r06.pdf (January 2018), 2013

References

- /MÜL 2010/ Müller-Hoeppe, N. *Untersuchung der Kontaktzone am Asse-Vordamm – Gesamtinterpretation*. Technical Report, 2010. (Unpublished)
- /MÜL 2012/ Müller-Hoeppe, N., Breustedt, M., Wolf, J., Czaikowski, O. and Wieczorek, K. *Integrität geotechnischer Barrieren. Teil 2: Vertiefte Nachweisführung*. Bericht zum Arbeitspaket 9.2. Vorläufige Sicherheitsanalyse für den Standort Gorleben. Gesellschaft für Anlagen- und Reaktorsicherheit (GRS) mbH, DBE Technology GmbH (DBE Tec), GRS-288, ISBN 978-3-939355-64-9, Technical Report, Köln, 2012.
- /OES 2009/ Oestreich, M., Freyer, D., Voigt, W. and Dinnebier, R. *Untersuchungen zu Lösegleichgewichten von Bindemittelphasen für MgO-Baustoffe: Magnesiumsalzhydrate im System MgO-MgCl₂-H₂O*. ISBN 978-3-936028-61-4, In: Band 41: Bauchemie: Tagung der GDCh-Fachgruppe Bauchemie, 8./9. Oktober 2009 in Freiberg. Gesellschaft Deutscher Chemiker, 2009.
- /PAN 2015/ Pannach, M., Freyer, D. and Voigt, W. *Temperaturabhängige Lösungsgleichgewichte der Sorelphasen*. In: Fachgespräch "Verschlussysteme – In-situ-Bauwerke aus Magnesiabaustoff und dessen chemisch-mechanische Eigenschaften im Hinblick auf HAW-Endlager“, 28.-29. April 2015, Freiberg, http://www.ptka.kit.edu/downloads/ptka-wte-e/FG_Verschluss_2015_Vortraege_Web-Version.pdf (January 2018), 2015.
- /PAN 2017/ Pannach, M., Bette, S. and Freyer, D. *Solubility equilibria in the system Mg(OH)₂-MgCl₂-H₂O from 298 to 393 K*. Journal of chemical and engineering data, 62, S. 1384 – 1396, 2017.

References

- /PAR 2013/ Parkhurst, D.L. and Appelo, C.A.J. *Description of input and examples for PHREEQC version 3: A computer program for speciation, batch-reaction, one-dimensional transport, and inverse geochemical calculations*. In: U.S. Geological Survey Techniques and Methods, book 6. Modeling Techniques, A43, U.S. Geological Survey, Denver, Colorado, 497 p, <https://pubs.usgs.gov/tm/06/a43/> (19 January 2018), 2013.
- /PAS 2015/ Paschke, I. and Freyer, D. *Das rezepturbedingte Abbindeverhalten des Magnesiabaustoffs*. In: Fachgespräch "Verschlussysteme – In-situ-Bauwerke aus Magnesiabaustoff und dessen chemisch-mechanische Eigenschaften im Hinblick auf HAW-Endlager“, 28.-29. April 2015, Freiberg, http://www.ptka.kit.edu/downloads/ptka-wte-e/FG_Verschluss_2015_Vortraege_Web-Version.pdf (January 2018), 2015.
- /PIT 1991/ Pitzer, K.S. *Theory and data correlation*. ISBN 978-0849354151, In: Activity coefficients in electrolyte solutions. CRC Press, Florida, S. 75-153, 1991.
- /PRI 2006/ Priestel, U., Kudla, W. and Gruner, M. *Aktuelle Erfahrungen beim Einsatz von MgO-Beton in untertägigen Bauwerken im Carnallit*. 35. Geomechanik-Kolloquium Freiberg, 2006-5, 2006.
- /RÜB 2014/ Rübel, A., Buhmann, D. and Kindlein, J. *Status report on conceptual and integrated modelling activities*. Contract Number: FP7 – 323273, DOPAS Deliverable n°5.6, Project Report, <http://www.posiva.fi/en/dopas/deliverables> (January 2018), 2014.

References

- /SCH 2009/ Schmidt-Döhl, F. *Was ist Salzbeton?* ISBN 978-3-936028-61-4, In: Band 41: Bauchemie: Tagung der GDCh-Fachgruppe Bauchemie, 8./9. Oktober 2009 in Freiberg. Gesellschaft Deutscher Chemiker, 2009.
- /STO 1994/ Stockmann, N., Beinlich, A., Droste, J., Flach, D., Gläß, F., Jockwer, N., Krogmann, P., Miehe, R., Möller, J., Schwägermann, F., Wallmüller, R., Walter, F. and Yaramanci, U. *Dammbau im Salzgebirge*. Abschlussbericht Projektphase II, GSF-Bericht 18/94, 1994
- /TEI 2009/ Teichmann, L. and Meyer, T. *Beschreibung der zur Verfüllung der Firstspalten und Resthohlräume in der Südflanke der Schachtanlage ASSE ausgewählten Baustoffe Sorelbeton A1 und A1-560*. Technical Report, Bundesamt für Strahlenschutz, 2009. (Unpublished)
- /WED 1982/ Wedler, G.: *Lehrbuch der physikalischen Chemie*. ISBN 3-527-25880-9, Verlag Chemie, 1982.
- /ZHA 2014/ Zhang, T., Vandeperre, L.J. und Cheeseman, C.R. *Formation of magnesium silicate hydrate (M-S-H) cement pastes using sodium hexametaphosphate*. 10.1016/j.cemconres.2014.07., ISSN 0008-8846, Cement and Concrete Research, 65, S. 8-14, 2014.

Glossary, Symbols and Abbreviations

Convergence	Time dependent contraction of cross sections in mines. Cause is the stress redistribution in the rock mass after excavation.
CRZ	The containment providing rock zone is the part of the repository system, which ensures the safe enclosure of the waste together with the technical seals.
EDZ	Excavation damaged zone, which develops in the contour zone by the installation of disposal facilities. Stress redistributions occur and a new state of secondary stress develops.
pH	Negative decade logarithm of hydrogen ion activity
p _{C_H}	Negative decade logarithm of hydrogen ion concentration
Saturation index (SI)	Logarithm of the ionic activity product divided by solubility product. Saturation index (SI) describes the Equilibrium in a system: SI < 0 → undersaturation, SI = 0 → saturation, SI > 0 → supersaturation

Terms

Symbol / Abbreviation	Labelling
CSH-Phases	Calcium Silicate Hydrate Phases
EDZ	Excavation Damage Zone
ICP-MS	Inductively Coupled Plasma - Mass Spectrometry
ICP-OES	Inductively Coupled Plasma - Optical Emission Spectrometry
MSH	Magnesium Silicate Hydrate Phases
SI	Saturation index
SSR	Solid solution ratio
TTF	Temperature time frame
wc-value	Water cement value

Capital letters

Symbol / Abbreviation	Labelling	Unit
<i>A</i>	Cross section area	m ²
<i>D</i>	Diffusion coefficient	m ² /s
<i>F</i>	Diffusion current density	mol/(m ² /s)
\vec{J}	Diffusion flow	mol/(m ² /s)
<i>k</i>	Permeability	m ²
<i>K</i>	Solubility constant	-
<i>L</i>	Length	m

N	Number of molecules	mol
q	Volume flow	m^3/s
Q	Ionic activity product	-

Small letters

Symbol / Abbreviation	Labelling	Unit
c_1	Tracer concentration at the lower part of the diffusion cell	mol/l
c_2	Initial concentration of tracer at the upper part of the diffusion cell	mol/l
p_1	Gas pressure at the outflowing surface	$\text{kg}/(\text{m}\cdot\text{s}^2)$
p_2	Gas pressure at the inflowing surface	$\text{kg}/(\text{m}\cdot\text{s}^2)$
p^*	Average internal pressure in the pores $((p_1+p_2)/2)$	$\text{kg}/(\text{m}\cdot\text{s}^2)$
Δp	Difference pressure (p_2-p_1)	$\text{kg}/(\text{m}\cdot\text{s}^2)$

Units

Labelling	Unit
Density	kg/m ³
Kilogramme	kg
Cubic metre	m ³
Millimetre	mm
Mol	mol
Newton	N
Revolutions per minute	rpm
Second	s
Square metre	m ²

Chemical equations

Labelling	Symbol / Abbreviation
Anhydrite / Calciumsulphate	CaSO_4
Bischofite	$\text{MgCl}_2 \cdot 6\text{H}_2\text{O}$
Bloedite	$\text{Na}_2\text{Mg}(\text{SO}_4)_2 \cdot 4\text{H}_2\text{O}$
Brucite / Magnesiumhydroxide	$\text{Mg}(\text{OH})_2$
Calcium chloride	CaCl_2
Carbon dioxide	CO_2
Carnallite	$\text{KMgCl}_3 \cdot 6\text{H}_2\text{O}$
Chlorartinite	$\text{Mg}_2[\text{ClOHCO}_3] \cdot 3\text{H}_2\text{O}$
Dansite	$\text{Na}_{21}\text{MgCl}_3(\text{SO}_4)_{10}$
Epsomite	$\text{MgSO}_4 \cdot 7\text{H}_2\text{O}$
Ettringite	$3\text{CaO} \cdot \text{Al}_2\text{O}_3 \cdot 3\text{CaSO}_4 \cdot 31\text{H}_2\text{O}$
Friedels' salt	$3\text{CaO} \cdot \text{Al}_2\text{O}_3 \cdot \text{CaCl}_2 \cdot 10\text{H}_2\text{O}$
Gibbsite	$\text{Al}(\text{OH})_3$
Glauberite	$\text{Na}_2\text{Ca}(\text{SO}_4)_2$
Gypsum	$\text{CaSO}_4 \cdot 2\text{H}_2\text{O}$
Halite / Sodiumchloride	NaCl
Hemicarbonate	$\text{Ca}_4\text{Al}_2(\text{CO}_3)0.5(\text{OH})_{13} \cdot 5.5\text{H}_2\text{O}$
Hexahydrate	$\text{MgSO}_4 \cdot 6\text{H}_2\text{O}$
Hydrogarnet	$\text{C}_3\text{AH}_6 / \text{Ca}_3\text{Al}_2(\text{OH})_{12}$
Hydrotalcite	$\text{Mg}_6\text{Al}_2(\text{CO}_3)(\text{OH})_{18} \cdot 4\text{H}_2\text{O}$
Jennite	$\text{Ca}_5(\text{SiO}_2)_3(\text{OH})_{10} \cdot 1.3\text{H}_2\text{O}$
Kainite	$\text{K}_4\text{Mg}_4[\text{Cl}_4\text{SO}_4]_4 \cdot 11\text{H}_2\text{O}$
Kerolite	$(\text{Mg}, \text{Ni})_3\text{Si}_4\text{O}_{10}(\text{OH})_2 \cdot \text{H}_2\text{O}$
Kieserite	$\text{MgSO}_4 \cdot \text{H}_2\text{O}$
Leonite	$\text{K}_2\text{Mg}(\text{SO}_4)_2 \cdot 4\text{H}_2\text{O}$

Labelling	Symbol / Abbreviation
Loeweite	$\text{Na}_{12}\text{Mg}_7(\text{SO}_4)_{13} \cdot 15\text{H}_2\text{O}$
Magnesium chloride	MgCl_2
Magnesium oxide	MgO
Magnesium sulphate	MgSO_4
Monocarbonate	$\text{Ca}_4\text{Al}_2(\text{CO}_3)(\text{OH})_{12} \cdot 5\text{H}_2\text{O}$
Monosulphate	$\text{Ca}_4\text{Al}_2(\text{SO}_4)(\text{OH})_{12} \cdot 6\text{H}_2\text{O}$
Pentasalt	$\text{K}_2\text{Ca}_5(\text{SO}_4)_6 \cdot \text{H}_2\text{O}$
Phosphorpentoxide	P_4O_{10}
Polyhalite	$\text{K}_2\text{Ca}_2\text{Mg}[\text{SO}_4] \cdot 2\text{H}_2\text{O}$
Portlandite / Calciumhydroxide	$\text{Ca}(\text{OH})_2$
Sepiolite	$\text{Mg}_4\text{Si}_6\text{O}_{15}(\text{OH})_2 \cdot 6\text{H}_2\text{O}$
Silica gel	SiO_2
Si-Hydrogarnet	$\text{Ca}_3\text{Al}_2(\text{SiO}_4)_{0.8}(\text{OH})_{8.8}$
Strätlingite	$\text{Ca}_2\text{Al}[(\text{OH})_6\text{AlSiO}_2(\text{OH})_4] \cdot 2.5\text{H}_2\text{O}$
Sylvine / Sylvite	KCl
Syngenite	$\text{K}_2\text{Ca}[\text{SO}_4]_2 \cdot 2\text{H}_2\text{O}$
Tobermorite	$\text{Ca}_{2.5}(\text{SiO})_3(\text{OH})_5 \cdot 1.5\text{H}_2\text{O}$
Tricalcium aluminate	C_3A
318-Phase / Oxychloride-Mg	$3\text{Mg}(\text{OH})_2 \cdot \text{H}_2\text{O} \cdot 8\text{MgCl}_2$

List of tables

Tab. 3.1	Composition of sored concrete A1 according to /FRE 2015a/ and /TEI 2009/	9
Tab. 3.2	Composition of salt concrete /MÜL 210/.....	15
Tab. 3.3	Evaporite minerals of NaCl and MgCl ₂ solution fabricated in laboratory	21
Tab. 3.4	Composition of concretes according to decomposition	22
Tab. 3.5	Mineral phase composition of concretes based on X-ray diffraction	22
Tab. 3.6	Composition of saturated NaCl solution, IP21-solution /MEY 2003a/ and MgCl ₂ solution	26
Tab. 4.1	Reaction time per cascade and temperature during cascade experiments in the system sored concrete – A1 / NaCl solution.	58
Tab. 4.2	Reaction time for each cascade and temperature during cascade experiments in the system salt concrete / MgCl ₂ solution. Vessel 1 bled during pressure filtration. Hence, the experiment in this vessel had to be restarted.....	63
Tab. 4.3	Calculated diffusion coefficients in pilot through-diffusion experiments	79
Tab. 4.4	Calculated diffusion coefficients in main through-diffusion experiments	83
Tab. 4.5	Overview of volume of passed through solution in [ml] and measured permeability in [m ²] in various cores during percolation of NaCl solution. Blue marked measurements present time periods of continuous percolation. after stop of percolation.	95
Tab. 4.6	Overview to volume of passed through solution in [ml] and measured permeability in [m ²] in various cores during percolation of MgCl ₂ solution. Blue marked measurements present time periods of continuous percolation. With * signed lines give measurement values after stop of percolation.	102

List of tables

Tab. 4.7	Calculated volume flow through a sealing element	119
Tab. 5.1	Composition of sorel concrete for PHREEQC based on laboratory decomposition	140
Tab. 5.2	Boundary conditions of calculation step 1 (sorel concrete / NaCl solution).....	141
Tab. 5.3	Boundary conditions of calculation step 2 (sorel concrete / NaCl solution).....	142
Tab. 5.4	Boundary conditions of calculation step 3 (sorel concrete / NaCl solution).....	143
Tab. 5.5	Composition of salt concrete for PHREEQC based on laboratory decomposition	144
Tab. 5.6	Boundary conditions of calculation step 1 (salt concrete).....	146
Tab. 5.7	Boundary conditions of calculation step 2a and 2b (salt concrete) - I.....	147
Tab. 5.8	Boundary conditions of calculation step 2a and 2b (salt concrete) - II....	148
Tab. 5.9	Boundary conditions of calculation step 3 (salt concrete / MgCl ₂ solution) - I.....	149

List of tables

Tab. 5.10	Boundary conditions of calculation step 3 (salt concrete / MgCl ₂ solution) - II.....	150
Tab. 5.11	Saturation index in step 1 (sorel concrete / NaCl solution). Phases, which are not listed, were undersaturated during complete reaction.	170
Tab. 5.12	Saturation index in step 1 (salt concrete / MgCl ₂ solution). Phases, which are not listed, were undersaturated during complete reaction.	175
Tab. 5.13	Saturation index in step 2 (salt concrete / MgCl ₂ solution). Phases, which are not listed, were undersaturated during complete reaction.	179
Tab. 5.14	Saturation index in Step 3 (salt concrete / MgCl ₂ solution). Phases, which are not listed, were undersaturated during complete reaction.	183
Tab. A.1.1	Detection limits of ICP-OES.....	245
Tab. A.1.2	Detection limits of ICP-MS.....	245
Tab. A.1.3	Measurement range of titration for chloride.....	245
Tab. A.1.4	Batch experiment: Sorel concrete - old / NaCl solution.....	246
Tab. A.1.5	Batch experiment: Sorel concrete - old / MgCl ₂ solution.....	247
Tab. A.1.6	Batch experiment: Sorel concrete / NaCl solution.....	248
Tab. A.1.7	Batch experiment: Salt concrete / MgCl ₂ solution.....	249
Tab. A.1.8	Cascade experiment: Sorel concrete – A1 / NaCl solution.....	250
Tab. A.1.9	Cascade experiment: Salt concrete / MgCl ₂ solution.....	251
Tab. A.1.10	Pilot test of through-diffusion experiments – NaCl solution.....	252
Tab. A.1.11	Pilot test of through-diffusion experiments – MgCl ₂ solution.....	253

List of tables

Tab. A.1.12 Main through-diffusion experiments – NaCl solution	254
Tab. A.1.13 Main through-diffusion experiments – MgCl ₂ solution.....	255
Tab. A.1.14 Advection experiment: Sorel concrete – A1 / NaCl solution - I	256
Tab. A.1.15 Advection experiment: Sorel concrete – A1 / NaCl solution - II	257
Tab. A.1.16 Advection experiment: Sorel concrete – A1 / MgCl ₂ solution - I.....	258
Tab. A.1.17 Advection experiment: Sorel concrete – A1 / MgCl ₂ solution - II.....	259
Tab. A.1.18 Advection experiment: Combined sample Salt concrete / Rock salt – Isostatic cells – NaCl solution	260
Tab. A.1.19 Advection experiment: Combined sample Salt concrete / Rock salt – Isostatic cells – MgCl ₂ solution.....	261
Tab. A.1.20 Advection experiment: Combined sample Salt concrete / Rock salt – Advection cells.....	262
Tab. A.1.21 Tracer test with NaCl and MgCl ₂ solution: comparison of initial and final concentrations of tracer	263
Tab. A.1.22 Permeability to gas in cores of sorel concrete - A1 with 1 MPa confining pressure	267
Tab. A.1.23 Permeability to gas in cores of salt concrete with 1 MPa confining pressure	268
Tab. A.1.24 Permeability to gas in cores of rock salt with 1 MPa confining pressure	268
Tab. A.2.1 Batch experiment: Sorel concrete - old / NaCl solution – Saturation indices calculated	269
Tab. A.2.2 Batch experiment: Sorel concrete - old / MgCl ₂ solution – Saturation indices calculated - I	270

List of tables

Tab. A.2.3 Batch experiment: Sorel concrete - old / $MgCl_2$ solution – Saturation indices calculated - II	271
Tab. A.2.4 Batch experiment: Salt concrete / NaCl solution – Saturation indices calculated - I	272
Tab. A.2.5 Batch experiment: Salt concrete / NaCl solution – Saturation indices calculated - II	273
Tab. A.2.6 Batch experiment: Salt concrete / $MgCl_2$ solution – Saturation indices calculated - I	274
Tab. A.2.7 Batch experiment: Salt concrete / $MgCl_2$ solution – Saturation indices calculated - II	275
Tab. A.2.8 Cascade experiment: Sorel concrete – A1 / NaCl solution – Saturation indices calculated	276
Tab. A.2.9 Cascade experiment: Salt concrete / $MgCl_2$ solution – Saturation indices calculated - I	277
Tab. A.2.10 Cascade experiment: Salt concrete / $MgCl_2$ solution – Saturation indices calculated - II	278
Tab. A.2.11 Advection experiment: Sorel concrete – A1 / NaCl solution – Saturation indices calculated - I	279
Tab. A.2.12 Advection experiment: Sorel concrete – A1 / NaCl solution – Saturation indices calculated - II	280
Tab. A.2.13 Advection experiment: Sorel concrete – A1 / $MgCl_2$ solution – Saturation indices calculated - I	281
Tab. A.2.14 Advection experiment: Sorel concrete – A1 / $MgCl_2$ solution – Saturation indices calculated - II	282

List of tables

Tab. A.2.15 Advection experiment: Sorel concrete – A1 / MgCl ₂ solution – Saturation indices calculated - III	283
Tab. A.2.16 Advection experiment: Sorel concrete – A1 / MgCl ₂ solution – Saturation indices calculated - IV.....	284
Tab. A.2.17 Advection experiment: Sorel concrete – A1 / MgCl ₂ solution – Saturation indices calculated - V.....	285
Tab. A.2.18 Potential equilibrium phases in system sorel concrete / NaCl solution according to calculation step 1	286
Tab. A.2.19 Potential equilibrium phases in system salt concrete / MgCl ₂ solution according to calculation step 1.....	287
Tab. A.2.20 Translation of logK from CEMDATA 07 to THEREDA – Substitution of OH ⁻ : H ⁺ + OH ⁻ = H ₂ O / Substitution of HSiO ₃ ⁻ : H ⁺ + HSiO(OH) ₃ ⁻ = Si(OH) ₄ / Substitution of AlO ₂ ⁻ : AlO ₂ ⁻ + 2*H ₂ O = Al(OH) ₄	288
Tab. A.2.21 Translation of logK from CEMDATA 07 to THEREDA – Substitution of OH ⁻ : H ⁺ + OH ⁻ = H ₂ O / Substitution of HSiO ₃ ⁻ : H ⁺ + HSiO(OH) ₃ ⁻ = Si(OH) ₄ / Substitution of AlO ₂ ⁻ : AlO ₂ ⁻ + 2*H ₂ O = Al(OH) ₄	289
Tab. A.2.22 Modelling of cascade experiment: Sorel concrete – A1 / NaCl solution	290
Tab. A.2.23 Modelling of cascade experiment: Salt concrete / MgCl ₂ solution.....	291
Tab. A.3.1 Parameter x _{j,ca} for description of ΔpH in the binary systems as adopted from GRS-internal quality system procedure for the description of calculation of pc _H	293
Tab. A.3.2 Parameter y _{j,mkl} for description of ΔpH in the ternary systems as adopted from GRS-internal quality system procedure for the description of calculation of pc _H	294

List of figures

Fig. 3.1 Continuous temperature time frame (TTF) of 90 °C for sorel concrete A1 /PAS 2015/..... 12

Fig. 3.2 Production of sorel concrete A1 in laboratory: Mixing of sorel concrete in compulsory mixer (left) and hardening of samples in air tide vessels in climate cabinet (right) 14

Fig. 3.3 Left: sample of salt concrete - dark-grey areas present the crushed salt inclusions, light-grey areas the cement-gel-matrix; Right: sample of sorel concrete: dark areas describe inclusions of crushed salt, light areas the MgO-matrix 21

Fig. 3.4 Initial phase composition of unreacted sorel concrete – old 23

Fig. 3.5 Initial phase composition of unreacted sorel concrete – A1 24

Fig. 3.6 Initial phase composition of unreacted salt concrete 25

Fig. 4.1 Preparation of batch experiments in PE-bottles (left) and storage of PE-vessels in exsiccator (right)..... 28

Fig. 4.2 Test tube with mixture of saline solution and concrete after sample drawing and before centrifugation (left) and sample after centrifugation with explicit separation of concrete and solution (right)..... 29

Fig. 4.3 X-ray-diffraction of sorel concrete – old after reaction with NaCl solution; A – Anhydrite, Cl – Chlorartinite, H – Halite, 318 – 318-phase..... 30

Fig. 4.4 Batch experiments in the system sorel concrete – old / NaCl solution: Development of chloride and sodium concentrations. Blue data points describe solution composition of initial NaCl solution..... 31

Fig. 4.5 Batch experiments in the system sorel concrete – old / NaCl solution: Development of calcium and potassium concentrations in the

List of figures

	solution. Blue data points describe solution composition of initial NaCl solution.	32
Fig. 4.6	Batch experiments in the system sorel concrete – old / NaCl solution: Development of magnesium and sulphate concentrations in the solution. Blue data points describe solution composition of initial NaCl solution	33
Fig. 4.7	Development of p_{cH} and density in the system sorel concrete – old / NaCl solution. Blue data points describe p_{cH} and density of initial NaCl solution	34
Fig. 4.8	X-ray-diffraction of sorel concrete – old after reaction with $MgCl_2$ solution; A – Anhydrite, Bi – Bischofite, C- Carnallite, Cl – Chlorartinite, H – Halite, 318 – 318-phase	35
Fig. 4.9	Batch experiments in the system sorel concrete – old / $MgCl_2$ solution: Development of chloride and magnesium concentrations. Blue data points describe solution composition of initial $MgCl_2$ solution	36
Fig. 4.10	Batch experiments in the system sorel concrete – old / $MgCl_2$ solution: Development of calcium, potassium, sodium and sulphate concentrations in the solution (below). Blue data points describe solution composition of initial $MgCl_2$ solution	37
Fig. 4.11	Development of p_{cH} and density in the system sorel concrete – old / $MgCl_2$ solution. Blue data points describe p_{cH} and density of initial $MgCl_2$ solution.....	38
Fig. 4.12	X-ray-diffraction of salt concrete after reaction with NaCl solution; A – Anhydrite, F- Friedels' salt, H – Halite, P - Portlandite	39
Fig. 4.13	Batch experiments in the system salt concrete / NaCl solution: Development of chloride and sodium concentrations. Blue data points describe solution composition of initial NaCl solution.....	40

List of figures

Fig. 4.14	Batch experiments in the system salt concrete / NaCl solution: Development of calcium, magnesium, potassium and sulphate concentrations. Blue data points describe solution composition of initial NaCl solution	41
Fig. 4.15	Development of p _{cH} and density in the system salt concrete / NaCl solution. Blue data points describe p _{cH} and density of initial NaCl solution	42
Fig. 4.16	X-ray diffraction of salt concrete after reaction with MgCl ₂ solution; A – Anhydrite, Bi – Bischofite, C – Carnallite, F- Friedels' salt, G- Gypsum, H – Halite, P – Portlandite.....	43
Fig. 4.17	Batch experiments in the system salt concrete / MgCl ₂ solution: Development of chloride, sodium and magnesium concentrations. Blue data points describe solution composition of initial NaCl solution.....	44
Fig. 4.18	Batch experiments in the system salt concrete / MgCl ₂ solution: Development calcium, potassium and sulphate concentrations in the solution. Blue data points describe solution composition of initial NaCl solution	45
Fig. 4.19	Development of p _{cH} and density in the system salt concrete / MgCl ₂ solution. Blue data points describe p _{cH} and density of initial MgCl ₂ solution	46
Fig. 4.20	Results of tracer test in NaCl solution. Blind sample of caesium is equal to caesium concentration in salt concrete samples in the beginning and end of tracer test.....	47
Fig. 4.21	Results of tracer test in MgCl ₂ solution. Blind sample of lithium is equal to lithium concentration in NaCl solution with salt concrete sample in the beginning of tracer test. Additionally, lithium concentrations of NaCl solution with salt and sored concrete are identically.....	48
Fig. 4.22	Test procedure of the cascade experiment /HER 1996/.....	56

List of figures

Fig. 4.23	Execution of cascade experiment in laboratory: pressure vessels in overhead shaker (left) and separation of reacted solution from concrete at the end of cascade (right).....	57
Fig. 4.24	Phase composition of sorel concrete – A1 after reaction with NaCl solution in approach 1; A – Anhydrite, B – Brucite, H – Halite, 318 – 318-phase (See appendix for X-ray diffraction analysis of approaches 2 and 3.).....	59
Fig. 4.25	Cascade experiment: Development of solution composition in the system sorel concrete – A1 / NaCl solution for sodium and chloride concentrations. Blue data points describe solution composition of initial NaCl solution	60
Fig. 4.26	Cascade experiment: Development of solution composition in the system sorel concrete – A1 / NaCl solution for calcium, magnesium, potassium and sulphate concentrations. Blue data points describe solution composition of initial NaCl solution.	61
Fig. 4.27	Cascade experiment: Development of p_{cH} and density in the system sorel concrete – A1 / NaCl solution.....	62
Fig. 4.28	Phase composition of salt concrete after reaction with $MgCl_2$ solution in approach 1; A – Anhydrite, C – Carnallite, F- Friedels' salt, G- Gypsum, H – Halite, P – Portlandite (See appendix for X-ray diffraction analysis of approaches 2 and 3.).....	64
Fig. 4.29	Cascade experiment: Development of solution composition in the system salt concrete / $MgCl_2$ solution for sodium and chloride concentrations. Blue data points describe solution composition of initial NaCl solution	65
Fig. 4.30	Cascade experiment: Development of solution composition in the system salt concrete / $MgCl_2$ solution for calcium, magnesium, potassium and sulphate concentrations. Blue data points describe solution composition of initial NaCl solution	66

List of figures

Fig. 4.31	Cascade experiment: Development of p_{cH} and density in the system salt concrete / $MgCl_2$ solution.....	67
Fig. 4.32	Concrete sample inserted in the lower part of a diffusion cell. Concrete sample was inserted in an acrylic glass tube and afterwards cast in araldite	72
Fig. 4.33	Schematic depiction of a diffusion-cell	73
Fig. 4.34	Diffusion cell with insert concrete sample (left) and arrangement of through-diffusion experiments in laboratory (right)	74
Fig. 4.35	Cumulated mass of tracer caesium (above) and lithium (below) in pilot tests of through-diffusion experiments with NaCl solution in samples of 1 cm, 2 cm and 3 cm in length	76
Fig. 4.36	Cumulated mass of tracer caesium (abv.) and lithium (bel.) in pilot tests of through-diffusion experiments with $MgCl_2$ solution in samples of 1,2,3 cm in length. Break through of lithium in 2,3 cm were not detectable.....	77
Fig. 4.37	Sorel concrete sample from through-diffusion experiments in coloured tracer solution. The violet colour occurs in the middle of sample only verifying that diffusion occurred in the concrete matrix.....	78
Fig. 4.38	Cumulated mass of tracer caesium (abv.) and lithium (bel.) in main through-diffusion experiments with NaCl solution in samples with 3 cm in length	81
Fig. 4.39	Cumulated mass of tracer caesium in main through-diffusion experiments with $MgCl_2$ solution in samples with 3 cm in length	82
Fig. 4.40	Sorel concrete samples after dismantling from through-diffusion cells. Left: $MgCl_2$ solution; Right: NaCl solution.....	85
Fig. 4.41	Schematic depiction of a concrete sealing: saturation of solution starts in the lower part of a sealing element. Affected by the higher	

List of figures

	degree of compaction in the lower part of a sealing an improved sealing capacity in this section of a sealing is assumed.....	87
Fig. 4.42	Functional principle of an advection cell.....	88
Fig. 4.43	Combined sample of salt concrete and rock salt.....	91
Fig. 4.44	Installation of the combined sample in the isostatic cell with rubber jacket.....	92
Fig. 4.45	Permeability development in advection experiments with sored concrete – A1 and NaCl solution. Light grey rectangle marks time of continuous percolation in the beginning of experiments. Percolation was also continuous in the end of experiments (days 159/160). Blue data points describe solution composition of initial NaCl solution.....	94
Fig. 4.46	Development of sodium and chloride concentrations in advection experiment with sored concrete – A1 and NaCl solution. Light grey rectangle marks time of continuous percolation in the beginning of experiments. Percolation was also continuous at the end of experiments (days 159/160). Blue data points describe solution composition of initial NaCl solution	96
Fig. 4.47	Development of magnesium and sulphate concentrations in advection experiment with sored concrete – A1 and NaCl solution. Light grey rectangle marks time of continuous percolation at the beginning of experiments. Percolation was also continuous in the end of experiments (days 159/160). Blue data points describe solution composition of initial NaCl solution	97
Fig. 4.48	Development of calcium and potassium concentrations in advection experiment with sored concrete – A1 and NaCl solution. Light grey rectangle marks time of continuous percolation at the beginning of experiments. Percolation was also continuous at the end of experiments (days 159/160). Blue data points describe solution composition of initial NaCl solution.....	98

List of figures

- Fig. 4.49 Development of p_{cH} and density in advection experiment with sorel concrete – A1 and NaCl solution. Light grey rectangle marks time of continuous percolation at the beginning of experiments. Percolation was also continuous at the end of experiments (days 159/160). Blue data points describe p_{cH} and density of initial NaCl solution 99
- Fig. 4.50 Permeability development in advection experiments with sorel concrete – A1 and $MgCl_2$ solution. Light grey rectangles mark time of continuous percolation at the beginning and end of experiments. Time period between is characterized by “Stop and flow” experiments 100
- Fig. 4.51 Development of sodium and chloride concentrations in advection experiment with sorel concrete – A1 and $MgCl_2$ solution. Light grey rectangles mark time of continuous percolation at the beginning and end of experiments. Time period between is characterized by “Stop and flow” experiments. Blue data points describe solution composition of initial $MgCl_2$ solution 103
- Fig. 4.52 Development of magnesium concentrations in advection experiment with sorel concrete – A1 and $MgCl_2$ solution. Light grey rectangles mark time of continuous percolation at the beginning and end of experiments. Time period between is characterized by “Stop and flow” experiments. Blue data points describe solution composition of initial $MgCl_2$ solution 104
- Fig. 4.53 Development of calcium, potassium and sulphate concentrations in advection experiment with sorel concrete – A1 and $MgCl_2$ solution. Light grey rectangles mark time of continuous percolation at the beginning and end of experiments. Time period between is characterized by “Stop and flow” experiments. Blue data points describe solution composition of initial $MgCl_2$ solution 105
- Fig. 4.54 Development of p_{cH} and density in advection experiment with sorel concrete – A1 and $MgCl_2$ solution. Light grey rectangles mark time of continuous percolation at the beginning and end of experiments.

List of figures

	Time period between is characterized by “Stop and flow” experiments. Blue data points describe p_{cH} and density of initial $MgCl_2$ solution.....	106
Fig. 4.55	Pilot test of advection experiment in isostatic cell with combined samples of salt concrete and rock salt	108
Fig. 4.56	Development of solution composition in pilot test of advection experiments in isostatic cell with combined samples of salt concrete and rock salt. Blue data points describe solution composition of initial $MgCl_2$ solution.....	108
Fig. 4.57	Development of permeability in combined samples in isostatic cells with influence of saturated NaCl solution and confining stress	110
Fig. 4.58	Development of permeability of core 3 and core 8 in isostatic cells after changing to $MgCl_2$ solution	111
Fig. 4.59	Development of solution composition during flowing through of $MgCl_2$ solution in core 3 in isostatic cells. Blue data points describe solution composition of initial $MgCl_2$ solution.....	112
Fig. 4.60	Verification of the contact seam between salt concrete and rock salt after dismantling from isostatic cells. Left: Saline solution pathed the samples driven by compressed air (Core 4). Right: Visualization of path ways using leakage spray (Core 5)	113
Fig. 4.61	Development of permeability after dismantling of combined samples (core 4 and core 5) from isostatic cells and pressure less cast in advection cells. Samples were first percolated with NaCl solution and afterwards with $MgCl_2$ solution	114
Fig. 4.62	Development of solution composition during flowing through of $MgCl_2$ solution in core 4 and core 5 in advection cells. Blue data points describe solution composition of initial $MgCl_2$ solution	116
Fig. 4.63	Sample “Halit_Zement_1”	126

List of figures

Fig. 4.64	Compiled 3D-presentation of all 16 PET time frames.....	129
Fig. 4.65	Estimation of the layer thickness δ from the activity concentration a on the joint surface (as cylinder slice)	131
Fig. 4.66	Circular mean values of the activity a_{mean} for three frames (0.2, 21.8, 70.8 days) in grey. The mean radial activity a_r is plotted in red. The sample axis is at 0 mm, the joint zone is clearly visible in the top profile at 17.5 mm, and the halite mantle extends to 35 mm (scaling in voxel sizes (1.15 mm)). The spreading on the left hand side from the joint is significant, whereas the variations on the right hand side are not exceeding statistical variations. The vertical lines are the first, second (median), and third quartiles of the radial tracer concentration profile, interpreted as a distribution density function.....	133
Fig. 4.67	The interquartile ranges (interval length of the 50%-25% (cement, red) and 75%-50% (halite, blue) values of the circular distribution in Fig. 4) was interpreted as penetration depth of the tracer (applying the interquartile range as robust measure of the standard deviation). The error range is in the order of the voxel dimension of 1.15 mm, therefore, the increase becomes significant after about 150 h	134
Fig. 5.1	Calculated SI of experimental solution in batch experiment in system sorel concrete - old / NaCl solution	153
Fig. 5.2	Calculated SI of experimental solution in batch experiment in system sorel concrete - old / MgCl ₂ solution.....	154
Fig. 5.3	Calculated SI of experimental solution in batch experiment in system salt concrete / NaCl solution	156
Fig. 5.4	Calculated SI of experimental solution in batch experiment in system salt concrete / MgCl ₂ solution.....	158
Fig. 5.5	Calculated SI of experimental solution in cascade experiment in system sorel concrete – A1 / NaCl solution.....	159

List of figures

Fig. 5.6	Calculated SI of experimental solution in cascade experiment in system salt concrete/MgCl ₂ solution. As to the sudden drop of SI, s. chap, 4.2.3.2.....	161
Fig. 5.7	Calculated SI of experimental solution in advection experiment in system sorel concrete – A1 / NaCl solution. Light grey rectangle marks time of continuous percolation at the beginning of experiments. Percolation was also continuous at the end of experiments (days 159/160)	162
Fig. 5.8	Calculated SI of experimental solution in advection experiment in system sorel concrete – A1 / MgCl ₂ solution	164
Fig. 5.9	Step 1 (sorel concrete / NaCl solution): Comparison of calculated (cal) and experimental (exp) concentrations of sodium and chloride. Additionally, the initial (in) concentrations of elements in NaCl solution and the saturation index of chloride and sodium containing phases in cascade experiment are given	166
Fig. 5.10	Step 1 (sorel concrete / NaCl solution): Comparison of calculated (cal) and experimental (exp) concentrations of magnesium and sulphate. Additionally, the initial (in) concentration of elements in NaCl solution and the saturation index of calcium, magnesium, potassium and sulphate containing phases in cascade experiments are given.....	168
Fig. 5.11	Step 1 (sorel concrete / NaCl solution): Comparison of calculated (cal) and experimental (exp) concentrations of calcium and potassium. Additionally, the initial (in) concentration of elements in NaCl solution and the saturation index of calcium, magnesium, potassium and sulphate containing phases in cascade experiments are given.....	169
Fig. 5.12	Step 1 (salt concrete / MgCl ₂ solution): Comparison of calculated (cal) and experimental (exp) concentrations of sodium and chloride. Additionally, the initial (in) concentrations of elements in MgCl ₂ solution and the saturation index of Halite are given	172

List of figures

- Fig. 5.13 Step 1 (salt concrete / MgCl₂ solution): Comparison of calculated (cal) and experimental (exp) concentrations of calcium and magnesium. Additionally, the initial (in) concentrations of elements in MgCl₂ solution and the saturation index of selected phases are given ... 173
- Fig. 5.14 Step 1 (salt concrete / MgCl₂ solution): Comparison of calculated (cal) and experimental (exp) concentrations of potassium and sulphate. Additionally, the initial (in) concentrations of elements in MgCl₂ solution and the saturation index of selected phases are given ... 174
- Fig. 5.15 Step 2 (salt concrete / MgCl₂ solution): Comparison of calculated (cal) and experimental (exp) concentrations of sodium and chloride. Additionally, the initial (in) concentrations of elements in MgCl₂ solution and the saturation index of Halite are given 176
- Fig. 5.16 Step 2 (salt concrete / MgCl₂ solution): Comparison of calculated (cal) and experimental (exp) concentrations of calcium and magnesium. Additionally, the initial (in) concentrations of elements in MgCl₂ solution and the saturation index of selected phases are given ... 177
- Fig. 5.17 Step 2 (salt concrete / MgCl₂ solution): Comparison of calculated (cal) and experimental (exp) concentrations of potassium and sulphate. Additionally, the initial (in) concentrations of elements in MgCl₂ solution and the saturation index of selected phases are given ... 178
- Fig. 5.18 Step 3 (salt concrete / MgCl₂ solution): Comparison of calculated (cal) and experimental (exp) concentrations of sodium and chloride. Additionally, the initial (in) concentrations of elements in MgCl₂ solution and the saturation index of Halite are given 180
- Fig. 5.19 Step 3 (salt concrete / MgCl₂ solution): Comparison of calculated (cal) and experimental (exp) concentrations of calcium and magnesium. Additionally, the initial (in) concentrations of elements in MgCl₂ solution and the saturation index of selected phases are given ... 181
- Fig. 5.20 Step 3 (salt concrete / MgCl₂ solution): Comparison of calculated (cal) and experimental (exp) concentrations of potassium and

List of figures

	sulphate. Additionally, the initial (in) concentrations of elements in MgCl ₂ solution and the saturation index of selected phases are given ...	182
Fig. A.1.1	X-ray diffraction of approach 2 in cascade experiments in system sores concrete – A1 / NaCl solution	264
Fig. A.1.2	X-ray diffraction of approach 3 in cascade experiments in system sores concrete – A1 / NaCl solution	265
Fig. A.1.3	X-ray diffraction of approach 2 in cascade experiments in system salt concrete / MgCl ₂ solution	265
Fig. A.1.4	X-ray diffraction of approach 3 in cascade experiments in system salt concrete / MgCl ₂ solution	266

Appendix**A 1 Experimental data****A 1.1 Detection limits of ICP-OES and ICP-MS****Tab. A.1.1** Detection limits of ICP-OES

Element	Detection limit [$\mu\text{g/l}$]
Aluminium	0.02
Calcium	0.06 – 1.42
Magnesium	0.04 – 1.02
Potassium	0.04 – 3.9
Sodium	0.04 – 0.22
Silicon	0.06
Sulphur	0.12 – 1.36

Tab. A.1.2 Detection limits of ICP-MS

Element	Detection limit [$\mu\text{g/l}$]
Caesium	0.1 – 1.0
Lithium	0.1 – 1.0

Tab. A.1.3 Measurement range of titration for chloride

Element	Measurement range [mg/l]
Chloride	35.0 – 700.0

A 1.2 Solution analysis batch experiments

Tab. A.1.4 Batch experiment: Sorel concrete - old / NaCl solution

Batch experiment: Sorel concrete - old / NaCl solution										
Sorel concrete/NaCl 1 (35538)										
Reaction time [d]	Ca [mg/l]	K [mg/l]	Mg [mg/l]	Na [mg/l]	SO ₄ ²⁻ [mg/l]	Cl [mg/l]	Al [mg/l]	Si [mg/l]	Density [g/cm ³]	p _{C_H}
2	78.25	89.68	2403	132750	5950	221500	n.b.	n.b.	1.203	10.03
4	103.50	91.97	2796	144433	6737	225000	n.b.	n.b.	1.204	10.13
7	47.62	101.10	2630	146033	6860	224500	n.b.	n.b.	1.204	10.13
9	60.78	104.20	2706	145000	6828	225500	n.b.	n.b.	1.203	10.14
11	67.70	105.70	2651	142167	6735	222500	n.b.	n.b.	1.204	10.10
18	109.40	152.50	2747	143900	6827	224500	n.b.	n.b.	1.205	10.18
88	49.40	82.92	2375	116167	6321	179000	n.b.	n.b.	1.204	9.78
200	53.78	75.92	2468	102867	2700	-	n.b.	n.b.	1.204	-
510	-	-	-	-	-	-	-	-	-	-
Sorel concrete/NaCl 2 (35539)										
Reaction time [d]	Ca [mg/l]	K [mg/l]	Mg [mg/l]	Na [mg/l]	SO ₄ ²⁻ [mg/l]	Cl [mg/l]	Al [mg/l]	Si [mg/l]	Density [g/cm ³]	p _{C_H}
2	78.05	84.22	2414	142933	6120	220000	n.b.	n.b.	1.204	10.09
4	73.07	85.55	2561	142500	6554	221667	n.b.	n.b.	1.204	10.10
7	50.99	81.53	2511	141733	6684	221500	n.b.	n.b.	1.204	10.11
9	37.06	87.01	2494	147300	6681	225000	n.b.	n.b.	1.204	10.14
11	161.40	88.10	2844	145700	6616	224500	n.b.	n.b.	1.204	10.10
18	65.14	84.55	2474	146400	6586	226500	n.b.	n.b.	1.205	10.19
Sorel concrete/NaCl 3 (35540)										
Reaction time [d]	Ca [mg/l]	K [mg/l]	Mg [mg/l]	Na [mg/l]	SO ₄ ²⁻ [mg/l]	Cl [mg/l]	Al [mg/l]	Si [mg/l]	Density [g/cm ³]	p _{C_H}
2	79.48	83.77	2504	139750	6313	222500	n.b.	n.b.	1.204	10.09
4	67.35	96.36	2639	141233	6690	224500	n.b.	n.b.	1.205	10.11
7	40.11	83.18	2536	139400	6681	221500	n.b.	n.b.	1.204	10.07
9	92.91	82.20	2760	143733	6757	227000	n.b.	n.b.	1.204	10.15
11	51.43	77.39	2523	139400	6660	221500	n.b.	n.b.	1.204	10.04
18	69.91	72.32	2239	120400	5815	196000	n.b.	n.b.	1.205	9.85
88	50.16	86.22	2443	117467	6479	180500	n.b.	n.b.	1.204	9.68
200	52.52	72.75	2319	112167	5297	-	n.b.	n.b.	1.205	-
510	-	-	-	-	-	-	-	-	-	-
Sorel concrete/NaCl 4 (35541)										
Reaction time [d]	Ca [mg/l]	K [mg/l]	Mg [mg/l]	Na [mg/l]	SO ₄ ²⁻ [mg/l]	Cl [mg/l]	Al [mg/l]	Si [mg/l]	Density [g/cm ³]	p _{C_H}
2	75.49	94.00	2534	139800	6399	221500	n.b.	n.b.	1.204	10.08
4	95.45	89.35	2772	141700	6789	224000	n.b.	n.b.	1.204	10.09
7	55.68	78.28	2609	141033	6812	220000	n.b.	n.b.	1.204	10.08
9	84.56	92.53	2758	143733	6941	226000	n.b.	n.b.	1.204	10.14
11	59.36	91.74	2616	145533	6865	223000	n.b.	n.b.	1.204	-
18	67.15	83.15	2623	145900	6982	225500	n.b.	n.b.	1.205	10.15

Tab. A.1.5 Batch experiment: Sorel concrete - old / MgCl₂ solution

Batch experiment: Sorel concrete - old / MgCl₂ solution										
Sorel concrete/MgCl₂ 1 (35534)										
Reaction time [d]	Ca [mg/l]	K [mg/l]	Mg [mg/l]	Na [mg/l]	SO ₄ ²⁻ [mg/l]	Cl [mg/l]	Al [mg/l]	Si [mg/l]	Density [g/cm ³]	p _{CH}
2	104.40	15203	108733	10805	25780	305000	n.b.	n.b.	1.290	9.56
4	106.60	13670	108733	10733	19575	-	n.b.	n.b.	1.289	9.59
7	104.90	12377	108900	10420	18983	-	n.b.	n.b.	1.288	9.57
9	109.90	12437	108200	10603	22367	-	n.b.	n.b.	1.289	9.54
11	111.50	12487	107233	10453	18365	-	n.b.	n.b.	1.290	9.50
18	105.90	12240	105767	10543	21371	301500	n.b.	n.b.	1.286	9.45
46	107.80	19545	92115	9663	23966	-	n.b.	n.b.	1.290	8.93
158	60.18	6908	88850	8960	23874	-	n.b.	n.b.	1.289	-
510	42.90	20557	89710	10507	22904	273500	n.b.	n.b.	1.289	8.70
Sorel concrete/MgCl₂ 2 (35535)										
Reaction time [d]	Ca [mg/l]	K [mg/l]	Mg [mg/l]	Na [mg/l]	SO ₄ ²⁻ [mg/l]	Cl [mg/l]	Al [mg/l]	Si [mg/l]	Density [g/cm ³]	p _{CH}
2	100.40	15857	108867	8946	26803	308000	n.b.	n.b.	1.289	9.56
4	109.00	12797	108200	7489	22429	-	n.b.	n.b.	1.289	9.52
7	109.80	9704	107133	5309	15908	-	n.b.	n.b.	1.288	9.50
9	110.10	12113	106067	5114	15324	-	n.b.	n.b.	1.289	9.47
11	108.50	14337	106300	6271	18789	-	n.b.	n.b.	1.289	9.48
18	109.90	10002	106467	7399	22168	298500	n.b.	n.b.	1.287	9.45
46	83.65	18697	91827	8246	24706	-	n.b.	n.b.	1.291	8.90
158	61.88	10730	88237	6669	19982	-	n.b.	n.b.	1.290	-
510	41.90	20593	89897	7641	22895	274500	n.b.	n.b.	1.288	8.70
Sorel concrete/MgCl₂ 3 (35536)										
Reaction time [d]	Ca [mg/l]	K [mg/l]	Mg [mg/l]	Na [mg/l]	SO ₄ ²⁻ [mg/l]	Cl [mg/l]	Al [mg/l]	Si [mg/l]	Density [g/cm ³]	p _{CH}
2	107.80	15443	109167	10980	25509	309000	n.b.	n.b.	1.291	9.57
4	109.40	13157	107233	10560	24149	-	n.b.	n.b.	1.288	9.50
7	111.50	10887	106467	10029	15695	-	n.b.	n.b.	1.289	9.50
9	112.80	12047	106100	10260	15817	-	n.b.	n.b.	1.287	9.48
11	113.40	11950	106933	10213	17094	-	n.b.	n.b.	1.291	9.49
18	115.90	10207	106233	10410	17597	302500	n.b.	n.b.	1.288	9.45
46	77.89	18497	92667	9714	28556	-	n.b.	n.b.	1.290	8.91
158	63.46	11253	89813	9304	16904	-	n.b.	n.b.	1.289	-
510	42.68	20577	89843	10607	22898	274500	n.b.	n.b.	1.288	8.80
Sorel concrete/MgCl₂ 4 (35537)										
Reaction time [d]	Ca [mg/l]	K [mg/l]	Mg [mg/l]	Na [mg/l]	SO ₄ ²⁻ [mg/l]	Cl [mg/l]	Al [mg/l]	Si [mg/l]	Density [g/cm ³]	p _{CH}
2	103.80	16500	108633	10853	23387	307500	n.b.	n.b.	1.289	9.58
4	113.40	11197	106667	10153	15393	-	n.b.	n.b.	1.291	9.49
7	108.80	12107	107133	10540	22138	-	n.b.	n.b.	1.289	9.47
9	109.70	13573	105933	10337	16147	-	n.b.	n.b.	1.288	9.48
11	107.40	15690	107433	10803	26234	-	n.b.	n.b.	1.287	9.52
18	112.20	12543	108533	10540	22341	327870	n.b.	n.b.	1.287	9.56
46	75.23	19480	92687	9793	28123	-	n.b.	n.b.	1.291	8.93
158	84.34	9489	91547	8852	22710	-	n.b.	n.b.	1.290	-
510	40.53	20820	90153	10633	23002	281297	n.b.	n.b.	1.288	8.70

Tab. A.1.6 Batch experiment: Sorel concrete / NaCl solution

Batch experiment: Sorel concrete / NaCl solution										
Sorel concrete/NaCl 1 (35528)										
Reaction time [d]	Ca [mg/l]	K [mg/l]	Mg [mg/l]	Na [mg/l]	SO ₄ ²⁻ [mg/l]	Cl [mg/l]	Al [mg/l]	Si [mg/l]	Density [g/cm ³]	pC _H
2	1231	644.10	1.74	143800	5348	225333	11.31	102.80	1.203	13.08
4	1275	592.00	2.72	136367	5585	211500	11.29	102.80	1.204	13.11
7	1401	639.80	1.80	155500	6516	241500	11.78	108.60	1.204	13.09
9	1278	570.90	1.65	143767	6048	222000	10.42	102.40	1.204	13.14
11	1046	461.90	1.29	120567	4881	183500	12.03	84.19	1.204	13.04
18	1184	586.40	1.65	146767	5962	111613	11.69	91.14	1.204	13.06
88	989	527.30	3.45	118767	6261	182000	n.b.	27.88	1.204	12.67
200	1048	571.70	264.90	96717	2115	-	n.b.	n.b.	1.204	-
552	-	-	-	-	-	-	-	-	-	-
Sorel concrete/NaCl 2 (35529)										
Reaction time [d]	Ca [mg/l]	K [mg/l]	Mg [mg/l]	Na [mg/l]	SO ₄ ²⁻ [mg/l]	Cl [mg/l]	Al [mg/l]	Si [mg/l]	Density [g/cm ³]	pC _H
2	1240	573.70	1.48	144450	5368	227500	9.36	90.61	1.203	13.12
4	1282	537.20	2.45	137400	5629	215000	12.55	92.71	1.204	13.11
7	1386	546.40	10.90	131750	5754	213500	22.38	120.50	1.204	13.44
9	1428	592.50	10.26	140267	6120	227500	25.79	145.20	1.204	13.20
11	1377	610.70	8.34	140100	6055	223000	21.28	136.10	1.204	13.14
18	1203	624.50	1.96	139900	6084	225000	12.30	102.70	1.204	13.23
Sorel concrete/NaCl 3 (35530)										
Reaction time [d]	Ca [mg/l]	K [mg/l]	Mg [mg/l]	Na [mg/l]	SO ₄ ²⁻ [mg/l]	Cl [mg/l]	Al [mg/l]	Si [mg/l]	Density [g/cm ³]	pC _H
2	1305	540.30	9.23	140767	5226	220500	22.15	143.40	1.203	13.08
4	1340	549.30	3.14	142233	5825	225000	14.55	101.60	1.204	13.11
7	1289	553.40	1.25	142600	5918	223000	9.67	106.30	1.204	13.09
9	1766	579.90	35.57	141533	5979	224500	58.02	253.30	1.204	13.14
11	1314	570.60	4.99	141100	5905	222000	17.52	110.80	1.204	13.04
18	1210	585.20	2.01	141733	6002	223500	12.76	98.03	1.204	13.06
88	930	508.20	n.b.	120433	6223	181500	n.b.	27.99	1.205	12.67
200	1104	659.10	n.b.	101133	4469	-	n.b.	n.b.	1.205	-
552	-	-	-	-	-	-	-	-	-	-
Sorel concrete/NaCl 4 (35531)										
Reaction time [d]	Ca [mg/l]	K [mg/l]	Mg [mg/l]	Na [mg/l]	SO ₄ ²⁻ [mg/l]	Cl [mg/l]	Al [mg/l]	Si [mg/l]	Density [g/cm ³]	pC _H
2	1236	576.40	6.83	147600	5055	221500	17.73	125.40	1.204	13.12
4	1281	584.90	3.54	148067	5537	220500	14.32	105.30	1.204	13.11
7	1408	681.80	n.b.	165267	6553	250000	10.67	102.80	1.204	13.44
9	1403	635.90	9.36	154367	6159	225000	23.61	143.70	1.204	13.20
11	1227	638.00	1.34	152333	6036	222500	10.68	93.11	1.204	13.14
18	1155	581.00	1.91	157367	5917	226000	10.64	98.56	1.204	13.23

Tab. A.1.7 Batch experiment: Salt concrete / MgCl₂ solution

Batch experiment: Salt concrete / MgCl₂ solution										
Sorel concrete/MgCl₂ 1 (35524)										
Reaction time [d]	Ca [mg/l]	K [mg/l]	Mg [mg/l]	Na [mg/l]	SO ₄ ²⁻ [mg/l]	Cl [mg/l]	Al [mg/l]	Si [mg/l]	Density [g/cm ³]	p _{C,H}
2	593	17493	99727	11717	7240	320571	n.b.	n.b.	1.271	9.67
4	2340	12610	97860	11220	2722	316330	n.b.	n.b.	1.267	9.44
7	5261	11697	95560	11000	1944	314203	n.b.	n.b.	1.268	9.24
9	7416	12250	94020	11170	1840	314354	n.b.	n.b.	1.270	9.10
11	8919	11870	93553	11087	1748	315253	n.b.	n.b.	1.271	9.03
18	11007	12187	91283	11370	1644	313124	n.b.	n.b.	1.271	8.89
46	9495	19390	77670	11480	1779	277413	n.b.	n.b.	1.272	8.33
158	11663	7236	77913	8651	797.3	267176	n.b.	n.b.	1.272	-
510	10757	21760	77007	13380	1665	282751	n.b.	n.b.	1.273	8.00
Sorel concrete/MgCl₂ 2 (35525)										
Reaction time [d]	Ca [mg/l]	K [mg/l]	Mg [mg/l]	Na [mg/l]	SO ₄ ²⁻ [mg/l]	Cl [mg/l]	Al [mg/l]	Si [mg/l]	Density [g/cm ³]	p _{C,H}
2	570.4	14443	103233	2448	7334	313598	n.b.	n.b.	1.273	9.74
4	2559	11707	99483	1009	3023	304680	n.b.	n.b.	1.269	9.47
7	5622	11737	97123	641.2	1921	303466	n.b.	n.b.	1.268	9.29
9	7823	13453	95940	570.3	1709	305481	n.b.	n.b.	1.268	9.23
11	9413	11843	95110	635.7	1905	304409	n.b.	n.b.	1.271	9.12
18	11657	12200	93720	556.6	1668	304702	n.b.	n.b.	1.269	8.99
46	9749	19387	77513	594.1	1780	260587	n.b.	n.b.	1.273	8.28
158	11903	8316	77890	341.4	1023	255533	n.b.	n.b.	1.273	-
510	11233	21393	75973	564.8	1692	260463	n.b.	n.b.	1.272	8.00
Sorel concrete/MgCl₂ 3 (35526)										
Reaction time [d]	Ca [mg/l]	K [mg/l]	Mg [mg/l]	Na [mg/l]	SO ₄ ²⁻ [mg/l]	Cl [mg/l]	Al [mg/l]	Si [mg/l]	Density [g/cm ³]	p _{C,H}
2	565.1	12990	101033	11143	7313	319287	n.b.	n.b.	1.273	9.62
4	2536	11713	99520	10890	3070	319929	n.b.	n.b.	1.268	9.48
7	5600	13217	98057	11357	1946	323969	n.b.	n.b.	1.270	9.29
9	7974	12157	95520	11007	1782	319446	n.b.	n.b.	1.268	9.17
11	9369	11257	95053	10960	1832	319643	n.b.	n.b.	1.270	9.10
18	11507	11943	94593	11177	1721	323088	n.b.	n.b.	1.268	9.05
46	9754	19410	76227	11550	1795	273704	n.b.	n.b.	1.272	8.26
158	11737	6951	77217	8587	1916	264094	n.b.	n.b.	1.273	-
510	11093	21400	76447	13433	1660	281471	n.b.	n.b.	1.272	8.00
Sorel concrete/MgCl₂ 4 (35527)										
Reaction time [d]	Ca [mg/l]	K [mg/l]	Mg [mg/l]	Na [mg/l]	SO ₄ ²⁻ [mg/l]	Cl [mg/l]	Al [mg/l]	Si [mg/l]	Density [g/cm ³]	p _{C,H}
2	556.2	14523	103667	11087	7406	328195	n.b.	n.b.	1.272	9.75
4	2577	12220	101033	10817	2809	324954	n.b.	n.b.	1.267	9.54
7	4653	11143	99293	10707	2160	322887	n.b.	n.b.	1.268	9.33
9	8203	11533	96003	10703	1937	320081	n.b.	n.b.	1.268	9.18
11	9402	12827	94617	10840	1858	319612	n.b.	n.b.	1.267	9.12
18	11623	12753	95020	11177	1806	325208	n.b.	n.b.	1.267	9.05
46	9870	19423	78340	11483	1791	280055	n.b.	n.b.	1.272	8.33
158	11827	6797	78047	8266	1945	266018	n.b.	n.b.	1.272	-
510	10937	21103	75647	13133	1660	278130	n.b.	n.b.	1.272	7.90

A 1.3 Solution analysis cascade experiments

Tab. A.1.8 Cascade experiment: Sorel concrete – A1 / NaCl solution

Cascade experiment: Sorel concrete – A1 / NaCl solution										
Sorel concrete/NaCl 1 (36672)										
Reacted solid [g]	Ca [mg/l]	K [mg/l]	Mg [mg/l]	Na [mg/l]	SO ₄ ²⁻ [mg/l]	Cl [mg/l]	Al [mg/l]	Si [mg/l]	Density [g/cm ³]	p _{C_H}
100.01	1439	41.13	3590	120167	3391	192500	n.b.	n.b.	1.201	7.38
192.13	1440	58.36	3136	119433	3251	192000	n.b.	n.b.	1.202	7.51
257.91	1428	74.96	2895	122400	3218	193500	n.b.	n.b.	1.202	7.70
304.60	1452	93.84	2774	121500	3241	191000	n.b.	n.b.	1.202	7.71
337.04	1489	106.5	2725	121733	3338	192000	n.b.	n.b.	1.202	7.69
357.34	1504	117.7	2330	120367	3359	193500	n.b.	n.b.	1.203	7.82
367.71	1491	140.8	2090	123000	3366	192000	n.b.	n.b.	1.202	9.13
Sorel concrete/NaCl 2 (36673)										
Reacted solid [g]	Ca [mg/l]	K [mg/l]	Mg [mg/l]	Na [mg/l]	SO ₄ ²⁻ [mg/l]	Cl [mg/l]	Al [mg/l]	Si [mg/l]	Density [g/cm ³]	p _{C_H}
99.99	1364	<0.04	3414	118733	3485	193500	n.b.	n.b.	1.201	7.88
190.82	1418	<0.04	2933	120100	3485	194500	n.b.	n.b.	1.202	7.55
255.45	1384	262.9	2769	120600	3387	193500	n.b.	n.b.	1.202	7.79
300.85	1383	75.58	2717	118700	3472	190500	n.b.	n.b.	1.202	7.91
332.36	1310	89.87	2862	120433	3626	192500	n.b.	n.b.	1.202	7.97
349.35	1324	116.6	2431	122167	3662	192000	n.b.	n.b.	1.202	7.93
355.59	1334	154	2123	120567	3821	191500	n.b.	n.b.	1.202	7.83
Sorel concrete/NaCl 3 (36674)										
Reacted solid [g]	Ca [mg/l]	K [mg/l]	Mg [mg/l]	Na [mg/l]	SO ₄ ²⁻ [mg/l]	Cl [mg/l]	Al [mg/l]	Si [mg/l]	Density [g/cm ³]	p _{C_H}
100.00	1393	<0.04	3442	120467	3486	192500	n.b.	n.b.	1.201	7.91
190.67	1443	<0.04	3056	120300	3450	193500	n.b.	n.b.	1.202	8.05
254.29	1452	81.74	2764	119133	3405	192000	n.b.	n.b.	1.201	7.90
300.98	1489	92.01	2728	117500	3451	188500	n.b.	n.b.	1.202	7.93
329.97	1368	121.6	2791	120067	3419	191000	n.b.	n.b.	1.202	8.02
347.93	1431	132.2	2351	119933	3488	190000	n.b.	n.b.	1.202	7.94
356.84	1321	158.4	2178	121533	3577	192500	n.b.	n.b.	1.202	8.00

Tab. A.1.9 Cascade experiment: Salt concrete / MgCl₂ solution

Cascade experiment: Salt concrete / MgCl₂ solution										
Salt concrete/MgCl₂ 1 (36370)										
Reacted solid [g]	Ca [mg/l]	K [mg/l]	Mg [mg/l]	Na [mg/l]	SO ₄ ²⁻ [mg/l]	Cl [mg/l]	Al [mg/l]	Si [mg/l]	Density [g/cm ³]	pC _H
100.00	10723	18317	74933	11467	2106	270500	n.b.	n.b.	1.203	8.29
181.71	28353	17783	63183	12597	3686	-	n.b.	n.b.	1.204	8.11
249.31	47093	17067	49007	15380	5579	-	n.b.	n.b.	1.204	8.17
295.70	66140	17043	35570	17940	7557	-	n.b.	n.b.	1.209	8.09
331.41	82660	16563	22743	20250	9889	260000	n.b.	n.b.	1.211	7.91
358.48	100407	16447	10893	22573	11637	-	n.b.	n.b.	1.214	-
378.07	116967	16337	912.9	24420	13493	-	n.b.	n.b.	1.216	7.89
390.34	116233	16373	<0.013	26440	14932	-	n.b.	n.b.	1.219	8.67
Salt concrete/MgCl₂ 2 (36371)										
Reacted solid [g]	Ca [mg/l]	K [mg/l]	Mg [mg/l]	Na [mg/l]	SO ₄ ²⁻ [mg/l]	Cl [mg/l]	Al [mg/l]	Si [mg/l]	Density [g/cm ³]	pC _H
100.01	6821	16913	65955	10097	-	268500	n.b.	n.b.	1.203	n.m.
182.16	27213	18010	64553	13310	4018	-	n.b.	n.b.	1.205	8.37
250.42	47660	17883	50540	15230	5791	-	n.b.	n.b.	1.207	8.13
305.51	64707	17163	37697	16600	7682	-	n.b.	n.b.	1.211	8.10
349.2	83393	17200	24717	20163	9994	257500	n.b.	n.b.	1.212	8.02
381.87	101700	16857	11770	22557	11804	-	n.b.	n.b.	1.216	-
406.26	116300	16430	1482	24890	13445	-	n.b.	n.b.	1.218	7.93
423.77	119400	17533	<0.013	27643	15559	-	n.b.	n.b.	1.219	8.17
435.13	108600	16223	<0.013	27420	14630	-	n.b.	n.b.	1.219	7.68
Salt concrete/MgCl₂ 3 (36372)										
Reacted solid [g]	Ca [mg/l]	K [mg/l]	Mg [mg/l]	Na [mg/l]	SO ₄ ²⁻ [mg/l]	Cl [mg/l]	Al [mg/l]	Si [mg/l]	Density [g/cm ³]	pC _H
100.02	8245	17867	76017	10570	2310	270500	n.b.	n.b.	1.206	8.26
181.82	26233	17233	60813	12357	3862	-	n.b.	n.b.	1.207	8.11
250.15	46420	17055	49950	14355	5549	-	n.b.	n.b.	1.211	8.04
304.12	49300	16910	36993	16767	7754	-	n.b.	n.b.	1.212	7.75
343.52	67623	17333	25193	20320	10436	259500	n.b.	n.b.	1.216	7.74
373.54	79853	16870	11530	22770	11498	-	n.b.	n.b.	1.219	-

A 1.4 Tracer concentrations through-diffusion experiments

Tab. A.1.10 Pilot test of through-diffusion experiments – NaCl solution

Pilot test of through-diffusion experiments – NaCl solution								
Sorel concrete – old/NaCl 1 cm			Sorel concrete – old/NaCl 2 cm			Sorel concrete – old/NaCl 3 cm		
Time [d]	Cumulated mass caesium [mol/m ²]	Cumulated mass lithium [mol/m ²]	Time [d]	Cumulated mass caesium [mol/m ²]	Cumulated mass lithium [mol/m ²]	Time [d]	Cumulated mass caesium [mol/m ²]	Cumulated mass lithium [mol/m ²]
3	4.53E-08	2.89E-08	3	3.32E-08	3.44E-08	3	1.32E-08	8.53E-09
7	7.14E-08	4.61E-08	7	5.51E-08	5.38E-08	7	2.10E-08	1.56E-08
10	1.02E-07	6.65E-08	9	8.26E-08	7.43E-08	11	3.43E-08	2.68E-08
14	2.68E-07	1.81E-07	14	8.84E-08	7.85E-08	13	3.79E-08	2.95E-08
21	2.90E-07	1.97E-07	18	1.04E-07	9.10E-08	17	4.71E-08	3.71E-08
25	3.05E-07	2.06E-07	22	1.18E-07	1.02E-07	20	5.41E-08	4.33E-08
29	3.25E-07	2.20E-07	24	1.32E-07	1.13E-07	24	6.33E-08	5.14E-08
31	3.56E-07	2.40E-07	28	1.41E-07	1.20E-07	27	6.72E-08	5.45E-08
35	3.72E-07	2.50E-07	31	1.59E-07	1.34E-07	31	7.16E-08	5.78E-08
38	3.96E-07	2.62E-07	35	1.67E-07	1.40E-07	35	7.68E-08	6.19E-08
42	4.54E-07	2.96E-07	38	1.80E-07	1.51E-07	-	-	-
45	4.79E-07	3.10E-07	42	1.88E-07	1.58E-07	-	-	-
49	4.98E-07	3.22E-07	46	1.97E-07	1.65E-07	-	-	-
53	5.20E-07	3.35E-07	49	2.07E-07	1.74E-07	-	-	-
56	5.49E-07	3.53E-07	-	-	-	-	-	-

Tab. A.1.11 Pilot test of through-diffusion experiments – MgCl₂ solution

Pilot test of through-diffusion experiments – MgCl₂ solution								
Sorel concrete – old/ MgCl ₂ 1 cm			Sorel concrete – old/ MgCl ₂ 2 cm			Sorel concrete – old/ MgCl ₂ 3 cm		
Time [d]	Cumulated mass caesium [mol/m ²]	Cumulated mass lithium [mol/m ²]	Time [d]	Cumulated mass caesium [mol/m ²]	Cumulated mass lithium [mol/m ²]	Time [d]	Cumulated mass caesium [mol/m ²]	Cumulated mass lithium [mol/m ²]
3	3.39E-09	6.33E-09	3	4.77E-10	n.b.	3	0.00E+00	n.b.
7	5.15E-09	9.82E-09	7	7.15E-10	n.b.	7	0.00E+00	n.b.
10	7.03E-09	1.35E-08	10	1.07E-09	n.b.	10	0.00E+00	n.b.
14	8.22E-09	1.59E-08	14	1.36E-09	n.b.	14	0.00E+00	n.b.
16	1.06E-08	1.59E-08	16	1.98E-09	n.b.	16	0.00E+00	n.b.
21	1.16E-08	1.80E-08	21	2.27E-09	n.b.	21	0.00E+00	n.b.
25	1.27E-08	2.02E-08	25	2.60E-09	n.b.	25	8.08E-11	n.b.
29	1.39E-08	2.25E-08	29	3.00E-09	n.b.	29	1.92E-10	n.b.
31	1.60E-08	2.64E-08	31	3.69E-09	n.b.	31	3.92E-10	n.b.
35	1.70E-08	2.85E-08	35	4.05E-09	n.b.	35	5.30E-10	n.b.
38	1.87E-08	3.17E-08	38	4.59E-09	n.b.	38	7.10E-10	n.b.
42	1.98E-08	3.37E-08	42	4.95E-09	n.b.	42	8.37E-10	n.b.
45	2.13E-08	3.66E-08	45	5.49E-09	n.b.	45	1.04E-09	n.b.
49	2.25E-08	3.86E-08	49	5.88E-09	n.b.	49	1.23E-09	n.b.
53	2.39E-08	4.17E-08	53	6.29E-09	n.b.	53	1.42E-09	n.b.
56	2.53E-08	4.44E-08	56	6.77E-09	n.b.	56	1.63E-09	n.b.
-	-	-	59	7.49E-09	n.b.	59	1.94E-09	n.b.
-	-	-	63	7.95E-09	n.b.	63	2.15E-09	n.b.
-	-	-	66	8.60E-09	n.b.	66	2.44E-09	n.b.
-	-	-	70	9.08E-09	n.b.	70	2.67E-09	n.b.
-	-	-	73	9.79E-09	n.b.	73	2.99E-09	n.b.
-	-	-	77	1.03E-08	n.b.	77	3.22E-09	n.b.
-	-	-	80	1.10E-08	n.b.	80	3.56E-09	n.b.
-	-	-	84	1.14E-08	n.b.	84	3.80E-09	n.b.
-	-	-	88	1.20E-08	n.b.	88	4.05E-09	n.b.
-	-	-	91	1.26E-08	n.b.	91	4.36E-09	n.b.
-	-	-	94	1.32E-08	n.b.	94	4.69E-09	n.b.
-	-	-	99	1.36E-08	n.b.	99	4.90E-09	n.b.

Tab. A.1.12 Main through-diffusion experiments – NaCl solution

Main through-diffusion experiments – NaCl solution								
Core NaCl 4			Core NaCl 5			Core NaCl 6		
Time [d]	Cumulated mass caesium [mol/m ²]	Cumulated mass lithium [mol/m ²]	Time [d]	Cumulated mass caesium [mol/m ²]	Cumulated mass lithium [mol/m ²]	Time [d]	Cumulated mass caesium [mol/m ²]	Cumulated mass lithium [mol/m ²]
3	0.00E+00	0.00E+00	3	2.92E-08	2.88E-08	-	-	-
6	0.00E+00	0.00E+00	6	5.37E-08	5.50E-08	-	-	-
10	2.08E-08	1.64E-08	10	7.84E-08	8.47E-08	-	-	-
14	3.82E-08	3.81E-08	14	9.54E-08	1.05E-07	-	-	-
17	5.77E-08	3.81E-08	17	1.16E-07	1.33E-07	-	-	-
20	7.51E-08	5.85E-08	20	1.38E-07	1.61E-07	-	-	-
26	8.42E-08	6.94E-08	26	1.49E-07	1.77E-07	-	-	-
28	9.73E-08	7.97E-08	28	1.76E-07	2.12E-07	-	-	-
32	1.05E-07	8.55E-08	32	1.92E-07	2.33E-07	-	-	-
36	1.18E-07	9.65E-08	36	2.18E-07	2.70E-07	-	-	-
40	2.51E-07	2.60E-07	40	2.39E-07	3.00E-07	-	-	-
42	2.68E-07	2.78E-07	42	2.78E-07	3.54E-07	-	-	-
46	4.84E-07	5.33E-07	46	2.98E-07	3.82E-07	-	-	-
49	4.87E-07	5.36E-07	49	3.08E-07	3.92E-07	-	-	-
53	6.11E-07	6.85E-07	53	3.20E-07	4.06E-07	-	-	-
56	6.37E-07	7.11E-07	56	3.53E-07	4.55E-07	-	-	-
60	6.68E-07	7.44E-07	60	4.07E-07	5.34E-07	-	-	-
62	7.29E-07	8.13E-07	62	5.58E-07	7.47E-07	-	-	-
67	7.42E-07	8.24E-07	67	6.21E-07	8.32E-07	-	-	-

Tab. A.1.13 Main through-diffusion experiments – MgCl₂ solution

Main through-diffusion experiments – MgCl ₂ solution								
Core MgCl ₂ 1			Core MgCl ₂ 2			Core MgCl ₂ 3		
Time [d]	Cumulated mass caesium [mol/m ²]	Cumulated mass lithium [mol/m ²]	Time [d]	Cumulated mass caesium [mol/m ²]	Cumulated mass lithium [mol/m ²]	Time [d]	Cumulated mass caesium [mol/m ²]	Cumulated mass lithium [mol/m ²]
3	2.09E-10	-	3	6.92E-11	-	3	6.88E-11	-
6	5.15E-10	-	6	1.63E-10	-	6	2.10E-10	-
10	8.97E-10	-	10	2.91E-10	-	10	4.46E-10	-
14	1.22E-09	-	14	4.04E-10	-	14	6.79E-10	-
17	1.63E-09	-	17	5.66E-10	-	17	1.05E-09	-
20	2.05E-09	-	20	7.29E-10	-	20	1.42E-09	-
26	2.32E-09	-	26	8.32E-10	-	26	1.67E-09	-
28	3.23E-09	-	28	1.02E-09	-	28	2.38E-09	-
32	3.62E-09	-	32	1.13E-09	-	32	2.77E-09	-
36	4.23E-09	-	36	1.28E-09	-	36	3.38E-09	-
40	4.70E-09	-	40	1.41E-09	-	40	3.87E-09	-
42	5.72E-09	-	42	1.70E-09	-	42	4.94E-09	-
46	6.25E-09	-	46	1.87E-09	-	46	5.50E-09	-
49	7.00E-09	-	49	2.09E-09	-	49	6.30E-09	-
53	7.60E-09	-	53	2.26E-09	-	53	6.94E-09	-
56	8.35E-09	-	56	2.49E-09	-	56	7.68E-09	-
60	9.07E-09	-	60	2.71E-09	-	60	8.40E-09	-
62	1.02E-08	-	62	2.93E-09	-	62	9.52E-09	-
67	1.07E-08	-	67	3.07E-09	-	67	1.00E-08	-

A 1.5 Solution analysis advection experiments – sorel concrete – A1

Tab. A.1.14 Advection experiment: Sorel concrete – A1 / NaCl solution - I

Advection experiment: Sorel concrete – A1 / NaCl solution - I									
MgB-A1-3 (35801)									
Reaction time [d]	Passed through solution [ml]	Ca [mg/l]	K [mg/l]	Mg [mg/l]	Na [mg/l]	SO ₄ ²⁻ [mg/l]	Cl [mg/l]	Density [g/cm ³]	p _{CH}
2	16	4479	293.7	40360	61720	1770	217000	1.212	8.40
5	59	1687	43.99	8612	115300	3414	203500	1.203	8.41
7	97	1416	n.b.	3855	123900	3360	200000	1.203	8.23
19	100	1232	n.b.	5134	117700	2819	195500	1.203	-
20	125	1601	n.b.	7699	112500	2832	199500	1.202	8.09
42	130	1458	n.b.	6966	116600	3433	198500	1.204	8.01
43	171	1440	48.3	7193	115100	3287	197500	1.203	8.10
75	173	1526	62.89	6931	112000	3500	199000	-	-
75	196	1555	58.66	8431	110600	3395	198000	1.203	8.04
159	221	1522	32.2	8379	112200	3406	197500	1.203	8.03
159	238	1413	30.86	6043	116733	3455	197000	1.203	7.90
160	256	1373	n.b.	3348	121667	3573	197000	1.201	7.72
160	282	1313	n.b.	2548	122833	3336	195500	1.202	7.68
MgB-A1-5 (35802)									
Reaction time [d]	Passed through solution [ml]	Ca [mg/l]	K [mg/l]	Mg [mg/l]	Na [mg/l]	SO ₄ ²⁻ [mg/l]	Cl [mg/l]	Density [g/cm ³]	p _{CH}
2	16	3912	325.4	34680	68840	1092	211000	1.210	8.33
5	59	2033	37.34	6346	117300	4282	196500	1.203	8.31
7	97	1422	n.b.	3997	121000	3455	195500	1.202	8.09
19	100	1465	n.b.	5187	118800	3416	199000	1.203	-
20	126	1519	n.b.	7248	114800	3407	197000	1.203	8.07
42	131	1420	n.b.	6862	113350	3401	199000	1.203	7.79
43	173	1369	47	6196	115700	3223	198500	1.203	8.04
75	176	1524	60.43	6830	115400	3513	199000	1.203	-
75	200	1557	59.48	7947	111900	3411	198000	1.203	8.05
159	227	1500	n.b.	7872	113367	3469	197500	1.203	8.03
159	253	1337	n.b.	3835	119333	3507	196000	1.202	7.83
160	273	1380	n.b.	2618	122400	3448	196000	1.202	7.70
160	304	1232	n.b.	2074	123367	3187	195000	1.202	7.73
MgB-A1-7 (35803)									
Reaction time [d]	Passed through solution [ml]	Ca [mg/l]	K [mg/l]	Mg [mg/l]	Na [mg/l]	SO ₄ ²⁻ [mg/l]	Cl [mg/l]	Density [g/cm ³]	p _{CH}
2	19	3351	280.1	35970	65520	1178	211500	1.211	8.10
5	68	1557	42.96	6207	115650	3185	197000	1.203	8.37
7	111	1343	n.b.	3643	119800	3217	196000	1.203	8.25
19	114	1205	n.b.	4539	118300	2934	196000	1.203	-
20	141	1909	n.b.	6873	114200	4375	197000	1.203	8.14
42	146	1373	n.b.	6017	117400	3477	198000	1.204	7.90
43	187	1444	n.b.	6996	115000	3431	198500	1.203	8.16
75	189	1510	51.3	6582	116500	3554	198000	1.203	-
75	211	1543	58.54	7841	113700	3461	198500	1.203	8.03
159	235	1466	n.b.	7316	115100	3311	198000	1.203	8.09
159	258	1378	n.b.	5304	117833	3504	196000	1.202	7.91
160	274	1377	n.b.	3074	121433	3529	196000	1.202	7.72
160	301	1279	n.b.	2484	123400	3339	195000	1.202	7.66

Tab. A.1.15 Advection experiment: Sorel concrete – A1 / NaCl solution - II

Advection experiment: Sorel concrete – A1 / NaCl solution - II									
MgB-A1-9 (36507)									
Reaction time [d]	Passed through solution [ml]	Ca [mg/l]	K [mg/l]	Mg [mg/l]	Na [mg/l]	SO ₄ ²⁻ [mg/l]	Cl [mg/l]	Density [g/cm ³]	p _{CH}
2	19	3567	295.3	34880	65860	1239	212000	1.211	8.11
5	68	1524	31.73	5571	116700	3241	197000	2.203	7.71
7	112	1309	n.b.	3958	119867	3154	197000	1.203	8.42
19	115	1393	25.69	4620	118767	3376	196000	1.204	-
20	115	1502	n.b.	6845	117700	3427	198000	1.203	8.22
42	148	1418	39.14	5957	114367	3588	197000	1.203	7.80
43	189	1495	n.b.	6718	113367	3437	197000	1.203	8.13
75	192	1497	55.95	6858	115200	3534	197500	1.203	-
75	215	1532	21.88	7967	114400	3423	198000	1.203	8.03
159	241	1513	n.b.	7765	112800	3419	196500	1.203	8.02
159	266	1374	n.b.	5120	118100	3470	196500	1.203	7.88
160	286	1369	n.b.	2986	121300	3485	196000	1.202	7.68
160	317	1256	n.b.	2225	123867	3253	195000	1.202	7.62
MgB-A1-10 (36508)									
Reaction time [d]	Passed through solution [ml]	Ca [mg/l]	K [mg/l]	Mg [mg/l]	Na [mg/l]	SO ₄ ²⁻ [mg/l]	Cl [mg/l]	Density [g/cm ³]	p _{CH}
2	17	4417	300.5	34417	65850	1169	209500	1.210	8.28
5	64	1626	26.89	6960	113900	3392	196500	1.203	8.32
7	107	1577	n.b.	4329	118200	3747	196000	1.202	8.13
19	111	1404	n.b.	5623	116633	3217	197000	1.203	-
20	141	1350	n.b.	7657	112267	2961	198500	1.203	8.11
42	147	1462	n.b.	7189	114900	3487	198500	1.203	7.93
43	189	1449	n.b.	6565	115267	3387	198500	1.203	8.05
75	202	1564	25.29	7734	113800	3500	198500	1.204	7.42
75	229	1526	19.76	7758	111700	3401	198500	1.203	8.04
159	277	1400	n.b.	6447	115800	3448	197000	1.203	8.03
159	313	1137	n.b.	1797	123767	2993	197000	1.202	7.98
160	344	1241	n.b.	2188	123267	3100	196000	1.202	7.99
160	381	895.1	n.b.	1214	126267	2348	196000	1.201	8.03

Tab. A.1.16 Advection experiment: Sorel concrete – A1 / MgCl₂ solution - I

Advection experiment: Sorel concrete – A1 / MgCl ₂ solution - I									
MgB-A1-1 (35804)									
Reaction time [d]	Passed through solution [ml]	Ca [mg/l]	K [mg/l]	Mg [mg/l]	Na [mg/l]	SO ₄ ²⁻ [mg/l]	Cl [mg/l]	Density [g/cm ³]	p _{CH}
4	11	4720	1114	38090	60783	1217	214000	1.213	8.39
8	26	519.7	13300	66003	26325	7155	240500	1.242	8.53
12	40	133.5	18497	84133	12097	18163	267000	1.279	8.77
27	43	112.8	21920	85977	12410	23584	267500	1.284	8.36
33	62	117.4	22277	84260	13307	23573	265000	1.283	8.60
54	64	107.3	23023	81627	13950	27076	262000	1.282	-
63	81	117	24383	80353	15123	27864	259500	1.280	8.60
99	84	115.1	25325	80013	16030	29912	258500	1.282	-
112	98	98.07	27943	76870	18730	33198	251500	1.279	8.54
175	109	77.96	24677	88373	12157	29092	271000	1.290	8.48
193	122	93.36	19077	92030	10450	26192	277500	1.291	8.45
209	135	84.82	18173	94090	8975	25913	278500	1.292	8.43
230	151	81.52	17757	93440	9701	25333	279000	1.292	8.43
249	165	80.56	18223	91400	9980	25213	277000	1.291	8.40
MgB-A1-2 (35805)									
Reaction time [d]	Passed through solution [ml]	Ca [mg/l]	K [mg/l]	Mg [mg/l]	Na [mg/l]	SO ₄ ²⁻ [mg/l]	Cl [mg/l]	Density [g/cm ³]	p _{CH}
4	11	4117	855.7	44100	52500	1294	217000	1.216	8.37
8	27	485.6	15453	67897	24570	8185	243500	1.245	8.52
12	43	134.3	18440	84533	12903	21063	267500	1.281	8.47
27	46	111.3	20790	86363	11555	22092	270000	1.285	8.61
33	66	120.8	21403	84187	12163	23066	266000	1.284	8.61
54	69	110.4	23195	83523	13980	27208	265500	1.285	-
63	89	117.1	22795	81100	16197	28568	260500	1.280	8.58
99	93	111.7	25780	80630	15153	29828	261000	1.284	8.48
112	110	100.4	27387	79040	17450	32738	254000	1.281	8.38
175	124	94.27	23727	88790	11923	27305	272500	1.290	8.36
193	142	89.38	17860	92430	9916	25686	278000	1.293	8.36
209	158	85.52	18490	93410	8973	25701	278500	1.291	8.40
230	179	83.88	19660	92570	8973	24480	276000	1.292	8.36
249	199	82.33	19273	92100	10217	24679	274500	1.293	8.40
MgB-A1-4 (35806)									
Reaction time [d]	Passed through solution [ml]	Ca [mg/l]	K [mg/l]	Mg [mg/l]	Na [mg/l]	SO ₄ ²⁻ [mg/l]	Cl [mg/l]	Density [g/cm ³]	p _{CH}
4	8	3982	497.4	40870	56807	1225	213500	1.214	8.36
8	23	1254	10290	58853	34820	3598	232000	1.232	8.49
12	36	178.7	18503	82070	14157	18942	263000	1.273	8.74
27	39	118.9	19947	85147	12943	22654	269000	1.282	-
33	51	124.3	21287	84190	12707	21813	266000	1.282	8.59
54	54	129.2	24307	82207	14897	26372	264500	1.282	-
63	66	122.6	23583	76707	15930	27995	249500	1.278	8.48
99	68	77.58	27597	86130	12343	35425	269000	1.293	-
112	82	92.06	28757	75673	19633	34017	250900	1.278	8.51
175	94	102.7	25797	82937	14847	30721	261000	1.285	8.46
193	111	91.12	22140	90943	10497	25659	276500	1.292	8.47
209	125	82.71	18877	93270	9135	25438	278000	1.292	8.47
230	144	83.69	19057	92530	10263	24523	276500	1.292	8.44
249	162	80.35	19713	92310	10520	24145	278000	1.291	8.51

Tab. A.1.17 Advection experiment: Sorel concrete – A1 / MgCl₂ solution - II

Advection experiment: Sorel concrete – A1 / MgCl₂ solution - II									
MgB-A1-6 (36509)									
Reaction time [d]	Passed through solution [ml]	Ca [mg/l]	K [mg/l]	Mg [mg/l]	Na [mg/l]	SO ₄ ²⁻ [mg/l]	Cl [mg/l]	Density [g/cm ³]	p _{CH}
4	9	4518	778.7	39427	58457	1187	212500	1.214	8.39
8	23	754.5	10433	61690	30933	4593	236500	1.236	8.47
12	37	152.6	19427	82020	14510	19563	264000	1.275	8.73
27	41	116.5	20905	85427	12667	25062	267500	1.283	-
33	58	120.9	21307	82777	12683	21706	265500	1.283	8.60
54	60	107.9	23533	83113	14263	27254	263500	1.283	-
63	78	117.5	21865	82527	15497	28061	263500	1.281	8.62
99	81	105.5	24670	81873	15333	29278	259000	1.282	-
112	95	95.52	28007	77230	17857	33018	252500	1.280	8.48
175	103	77.2	25607	86023	12780	32439	265000	1.291	8.50
193	114	97.05	21023	89345	10717	27803	274000	1.293	8.43
209	124	86.31	16950	94887	8559	26825	278000	1.294	8.43
230	137	85.59	16960	94663	9692	25553	280000	1.293	8.45
249	148	81.08	16653	94477	9728	25505	279000	1.293	8.49
MgB-A1-8 (36510)									
Reaction time [d]	Passed through solution [ml]	Ca [mg/l]	K [mg/l]	Mg [mg/l]	Na [mg/l]	SO ₄ ²⁻ [mg/l]	Cl [mg/l]	Density [g/cm ³]	p _{CH}
4	12	4146	747.6	43770	53260	1271	220000	1.216	8.38
8	28	459.8	13507	68547	24960	7906	245000	1.246	8.55
12	43	131.7	20230	83253	12480	19035	268000	1.281	8.76
27	47	112.5	21483	85340	11923	20392	271000	1.285	8.57
33	68	120	22607	82263	13117	22036	265500	1.283	8.63
54	70	108.7	25060	80037	16093	29089	258500	1.281	-
63	91	118	24427	79770	16007	27902	260000	1.280	8.56
99	95	104.5	25603	82993	14560	33018	261500	1.285	-
112	112	90.93	26833	78353	17227	30013	253000	1.280	8.44
175	125	90.46	23633	88587	11367	27006	272500	1.291	8.38
193	142	89.52	18773	91673	10193	25477	277000	1.292	8.41
209	156	84.97	18480	93763	9013	25546	276500	1.293	8.41
230	176	85.57	18713	92293	10250	24545	276500	1.292	8.40
249	193	83.65	18670	91820	10383	24374	277000	1.292	8.45

A 1.6 Solution analysis and permeability measurements advection experiments – combined samples

Tab. A.1.18 Advection experiment: Combined sample Salt concrete / Rock salt – Isostatic cells – NaCl solution

Advection experiment: Combined sample Salt concrete / Rock salt – Isostatic cells – NaCl solution							
Core 1		Core 2		Core 3		Core 4	
Reaction time [d]	Permeability [m ²]	Reaction time [d]	Permeability [m ²]	Reaction time [d]	Permeability [m ²]	Reaction time [d]	Permeability [m ²]
5	4.14E-13	2	3.82E-14	2	1.95E-14	19	9.88E-15
5	4.14E-13	10	6.80E-15	2	1.95E-14	22	6.49E-16
6	4.27E-13	10	6.80E-15	14	6.52E-16	25	1.85E-16
6	4.27E-13	22	2.20E-15	14	6.52E-16	28	6.16E-17
6	4.27E-13	22	2.20E-15	22	4.07E-16	32	1.71E-17
14	2.74E-13	32	1.32E-15	22	4.07E-16	40	3.02E-18
14	2.74E-13	39	6.75E-16	30	3.65E-17	64	1.47E-19
14	2.74E-13	49	2.90E-16	30	3.65E-17		
21	1.31E-13	58	1.00E-16	30	3.65E-17		
28	7.42E-14	71	5.26E-17	43	8.39E-18		
28	7.42E-14	86	1.13E-17	43	8.39E-18		
28	7.42E-14	113	1.67E-18	58	8.97E-18		
28	7.42E-14						
41	1.90E-14						
41	1.90E-14						
41	1.90E-14						
41	1.90E-14						
48	1.14E-14						
48	1.14E-14						
48	1.14E-14						
55	6.23E-15						
55	6.23E-15						
67	3.76E-15						
67	3.76E-15						
67	3.76E-15						
75	2.23E-15						
75	2.23E-15						
83	6.32E-16						
83	6.32E-16						
91	3.11E-16						
98	2.32E-16						
106	2.22E-16						
118	9.16E-17						
131	4.28E-17						
148	2.37E-17						
195	2.29E-18						
195	2.29E-18						
195	2.29E-18						
203	2.64E-17						
209	5.56E-18						
209	5.56E-18						
217	3.02E-18						
Core 5		Core 6		Core 7		Core 8	
Reaction time [d]	Permeability [m ²]	Reaction time [d]	Permeability [m ²]	Reaction time [d]	Permeability [m ²]	Reaction time [d]	Permeability [m ²]
1	9.51E-16	4	3.06E-13	2	6.70E-17	1	8.40E-15
2	4.03E-16	12	4.78E-14	5	2.07E-18	13	1.72E-18
9	1.79E-17	18	1.84E-14	8	7.57E-20		
17	1.15E-18	25	7.80E-15				

Tab. A.1.19 Advection experiment: Combined sample Salt concrete / Rock salt – Isostatic cells – MgCl₂ solution

Advection experiment: Combined sample Salt concrete / Rock salt – Isostatic cells – MgCl ₂ solution								
Pilot test (35827) – MgCl₂ solution								
Reaction time [d]	Passed through solution [ml]	Ca [mg/l]	K [mg/l]	Mg [mg/l]	Na [mg/l]	SO ₄ ²⁻ [mg/l]	Cl [mg/l]	Permeability [m ²]
79	-	47.88	18293	79410	17707	20583	-	-
88	51	28.32	20410	89815	11030	23288	-	7.68E-17
108	143	30.53	19650	88425	11960	21391	-	1.99E-17
163	185	25.97	19947	91623	10760	23519	-	2.93E-17
172	203	25.91	20380	92343	10750	23881	-	3.37E-17
184	229	72.9	20883	90570	10450	23995	-	3.47E-17
189	258	79.51	15937	95200	9606	26521	-	7.71E-17
193	274	80.78	20833	93067	10570	23830	-	7.23E-17
198	297	83.81	22545	99793	11335	25691	-	9.65E-17
201	306	78.45	20475	90953	10290	23213	-	6.76E-17
206	333	79.67	20645	91120	10430	23689	-	1.15E-16
207	350	75.25	20620	93480	10283	23968	-	2.36E-16
212	403	69.73	19710	92625	9877	23516	-	2.11E-16
214	426	404.8	1117	n.b.	123700	7577	-	2.08E-16
219	474	72.23	20097	87773	10107	23750	-	2.22E-16
220	484	73.18	20930	93500	10565	24018	-	1.49E-16
Core 3 (35835) – MgCl₂ solution								
Reaction time [d]	Passed through solution [ml]	Ca [mg/l]	K [mg/l]	Mg [mg/l]	Na [mg/l]	SO ₄ ²⁻ [mg/l]	Cl [mg/l]	Permeability [m ²]
70	0.2	-	-	-	-	-	-	3.63E-19
79	15	1083	12627	49570	45350	6719	220500	2.84E-18
84	33	106.1	20557	88150	11253	21784	272000	2.73E-18
93	53	103.8	20557	89367	10950	22774	273000	1.63E-18
101	67	97.46	20823	89993	10747	23755	273500	1.53E-18
108	85	101	21047	90770	10663	24159	274000	1.88E-18
118	108	88.8	21283	90267	10770	24188	276500	2.22E-18
127	133	85.38	21253	89740	10627	24187	274500	2.40E-18
136	156	89.99	21217	89507	10933	24000	274000	2.07E-18
148	180	89.49	21493	89520	10540	24751	272500	1.68E-18
163	209	88.59	20770	89003	10533	23905	276500	1.64E-18
176	232	-	-	-	-	-	-	1.55E-18
185	251	-	-	-	-	-	-	1.72E-18
190	262	-	-	-	-	-	-	2.02E-18
Core 8 (-) – MgCl₂ solution								
Reaction time [d]	Passed through solution [ml]	Ca [mg/l]	K [mg/l]	Mg [mg/l]	Na [mg/l]	SO ₄ ²⁻ [mg/l]	Cl [mg/l]	Permeability [m ²]
63		-	-	-	-	-	-	1.26E-19
78		-	-	-	-	-	-	1.84E-19
91		-	-	-	-	-	-	2.51E-19
102		-	-	-	-	-	-	2.77E-19
116		-	-	-	-	-	-	3.39E-19
130		-	-	-	-	-	-	2.78E-19

Tab. A.1.20 Advection experiment: Combined sample Salt concrete / Rock salt – Advection cells

Advection experiment: Combined sample Salt concrete / Rock salt – Advection cells								
Core 4 (35828) – NaCl solution								
Reaction time [d]	Passed through solution [ml]	Ca [mg/l]	K [mg/l]	Mg [mg/l]	Na [mg/l]	SO ₄ ²⁻ [mg/l]	Cl [mg/l]	Permeability [m ²]
48	12	1655	1579	694	126233	6250	196000	1.69E-18
62	17	1501	1849	1640	123833	4704	197500	7.41E-19
Core 4 (35829) – MgCl₂ solution								
Reaction time [d]	Passed through solution [ml]	Ca [mg/l]	K [mg/l]	Mg [mg/l]	Na [mg/l]	SO ₄ ²⁻ [mg/l]	Cl [mg/l]	Permeability [m ²]
82	5	1321	3018	8737	112567	7153	198000	1.04E-18
112	20	625.9	9380	38450	63783	6814	212000	1.80E-18
133	39	226.9	16305	70497	23373	18238	244000	3.88E-18
147	62	123.9	19010	85193	13180	22757	267000	4.67E-18
159	85	-	-	-	-	-	-	6.64E-18
170	104	-	-	-	-	-	-	5.40E-18
182	124	-	-	-	-	-	-	5.96E-18
196	147	-	-	-	-	-	-	5.45E-18
209	168	-	-	-	-	-	-	5.25E-18
Core 5 (35843) – NaCl solution								
Reaction time [d]	Passed through solution [ml]	Ca [mg/l]	K [mg/l]	Mg [mg/l]	Na [mg/l]	SO ₄ ²⁻ [mg/l]	Cl [mg/l]	Permeability [m ²]
48	29	1406	486.5	n.b.	125533	3643	195500	1.09E-17
62	46	1653	1078	540.8	124433	3391	196000	1.63E-18
Core 5 (35843) – MgCl₂ solution								
Reaction time [d]	Passed through solution [ml]	Ca [mg/l]	K [mg/l]	Mg [mg/l]	Na [mg/l]	SO ₄ ²⁻ [mg/l]	Cl [mg/l]	Permeability [m ²]
82	26	511.4	9514	41698	60567	11732	212000	1.31E-17
91	53	149	18317	79907	16147	21483	257500	1.68E-17
97	66	112	19860	86430	12210	23361	268500	1.36E-17
112	102	96.37	20513	89513	10927	24026	271000	1.29E-17
121	126	93.29	20450	89693	10423	24058	276500	1.33E-17
133	150	94.33	20740	90917	10233	24394	279500	1.11E-17
147	177	90.94	20420	91430	10427	24678	278500	1.08E-17
159	203	-	-	-	-	-	-	1.25E-17
170	223	-	-	-	-	-	-	9.98E-18
182	244	-	-	-	-	-	-	9.79E-18
196	268	-	-	-	-	-	-	9.38E-18
209	289	-	-	-	-	-	-	8.64E-18

A 1.7 Tracer test

Tab. A.1.21 Tracer test with NaCl and MgCl₂ solution: comparison of initial and final concentrations of tracer

Tracer test				
NaCl solution				
	Caesium		Lithium	
	Initial concentration [mg/l]	Final concentration [mg/l]	Initial concentration [mg/l]	Final concentration [mg/l]
Blind sample – NaCl solution				
	0.012	0.012	0.015	0.015
Salt concrete – NaCl solution				
35528	0.012	0.010	0.014	0.013
35530	0.012	0.012	0.013	0.013
Sorel concrete – NaCl solution				
35538	0.011	0.010	0.014	0.014
35540	0.011	0.010	0.014	0.013
MgCl₂ solution				
	Caesium		Lithium	
	Initial concentration [mg/l]	Final concentration [mg/l]	Initial concentration [mg/l]	Final concentration [mg/l]
Blind sample – MgCl ₂ solution				
	0.003	0.004	0.014	0.014
Salt concrete – MgCl ₂ solution				
35524	0.002	0.003	0.014	0.008
35525	0.002	0.003	0.014	0.008
35526	0.002	0.003	0.014	0.008
35527	0.002	0.003	0.014	0.008
Sorel concrete – MgCl ₂ solution				
35534	0.002	0.003	0.015	0.012
35535	0.002	0.003	0.015	0.012
35536	0.002	0.003	0.015	0.012
35537	0.002	0.003	0.015	0.012

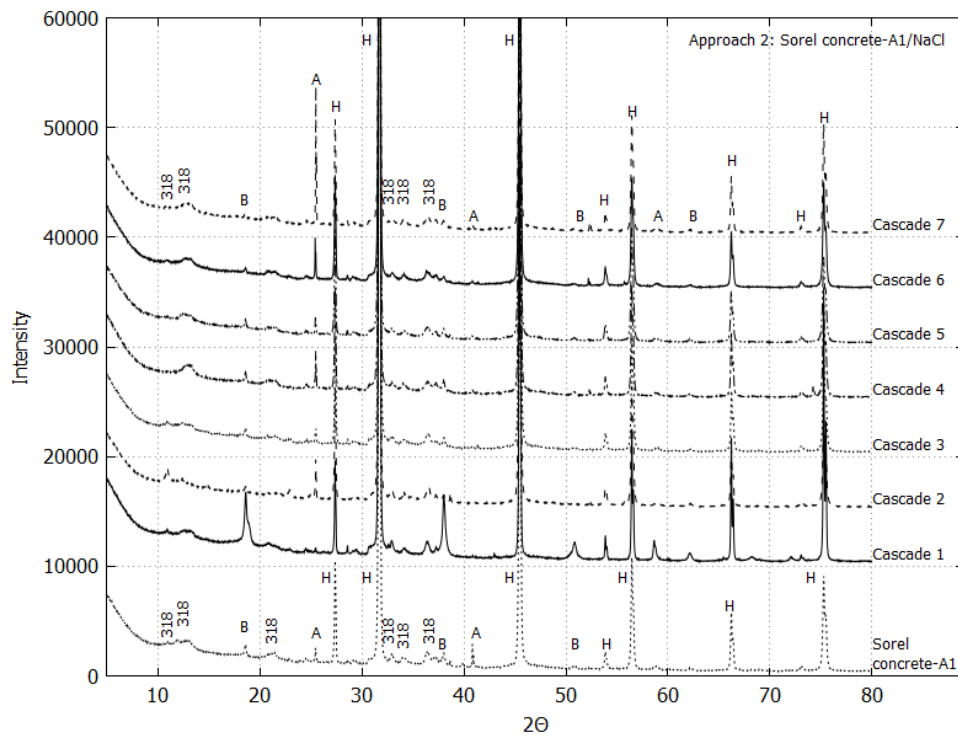
A 1.8 X-ray analysis

Fig. A.1.1 X-ray diffraction of approach 2 in cascade experiments in system sorel concrete – A1 / NaCl solution

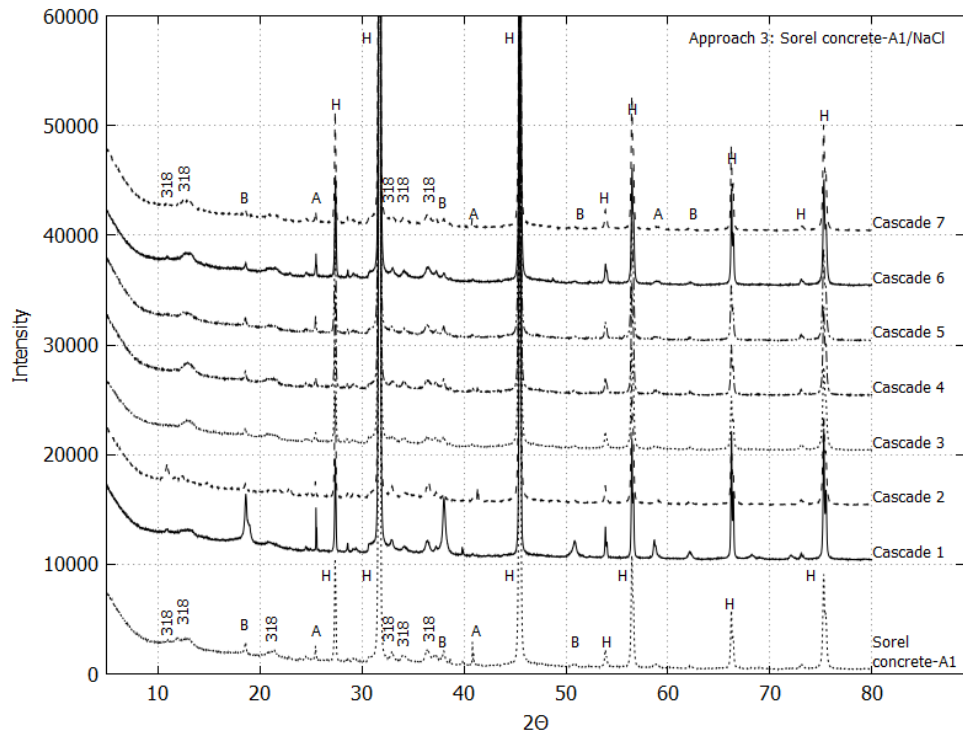


Fig. A.1.2 X-ray diffraction of approach 3 in cascade experiments in system sorel concrete – A1 / NaCl solution

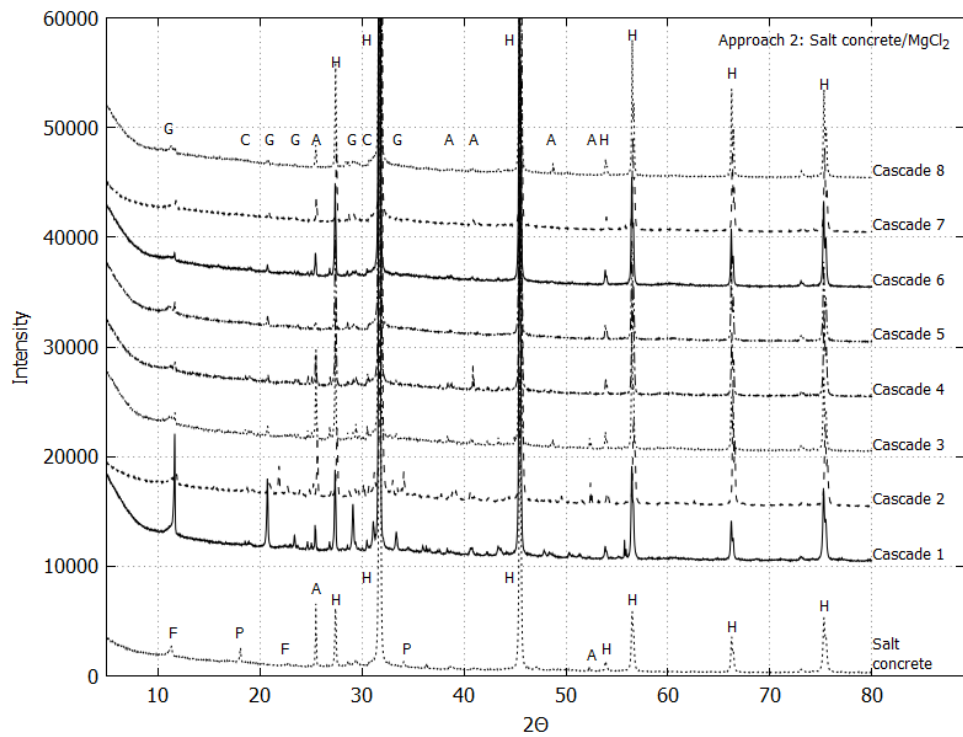


Fig. A.1.3 X-ray diffraction of approach 2 in cascade experiments in system salt concrete / MgCl₂ solution

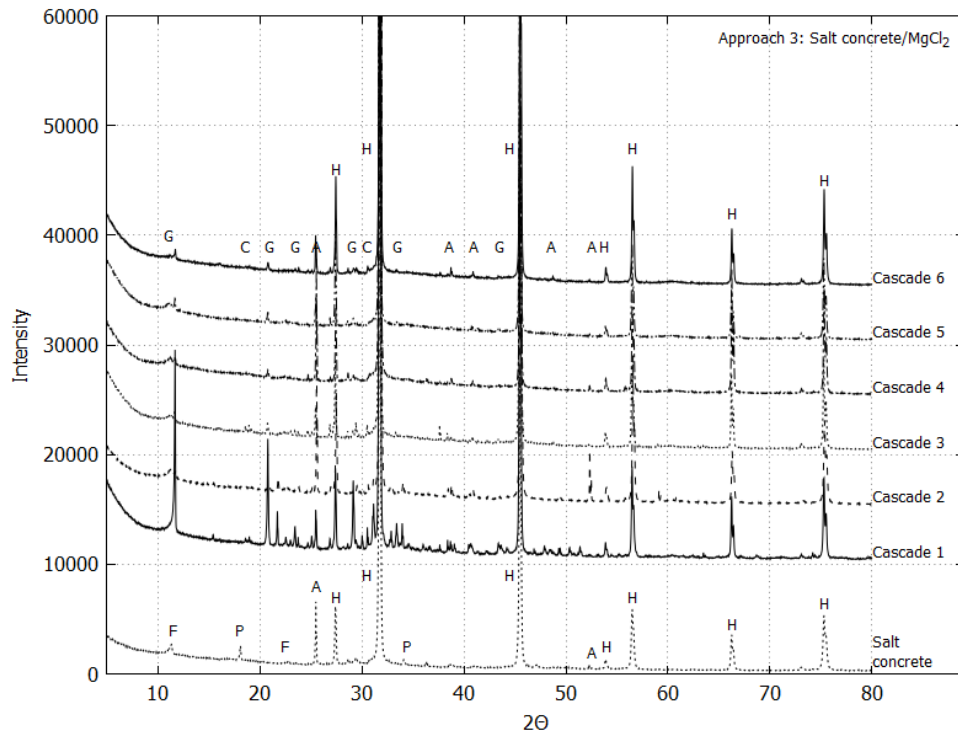


Fig. A.1.4 X-ray diffraction of approach 3 in cascade experiments in system salt concrete / MgCl₂ solution

A 1.9 Permeability measurements to gas – sored concrete – A1**Tab. A.1.22** Permeability to gas in cores of sored concrete - A1 with 1 MPa confining pressure

Core-Nr.	Permeability [m²]	Percolation with
Core A1-1	$3.1 \cdot 10^{-17}$	MgCl ₂
Core A1-2	$6.7 \cdot 10^{-18}$	MgCl ₂
Core A1-3	$2.6 \cdot 10^{-17}$	NaCl
Core A1-4	$5.6 \cdot 10^{-17}$	MgCl ₂
Core A1-5	$6.7 \cdot 10^{-18}$	NaCl
Core A1-6	$9.4 \cdot 10^{-17}$	MgCl ₂
Core A1-7	$7.1 \cdot 10^{-18}$	NaCl
Core A1-8	$1.3 \cdot 10^{-16}$	MgCl ₂
Core A1-9	$3.6 \cdot 10^{-17}$	NaCl
Core A1-10	$8.2 \cdot 10^{-17}$	NaCl

A 1.10 Permeability measurements to gas – combined samples**Tab. A.1.23** Permeability to gas in cores of salt concrete with 1 MPa confining pressure

Core-Nr.	Permeability [m ²]	Used in
Kern_B5_KK3_396_406_Salzbeton	$7.90 \cdot 10^{-19}$	Core 5
Kern_B5_KK4_535_545_Salzbeton	$7.49 \cdot 10^{-20}$	Core 3
Kern_B5_KK4_550_560_Salzbeton	no flux	Core 2
Kern_B5_KK4_584_594_Salzbeton	no flux	Core 1
Kern_B5_KK4_600_610_Salzbeton	no flux	Core 8
Kern_B5_KK4_622_632_Salzbeton	no flux	Core 6
Kern_B5_KK4_657_667_Salzbeton	$4.2 \cdot 10^{-20}$	-
Kern_B5_KK4_678_688_Salzbeton	no flux	Core 7
Kern_B5_KK4_693_703_Salzbeton	no flux	-
Kern_B5_KK4_712_722_Salzbeton	no flux	Core 4
Kern_B5_KK4_723_733_Salzbeton	no flux	-

Tab. A.1.24 Permeability to gas in cores of rock salt with 1 MPa confining pressure

Core-Nr.	Permeability [m ²]	Used in
Kern_B20_KK3_455_565_Salz	$1.20 \cdot 10^{-19}$	Core 5
Kern_B20_KK2_397_407_Salz	low flux	Core 3
Kern_B20_KK2_233_243_Salz	no flux	Core 2
Kern_B20_KK2_244_254_Salz	no flux	Core 1
Kern_B20_KK2_293_303_Salz	no flux	Core 8
Kern_B20_KK2_262_272_Salz	no flux	Core 4
Kern_B20_KK3_415_425_Salz	low flux	-
Kern_B20_KK2_382_292_Salz	no flux	Core 7
Kern_B20_KK2_204_314_Salz	no flux	-
Kern_B20_KK2_214_224_Salz	no flux	Core 6
Kern_B20_KK3_440_450_Salz	no flux	-

A 2 Modelling data

A 2.1 Calculated saturation indices from batch experiments

Tab. A.2.1 Batch experiment: Sorel concrete - old / NaCl solution – Saturation indices calculated

Batch experiment: Sorel concrete - old / NaCl solution – Saturation indices									
Sorel concrete/NaCl 1 (35538)									
Reaction time [d]	Anhydrite	Brucite	Dansite	Glauberite	Gypsum	Halite	Na ₂ Ca ₅ (SO ₄) ₆ ·3H ₂ O	318-Phase	Polyhalite
2	0.156	-2.469	0.322	0.532	-0.189	0.810	0.260	-3.617	-5.547
4	0.480	-2.261	3.438	1.117	0.073	0.985	2.048	-3.263	-4.600
7	0.154	-2.288	3.663	0.814	-0.258	0.996	0.434	-3.322	-5.181
9	0.268	-2.266	3.629	0.922	-0.143	0.994	0.997	-3.275	-4.907
11	0.233	-2.342	2.667	0.810	-0.155	0.933	0.783	-3.409	-5.047
18	0.496	-2.281	3.325	1.125	0.092	0.974	2.125	-3.299	-4.137
88	-0.724	-3.162	-6.540	-0.863	-0.911	0.293	-4.418	-4.938	-7.989
200	-1.269	-3.395	-13.396	-2.025	-1.395	0.050	-7.666	-5.388	-10.064
Sorel concrete/NaCl 2 (35539)									
Reaction time [d]	Anhydrite	Brucite	Dansite	Glauberite	Gypsum	Halite	Na ₂ Ca ₅ (SO ₄) ₆ ·3H ₂ O	318-Phase	Polyhalite
2	0.215	-2.422	1.952	0.733	-0.166	0.915	0.642	-3.567	-5.448
4	0.242	-2.370	2.457	0.803	-0.144	0.928	0.815	-3.464	-5.266
7	0.079	-2.388	2.308	0.628	-0.303	0.916	-0.007	-3.495	-5.643
9	0.052	-2.298	3.777	0.721	-0.365	1.012	-0.075	-3.348	-5.548
11	0.667	-2.251	3.524	1.309	0.255	0.997	2.981	-3.249	-4.280
18	0.309	-2.286	3.755	0.974	-0.109	1.015	1.206	-3.320	-5.053
Sorel concrete/NaCl 3 (35540)									
Reaction time [d]	Anhydrite	Brucite	Dansite	Glauberite	Gypsum	Halite	Na ₂ Ca ₅ (SO ₄) ₆ ·3H ₂ O	318-Phase	Polyhalite
2	0.256	-2.388	1.916	0.768	-0.121	0.902	0.847	-3.487	-5.296
4	0.256	-2.320	2.738	0.836	-0.135	0.940	0.894	-3.363	-5.060
7	-0.036	-2.398	1.995	0.487	-0.408	0.890	-0.592	-3.505	-5.845
9	0.464	-2.242	3.587	1.111	0.053	0.994	1.973	-3.224	-4.701
11	0.071	-2.401	1.976	0.592	-0.302	0.889	-0.061	-3.510	-5.701
18	-0.362	-2.941	-4.674	-0.371	-0.596	0.464	-2.547	-4.502	-7.244
88	-0.681	-3.123	-6.084	-0.783	-0.874	0.319	-4.175	-4.862	-7.814
200	-0.823	-3.233	-8.183	-1.107	-0.992	0.228	-5.030	-5.070	-8.506
Sorel concrete/NaCl 4 (35541)									
Reaction time [d]	Anhydrite	Brucite	Dansite	Glauberite	Gypsum	Halite	Na ₂ Ca ₅ (SO ₄) ₆ ·3H ₂ O	318-Phase	Polyhalite
2	0.223	-2.396	1.869	0.732	-0.151	0.894	0.685	-3.504	-5.261
4	0.409	-2.300	2.866	1.000	0.017	0.944	1.671	-3.325	-4.792
7	0.103	-2.396	2.190	0.644	-0.273	0.897	0.114	-3.506	-5.612
9	0.417	-2.257	3.574	1.066	0.010	0.985	1.746	-3.253	-4.685
11	0.220	-2.317	3.375	0.858	-0.184	0.977	0.752	-3.375	-5.165
18	0.328	-2.275	3.853	1.003	-0.087	1.004	1.314	-3.296	-4.974

Tab. A.2.2 Batch experiment: Sorel concrete - old / $MgCl_2$ solution – Saturation indices calculated - I

Batch experiment: Sorel concrete - old / $MgCl_2$ solution – Saturation indices - I										
Sorel concrete/ $MgCl_2$ 1 (35534)										
Reaction time [d]	Anhydrite	Bischofite	Bloedite	Brucite	Carnallite	Dansite	Epsomite	Glauberite	Gypsum	Halite
2	0.521	0.735	0.618	0.778	1.306	-14.599	1.517	-0.918	0.078	-0.071
4	0.775	0.626	0.327	1.118	1.316	-13.679	0.879	-0.650	0.109	0.145
7	1.015	0.536	-0.203	1.532	1.396	-13.944	0.088	-0.525	0.098	0.375
9	0.967	0.520	-0.331	1.584	1.534	-14.073	-0.067	-0.600	0.014	0.422
11	0.853	0.546	-0.033	1.409	1.508	-13.273	0.265	-0.600	-0.002	0.351
18	1.120	0.516	0.422	1.555	1.377	-8.761	0.184	0.075	0.181	0.559
46	0.966	0.224	0.437	1.559	1.797	-2.776	-0.483	0.479	-0.056	1.005
158	0.811	0.008	-0.178	1.157	1.283	-7.956	-0.432	-0.092	-0.045	0.705
510	0.585	0.161	0.215	1.434	1.765	-4.514	-0.492	-0.047	-0.391	0.917
Reaction time [d]	Hexahydrate	Kainite	Kieserite	Leonite	Loweite	$Na_2Ca_5(SO_4)_6 \cdot 3H_2O$	318-Phase	Pentahydrate	Polyhalite	Sylvite
2	1.561	5.767	1.498	0.111	4.936	0.124	3.109	1.150	3.046	-0.469
4	1.034	5.580	1.526	-0.373	4.335	1.072	3.454	2.126	3.291	-0.350
7	0.369	5.232	1.488	-1.021	2.371	1.782	3.904	2.969	3.374	-0.180
9	0.231	5.531	1.441	-0.938	1.734	1.460	3.956	2.895	3.398	-0.026
11	0.514	5.810	1.477	-0.601	3.064	1.151	3.756	2.525	3.407	-0.078
18	0.475	5.810	1.652	-0.763	6.396	2.768	3.918	3.611	3.865	-0.179
46	-0.150	6.689	1.231	-0.216	6.476	2.431	3.737	3.888	4.185	0.533
158	-0.182	4.290	0.785	-0.828	1.515	1.492	3.108	2.787	3.100	0.235
510	-0.182	6.392	1.086	-0.200	4.770	0.450	3.541	2.100	3.395	0.564
Sorel concrete/ $MgCl_2$ 2 (35535)										
Reaction time [d]	Anhydrite	Bischofite	Bloedite	Brucite	Carnallite	Dansite	Epsomite	Glauberite	Gypsum	Halite
2	0.420	0.839	0.798	0.527	1.260	-15.069	1.952	-1.012	0.151	-0.190
4	0.733	0.648	0.710	0.997	1.280	-11.079	1.094	-0.418	0.138	0.203
7	0.760	0.619	0.284	1.122	1.282	-12.345	0.710	-0.546	0.089	0.284
9	0.725	0.620	0.282	1.102	1.322	-12.363	0.721	-0.579	0.064	0.283
11	0.683	0.659	0.355	0.992	1.277	-13.181	0.959	-0.674	0.097	0.175
18	0.881	0.591	0.454	1.204	1.266	-10.453	0.631	-0.259	0.155	0.379
46	0.981	0.253	0.756	1.626	1.815	-0.243	-0.439	0.726	-0.070	1.106
158	0.882	0.140	0.150	1.395	1.485	-4.105	-0.559	0.297	-0.065	0.970
510	0.622	0.201	0.559	1.517	1.812	-1.016	-0.520	0.307	-0.392	1.099
Reaction time [d]	Hexahydrate	Kainite	Kieserite	Leonite	Loweite	$Na_2Ca_5(SO_4)_6 \cdot 3H_2O$	318-Phase	Pentahydrate	Polyhalite	Sylvite
2	1.909	5.426	1.409	0.230	5.055	-0.112	2.872	0.679	2.789	-0.619
4	1.213	5.608	1.529	-0.223	6.278	1.245	3.318	1.997	3.288	-0.408
7	0.867	4.835	1.371	-0.749	3.943	1.110	3.453	1.837	2.890	-0.377
9	0.873	4.954	1.353	-0.670	3.863	0.951	3.429	1.749	2.890	-0.338
11	1.074	4.933	1.367	-0.550	3.943	0.802	3.320	1.572	2.851	-0.423
18	0.816	5.034	1.457	-0.746	5.320	1.797	3.535	2.413	3.190	-0.365
46	-0.092	7.073	1.364	-0.120	8.672	2.694	3.836	3.958	4.341	0.523
158	-0.263	4.835	0.931	-0.892	4.080	2.025	3.485	3.018	3.267	0.304
510	-0.192	6.625	1.171	-0.208	7.109	0.894	3.666	2.230	3.498	0.571

Tab. A.2.3 Batch experiment: Sorel concrete - old / MgCl₂ solution – Saturation indices calculated - II

Batch experiment: Sorel concrete - old / MgCl ₂ solution – Saturation indices - II										
Sorel concrete/MgCl ₂ 3 (35536)										
Reaction time [d]	Anhydrite	Bischofite	Bloedite	Brucite	Carnallite	Dansite	Epsomite	Glauberite	Gypsum	Halite
2	0.358	0.836	0.675	0.528	1.304	-15.673	1.886	-1.135	0.086	-0.189
4	0.710	0.642	0.266	1.049	1.274	-13.109	0.821	-0.654	0.087	0.223
7	0.755	0.641	0.643	1.029	1.261	-11.150	1.013	-0.410	0.141	0.227
9	0.647	0.634	0.270	1.047	1.360	-12.865	0.797	-0.695	0.019	0.241
11	0.597	0.697	0.767	0.843	1.316	-12.099	1.365	-0.619	0.101	0.084
18	0.600	0.746	0.651	0.759	1.212	-13.885	1.506	-0.769	0.173	-0.021
46	0.949	0.262	0.750	1.642	1.847	-0.214	-0.457	0.693	-0.110	1.116
158	1.125	0.165	0.416	1.448	1.433	-2.876	-0.434	0.655	0.161	0.973
510	0.602	0.214	0.578	1.542	1.832	-0.862	-0.527	0.297	-0.422	1.112
Reaction time [d]	Hexahydrate	Kainite	Kieserite	Leonite	Loweite	Na ₂ Ca ₅ (SO ₄) ₆ ·3H ₂ O	318-Phase	Pentahydrate	Polyhalite	Sylvite
2	1.844	5.371	1.352	0.198	4.276	-0.489	2.870	0.395	2.635	-0.573
4	0.955	4.751	1.339	-0.707	3.562	0.872	3.380	1.612	2.784	-0.408
7	1.142	5.402	1.506	-0.361	5.951	1.311	3.354	2.010	3.213	-0.420
9	0.932	5.070	1.330	-0.550	3.605	0.572	3.370	1.467	2.819	-0.314
11	1.435	5.798	1.503	0.047	6.100	0.646	3.162	1.511	3.186	-0.421
18	1.541	5.161	1.436	-0.165	4.993	0.613	3.094	1.312	2.911	-0.574
46	-0.105	7.164	1.371	-0.102	8.679	2.521	3.861	3.818	4.304	0.546
158	-0.130	5.175	1.106	-0.783	5.931	3.330	3.569	4.183	3.878	0.229
510	-0.193	6.714	1.195	-0.199	7.294	0.792	3.704	2.128	3.478	0.578
Sorel concrete/MgCl ₂ 4 (35537)										
Reaction time [d]	Anhydrite	Bischofite	Bloedite	Brucite	Carnallite	Dansite	Epsomite	Glauberite	Gypsum	Halite
2	0.472	0.791	0.782	0.632	1.264	-14.208	1.763	-0.900	0.128	-0.108
4	0.417	0.819	0.525	0.590	1.242	-16.056	1.733	-1.127	0.109	-0.156
7	0.463	0.799	0.487	0.646	1.206	-15.936	1.640	-1.081	0.118	-0.128
9	0.626	0.721	0.657	0.818	1.220	-13.225	1.398	-0.692	0.158	0.035
11	0.635	0.685	0.437	0.912	1.268	-13.430	1.125	-0.727	0.102	0.116
18	0.860	0.569	0.611	1.249	1.345	-8.993	0.604	-0.148	0.099	0.439
46	1.077	0.260	0.582	1.631	1.855	-1.163	-0.525	0.729	0.023	1.105
158	0.948	0.013	0.275	1.178	1.093	-4.215	-0.347	0.403	0.086	0.842
510	0.620	0.194	0.544	1.504	1.803	-1.164	-0.516	0.294	-0.388	1.090
Reaction time [d]	Hexahydrate	Kainite	Kieserite	Leonite	Loweite	Na ₂ Ca ₅ (SO ₄) ₆ ·3H ₂ O	318-Phase	Pentahydrate	Polyhalite	Sylvite
2	1.757	5.520	1.446	0.156	5.374	0.093	2.968	0.900	2.893	-0.566
4	1.709	4.887	1.307	-0.108	3.515	-0.297	2.936	0.466	2.484	-0.618
7	1.634	4.760	1.323	-0.234	3.481	-0.125	2.993	0.588	2.485	-0.633
9	1.454	5.216	1.454	-0.206	5.252	0.732	3.149	1.426	2.964	-0.541
11	1.214	5.013	1.376	-0.419	4.179	0.635	3.241	1.402	2.834	-0.457
18	0.806	5.629	1.536	-0.506	6.522	1.774	3.574	2.507	3.424	-0.265
46	-0.176	6.887	1.287	-0.227	7.564	3.079	3.846	4.413	4.431	0.555
158	-0.094	3.910	0.890	-1.036	4.368	2.524	3.139	3.163	3.171	0.041
510	-0.190	6.591	1.159	-0.207	6.980	0.884	3.646	2.231	3.492	0.569

Tab. A.2.4 Batch experiment: Salt concrete / NaCl solution – Saturation indices calculated - I

Batch experiment: Salt concrete / NaCl solution – Saturation indices - I							
Salt concrete NaCl 1 (35528)							
Reaction time [d]	Anhydrite	Glauberite	Gypsum	Halite	Kerolite	$\text{Na}_2\text{Ca}_5(\text{SO}_4)_6 \cdot 3\text{H}_2\text{O}$	Pentasalt
2	1.4259	1.9184	1.036	0.9431	5.5448	6.6592	3.4692
4	1.1838	1.4674	0.8648	0.7397	4.7253	5.346	2.1943
7	1.9509	2.8724	1.4455	1.2395	7.7701	9.5398	6.1363
9	1.4403	1.9556	1.0605	0.9147	5.2645	6.7689	3.4833
11	0.5599	0.3714	0.361	0.3443	0.7841	1.9345	-1.2124
18	-0.0793	-0.2744	-0.1988	0.0371	-1.029	-1.1489	-4.1015
88	0.6172	0.505	0.426	0.3147	-0.0256	2.309	-0.7059
200	-0.2332	-1.2438	-0.3198	-0.1256	0.6176	-2.6845	-5.3472
Reaction time [d]	Portlandite	Sepiolite	CSH (0.8)	CSH (1.1)	CSH (1.8)	SiO_2 (am)	SiO_2 (cr)
2	-8.7698	4.287	-0.5296	-2.4684	-8.2924	1.8446	2.8766
4	-9.0218	3.7665	-0.8557	-2.8595	-8.835	1.6918	2.7238
7	-8.3479	5.7361	0.0338	-1.7958	-7.3649	2.1167	3.1487
9	-8.8037	4.1056	-0.5693	-2.5168	-8.3609	1.828	2.86
11	-9.6004	1.1463	-1.6391	-3.7984	-10.1369	1.3232	2.3552
18	-10.2457	0.036	-2.0865	-4.4275	-11.1899	1.3602	2.3922
88	-9.6573	0.4482	-2.1816	-4.3569	-10.7325	0.823	1.855
200	-10.0945	0.6953	-3.3746	-5.6653	-12.3104	-0.0619	0.9701
Salt concrete NaCl 2 (35529)							
Reaction time [d]	Anhydrite	Glauberite	Gypsum	Halite	Kerolite	$\text{Na}_2\text{Ca}_5(\text{SO}_4)_6 \cdot 3\text{H}_2\text{O}$	Pentasalt
2	1.4753	2.0015	1.0756	0.9698	5.3031	6.925	3.6186
4	1.2522	1.5836	0.9194	0.7807	4.6928	5.7152	2.4572
7	1.2374	1.49	0.9292	0.7067	6.6459	5.5993	2.4028
9	1.5606	2.0856	1.177	0.925	8.3893	7.3747	4.1163
11	1.4632	1.9379	1.0947	0.8828	7.6873	6.86	3.6533
18	1.4383	1.9305	1.0655	0.8953	5.4162	6.7464	3.5566
88	-	-	-	-	-	-	-
200	-	-	-	-	-	-	-
Reaction time [d]	Portlandite	Sepiolite	CSH (0.8)	CSH (1.1)	CSH (1.8)	SiO_2 (am)	SiO_2 (cr)
2	-8.727	4.1033	-0.5352	-2.4627	-8.2601	1.8086	2.8406
4	-8.9601	3.7242	-0.8292	-2.8165	-8.7537	1.6744	2.7064
7	-8.9923	5.0678	-0.8004	-2.7937	-8.7447	1.7191	2.7511
9	-8.7026	6.2309	-0.3509	-2.2686	-8.0433	1.967	2.999
11	-8.788	5.7616	-0.4663	-2.4073	-8.2365	1.914	2.946
18	-8.8218	4.2038	-0.6125	-2.5643	-8.4186	1.7964	2.8284
88	-	-	-	-	-	-	-
200	-	-	-	-	-	-	-

Tab. A.2.5 Batch experiment: Salt concrete / NaCl solution – Saturation indices calculated - II

Batch experiment: Salt concrete / NaCl solution – Saturation indices - II							
Salt concrete/NaCl 3 (35530)							
Reaction time [d]	Anhydrite	Glauberite	Gypsum	Halite	Kerolite	Na ₂ Ca ₅ (SO ₄) ₆ ·3H ₂ O	Pentasalt
2	1.3405	1.7357	0.9781	0.8664	7.768	6.1761	2.8762
4	1.484	1.9897	1.1009	0.9237	6.1829	6.973	3.6512
7	1.4431	1.9419	1.0651	0.9098	4.9536	6.7693	3.4614
9	1.6029	2.1092	1.2211	0.9193	10.901	7.5701	4.288
11	1.4228	1.8905	1.054	0.8842	6.652	6.6504	3.3845
18	1.4234	1.9209	1.0478	0.9032	5.3914	6.673	3.4197
88	0.5868	0.4889	0.3924	0.3271	-999.999	2.1666	-0.8919
200	0.163	-0.4534	0.0612	-0.0545	-999.999	-0.3321	-2.9252
Reaction time [d]	Portlandite	Sepiolite	CSH (0.8)	CSH (1.1)	CSH (1.8)	SiO ₂ (am)	SiO ₂ (cr)
2	-8.8412	5.827	-0.4913	-2.4474	-8.3117	1.929	2.961
4	-8.7505	4.712	-0.5351	-2.4671	-8.2751	1.821	2.853
7	-8.795	3.9025	-0.5549	-2.4995	-8.3369	1.8347	2.8667
9	-8.6372	7.9898	-0.0502	-1.9481	-7.6764	2.2146	3.2466
11	-8.8147	5.0431	-0.5716	-2.5208	-8.3688	1.8301	2.8621
18	-8.8245	4.1823	-0.6215	-2.5746	-8.4318	1.7908	2.8228
88	-9.681	-999.999	-2.1866	-4.3695	-10.7629	0.8384	1.8704
200	-10.0122	-999.999	-3.3703	-5.6387	-12.2315	-0.1174	0.9146
Salt concrete/NaCl 4 (35531)							
Reaction time [d]	Anhydrite	Glauberite	Gypsum	Halite	Kerolite	Na ₂ Ca ₅ (SO ₄) ₆ ·3H ₂ O	Pentasalt
2	1.3682	1.8525	0.9748	0.9531	7.682	6.3572	3.0612
4	1.4092	1.9305	1.0165	0.9508	6.5005	6.6001	3.3136
7	2.2068	3.3815	1.6107	1.451	-999.999	10.9365	7.4249
9	1.622	2.3253	1.1847	1.0694	9.1136	7.7794	4.4885
11	1.4943	2.1333	1.0763	1.0189	5.4796	7.1056	3.8524
18	1.5643	2.3022	1.1116	1.11	6.6508	7.5024	4.1174
88	-	-	-	-	-	-	-
200	-	-	-	-	-	-	-
Reaction time [d]	Portlandite	Sepiolite	CSH (0.8)	CSH (1.1)	CSH (1.8)	SiO ₂ (am)	SiO ₂ (cr)
2	-8.7888	5.7456	-0.4335	-2.3786	-8.2171	1.9573	2.9893
4	-8.7847	4.9342	-0.5033	-2.447	-8.2823	1.8839	2.9159
7	-8.105	-999.999	0.3633	-1.407	-6.8377	2.2882	3.3202
9	-8.6151	6.7088	-0.1428	-2.0424	-7.7747	2.1266	3.1586
11	-8.7349	4.2299	-0.4624	-2.3949	-8.2043	1.8952	2.9272
18	-8.6568	5.0088	-0.3066	-2.221	-7.9878	2.0023	3.0343
88	-	-	-	-	-	-	-
200	-	-	-	-	-	-	-

Tab. A.2.6 Batch experiment: Salt concrete / MgCl₂ solution – Saturation indices calculated - I

Batch experiment: Salt concrete / MgCl ₂ solution – Saturation indices - I								
Salt concrete/ MgCl ₂ 1 (35524)								
Reaction time [d]	Anhydrite	Bischofite	Brucite	Carnallite	Epsomite	Glauberite	Gypsum	Halite
2	1.164	0.609	1.097	1.454	0.271	-0.434	0.496	0.353
4	1.802	0.486	1.564	1.573	-1.064	0.041	0.840	0.804
7	1.834	0.467	1.573	1.574	-1.536	-0.286	0.856	0.847
9	1.726	0.477	1.432	1.553	-1.533	-0.640	0.821	0.746
11	1.885	0.462	1.482	1.510	-1.605	-0.418	0.949	0.798
18	1.824	0.459	1.412	1.478	-1.675	-0.618	0.919	0.770
46	1.773	-0.012	1.108	1.508	-2.135	-0.264	0.897	0.974
158	1.757	-0.086	0.986	1.039	-2.120	-0.558	0.942	0.806
510	1.750	-0.001	1.131	1.564	-2.288	-0.265	0.854	1.062
Reaction time [d]	Kainite	Kieserite	Na ₂ Ca ₅ (S O ₄) ₆ ·3H ₂ O	318-Phase	Pentasalt	Polyhalite	Portlandite	Sylvite
2	3.783	0.923	2.841	3.413	3.791	3.185	-9.112	-0.195
4	1.917	0.473	5.427	3.904	6.254	3.283	-7.704	0.047
7	0.245	0.048	5.204	3.901	6.002	2.511	-7.245	0.068
9	-0.488	-0.167	4.529	3.730	5.394	2.010	-7.243	0.036
11	-0.621	-0.146	5.341	3.781	6.078	2.238	-7.071	0.008
18	-1.286	-0.311	4.941	3.691	5.644	1.824	-7.021	-0.021
46	-1.362	-0.855	5.137	3.014	6.405	2.192	-6.818	0.480
158	-3.407	-1.025	4.868	2.825	5.620	1.287	-6.755	0.085
510	-1.636	-0.952	5.014	3.045	6.213	1.974	-6.730	0.525
Salt concrete/MgCl ₂ 2 (35525)								
Reaction time [d]	Anhydrite	Bischofite	Brucite	Carnallite	Epsomite	Glauberite	Gypsum	Halite
2	1.489	0.492	1.560	1.603	-0.491	0.260	0.531	0.787
4	1.814	0.485	1.579	1.582	-1.078	0.056	0.843	0.810
7	1.669	0.509	1.358	1.519	-1.186	-0.607	0.818	0.647
9	1.850	0.456	1.547	1.566	-1.687	-0.413	0.879	0.847
11	1.909	0.455	1.523	1.510	-1.675	-0.378	0.949	0.832
18	1.800	0.480	1.337	1.433	-1.497	-0.688	0.943	0.680
46	1.745	-0.076	0.999	1.422	-2.078	-0.295	0.905	0.921
158	2.012	-0.160	0.866	0.849	-1.739	-0.070	1.241	0.706
510	1.750	0.021	1.169	1.593	-2.314	-0.261	0.841	1.084
Reaction time [d]	Kainite	Kieserite	Na ₂ Ca ₅ (S O ₄) ₆ ·3H ₂ O	318-Phase	Pentasalt	Polyhalite	Portlandite	Sylvite
2	4.269	1.033	4.402	3.903	5.306	3.834	-8.578	0.071
4	1.973	0.484	5.477	3.922	6.321	3.326	-7.692	0.057
7	0.171	0.016	4.414	3.662	5.289	2.260	-7.530	-0.030
9	-0.408	-0.123	5.153	3.859	5.948	2.236	-7.081	0.069
11	-0.676	-0.146	5.439	3.829	6.144	2.234	-7.017	0.015
18	-1.253	-0.278	4.848	3.614	5.548	1.833	-7.129	-0.088
46	-1.535	-0.909	5.046	2.837	6.339	2.159	-6.882	0.458
158	-2.718	-0.776	6.445	2.630	7.122	2.272	-6.846	-0.031
510	-1.594	-0.937	4.996	3.106	6.180	1.956	-6.714	0.532

Tab. A.2.7 Batch experiment: Salt concrete / MgCl₂ solution – Saturation indices calculated - II

Batch experiment: Salt concrete / MgCl ₂ solution – Saturation indices - II								
Salt concrete/MgCl ₂ 3 (35526)								
Reaction time [d]	Anhydrite	Bischofite	Brucite	Carnallite	Epsomite	Glauberite	Gypsum	Halite
2	1.129	0.623	1.063	1.445	0.340	-0.530	0.485	0.301
4	1.605	0.540	1.333	1.483	-0.704	-0.411	0.786	0.559
7	1.761	0.507	1.431	1.479	-1.128	-0.392	0.875	0.670
9	1.893	0.464	1.520	1.524	-1.582	-0.370	0.939	0.804
11	1.869	0.452	1.521	1.569	-1.721	-0.458	0.907	0.832
18	1.738	0.507	1.222	1.410	-1.290	-0.820	0.952	0.573
46	1.798	0.031	1.182	1.565	-2.177	-0.239	0.895	1.010
158	2.051	-0.121	0.928	0.891	-1.749	-0.040	1.260	0.721
510	1.729	-0.030	1.082	1.521	-2.252	-0.295	0.852	1.030
Reaction time [d]	Kainite	Kieserite	Na ₂ Ca ₅ (S O ₄) ₆ ·3H ₂ O	318-Phase	Pentasalt	Polyhalite	Portlandite	Sylvite
2	3.767	0.921	2.642	3.381	3.627	3.124	-9.165	-0.218
4	1.572	0.405	4.403	3.656	5.291	2.842	-7.992	-0.097
7	0.552	0.179	4.944	3.754	5.734	2.593	-7.545	-0.068
9	-0.338	-0.072	5.394	3.832	6.159	2.371	-7.107	0.020
11	-0.592	-0.185	5.195	3.823	6.026	2.197	-7.022	0.077
18	-1.222	-0.282	4.575	3.490	5.319	1.785	-7.267	-0.138
46	-1.247	-0.818	5.221	3.133	6.474	2.223	-6.769	0.495
158	-2.581	-0.728	6.599	2.733	7.272	2.354	-6.804	-0.027
510	-1.706	-0.971	4.928	2.966	6.144	1.948	-6.772	0.510
Salt concrete/MgCl ₂ 4 (35527)								
Reaction time [d]	Anhydrite	Bischofite	Brucite	Carnallite	Epsomite	Glauberite	Gypsum	Halite
2	1.372	0.491	1.489	1.705	-0.483	0.086	0.444	0.762
4	1.819	0.455	1.710	1.697	-1.380	0.157	0.768	0.974
7	1.941	0.434	1.741	1.678	-1.815	-0.002	0.866	1.034
9	1.955	0.424	1.710	1.672	-1.952	-0.117	0.890	1.035
11	1.955	0.424	1.673	1.628	-1.981	-0.219	0.907	1.004
18	1.978	0.400	1.692	1.648	-2.185	-0.228	0.910	1.073
46	1.769	-0.011	1.110	1.510	-2.125	-0.262	0.892	0.972
158	1.653	-0.113	0.941	0.944	-2.167	-0.805	0.857	0.749
510	1.750	0.041	1.205	1.628	-2.324	-0.257	0.829	1.099
Reaction time [d]	Kainite	Kieserite	Na ₂ Ca ₅ (S O ₄) ₆ ·3H ₂ O	318-Phase	Pentasalt	Polyhalite	Portlandite	Sylvite
2	4.456	0.950	3.803	3.811	4.934	3.731	-8.668	0.175
4	2.023	0.422	5.478	4.064	6.363	3.291	-7.533	0.202
7	0.496	0.058	5.771	4.088	6.565	2.762	-7.029	0.204
9	-0.115	-0.106	5.728	4.041	6.517	2.508	-6.877	0.208
11	-0.552	-0.186	5.651	3.994	6.399	2.310	-6.825	0.164
18	-1.023	-0.330	5.704	4.001	6.421	2.119	-6.649	0.208
46	-1.318	-0.845	5.122	3.017	6.395	2.205	-6.830	0.481
158	-4.026	-1.128	4.234	2.753	4.945	0.820	-6.791	0.017
510	-1.471	-0.910	4.982	3.163	6.179	1.981	-6.711	0.547

A 2.2 Calculated saturation indices from cascade experiments

Tab. A.2.8 Cascade experiment: Sorel concrete – A1 / NaCl solution – Saturation indices calculated

Cascade experiment: Sorel concrete – A1 / NaCl solution – Saturation indices									
A1/NaCl 1 (36672)									
Reacted solid [g]	Anhydrite	Brucite	Dansite	Glauberite	Gypsum	Halite	Na ₂ Ca ₅ (SO ₄) ₆ ·3H ₂ O	318-Phase	Polyhalite
100.01	0.666	-2.753	-6.968	0.408	0.428	0.472	2.336	-4.139	-6.027
192.13	0.636	-2.832	-7.443	0.342	0.404	0.453	2.161	-4.291	-5.885
257.91	0.662	-2.835	-6.960	0.410	0.419	0.491	2.313	-4.305	-5.634
304.60	0.632	-2.894	-7.353	0.353	0.399	0.461	2.155	-4.420	-5.545
337.04	0.671	-2.887	-7.102	0.414	0.434	0.471	2.365	-4.408	-5.327
357.34	0.692	-2.949	-7.258	0.426	0.458	0.461	2.465	-4.525	-5.242
367.71	0.679	-3.008	-7.088	0.435	0.442	0.473	2.418	-4.648	-5.174
A1/NaCl 2 (36673)									
Reacted solid [g]	Anhydrite	Brucite	Dansite	Glauberite	Gypsum	Halite	Na ₂ Ca ₅ (SO ₄) ₆ ·3H ₂ O	318-Phase	Polyhalite
99.99	0.662	-2.773	-7.019	0.402	0.427	0.461	2.319	-4.172	-999.999
190.82	0.697	-2.826	-6.848	0.458	0.459	0.475	2.511	-4.281	-999.999
255.45	0.661	-2.866	-7.049	0.407	0.424	0.470	2.318	-4.362	-4.523
300.85	0.623	-2.926	-7.543	0.333	0.399	0.426	2.110	-4.475	-5.712
332.36	0.653	-2.865	-6.851	0.421	0.419	0.461	2.305	-4.358	-5.409
349.35	0.662	-2.941	-6.733	0.448	0.426	0.468	2.363	-4.514	-5.232
355.59	0.669	-3.020	-6.942	0.446	0.441	0.443	2.401	-4.666	-5.007
A1/NaCl 3 (36674)									
Reacted solid [g]	Anhydrite	Brucite	Dansite	Glauberite	Gypsum	Halite	Na ₂ Ca ₅ (SO ₄) ₆ ·3H ₂ O	318-Phase	Polyhalite
100.00	0.665	-2.773	-6.845	0.422	0.427	0.472	2.346	-4.178	-999.999
190.67	0.688	-2.819	-6.924	0.441	0.450	0.472	2.457	-4.267	-999.999
254.29	0.658	-2.894	-7.397	0.376	0.429	0.443	2.285	-4.414	-5.564
300.98	0.620	-2.956	-7.936	0.299	0.403	0.399	2.075	-4.532	-5.581
329.97	0.624	-2.899	-7.333	0.350	0.394	0.445	2.123	-4.426	-5.289
347.93	0.637	-2.995	-7.502	0.358	0.412	0.429	2.190	-4.616	-5.262
356.84	0.654	-2.990	-6.968	0.422	0.420	0.461	2.309	-4.609	-5.043

Tab. A.2.9 Cascade experiment: Salt concrete / MgCl₂ solution – Saturation indices calculated - I

Cascade experiment: Salt concrete / MgCl ₂ solution – Saturation indices - I								
Salt concrete MgCl ₂ 1 (36370)								
Reacted solid [g]	Anhydrite	Bischofite	Brucite	Carnallite	Epsomite	Glauberite	Gypsum	Halite
100.00	1.819	-0.134	0.906	1.315	-1.976	-0.174	1.011	0.872
181.71	2.176	-0.292	0.675	1.058	-2.107	0.207	1.408	0.881
249.31	2.390	-0.556	0.319	0.673	-2.172	0.611	1.683	0.892
295.70	2.551	-0.810	0.016	0.338	-2.346	0.926	1.870	0.936
331.41	2.668	-1.181	-0.415	-0.133	-2.486	1.196	2.038	0.909
358.48	2.775	-1.590	-0.824	-0.594	-2.927	1.419	2.140	0.981
378.07	2.904	-2.710	-1.907	-1.752	-4.176	1.665	2.233	1.097
390.34	2.940	-999.999	-999.999	-999.999	-999.999	1.810	2.282	1.098
Reacted solid [g]	Kainite	Kieserite	Na ₂ Ca ₅ (SO ₄) ₆ ·3H ₂ O	318-Phase	Pentasalt	Polyhalite	Portlandite	Sylvite
100.00	-1.594	-0.902	5.512	2.684	6.772	2.375	-6.893	0.409
181.71	-2.852	-1.153	7.380	2.278	8.386	2.668	-6.496	0.310
249.31	-4.120	-1.401	8.733	1.644	9.413	2.803	-6.358	0.189
295.70	-5.365	-1.656	9.730	1.076	10.133	2.788	-6.233	0.108
331.41	-6.748	-1.946	10.544	0.268	10.753	2.766	-6.232	0.009
358.48	-8.676	-2.370	11.188	-0.552	11.151	2.418	-6.112	-0.045
378.07	-13.525	-3.514	11.895	-2.754	11.588	1.325	-5.941	-0.082
390.34	-999.999	-999.999	12.204	-999.999	11.842	-999.999	-5.982	-0.101
Salt concrete/MgCl ₂ 2 (36371)								
Reacted solid [g]	Anhydrite	Bischofite	Brucite	Carnallite	Epsomite	Glauberite	Gypsum	Halite
100.01	-	-	-	-	-	-	-	-
182.16	2.230	-0.233	0.769	1.141	-2.098	0.362	1.432	0.949
250.42	2.437	-0.445	0.484	0.832	-2.261	0.661	1.678	0.980
305.51	2.569	-0.743	0.101	0.421	-2.319	0.902	1.874	0.930
349.20	2.726	-1.016	-0.188	0.080	-2.589	1.269	2.032	1.034
381.87	2.824	-1.472	-0.663	-0.449	-2.998	1.487	2.143	1.074
406.26	2.911	-2.477	-1.664	-1.512	-3.990	1.692	2.229	1.126
423.77	3.022	-999.999	-999.999	-999.999	-999.999	1.962	2.285	1.276
435.13	2.798	-999.999	-999.999	-999.999	-999.999	1.636	2.247	0.875
Reacted solid [g]	Kainite	Kieserite	Na ₂ Ca ₅ (SO ₄) ₆ ·3H ₂ O	318-Phase	Pentasalt	Polyhalite	Portlandite	Sylvite
100.01	-	-	-	-	-	-	-	-
182.16	-2.470	-1.054	7.706	2.434	8.651	2.870	-6.461	0.333
250.42	-3.836	-1.333	8.893	1.920	9.544	2.862	-6.241	0.237
305.51	-5.065	-1.583	9.757	1.228	10.217	2.890	-6.210	0.123
349.20	-6.422	-1.855	10.754	0.659	10.871	2.799	-6.069	0.056
381.87	-8.465	-2.305	11.383	-0.274	11.261	2.446	-5.989	-0.017
406.26	-12.653	-3.294	11.936	-2.279	11.596	1.531	-5.915	-0.074
423.77	-999.999	-999.999	12.567	-999.999	12.025	-999.999	-5.770	-0.053
435.13	-999.999	-999.999	11.623	-999.999	11.522	-999.999	-6.315	-0.140

Tab. A.2.10 Cascade experiment: Salt concrete / MgCl₂ solution – Saturation indices calculated - II

Cascade experiment: Salt concrete / MgCl ₂ solution – Saturation indices - II								
Salt concrete/MgCl ₂ 3 (36372)								
Reacted solid [g]	Anhydrite	Bischofite	Brucite	Carnallite	Epsomite	Glauberite	Gypsum	Halite
100.02	1.794	-0.167	0.850	1.260	-1.794	-0.155	1.011	0.794
181.82	2.103	-0.505	0.354	0.763	-1.875	0.144	1.439	0.689
250.15	2.388	-0.540	0.337	0.692	-2.154	0.556	1.680	0.864
304.12	2.293	-1.270	-0.620	-0.257	-1.753	0.617	1.830	0.437
343.52	2.483	-1.460	-0.817	-0.472	-2.009	1.007	2.005	0.566
373.54	2.422	-2.162	-1.587	-1.298	-2.273	0.960	2.042	0.380
Reacted solid [g]	Kainite	Kieserite	Na ₂ Ca ₅ (S O ₄) ₆ :3H ₂ O	318-Phase	Pentasalt	Polyhalite	Portlandite	Sylvite
100.02	-1.170	-0.797	5.468	2.596	6.817	2.601	-7.066	0.388
181.82	-3.137	-1.232	7.182	1.743	8.302	2.723	-6.758	0.228
250.15	-4.024	-1.380	8.667	1.679	9.410	2.829	-6.364	0.192
304.12	-5.374	-1.713	8.717	-0.001	9.631	3.000	-6.961	-0.027
343.52	-6.373	-1.924	9.845	-0.398	10.464	3.053	-6.764	-0.052
373.54	-8.762	-2.484	9.700	-1.854	10.347	2.560	-6.986	-0.176

A 2.3 Calculated saturation indices from advection experiments

Tab. A.2.11 Advection experiment: Sorel concrete – A1 / NaCl solution – Saturation indices calculated - I

Advection experiment: Sorel concrete – A1 / NaCl solution – Saturation indices - I										
MgB-A1-3 (35801)										
Reaction time [d]	Passed through solution [ml]	Anhydrite	Brucite	Dansite	Glauberite	Gypsum	Halite	Na ₂ Ca ₅ (SO ₄) ₆ :3H ₂ O	318-Phase	Polyhalite
2	16	1.100	-0.891	-10.069	0.288	0.722	0.683	3.743	-0.507	-2.751
5	59	0.889	-2.147	-5.290	0.711	0.605	0.602	3.462	-2.946	-5.004
7	97	0.781	-2.592	-5.531	0.631	0.511	0.579	2.973	-3.833	-999.99
19	100	0.554	-2.543	-7.413	0.225	0.307	0.497	1.692	-3.721	-999.99
20	125	0.708	-2.288	-7.196	0.370	0.451	0.521	2.439	-3.212	-999.99
42	130	0.756	-2.336	-5.967	0.542	0.493	0.544	2.793	-3.316	-999.99
43	171	0.711	-2.341	-6.450	0.452	0.453	0.524	2.530	-3.322	-5.469
75	173	0.768	-2.358	-6.574	0.502	0.517	0.498	2.819	-3.345	-5.075
75	196	0.747	-2.265	-6.701	0.459	0.494	0.501	2.688	-3.165	-5.137
159	221	0.740	-2.267	-6.491	0.471	0.484	0.514	2.669	-3.172	-5.674
159	238	0.721	-2.437	-6.291	0.490	0.467	0.517	2.615	-3.511	-5.872
160	256	0.738	-2.718	-6.069	0.557	0.486	0.522	2.754	-4.072	-999.99
160	282	0.671	-2.867	-6.595	0.455	0.424	0.508	2.390	-4.369	-999.99
MgB-A1-5 (35802)										
Reaction time [d]	Passed through solution [ml]	Anhydrite	Brucite	Dansite	Glauberite	Gypsum	Halite	Na ₂ Ca ₅ (SO ₄) ₆ :3H ₂ O	318-Phase	Polyhalite
2	16	0.746	-1.142	-12.482	-0.266	0.408	0.615	1.833	-0.979	-3.934
5	59	0.969	-2.405	-5.199	0.841	0.709	0.533	3.948	-3.454	-5.020
7	97	0.717	-2.652	-6.290	0.509	0.466	0.515	2.620	-3.944	-999.99
19	100	0.768	-2.480	-6.012	0.564	0.507	0.540	2.866	-3.599	-999.99
20	126	0.741	-2.344	-6.375	0.492	0.485	0.518	2.695	-3.328	-999.99
42	131	0.731	-2.357	-6.505	0.470	0.477	0.510	2.634	-3.347	-999.99
43	173	0.694	-2.409	-6.573	0.430	0.439	0.519	2.444	-3.453	-5.592
75	176	0.785	-2.347	-6.034	0.567	0.525	0.533	2.940	-3.333	-5.070
75	200	0.754	-2.293	-6.576	0.480	0.500	0.507	2.738	-3.221	-5.129
159	227	0.746	-2.297	-6.336	0.495	0.489	0.517	2.716	-3.234	-999.99
159	253	0.698	-2.673	-6.386	0.484	0.450	0.504	2.526	-3.980	-999.99
160	273	0.712	-2.848	-6.438	0.510	0.464	0.509	2.609	-4.331	-999.99
160	304	0.618	-2.970	-6.934	0.380	0.373	0.500	2.106	-4.574	-999.99
MgB-A1-7 (35803)										
Reaction time [d]	Passed through solution [ml]	Anhydrite	Brucite	Dansite	Glauberite	Gypsum	Halite	Na ₂ Ca ₅ (SO ₄) ₆ :3H ₂ O	318-Phase	Polyhalite
2	19	0.707	-1.119	-12.616	-0.319	0.371	0.591	1.625	-0.928	-4.055
5	68	0.723	-2.427	-6.772	0.444	0.471	0.509	2.578	-3.490	-5.646
7	111	0.661	-2.700	-6.838	0.405	0.415	0.499	2.302	-4.033	-999.99
19	114	0.570	-2.598	-7.244	0.263	0.324	0.496	1.795	-3.829	-999.99
20	141	0.945	-2.372	-5.432	0.793	0.691	0.511	3.813	-3.381	-999.99
42	146	0.729	-2.422	-6.063	0.516	0.471	0.531	2.667	-3.483	-999.99
43	187	0.743	-2.343	-6.221	0.507	0.485	0.527	2.716	-3.325	-999.99
75	189	0.777	-2.375	-5.969	0.569	0.517	0.533	2.909	-3.392	-5.246
75	211	0.772	-2.284	-6.194	0.532	0.512	0.529	2.854	-3.207	-5.088
159	235	0.729	-2.324	-6.338	0.479	0.470	0.530	2.629	-3.289	-999.99
159	258	0.705	-2.515	-6.337	0.479	0.455	0.507	2.547	-3.667	-999.99
160	274	0.718	-2.775	-6.343	0.518	0.470	0.507	2.641	-4.185	-999.99
160	301	0.655	-2.883	-6.580	0.443	0.408	0.508	2.316	-4.403	-999.99

Tab. A.2.12 Advection experiment: Sorel concrete – A1 / NaCl solution – Saturation indices calculated - II

Advection experiment: Sorel concrete – A1 / NaCl solution – Saturation indices - II										
MgB-A1-9 (36507)										
Reaction time [d]	Passed through solution [m]	Anhydrite	Brucite	Dansite	Glauberite	Gypsum	Halite	Na ₂ Ca ₅ (SO ₄) ₆ :3H ₂ O	318-Phase	Polyhalite
2	19	0.756	-1.146	-12.497	-0.254	0.424	0.581	1.893	-0.978	-3.884
5	68	0.724	-2.481	-6.682	0.459	0.473	0.509	2.600	-3.597	-5.934
7	112	0.657	-2.645	-6.728	0.404	0.407	0.512	2.277	-3.924	-999.99
19	115	0.696	-2.583	-6.524	0.459	0.447	0.506	2.490	-3.802	-6.226
20	115	0.766	-2.346	-5.877	0.562	0.502	0.551	2.851	-3.339	-999.99
42	148	0.727	-2.457	-6.519	0.479	0.481	0.490	2.641	-3.545	-5.632
43	189	0.729	-2.396	-6.687	0.458	0.481	0.493	2.624	-3.423	-999.99
75	192	0.758	-2.367	-6.189	0.529	0.502	0.520	2.800	-3.372	-5.205
75	215	0.762	-2.277	-6.153	0.525	0.500	0.535	2.801	-3.197	-5.971
159	241	0.726	-2.322	-6.614	0.453	0.474	0.502	2.602	-3.281	-999.99
159	266	0.707	-2.526	-6.333	0.482	0.456	0.511	2.557	-3.688	-999.99
160	286	0.709	-2.790	-6.445	0.501	0.463	0.504	2.590	-4.214	-999.99
160	317	0.638	-2.934	-6.713	0.417	0.391	0.509	2.219	-4.504	-999.99
MgB-A1-10 (36508)										
Reaction time [d]	Passed through solution [m]	Anhydrite	Brucite	Dansite	Glauberite	Gypsum	Halite	Na ₂ Ca ₅ (SO ₄) ₆ :3H ₂ O	318-Phase	Polyhalite
2	17	0.787	-1.190	-13.025	-0.267	0.463	0.563	2.016	-1.061	-3.905
5	64	0.756	-2.378	-6.647	0.486	0.506	0.501	2.756	-3.392	-5.893
7	107	0.791	-2.618	-6.219	0.589	0.545	0.497	3.007	-3.868	-999.99
19	111	0.685	-2.477	-6.720	0.417	0.435	0.508	2.404	-3.589	-999.99
20	141	0.639	-2.309	-7.164	0.308	0.386	0.507	2.105	-3.251	-999.99
42	147	0.756	-2.328	-6.120	0.528	0.497	0.529	2.786	-3.295	-999.99
43	189	0.739	-2.378	-6.333	0.496	0.483	0.522	2.690	-3.393	-999.99
75	202	0.783	-2.291	-6.151	0.549	0.524	0.528	2.914	-3.221	-5.791
75	229	0.750	-2.302	-6.615	0.473	0.497	0.505	2.714	-3.236	-6.101
159	277	0.713	-2.406	-6.353	0.473	0.460	0.514	2.567	-3.449	-999.99
159	313	0.585	-3.009	-7.053	0.337	0.337	0.514	1.927	-4.652	-999.99
160	344	0.623	-2.932	-6.926	0.380	0.376	0.509	2.123	-4.498	-999.99
160	381	0.372	-3.194	-8.117	0.036	0.123	0.519	0.772	-5.026	-999.99

Tab. A.2.13 Advection experiment: Sorel concrete – A1 / MgCl₂ solution – Saturation indices calculated - I

Advection experiment: Sorel concrete – A1 / MgCl ₂ solution – Saturation indices - I											
MgB-A1-1 (35804)											
Reaction time [d]	Passed through solution [ml]	Anhydrite	Bischofite	Bloedite	Brucite	Carnallite	Dansite	Epsomite	Glauberite	Gypsum	Halite
4	11	0.886	-1.667	-2.463	-1.024	-1.943	12.769	-1.807	-0.170	0.535	0.605
8	26	0.999	-0.722	-0.736	0.079	0.381	-6.563	-0.848	0.390	0.434	0.767
12	40	0.993	-0.024	0.208	1.110	1.480	-3.088	-0.521	0.552	0.128	0.962
27	43	0.943	0.027	0.516	1.213	1.627	-0.990	-0.462	0.686	0.036	1.039
33	62	0.929	-0.028	0.511	1.117	1.558	-0.920	-0.444	0.695	0.052	1.022
54	64	0.862	-0.104	0.591	0.985	1.456	-0.705	-0.351	0.674	0.025	0.971
63	81	0.866	-0.152	0.627	0.911	1.418	-0.254	-0.340	0.734	0.049	0.974
99	84	0.855	-0.163	0.730	0.898	1.420	0.563	-0.317	0.803	0.039	0.997
112	98	0.716	-0.295	0.803	0.700	1.287	1.310	-0.270	0.771	-0.046	0.974
175	109	0.818	0.110	0.777	1.371	1.784	0.701	-0.429	0.695	-0.152	1.116
193	122	1.022	0.217	0.698	1.565	1.807	-0.125	-0.483	0.787	-0.007	1.126
209	135	1.013	0.253	0.597	1.637	1.836	-1.188	-0.505	0.665	-0.037	1.093
230	151	0.998	0.248	0.644	1.624	1.816	-0.637	-0.506	0.704	-0.049	1.118
249	165	0.956	0.202	0.611	1.529	1.765	-0.934	-0.476	0.651	-0.056	1.084
Reaction time [d]	Passed through solution [ml]	Hexahydrate	Kainite	Kieserite	Leonite	Lowellite	Na ₂ Ca ₅ (SO ₄) ₆ :3H ₂ O	318-Phase	Pentahydrate	Polyhalite	Sylvite
4	11	-1.810	11.709	-2.106	-6.015	17.616	2.469	-0.748	0.356	-2.444	-1.316
8	26	-0.743	-0.532	-0.503	-1.853	-4.580	3.161	1.271	3.698	2.159	0.063
12	40	-0.267	4.926	0.723	-0.498	3.812	2.848	3.017	4.095	3.802	0.464
27	43	-0.186	5.911	0.910	-0.153	6.058	2.721	3.175	4.049	4.091	0.560
33	62	-0.184	5.666	0.836	-0.150	5.801	2.716	3.019	4.020	4.033	0.546
54	64	-0.110	5.593	0.809	-0.021	6.052	2.489	2.804	3.803	3.989	0.520
63	81	-0.109	5.508	0.760	0.030	6.123	2.595	2.678	3.903	4.027	0.530
99	84	-0.087	5.648	0.782	0.112	6.759	2.620	2.654	3.907	4.086	0.543
112	98	-0.067	5.376	0.668	0.228	6.815	2.115	2.318	3.391	3.872	0.542
175	109	-0.122	6.870	1.130	0.104	8.155	2.134	3.424	3.520	4.159	0.634
193	122	-0.147	6.812	1.252	-0.164	8.099	2.953	3.739	4.209	4.357	0.550
209	135	-0.158	6.886	1.296	-0.212	7.643	2.764	3.853	4.095	4.313	0.543
230	151	-0.161	6.794	1.284	-0.244	7.899	2.748	3.833	3.995	4.247	0.529
249	165	-0.148	6.599	1.210	-0.219	7.452	2.579	3.685	3.850	4.154	0.524

Appendix

Tab. A.2.14 Advection experiment: Sorel concrete – A1 / MgCl₂ solution – Saturation indices calculated - II

Advection experiment: Sorel concrete – A1 / MgCl ₂ solution – Saturation indices - II												
MgB-A1-2 (35805)												
Reaction time [d]	Passed through solution [ml]	Anhydrite	Bischofite	Bloedite	Brucite	Carnallite	Dansite	Epsomite	Glauberite	Gypsum	Halite	
4	11	0.892	-1.494	-2.378	-0.834	-1.841	-	12.960	-1.713	-0.208	0.518	0.616
8	27	1.046	-0.641	-0.595	0.187	0.560	-5.906	-0.798	0.482	0.451	0.798	
12	43	1.037	-0.003	0.429	1.151	1.503	-1.550	-0.467	0.738	0.156	1.012	
27	46	0.955	0.054	0.430	1.252	1.635	-1.760	-0.483	0.617	0.037	1.020	
33	66	0.948	-0.024	0.419	1.116	1.540	-1.918	-0.436	0.620	0.075	0.974	
54	69	0.911	-0.030	0.687	1.115	1.563	0.166	-0.380	0.783	0.030	1.041	
63	89	0.910	-0.121	0.758	0.967	1.432	0.892	-0.336	0.878	0.075	1.033	
99	93	0.850	-0.126	0.721	0.954	1.475	0.350	-0.323	0.768	0.016	0.999	
112	110	0.761	-0.224	0.809	0.811	1.377	1.283	-0.289	0.794	-0.034	1.001	
175	124	0.913	0.127	0.725	1.401	1.791	0.387	-0.458	0.755	-0.065	1.119	
193	142	1.025	0.226	0.652	1.579	1.788	-0.626	-0.483	0.741	-0.005	1.105	
209	158	1.002	0.243	0.575	1.612	1.828	-1.388	-0.499	0.639	-0.040	1.079	
230	179	0.948	0.210	0.483	1.550	1.823	-1.915	-0.516	0.545	-0.071	1.057	
249	199	0.943	0.193	0.593	1.524	1.797	-0.751	-0.510	0.656	-0.068	1.105	
Reaction time [d]	Passed through solution [ml]	Hexahydrate	Kainite	Kieserite	Leonite	Lowite	Na ₂ Ca ₅ (SO ₄) ₆ :3H ₂ O	318-Phase	Pentastalt	Polyhalite	Sylvite	
4	11	-1.704	11.414	-1.941	-6.093	16.821	2.423	-0.388	0.170	-2.486	-1.387	
8	27	-0.678	0.315	-0.363	-1.579	-3.445	3.396	1.459	4.097	2.557	0.161	
12	43	-0.204	5.292	0.826	-0.372	5.322	3.187	3.080	4.356	4.032	0.466	
27	46	-0.202	5.842	0.921	-0.237	5.604	2.681	3.242	4.021	4.040	0.541	
33	66	-0.178	5.575	0.833	-0.192	5.228	2.723	3.022	4.074	4.026	0.523	
54	69	-0.117	5.986	0.913	0.001	6.957	2.727	3.014	4.011	4.153	0.553	
63	89	-0.097	5.609	0.819	0.008	7.058	2.888	2.770	4.061	4.112	0.513	
99	93	-0.084	5.849	0.830	0.134	6.841	2.539	2.748	3.876	4.118	0.561	
112	110	-0.070	5.644	0.743	0.220	7.083	2.266	2.504	3.560	3.984	0.561	
175	124	-0.147	6.785	1.127	0.025	7.881	2.562	3.473	3.930	4.279	0.624	
193	142	-0.146	6.718	1.258	-0.224	7.836	2.919	3.763	4.162	4.306	0.522	
209	158	-0.156	6.845	1.277	-0.204	7.450	2.707	3.816	4.060	4.292	0.545	
230	179	-0.184	6.694	1.191	-0.195	6.699	2.431	3.717	3.861	4.169	0.573	
249	199	-0.183	6.610	1.172	-0.202	7.296	2.534	3.674	3.839	4.144	0.563	

Tab. A.2.15 Advection experiment: Sorel concrete – A1 / MgCl₂ solution – Saturation indices calculated - III

Advection experiment: Sorel concrete – A1 / MgCl ₂ solution – Saturation indices - III											
MgB-A1-4 (35806)											
Reaction time [d]	Passed through solution [ml]	Anhydrite	Bischofite	Bloedite	Brucite	Carnallite	Dansite	Epsomite	Glauberite	Gypsum	Halite
4	8	0.809	-1.618	-2.465	-0.969	-2.237	13.180	-1.767	-0.291	0.457	0.587
8	23	0.993	-0.985	-1.379	-0.248	-0.082	-9.031	-1.184	0.190	0.503	0.726
12	36	1.091	-0.100	0.295	0.989	1.377	-2.159	-0.490	0.760	0.263	0.973
27	39	0.989	0.026	0.529	1.205	1.576	-0.858	-0.456	0.746	0.086	1.044
33	51	0.955	-0.024	0.407	1.117	1.541	-1.729	-0.466	0.643	0.081	0.997
54	54	0.945	-0.064	0.671	1.057	1.539	0.271	-0.391	0.835	0.080	1.043
63	66	0.806	-0.345	0.444	0.611	1.139	-1.699	-0.297	0.591	0.085	0.838
99	68	0.776	0.061	0.907	1.279	1.747	1.134	-0.322	0.713	-0.169	1.074
112	82	0.672	-0.323	0.836	0.656	1.259	1.598	-0.257	0.762	-0.080	0.973
175	94	0.843	-0.079	0.782	1.043	1.549	0.895	-0.341	0.798	-0.020	1.043
193	111	0.943	0.191	0.632	1.516	1.844	-0.483	-0.502	0.681	-0.072	1.112
209	125	0.977	0.237	0.572	1.603	1.833	-1.307	-0.506	0.623	-0.062	1.085
230	144	0.965	0.216	0.618	1.566	1.817	-0.532	-0.521	0.691	-0.062	1.124
249	162	0.938	0.223	0.631	1.579	1.839	-0.344	-0.534	0.677	-0.096	1.140
Reaction time [d]	Passed through solution [ml]	Hexahydrate	Kainite	Kieserite	Leonite	Lowite	Na ₂ Ca ₅ (SO ₄) ₆ :3H ₂ O	318-Phase	Pentastalt	Polyhalite	Sylvite
4	8	-1.769	12.909	-2.062	-6.667	17.580	2.039	-0.643	-0.722	-3.249	-1.659
8	23	-1.117	-3.316	-1.065	-2.814	-9.375	3.049	0.687	3.193	1.111	-0.137
12	36	-0.254	4.630	0.644	-0.488	4.068	3.504	2.816	4.638	3.972	0.437
27	39	-0.183	5.697	0.903	-0.248	6.109	2.970	3.165	4.184	4.082	0.510
33	51	-0.207	5.473	0.806	-0.245	5.134	2.773	3.023	4.084	3.988	0.526
54	54	-0.137	5.843	0.853	0.001	6.714	2.938	2.917	4.223	4.204	0.563
63	66	-0.114	4.520	0.516	-0.056	4.296	2.356	2.180	3.666	3.726	0.444
99	68	-0.027	7.137	1.163	0.343	8.842	2.020	3.273	3.489	4.288	0.647
112	82	-0.058	5.343	0.651	0.262	6.944	1.944	2.242	3.213	3.809	0.542
175	94	-0.088	6.123	0.896	0.161	7.413	2.496	2.890	3.827	4.157	0.588
193	111	-0.173	6.874	1.193	-0.077	7.573	2.552	3.659	3.948	4.273	0.613
209	125	-0.165	6.834	1.260	-0.197	7.402	2.594	3.800	3.953	4.245	0.556
230	144	-0.186	6.694	1.209	-0.218	7.568	2.633	3.740	3.913	4.189	0.561
249	162	-0.195	6.760	1.218	-0.209	7.685	2.499	3.760	3.783	4.150	0.575

Tab. A.2.16 Advection experiment: Sorel concrete – A1 / MgCl₂ solution – Saturation indices calculated - IV

Advection experiment: Sorel concrete – A1 / MgCl ₂ solution – Saturation indices - IV											
MgB-A1-6 (36509)											
Reaction time [d]	Passed through solution [ml]	Anhydrite	Bischofite	Bloedite	Brucite	Carnallite	Dansite	Epsomite	Glauberite	Gypsum	Halite
4	9	0.834	-1.662	-2.516	-1.017	-2.097	13.293	-1.805	-0.271	0.488	0.582
8	23	0.938	-0.869	-1.133	-0.110	0.073	-8.209	-1.042	0.196	0.420	0.736
12	37	1.023	-0.087	0.361	1.010	1.415	-1.637	-0.484	0.738	0.185	0.996
27	41	0.978	0.020	0.589	1.198	1.588	-0.637	-0.419	0.759	0.076	1.034
33	58	0.923	-0.058	0.363	1.055	1.489	-2.194	-0.446	0.578	0.070	0.959
54	60	0.884	-0.057	0.671	1.071	1.536	0.109	-0.377	0.758	0.018	1.031
63	78	0.949	-0.064	0.776	1.061	1.490	0.970	-0.353	0.908	0.085	1.058
99	81	0.841	-0.123	0.717	0.968	1.470	0.512	-0.343	0.773	0.005	1.017
112	95	0.708	-0.278	0.773	0.721	1.308	0.951	-0.270	0.725	-0.060	0.962
175	103	0.772	0.018	0.812	1.209	1.674	0.727	-0.346	0.683	-0.144	1.059
193	114	0.975	0.148	0.685	1.429	1.753	-0.413	-0.425	0.738	-0.007	1.072
209	124	1.055	0.262	0.606	1.656	1.816	-1.327	-0.487	0.692	0.000	1.080
230	137	1.052	0.273	0.686	1.678	1.829	-0.294	-0.517	0.782	-0.014	1.143
249	148	1.029	0.263	0.680	1.660	1.812	-0.329	-0.511	0.759	-0.029	1.138
Reaction time [d]	Passed through solution [ml]	Hexahydrate	Kainite	Kieserite	Leonite	Lowite	Na ₂ Ca ₅ (SO ₄) ₆ :3H ₂ O	318-Phase	Pentastalt	Polyhalite	Sylvite
4	9	-1.810	12.369	-2.116	-6.340	17.967	2.168	-0.734	-0.221	-2.877	-1.475
8	23	-0.961	-2.348	-0.837	-2.510	-7.531	2.793	0.937	3.023	1.333	-0.098
12	37	-0.243	4.838	0.679	-0.417	4.550	3.196	2.849	4.344	3.916	0.462
27	41	-0.146	5.908	0.937	-0.134	6.493	2.938	3.152	4.206	4.172	0.528
33	58	-0.197	5.302	0.764	-0.250	4.722	2.611	2.923	3.940	3.897	0.507
54	60	-0.122	5.874	0.872	0.006	6.745	2.618	2.941	3.908	4.090	0.553
63	78	-0.099	5.791	0.888	-0.023	7.375	3.029	2.925	4.184	4.187	0.514
99	81	-0.103	5.755	0.815	0.080	6.812	2.506	2.770	3.794	4.048	0.553
112	95	-0.064	5.440	0.684	0.232	6.680	2.027	2.355	3.342	3.865	0.546
175	103	-0.067	6.664	1.050	0.215	8.013	2.018	3.162	3.425	4.123	0.616
193	114	-0.112	6.718	1.172	-0.038	7.712	2.787	3.523	4.135	4.343	0.565
209	124	-0.138	6.879	1.327	-0.234	7.752	2.951	3.884	4.254	4.378	0.514
230	137	-0.162	6.864	1.331	-0.278	8.291	3.012	3.917	4.204	4.341	0.516
249	148	-0.160	6.790	1.313	-0.288	8.201	2.911	3.889	4.090	4.278	0.509

Tab. A.2.17 Advection experiment: Sorel concrete – A1 / MgCl₂ solution – Saturation indices calculated - V

Advection experiment: Sorel concrete – A1 / MgCl ₂ solution – Saturation indices - V											
MgB-A1-8 (36510)											
Reaction time [d]	Passed through solution [ml]	Anhydrite	Bischofite	Bloedite	Brucite	Carnallite	Dansite	Epsomite	Glauberite	Gypsum	Halite
4	12	0.931	-1.456	-2.335	-0.795	-1.850	12.613	-1.711	-0.144	0.547	0.644
8	28	1.054	-0.605	-0.562	0.237	0.549	-5.581	-0.805	0.513	0.447	0.827
12	43	0.969	-0.028	0.270	1.101	1.509	-2.661	-0.504	0.569	0.102	0.972
27	47	0.931	0.043	0.370	1.228	1.634	-1.996	-0.512	0.572	0.019	1.020
33	68	0.901	-0.066	0.393	1.042	1.504	-1.884	-0.445	0.587	0.049	0.970
54	70	0.829	-0.164	0.708	0.896	1.415	0.469	-0.329	0.769	0.014	0.998
63	91	0.870	-0.156	0.679	0.906	1.412	0.264	-0.339	0.787	0.052	0.996
99	95	0.866	-0.069	0.845	1.058	1.551	1.105	-0.305	0.840	-0.002	1.038
112	112	0.695	-0.257	0.678	0.755	1.325	0.399	-0.315	0.653	-0.079	0.964
175	125	0.890	0.122	0.666	1.387	1.781	-0.210	-0.453	0.677	-0.082	1.088
193	142	0.998	0.207	0.641	1.542	1.787	-0.610	-0.484	0.721	-0.021	1.102
209	156	0.996	0.234	0.563	1.601	1.826	-1.362	-0.508	0.638	-0.040	1.083
230	176	0.978	0.212	0.617	1.557	1.802	-0.597	-0.513	0.699	-0.045	1.117
249	193	0.965	0.208	0.619	1.547	1.792	-0.588	-0.508	0.689	-0.054	1.115
Reaction time [d]	Passed through solution [ml]	Hexahydrate	Kainite	Kieserite	Leonite	Lowite	Na ₂ Ca ₅ (SO ₄) ₆ :3H ₂ O	318-Phase	Pentastalt	Polyhalite	Sylvite
4	12	-1.697	11.507	-1.908	-6.202	16.482	2.625	-0.316	0.232	-2.506	-1.434
8	28	-0.679	0.202	-0.334	-1.698	-3.159	3.441	1.545	4.001	2.466	0.114
12	43	-0.249	5.140	0.745	-0.391	4.212	2.766	3.001	4.061	3.862	0.496
27	47	-0.234	5.708	0.872	-0.279	5.167	2.550	3.204	3.901	3.943	0.551
33	68	-0.197	5.389	0.761	-0.196	4.896	2.534	2.900	3.886	3.907	0.530
54	70	-0.099	5.579	0.767	0.081	6.604	2.484	2.651	3.761	4.003	0.540
63	91	-0.108	5.510	0.763	0.033	6.437	2.662	2.668	3.922	4.038	0.528
99	95	-0.049	6.282	0.948	0.219	7.869	2.623	2.915	3.954	4.267	0.580
112	112	-0.105	5.297	0.658	0.125	6.114	1.894	2.414	3.203	3.738	0.542
175	125	-0.145	6.729	1.113	0.016	7.484	2.401	3.453	3.813	4.217	0.618
193	142	-0.153	6.687	1.221	-0.193	7.671	2.806	3.704	4.080	4.270	0.541
209	156	-0.168	6.793	1.251	-0.208	7.322	2.690	3.797	4.044	4.269	0.552
230	176	-0.179	6.649	1.206	-0.228	7.535	2.700	3.726	3.968	4.201	0.550
249	193	-0.176	6.617	1.201	-0.233	7.528	2.643	3.711	3.899	4.166	0.544

A 2.4 Potential equilibrium phases in modelling with PHREEQC

Tab. A.2.18 Potential equilibrium phases in system sorel concrete / NaCl solution according to calculation step 1

$\text{Al}(\text{OH})_3$ (mcr)	Glaserite	Monosulfat
Anhydrite	Glauberite	$\text{Na}(\text{HSO}_4) \cdot \text{H}_2\text{O}$ (cr)
Antarcticite	Gypsum	$\text{Na}_2\text{Ca}_5(\text{SO}_4)_6 \cdot 3\text{H}_2\text{O}$ (cr)
Bischofite	H_2O (g)	$\text{Na}_3(\text{HSO}_4)(\text{SO}_4)$ (cr)
Bloedite	Halite	Oxychloride-Mg (318-phase)
Brucite	Hexahydrite	Pentasalt
C_2AH_8	Hydrogarnet	Picromerite
C_4AH_{13}	Hydrotalcite	Polyhalite
$\text{Ca}(\text{SO}_4) \cdot 0.5\text{H}_2\text{O}$ (cr)	$\text{K}_3(\text{HSO}_4)(\text{SO}_4)$ (cr)	Portlandite
$\text{Ca}_2\text{Cl}_2(\text{OH})_2 \cdot \text{H}_2\text{O}$ (cr)	Kainite	Sepiolite
$\text{Ca}_4\text{Cl}_2(\text{OH})_6 \cdot 13\text{H}_2\text{O}$ (cr)	Kerolite	Si-Hydrogarnet
Carnallite	Kieserite	SiO_2 (am)
CSH(0.8)	Kuzels'salt	SiO_2 alpha Qrz (cr)
CSH(1.1)	Labile'salt	Stratlingite
CSH(1.8)	Langbeinite	Sylvite
Dansite	Leonite	Syngenite
Epsomite	Loeweite	Tachyhydrite
Ettringite	Mercallite	Thenardite
Friedels'salt	Mirabilite	Vanthoffite
Gibbsite	Misenite	

Tab. A.2.19 Potential equilibrium phases in system salt concrete / MgCl_2 solution according to calculation step 1

$\text{Al}(\text{OH})_3$ (mcr)	Glaserite	Monosulfat
Anhydrite	Glauberite	$\text{Na}(\text{HSO}_4) \cdot \text{H}_2\text{O}$ (cr)
Antarcticite	Gypsum	$\text{Na}_2\text{Ca}_5(\text{SO}_4)_6 \cdot 3\text{H}_2\text{O}$ (cr)
Bischofite	H_2O (g)	$\text{Na}_3(\text{HSO}_4)(\text{SO}_4)$ (cr)
Bloedite	Halite	Oxychloride-Mg (318-phase)
Brucite	Hexahydrite	Pentasalt
C_2AH_8	Hydrogarnet	Picromerite
C_4AH_{13}	Hydrotalcite	Polyhalite
$\text{Ca}(\text{SO}_4) \cdot 0.5\text{H}_2\text{O}$ (cr)	$\text{K}_3(\text{HSO}_4)(\text{SO}_4)$ (cr)	Portlandite
$\text{Ca}_2\text{Cl}_2(\text{OH})_2 \cdot \text{H}_2\text{O}$ (cr)	Kainite	Sepiolite
$\text{Ca}_4\text{Cl}_2(\text{OH})_6 \cdot 13\text{H}_2\text{O}$ (cr)	Kerolite	Si-Hydrogarnet
Carnallite	Kieserite	SiO_2 (am)
CSH(0.8)	Kuzels'salt	SiO_2 alpha Qrz (cr)
CSH(1.1)	Labile'salt	Stratlingite
CSH(1.8)	Langbeinite	Sylvite
Dansite	Leonite	Syngenite
Epsomite	Loeweite	Tachyhydrite
Ettringite	Mercallite	Thenardite
Friedels'salt	Mirabilite	Vanthoffite
Gibbsite	Misenite	

A 2.5 Translation of logK from cemdata07.dat to THEREDA

Tab. A.2.20 Translation of logK from CEMDATA 07 to THEREDA – Substitution of OH⁻: $H^+ + OH^- = H_2O$ / Substitution of $HSiO_3^-$: $H^+ + HSiO(OH)_3^- = Si(OH)_4$ / Substitution of AlO_2^- : $AlO_2^- + 2*H_2O = Al(OH)_4$

Mineral	Dissolution reaction														log k		
		H+	OH-	SiO(OH)3-	=	Ca+2	AlO2-	Al(OH)4-	HSiO3-	Si(OH)4	SO4-2	CO3-2	OH-	H2O			
Hydrogarnet	Ca3Al2(OH)12				=		3	2						4	4	-20.840	
			4	4	=										4	14.001	
	Ca3Al2(OH)12	4H+			=	3Ca+2		2Al(OH)4-						4H2O		35.164	
Siliceous Hydrogarnet	Ca3Al2(SiO4)0,8(OH)8,8				=		3	2		0.8				3.2	2.4	-29.870	
			3.2	3.2	=										3.2	14.001	
	Ca3Al2(SiO4)0,8(OH)8,8	3,2H+			=	3Ca+2		2Al(OH)4-	0,8HSiO3-					1,6H2O		14.933	
		4H+	0.8		=	3Ca+2		2Al(OH)4-		0.8				0.8	9.810		
					=	3Ca+2		2Al(OH)4-		0,8Si(OH)4				0,8H2O		22.781	
Aft																	
Ettringit	Ca6Al2(SO4)3(OH)12*26H2O				=		6	2				3		4	30	-44.900	
			4	4	=										4	14.001	
Ca6Al2(SO4)3(OH)12*26H2O	4H+				=	6Ca+2		2Al(OH)4-			3SO4-2			30H2O		11.104	
Tricarbonat	Ca6Al2(CO3)3(OH)12*26H2O				=		6	2					3	4	30	-46.500	
			4	4	=										4	14.001	
Ca6Al2(CO3)3(OH)12*26H2O	4H+				=	6Ca+2		2Al(OH)4-				3CO3-2		30H2O		9.504	
AFm																	
Monosulfat	Ca4Al2(SO4)(OH)12*6H2O				=		4	2				1		4	10	-29.260	
			4	4	=										4	14.001	
Ca4Al2(SO4)(OH)12*6H2O	4H+				=	4Ca+2		2Al(OH)4-			1SO4-2			10H2O		26.744	
Monocarbonat	Ca4Al2(CO3)(OH)12*5H2O				=		4	2					1	4	9	-31.470	
			4	4	=										4	14.001	
Ca4Al2(CO3)(OH)12*5H2O	4H+				=	4Ca+2		2Al(OH)4-				1CO3-2		9H2O		24.534	
Hemicarbonat	Ca4Al2(CO3)0,5(OH)13*5,5H2O				=		4	2					0.5	5	9.5	-29.130	
			5	5	=										5	14.001	
Ca4Al2(CO3)0,5(OH)13*5,5H2O	5H+				=	4Ca+2		2Al(OH)4-				0,5CO3-2		10,5H2O		40.875	

A 2.6 Modelled concentrations cascade experiment – sorel concrete – A1 / NaCl solution

Tab. A.2.22 Modelling of cascade experiment: Sorel concrete – A1 / NaCl solution

Modelling cascade experiment: Sorel concrete – A1 / NaCl solution						
Step 1 (sorel concrete / NaCl solution)						
Reacted solid [mol]	Ca [mol/kg H ₂ O]	K [mol/kg H ₂ O]	Mg [mol/kg H ₂ O]	Na [mol/kg H ₂ O]	SO ₄ ²⁻ [mol/kg H ₂ O]	Cl [mol/kg H ₂ O]
0.1	0.016	0.001	0.055	6.046	0.016	6.157
0.2	0.032	0.001	0.109	5.933	0.032	6.152
0.3	0.038	0.002	0.162	5.831	0.038	6.154
0.4	0.038	0.003	0.214	5.735	0.038	6.161
0.5	0.038	0.003	0.265	5.643	0.038	6.167
Step 2 (sorel concrete / NaCl solution)						
Reacted solid [mol]	Ca [mol/kg H ₂ O]	K [mol/kg H ₂ O]	Mg [mol/kg H ₂ O]	Na [mol/kg H ₂ O]	SO ₄ ²⁻ [mol/kg H ₂ O]	Cl [mol/kg H ₂ O]
0.1	0.016	0.001	0.055	6.046	0.016	6.157
0.2	0.032	0.001	0.109	5.933	0.032	6.152
0.3	0.038	0.002	0.162	5.831	0.038	6.154
0.4	0.038	0.003	0.214	5.735	0.038	6.161
0.5	0.038	0.003	0.265	5.643	0.038	6.167
Step 3 (sorel concrete / NaCl solution)						
Reacted solid [mol]	Ca [mol/kg H ₂ O]	K [mol/kg H ₂ O]	Mg [mol/kg H ₂ O]	Na [mol/kg H ₂ O]	SO ₄ ²⁻ [mol/kg H ₂ O]	Cl [mol/kg H ₂ O]
0.1	0.016	0.001	0.055	6.046	0.016	6.157
0.2	0.032	0.001	0.109	5.933	0.032	6.152
0.3	0.038	0.002	0.162	5.831	0.038	6.154
0.4	0.038	0.003	0.214	5.735	0.038	6.161
0.5	0.038	0.003	0.265	5.643	0.038	6.167

A 2.7 Modelled concentrations cascade experiment – salt concrete / MgCl₂ solution

Tab. A.2.23 Modelling of cascade experiment: Salt concrete / MgCl₂ solution

Modelling cascade experiment: Salt concrete / MgCl ₂ solution						
Step 1 (salt concrete / MgCl ₂ solution)						
Reacted solid [mol]	Ca [mol/kg H ₂ O]	K [mol/kg H ₂ O]	Mg [mol/kg H ₂ O]	Na [mol/kg H ₂ O]	SO ₄ ²⁻ [mol/kg H ₂ O]	Cl [mol/kg H ₂ O]
0.1	0.003	0.497	4.036	0.548	0.129	8.873
0.2	0.004	0.568	3.976	0.570	0.116	8.874
0.3	0.007	0.602	3.900	0.597	0.069	8.883
0.4	0.034	0.606	3.810	0.620	0.014	8.894
0.5	0.107	0.609	3.720	0.632	0.005	8.893
Step 2 (salt concrete / MgCl ₂ solution)						
Reacted solid [mol]	Ca [mol/kg H ₂ O]	K [mol/kg H ₂ O]	Mg [mol/kg H ₂ O]	Na [mol/kg H ₂ O]	SO ₄ ²⁻ [mol/kg H ₂ O]	Cl [mol/kg H ₂ O]
0.1	0.004	0.539	4.096	0.510	0.115	9.027
0.2	0.018	0.584	3.955	0.553	0.024	9.042
0.3	0.144	0.589	3.795	0.572	0.004	9.040
0.4	0.289	0.595	3.635	0.587	0.002	9.032
0.5	0.435	0.600	3.474	0.601	0.002	9.025
Step 3 (salt concrete / MgCl ₂ solution)						
Reacted solid [mol]	Ca [mol/kg H ₂ O]	K [mol/kg H ₂ O]	Mg [mol/kg H ₂ O]	Na [mol/kg H ₂ O]	SO ₄ ²⁻ [mol/kg H ₂ O]	Cl [mol/kg H ₂ O]
0.1	1.966	0.643	0.000	1.389	0.002	5.955
0.2	1.675	0.615	0.000	2.122	0.002	6.079
0.3	1.422	0.591	0.000	2.796	0.002	6.223
0.4	1.202	0.571	0.000	3.426	0.002	6.395
0.5	1.014	0.555	0.000	4.029	0.002	6.605

A 3 Calculation of pC_H

The pH-value is defined as negative decade logarithm of the hydrogen ion activity ($-\log(a_{H^+})$). Conventions for such activities are defined at defined boundary conditions. "pH-scales" are based on these conventions and defined pH-values of buffer solutions. Further conventions exist for typical transitional potentials of references electrodes in comparison with measuring solution. Hence, pH-values can be determined using typical pH-electrodes after calibration with buffer solution for solutions with low ionic activities.

But for high saline solutions thus conventions has no validity anymore. This is caused by the inconstant transitional potentials and the overlay of measurement signals by effects, which depend in ionic concentrations in the solution. Thus, the pH-values have no thermodynamically meaning anymore in high saline solutions.

The dependence of hydrogen ionic activity " c_{H^+} " and observed pH-value " pH_{mes} ", which results from application of the calibration function, is defined by

$$pH_{mes} = -\log c_{H^+} - \Delta pH = pC_H - \Delta pH \quad \text{Equation A3.1}$$

pC_H is defined as the negative decade logarithm of the hydrogen ion concentration. ΔpH describes the difference between pH_{mes} and pC_H . ΔpH is a function of the concentrations c of the saline solution and consists of two parts. Frist part describes the difference of the diffusion potential between inner electrolyte and reference electrode and second part the activity coefficient of H^+ .

$$\Delta pH = \sum_c \sum_a \sum_l x_{j,ca} Q_{ca}^j + \sum_k \sum_{l \neq k} \sum_{m \neq k,l} \sum_j y_{j,klm} T_{klm}^j + SIT(I) \quad \text{Equation A3.2}$$

$$SIT(I) = \log y_{H^+} = -A \frac{\sqrt{I}}{1 + 1.5\sqrt{I}} \quad \text{Equation A3.3}$$

Appendix A3

A is a Debye-Hückel parameter ($A = 0.5134 \text{ [kg}^{1/2}/\text{mol}^{1/2}]$) and I describes the ionic strength. $x_{j,ca}$ and $y_{j,klm}$ are parameters of the polynomic function with powers Q^j and T^j :

$$Q = \frac{c_c c_a}{Z} = \frac{c_c c_a}{\sum_j c_i |z_i|} \quad \text{Equation A3.4}$$

$$T = \frac{c_k c_l c_m}{Z} = \frac{c_k c_l c_m}{\sum_j c_i |z_i|} \quad \text{Equation A3.5}$$

Q describes the binary interdependency between cations (index c) and anions (index a). It is the quotient of product of solution concentration c and the charged balanced sum Z of solution concentrations. T describes the ternary interdependency of three ions.

This method is valid at temperatures of 25°C and pH-electrodes with an inner electrolyte of 3 molar KCl-solution. The method can be applied in system of oceanic salt (Na, K, Mg, Ca, Cl and SO₄) with concentrations between 0.35 mol/kg up to saturation approximately. The sum of further ions has to be < 0.1 mol/kg.

Tab. A.3.1 Parameter $x_{j,ca}$ for description of ΔpH in the binary systems as adopted from GRS-internal quality system procedure for the description of calculation of pC_H

System		Parameter $x_{j,ca}$	
c	a	j = 1	j = 2
Na ⁺	Cl ⁻	0.4116	0
K ⁺	Cl ⁻	0.2533	0
Mg ²⁺	Cl ⁻	1.1317	0
Ca ²⁺	Cl ⁻	1.0148	0
Na ⁺	SO ₄ ²⁻	0.3329	0.093
K ⁺	SO ₄ ²⁻	-0.7293	1.3199
Mg ²⁺	SO ₄ ²⁻	-0.0557	0.8848

Tab. A.3.2 Parameter $y_{j,mkl}$ for description of ΔpH in the ternary systems as adopted from GRS-internal quality system procedure for the description of calculation of pC_H

System		Parameter $y_{j,mkl}$		
m	k	l	j = 1	j = 2
Na ⁺	K ⁺	Cl ⁻	-0.0062	0
Na ⁺	Mg ²⁺	Cl ⁻	-0.0251	0
Na ⁺	Ca ²⁺	Cl ⁻	-0.0298	0
K ⁺	Mg ²⁺	Cl ⁻	-0.0423	0
K ⁺	Ca ²⁺	Cl ⁻	-0.0446	0
Mg ²⁺	Ca ²⁺	Cl ⁻	0	0
Na ⁺	K ⁺	SO ₄ ²⁻	0.3210	0
Na ⁺	Mg ²⁺	SO ₄ ²⁻	0.2033	0
K ⁺	Mg ²⁺	SO ₄ ²⁻	0.5141	0

**Gesellschaft für Anlagen-
und Reaktorsicherheit
(GRS) gGmbH**

Schwertnergasse 1
50667 Köln
Telefon +49 221 2068-0
Telefax +49 221 2068-888

Forschungszentrum
Boltzmannstraße 14
85748 Garching b. München
Telefon +49 89 32004-0
Telefax +49 89 32004-300

Kurfürstendamm 200
10719 Berlin
Telefon +49 30 88589-0
Telefax +49 30 88589-111

Theodor-Heuss-Straße 4
38122 Braunschweig
Telefon +49 531 8012-0
Telefax +49 531 8012-200

www.grs.de